Quantifying Rocky Coastline Evolution in North Torbay, Devon, using ^{36}Cl Exposure Dating and Structure-from-Motion Photogrammetry

Drone image of Hopes Nose captured with an eBee drone, used within this study.

Submitted by Victoria Rose Naylor, to the University of Exeter as a dissertation for the degree of Masters by Research in Geography, April 2019.

I certify that all material in this dissertation which is not my own work has been identified and that any material that has previously been submitted and approved for the award of a degree by this or any other University has been acknowledged.

……

Abstract

Around 70-80% of the world's coastline, and around 60% of the UK's coastline, can be considered as 'rocky'. Rocky coasts erode much slower than their softer sedimentary counterparts, but their rates of erosion and their evolutionary history are poorly known. In this dissertation I use a new combination of methods, cosmogenic nuclide exposure dating, structure-from-motion photogrammetry and sea-level modelling, to study a typical stretch of rocky coastline in north Torbay, Devon, southwest England. Torbay's coast is characterised by the presence of shore platforms and raised beaches above modern sea level, situated on the north headland peninsula, named Hopes Nose. These elevated landforms must relate to a previous interglacial period, with warmer environments and higher sea-levels, and their preservation indicates very slow rates of coastal evolution within the area. I apply exposure dating using ^{36}Cl to determine the degree of geomorphological inheritance from previous high sea-level stands, along north Torbay's rocky cliffs and across the main body of the raised shore platform at Hopes Nose. I combine this analysis with the measurement of a new digital surface model, collected via drone imagery and structure-from-motion photogrammetry, across the headland to perform a morphometric analysis of the modern and elevated interglacial platform. Lastly, I determine a new estimate of relative sea-level change at the site, considering glacio-isostatic adjustment, using the SELEN sea-level model. Cosmogenic nuclide exposure dating reveals that the rocky coastline around north Torbay has been actively eroding throughout the late Holocene, through a series of stochastic mass movements and some incremental loss. Similarly, the exposure dating of the raised shore platform at Hopes Nose reveals it has been covered by distinctive sediments during the late Pleistocene and hence survived surface erosion. Morphometric

analysis of the raised interglacial shore platform and the modern shore platform shows a similar evolutionary history, highlighting the changes in marine and aerial influence over the shore platforms formation. An analysis of the raised platform's elevation, evaluated relative to modelled relative sea-level change, is most consistent with the platform being formed during the last interglacial period (Marine Isotope Stage 5e). As a result, this research also puts into question the overall height of the sea-level during MIS 5e, or the presence of a double peak within the record. Overall, this research demonstrates that the unique combination of methodologies can quantify coastal erosion and help decipher a rocky coastline's history under both present and previous sea levels.

Acknowledgements

I would like to thank my fantastic supervisory team, Dr Steven Palmer, Professor Timothy Barrows, Dr Matteo Vacchi and Olly Bartlett, who have supported me greatly throughout my Masters by Research at Exeter. Their knowledge and passion for the subject area and the methodologies employed within this research was truly inspiring, infectious and immensely valuable. I am truly grateful for their frequent availability and ability to always reignite my passion for the research, even at my lowest points in my research and other areas of my life.

I am also grateful for the support of Dr Paolo Stocchi (Royal Netherlands Institute of Sea Research, Netherlands), who assisted me in sea-level modelling within this research. I am also grateful for Dr Keith. L Fifield (Australian National University, Australia), who provided his expertise to measure ^{36}Cl concentrations within the collected samples. Furthermore, I greatly appreciate Dr Karen Leslie and Dr Sharon Turners (Research Technicians in Geography, University of Exeter, UK) for assisting with sample collection within the early stages of this research.

I would like to acknowledge and thank Dr Richard Jones, without his early support and belief in my ability to persue a Masters by Research in Geography, I would not have reached this point.

Finally, thanks also to the University of Exeter Geography department, as well as the Cryosphere, Coastal and River Dynamics (CCoRDs) research group for their support and friendship throughout my time at the university.

Contents

Figures

Tables

Equations

Author's Declaration

The work presented in this dissertation is entirely my own, in my own words and all sources used within this research have been fully acknowledged.

I was assisted by my supervisory team Dr Steven Palmer (provided knowledge on coastal processes), Dr Timothy Barrows (assisted in exposure age calculations and provision of expert knowledge), Dr Matteo Vacchi (assisted in geomorphological interpretation and sea-level reconstruction) and Olly Bartlett (provided expertise in eBee operation within the field site).

The modelling of the relative sea-level at Hopes Nose was carried out by Dr Paolo Stocchi, with assistance from Dr Matteo Vacchi, who also contributed to its interpretation. However, the work presented within this dissertation is written in my own words and with further interpretation.

It must be noted, that this research has also been written into a manuscript for publication and at the time of marking may be in the submission process.

List of Abbreviations

Abbreviation	Explanation
^{36}Cl	Chlorine-36
A/I	D-alloisoleucine/L-isoleucine
AAR	Amino Acid Racemization
AIS	Antarctic Ice Sheet
AOI	Area of Interest
DEM/DSM	Digital Elevation Model/Digital Surface Model
EA	Environment Agency
GCP	Ground Control Point
GIA	Glacial-isostatic Adjustment
GIS	Geographical Information Systems
GPS	Global Positioning System
GrIS	Greenland Ice Sheet
Ka BP	Kilo Annum Before Present
LGM	Last Glacial Maximum
LiDAR	Light Detection and Ranging Methods
Lm	Lifton (2005) Scaling scheme
MEM	Micro Erosion Meter
MIS	Marine Isotope Stage
MVM	Multi-view Measurements
OD	Ordnance Datum
RSL	Relative Sea-Level
Sa/LSDn	Saito Scaling scheme (Lifton, 2014)
SD	Standard Deviation
SLE	Sea-level Equation
SfM	Structure-from-Motion
St	Stone (2000) Scaling scheme
UAV	Unmanned Aerial Vehicle
U-Series	Uranium-series Dating

CHAPTER 1: INTRODUCTION

1.1. Why are coastlines important?

Coastlines play a vital role in modern society. Currently, around 40% of the world's population resides in dense communities within 100 km of a coastline (Small and Nicholls, 2003; UN, 2007). Coastlines are historically important for establishing and developing communities on a global scale, with a dramatic increase in the utilisation of the coast during the 20th century (Nicholls, 2010). The increased utilisation of the coast can be attributed to rapidly growing populations and industrial practices at the global scales, both of which are set to increase into the 21st century (Nicholls, 2010; UN, 2007). This is evident in the UK, where over 30% of the population in England and Wales live within 10 km of the coast, with rapid population growth in these coastal communities peaking in 2016 (ONS, 2016; POST Report 363, 2010).

Coastlines have a significant socio-economic importance, and the entire global population is connected to the coast in some way. Coastlines provide an array of goods and services, which are highly valuable to human society (Martínez et al., 2007). Economic activity has increased along the coastline, almost exponentially with increasing populations (Coastal EBA, 2017). This is evident in the growth of megacities along many coastlines, with 21 of the 33 global megacities located along the coast. In particular, Lagos (Nigeria), Dhaka (Bangladesh) and Karachi (India), which have all seen significant growth over the last three decades (Martínez et al., 2007). The world's coastlines have diverse physiographical characteristics and contrasting environments, altering the resources and services which they can provide (Martínez et al., 2007).

Additionally, the economic value of coastlines is commonly based on the value of private dwellings, public infrastructure (e.g. transport links, such as the Dawlish railway line) and tourism income (e.g. arcades and holiday parks) (Dawson, 2012; GCC, nd; Lewsey et al., 2004). In most economically developed regions, coastal properties are higher in value than similar properties inland. For example, within the UK, where coastal houses along Sandbanks (Dorset) sold on average for £665,000 in 2016 (Turrill, 2017). Similarly, seaside tourism plays a significant part in the coastline economy, and is worth around £8 billion a year in the UK (Coastal Tourism Report, 2016).

In addition to this, coastlines also play an important role in the development of cultures around the world, such as heritage cultures, cultural identities and some aspects of spiritual cultures (Mwaipopo and Shalli, 2016). An example of the cultural identity that the coast can bring to people is seen in California's surfer culture along the west coast of the US, as well as the multi-cultural (or creolization) of the Gulf Coast of New Orleans (e.g. Cresent City) (NGS, 2017).

Similarly, coastline features and characteristics also play a role in how people interact and learn from the coastline. In the UK, the coastlines can hold significant importance to the population, this is seen in the UNESCO World Heritage status of the Jurassic Coast (established in 2001) which extends between Exmouth (east Devon) and Studland Ba (Dorset). The Jurassic coastline has proved significant in increasing our understanding of the last 185 million years of geological history (Jurassic Coast Website, 2018; Cochrane, 2008). The Jurassic Coast has also been a significant tourist attraction for generations. Those that have not visited are aware and familiar of the importance of this coastline through education, books, news, TV, Film and social media (Cochrane, 2008). As a result of the high engagement of the general public, scientists and governing bodies are

encouraged to maintain the importance and protection of this area and its history (Edwards, 1987).

Lastly, the diverse habitats along coastlines, serve as nurseries for rare species of flora and fauna, which are biologically diverse and accessible (Burke et al., 2001; Economidou, 1982). Within the UK, topographically complex and exposed coastlines provide unique habitats, rocky surface substrate and turbulent nutrient rich environments for plant growth, such as Dog Whelk, Kelp and Sea Palm, as well as marine life such as Mussels and Limpets (Boaden and Seed, 1985; Economidou, 1982). Coastal ecosystems also include salt marshes, dunes, beaches, barrier beaches, coral reefs and areas of brackish water (Economidou, 1982). It is possible to determine the stability of many coastlines by how established and diverse their associated habitats have become, with extremely diverse and well established environments possibly highlighting relative stability in the coastal environment (Bird, 2011; Burke et al., 2001)

Despite their wealth and diversity, many of the worlds coastlines are under stress as a direct and indirect result of anthropogenic activity. The primary threat to coastlines at a global scale is the rapid sea-level rise and increased storminess occurring over the latter part of the Holocene, which can be directly related to increased anthropogenic activity and influence (Thompson et al., 2002). Predicted sea-level rise varies significantly depending on the climate scenario and the geographical location, as reported in the most recent UKCP18 report (Table 1.1) (Palmer et al., 2018). Sea-level changes of such magnitudes are predicted to have a substantial impact on tidal amplitude, wave height and the frequency of storm surges and swells (Dawson, 2012; Nicholls, 2010; Palmer et al., 2018). As a direct result of these changes, the increase in future rates of coastal retreat is deemed inevitable, including erosion via mass movement

events which are more frequent and devastating in nature (Kennedy et al., 2014; Teixeira, 2006). These changes are set to threaten the numerous natural and manmade benefits that's the coast provides at the global scale (e.g. tourism, public infrastructure and natural diverse habitats).

	climate scenarios	
Place	**RCP 2.6** **Sea-level change (m)**	**RCP 8.5** **Sea-level change (m)**
London	0.29 – 0.70	0.53 – 1.15
Cardiff	0.27 – 0.69	0.51 – 1.13
Edinburgh	0.08 – 0.49	0.30 – 0.90
Belfast	0.11 – 0.52	0.33 – 0.94

***Table 1.1**: Table interpreted and modified from Palmer et al (2018), presenting predicted sea-level changes at 2100. RCP 2.6 represents a low emission scenarios, and RCP 8.5 represents a high emission scenario. Measurements are relative to 1981 – 2000 averages.*

The impact of climatic change has started to be seen along the UK coastline, especially during the 2013/14 winter storms, which caused significant damage along the coastline of Devon and Cornwall (Huntingford et al., 2014; Masselink et al., 2014). Coastal erosion at Dawlish (south Devon), led to a month-long suspension of the mainline rail services, a key transport link between the southwest and the rest of the country. The estimated cost of rebuilding the track at the time was around £35 million, with further attempts to protect the area estimated upwards of £650 million, leading to significant economic loss across the UK (BBC, 2016, 2014; Kendon and McCarthy, 2015).

Despite the threat of sea-level change on the worlds coastlines, Naylor et al (2010) noted that there is greater interest towards research on softer and predominantly sedimentary cliffs, beaches, dunes and barriers across the last century, rather than coastlines consisting of more resistant lithologies categorised as rocky coastlines. This is highlighted throughout a wide array of literature over the last few years, regarding rocky coast erosion and geomorphology, and this is also replicated in modern coastal management policies (Emery and Kuhn, 1982; Masselink et al., 2014). The minimal research interest in rocky coastline geomorphology, processes and retreat, is commonly associated with the typically slower recession rates of rocky cliffs. These rates supposedly pose less of an apparent and immediate threat to populations, with significant retreat events hardly occurring in an average person's lifespan (Bird, 2011; Earlie et al., 2013; Naylor et al., 2010b). Consequently, our overall understanding of rocky coastline evolution is hindered by the lack of measurements and quantification along rocky coastlines, leading to a reliance on theories and assumptions, which are not always supported by solid and real-time evidence.

Within the next sections I will outline the classification and characteristics of rocky coastlines, the mechanisms and theories of their evolution and analyse current literature which aims to further our understandings and quantify these variables.

1.2. Rocky Coastlines

1.2.1. What are rocky coastlines?

It is estimated that around 75-80% of the world's coastlines are classified as "rocky" coastlines (Emery and Kuhn, 1982; Masselink et al., 2011). This high percentage is lower within the UK, where 60% of the UK's open coastlines can

be categorised as rocky (Masselink and Russell, 2008). Rocky coastlines are unique for several reasons, yet arguably their most distinctive characteristics are their lithology, distinctive geomorphology, slow rates of retreat and exposure to harsh marine conditions (Bird, 2011; Naylor et al., 2010b; Trenhaile, 2016a).

Giuliano et al (2013), identifies that rocky coastlines consist of large areas of sinuous and heterogeneous lithologies, such as headlands and rocky outcrops. The geology of rocky coastlines consist of close-grained and cohesive structures, where strong bonds tying the overall structures together, forming a distinctive resistant lithology (e.g. very hard quartzites and granite, or moderately hard limestones and shales), which erode much slower than loose structured and soft-rock coastlines (Bird, 2011; Davidson-Arnott, 2010; Wright, 1970).

Rocky coastlines are often characterised by their distinctive geomorphology, as noted in pioneering work by Tsujimoto (1986) and further developed by Sunamura (1992). There are three distinctive geomorphologies which are seen along rocky coastlines: plunging cliffs, cliffs footed by a sloping shore platform, and cliffs that are footed by a sub-horizontal shore platform (Figure 1.1) (Bird, 2011; Masselink et al., 2014, 2011; Sunamura, 2015, 1992). Plunging cliffs are often found along many rocky coastlines, typically measuring around 100-150 m high, with the cliff face extending below the sea level to some considerable depth (Figure 1.1) (Davidson-Arnott, 2010; Sunamura, 2015; Woodroffe, 2002). Many plunging cliffs, seen today, are formed as a result of sea-level changes during the Holocene, which drowned the coastline after a period of abandonment, resulting in mass movement events which formed the shear vertical plunging cliffs (Isla, 2009). Examples of plunging cliffs can be seen along the rocky coastlines of Lord Howe Island (New Zealand), Esha Ness (mainland Sheltand) and St Agnes (Cornwall) (Cotton, 1949; Garnett, 1962; Hall et al., 2006; Isla, 2009).

Another distinctive geomorphological feature of rocky coastlines is the presence of shore platforms. Shore platforms are a common coastal features along rocky coastlines along south coast of Britain, where 38% of the rocky coastlines have a shore platform (Wright, 1970). Shore platforms are created as result of progressive cliff retreat over time. Cliff retreat occurs as a result of weakness within the cliff. These weaknesses occur in rocky coastlines due to the presence of joints, faults, bedding planes and varying lithologies (Bird, 2011; Masselink and Russell, 2008; McLean and Davidson, 1968). As a result, rocky coastlines experience erosion at the cliff toe, in addition to the vertical downwearing and lowering of the surfaces within the intertidal zone (Davidson-Arnott, 2010).

Different climatic and wave environments and rock lithologies, determine the geomorphology of the shore platform which is created. Shore platforms can be categorised as either Type-A or Type-B (Figure 1.1). “Type-A” shore platforms, slope away from the toe of the cliff, at a gradient around 1˚-5˚, with no breaks or abrupt terminus below the sea-level (Figure 1.1) (Masselink et al., 2014; Sunamura., 1992). Type-A platforms are the most common type of shore platform in macrotidal environments (tides >4 m), where tidal ranges dominate the erosive processes active within the environment (Woodroffe, 2002). These platforms can be up to 5000 m wide and 30 m deep, such as those along the west coast of Sakhalin (Russia) (Woodroffe, 2002).

However, shore platforms can also be categorised as Type-B platforms, often referred to as sub-horizontal shore platforms (Masselink et al., 2014; Sunamura, 2015). These platforms extend across the intertidal zone, either at high-tide or low-tide, terminating in a horizontal seaward drop (Figure 1.1) (Woodroffe, 2002). Type-B shore platforms commonly occur in microtidal environments (tides <2 m), and are especially characteristic of prominent headlands (Bourke et al., 2017;

Masselink et al., 2014; Sunamura, 1992). Type-B platforms measure between 10 m and 1000 m wide, increasing in width with increasing water depths, usually measuring 10 m to 20 m deep on average, yet some storm dominated areas may have platforms 50 m deep (Isla, 2009).

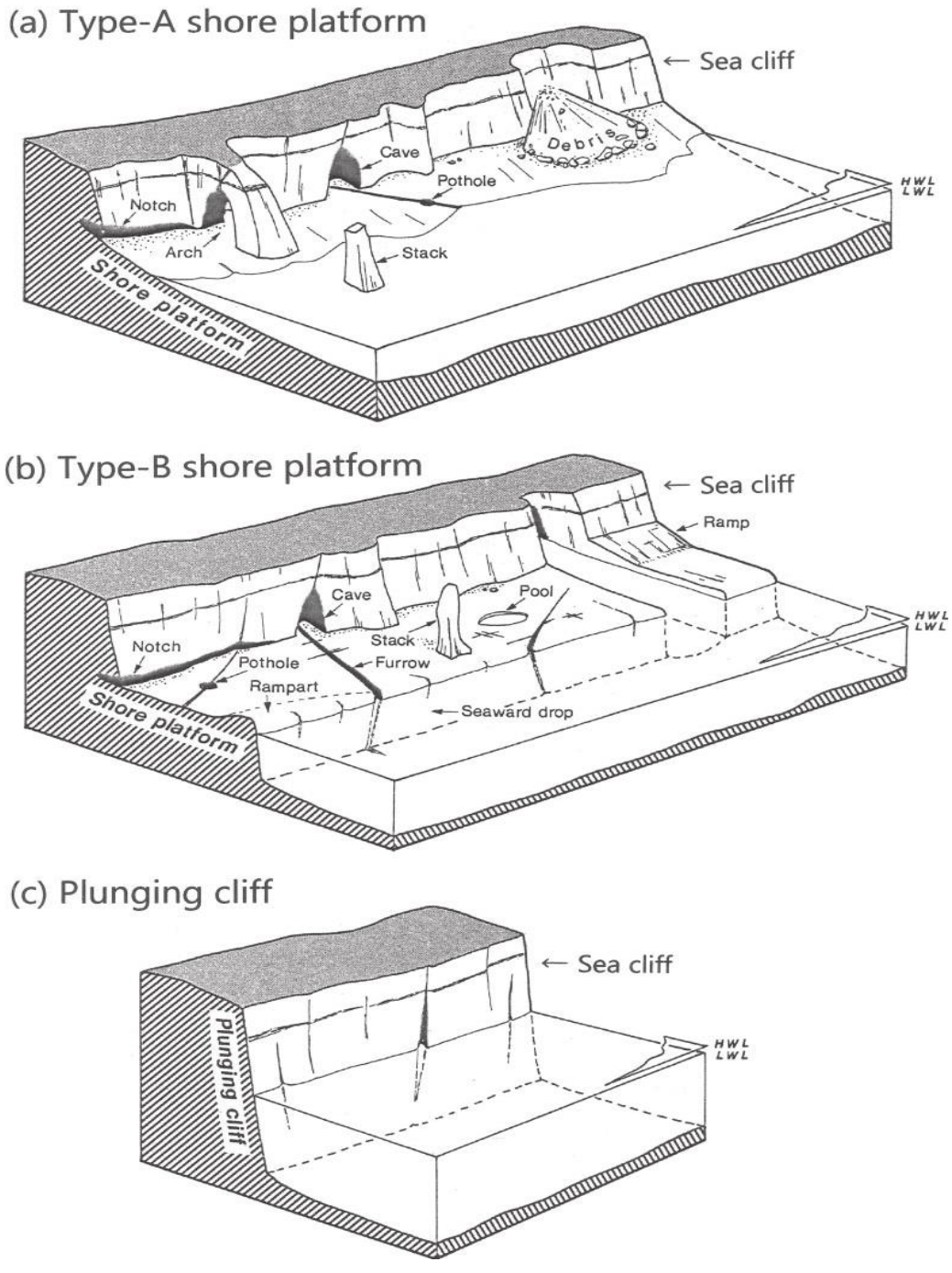

Figure 1.1: *Rocky coastline characteristics, taken from Sunamura (1992). (a) Type-A shore platform shows a sloping shore platform, (b) Type-B shore platform shows a sub-horizontal platform and (c) shows a plunging cliff.*

The geomorphological features of rocky coastlines, outlined above and in Figure 1.1, are an expression and legacy of the interactions of external forcing, such as marine and subaerial erosion, and the intrinsic properties of the rock's lithology and structure (Andriani and Walsh, 2007; Carter and Woodroffe, 1997; Giuliano et al., 2013; Limber and Murray, 2011). The formation of distinctive rocky coastline geomorphologies can be attributed to a number of different processes and mechanisms, which operate over different spatial and temporal scales.

1.2.2. Mechanisms and theories of coastal erosion and shore platform formation

Despite the minimal long-term quantitative research focussing on the coastal evolution of rocky coastlines, there are several existing theories regarding the erosional mechanisms and processes which shape the coastline. Rocky coastlines are primarily impacted and eroded by waves, weathering, bioerosion and mass movement processes. However, interpreting the dominant processes of evolution can be difficult within the coastal setting, as they all tend to occur concurrently (Masselink et al., 2014). Due to the resistant nature of the rocky coastline geology the incremental loss of material via mechanical erosion, weathering and bioerosion rates are often perceived to be relatively minimal (Earlie et al., 2013). Table 1.2 highlights the differences in the incremental erosion rates between more resistant rocky lithologies (e.g. granite and limestone), and softer sedimentary coastlines (e.g. volcanic ejecta) (Masselink et al., 2014; Trenhaile, 2011). The erosive difference is also summarised by, Trenhaile (2011), who estimates that cliff recession is around 1.5 to 2 orders of magnitude greater on softer cohesive clay cliffs (over the last 100 years), than the hard-rock lithologies of rocky coastlines.

Lithology	**Rate of Erosion (m/yr^{-1})**
Granite	<0.001
Limestone	0.001 - 0.01
Flysch and Shale	0.1 - 1
Clay	0.5 - 2
Quaternary Deposits	1 – 10
Volcanic Ejecta	>10

Table 1.2: *An example of incremental erosion along resistant rocks which can make up a "rocky" coastlines lithology, and the variations in rates for "soft" coastline lithologies (Masselink et al., 2014; Sunamura, 1992; Trenhaile, 2011).*

Long-term studies focused on rocky coastline evolution often identify that the recession of rocky coastlines is primarily driven by large episodic and localised mass movement events, extending over significantly long timescales. Wave action often dominates the initiation of mass movement events. The degree to which waves impact the rate of coastal erosion is determined by the specific wave climate which operates along the coastline, as well as the coasts lithology, geographical location and geomorphology itself (Woodroffe, 2002). The cliff face and geomorphological features can either reflect or dissipate breaking wave energy, thus altering the erosive processes which erode the coastline (Laker, 2016; Masselink et al., 2014). Coastal erosion is often characterised by either horizontal cliff retreat (backward) erosion or vertical lowering (downward) erosion. However, it is often difficult to fully separate these two types of erosion within rocky coast environments, as they are intrinsically linked to one another. Within

the following sections I outline the processes which can be deemed the primary drivers of horizontal and vertical erosion along a rocky coastline.

1.2.2.1. Horizontal erosion: Hydraulic erosion and mass movements

Hydraulic erosion can occur when waves break directly against the cliff face, due to the tension of receding water and the vertical shearing of water as it is forced up and down the cliff face (Davidson-Arnott, 2010). The direct breaking of waves on the cliff face has been dubbed as a “water hammer” or “geomorphic wrecking ball” due to significantly concentrated wave energy at the cliff face (Adams et al., 2005; Davidson-Arnott, 2010). As the waves break, air is compressed and trapped in cracks and fractures across the cliff face, resulting in the exploitation and expansion of these weaknesses (Davidson-Arnott, 2010). Hydraulic erosion can lead to the quarrying of the cliff face, plucking the material from the cliff face, which results in the horizontal retreat of the cliff. The lose material removed from the cliff face can often contribute to the vertical/downwards erosion and lowering of bedrock at the front of the cliff, possibly on a shore platform (Adams et al., 2005). These processes will be further outlined in section 1.2.2.2 (Adams et al., 2005). Hydraulic erosion tends to increase during periods of storm activity, due to the increased frequency, energy and thus impact of waves on the cliff face (Carter and Woodroffe, 1997; Masselink et al., 2014). Hydraulic erosion can have profound implications for rocky coastline evolution and is commonly attributed as a contributing process to the episodic occurrence of mass movements.

The direct breaking of waves on the cliffs face can also create microseismic shaking and low-frequency oscillations throughout the cliff (Adams et al., 2005). These oscillations are generated and controlled by a range of offshore, nearshore and at-cliff sources, such as tide, water depth and wave heights (Adams et al.,

2002; Norman et al., 2013; Vann Jones (née Norman) et al., 2015). Peak energy transfers to the cliffs face occur during large storm evens, increasing microseismic shaking and low-frequency oscillations (Vann Jones (née Norman) et al., 2015). An example of this is outlined in work by Earlie et al (2015b) along the southwest peninsula of the UK, where vertical ground displacements and microseismic motions increased an order of magnitude (10 µm to 100 µm) during large Atlantic storms in 2014.

Hydraulic erosion contributes to the horizontal retreat of rocky coastlines through undercutting at the cliff toe, via quarrying and the removal of large quantities of material. The undercutting of the cliff results in the destabilisation of the cliff and as a result triggers large and episodic mass movement along many rocky coastlines (Adams et al., 2005). When combined with an increase in rock stress, related to the microseismic shaking and low-frequency oscillations, further destabilisation of the cliff occurs (Adams et al., 2005; Kennedy et al., 2018; Vann Jones (née Norman) et al., 2015).

Mass movements are often seen as a mechanism which can re-establish “equilibrium” of the cliff face and angle (McLean and Davidson, 1968). The type of mass movement or wasting event is related to the environmental setting of the cliff and the cliff’s lithology (Masselink et al., 2014). Rock falls and topples occur on well-jointed rocky cliffs, which have become undercut by hydraulic erosive processes (Figure 1.2). During rock falls, most of the sediments are composed of cliff material, causing significant coastline retreat. Landslides can also occur along sections of rocky coastlines, which are more deep-seated failures where the comprehensive strength of the rock is exceeded by the load that is imparted onto it (Masselink et al., 2014). Landslides are often associated with sediments which overly the cliff, but it is possible for a significant amount of the cliff’s

sediments to also be incorporated within the debris. Landslides can be transitional (a controlled slide on a straight plane), rotational slides (occurs on a concave-upward surface and related to significant undercutting of the cliff) and block slides (related units slide down as uniform plains) (Masselink et al., 2014, 2011; McLean and Davidson, 1968).

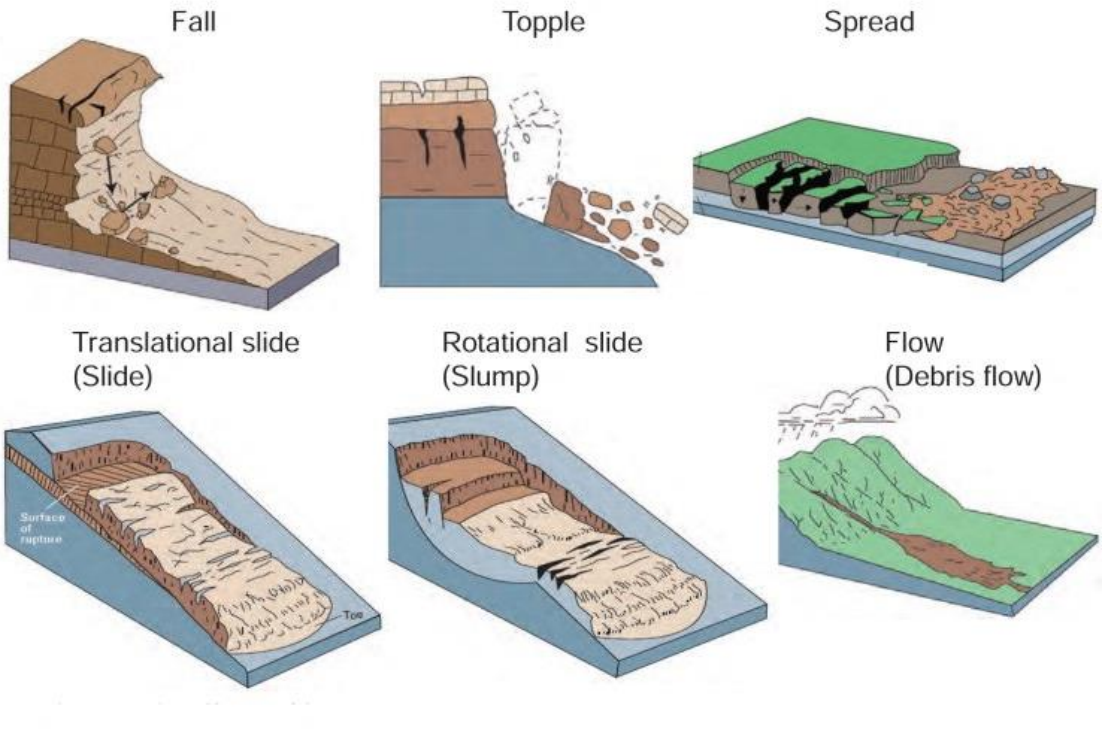

Figure 1.2: *Examples of mass movements events which can occur along coastal areas. Figure from Shanmugam and Wang (2015), interpreted from Varnes (1978).*

When a mass movement occurs debris from the cliff face falls to be the base of the cliff, known as talus. Talus influences mechanical processes and both vertical lowering and horizontal cliff retreat, which contributes to the evolution of the coastline (Bonneau and Hutchinson, 2019; McLean and Davidson, 1968; Melo et al., 2018). The overall quantity of the talus which is produced, is influenced by the height of the cliff with taller cliffs producing more talus during mass movement (Sunamura, 2015). Material is often produced via rock falls and topples, having

the same resistant lithology of the cliff itself. Consequently, it can take a long time (decades – millennia) for all the talus to be removed from in front of the cliff, via waves and tides (Carter and Woodroffe, 1997). The presence of talus is effective in momentarily ceasing the erosion of the cliff base, acting as a form of protection. The effectiveness of talus is often replicated as a form of coastal management, such as rock armour, as seen along Dawlish Warren (south Devon) and Saunton Sands (north Devon) (Masselink et al., 2014).

In contrast to the above, talus can also intensify some of the mechanical erosional processes which operate within the coastal environment. Over time, erosive process (e.g. hydraulic erosion) break the talus down into clast sizes which are easily mobilised by waves (Blanco Chao et al., 2006). The mobilization and presence of such clasts provides ammunition and tools for erosive processes, such as abrasion and attrition, which result in the incremental loss of material from the cliff face (Limber and Murray, 2011). The balance between wave energy and clast size determines the erosive frequency and efficiency, and thus the rate of incremental loss (Blanco Chao et al., 2006; Limber and Murray, 2011). These processes mainly occur at the cliff base, contributing to the undercutting and destabilisation of the cliff (Bezerra et al., 2011).

The recession of the cliff via wave driven mass movement events often creates near vertical plunging cliff faces along rocky coastlines. Similar mass movements and other processes which drive horizontal cliff retreat is also noted as the initiation mechanisms of shore platforms. Due to this, shore platforms are often noted as “wave-cut” platforms, which also refers to the vertical downwearing which is outlined within the next section.

1.2.2.2. Vertical erosion: mechanical erosion and subaerial processes

Mechanical erosion refers to the removal of material from the rocky coastlines by other material, which have been entrained by the orbital and turbulence of waves (Adams et al., 2005; Davidson-Arnott, 2010; Woodroffe, 2002). The entrained sediments are often made up of material removed from the horizontal cliff retreat, such as quarried sediments or talus (section 1.2.2.1) (Robinson, 1977; Woodroffe, 2002). Once sediments are entrained within the waves, the oscillatory motion results in abrasion (materials rubbing against the cliff face), and attrition (material hitting and fragmenting the cliff face and shore platform) (Kline et al., 2014). Mechanical erosion tends to occur at the mean water level and is limited to shallower water depths. Work by Robinson (1977), identifies that overall erosion rates can be 15-18.5 times greater where there is available sediments at the cliff foot. However, as water depth increases, there is a decrease in material mobilization, and hydraulic erosion is once again the primary drive of cliff retreat (Davidson-Arnott, 2010).

While horizontal cliff retreat is responsible for the initial formation of shoreline platforms and the retreat and evolution of the cliff, the type of shore platform (Figure 1.1), created is determined by the vertical lowering of the platform within the intertidal zone. (Davidson-Arnott, 2010; Stephenson, 2000; Tsujimoto, 1986). Tsujimoto (1986) identified that Type-A platforms occur when vertical lowering rates in the inter-tidal zone is similar to that experienced in the nearshore. This removes the low-tide cliff, creating the distinctive seaward slope of Type-A platforms (Bird, 2011; Davidson-Arnott, 2010). However, slower rates of vertical lowering and downwearing preserves the low-tide cliff in the intertidal zone, developing the characteristic sharp drop of the platform associated with Type-B platforms (Bird, 2011; Sunamura, 1978a; Woodroffe, 2002).

This is seen in studies which use micro-erosion meters (MEM), introduced in 1970 by High and Hanna (1970), to measure the small rates of vertical lowering on geomorphological features, like shore platforms. Stephenson and Kirk (1998) utilize MEM on a sloping Type-A mudstone platform, on the Kaikoura Peninsula (South Island, New Zealand). Vertical downwearing measured a rate of 1.98 mm yr^{-1}, whereas Type-B subhorizontal platforms measured a lower rate of 0.73 mm yr^{-1} (Stephenson and Kirk, 1998). Similar rates are measured by Trenhaile and Porter (2018), where mean vertical downwearing rates were measured at 0.162 mm yr^{-1} (Mont Louis), 2.006 mm yr^{-1} (Burntcoat Head) and 0.631 mm yr^{-1} (Scots Bay). Vertical lowering rates are influenced by the coasts lithology, as outlined and agreed upon by authors, such as Bird (2011) and Stephenson and Kirk (1998). On average Stephenson and Kirk (1998) recorded vertical lowering rates of 1.233 mm yr^{-1} on mudstone shore platforms, which is seemingly high when compared to the rate of 0.875 mm yr^{-1}, measured on the limestone platform (Stephenson and Kirk, 1998). However, when both mudstone and limestone lithologies are grouped, and subdivided as Type-A and Type-B shore platforms, the vertical lowering of Type-A shore platforms remains higher than Type-B (Stephenson and Kirk, 1998).

However, there is significant debate regarding the influence of marine and subaerial processes in the vertical surface lowering of shore platforms (Matsumoto et al., 2016a). Waves are considered the primary erosive agent in vertical lowering along rocky coastlines and shore platform development. Plunging waves assert instantaneous pressures up to 600 kPa across a shore platforms surface, and are responsible for the majority of erosive processes operating in their formation (section 1.2.2.1) (Davidson-Arnott, 2010; Summerfield, 1991). Vertical downwearing of the platform theoretically increases

with the increase of wave energy and frequency (e.g. storms and high swells), yet there is minimal quantification of the difference (Davidson-Arnott, 2010). The amount of vertical downwearing is also influenced by the presence of beach sediments. As previously mentioned, Robinson (1977) noted that overall erosion increases in areas where sediment is available in the active wave layer (e.g. beach sediments or talus). However, when sediment thickness exceeds around 5 cm it begins to protect the platform, rather than increasing its vertical downwearing rate (Kennedy et al., 2014; Robinson, 1977).

It is only in recent years that the influence of marine processes on total vertical downwearing has been debated, with an increasing number of studies identifying the significant influence of subaerial and weathering processes on shore platform development (Woodroffe, 2002). These processes occur when there is no protection to the coastal area, such as talus, vegetation or other sediments (Bird, 2011).

An example of coastal weathering is water-layer weathering (Summerfield, 1991; Wentworth, 1938). Water-layer weathering is the repeated wetting and drying of the shore platforms top layer (Summerfield, 1991). This is active mainly around the lower water mark, and the furthest limit of its influence is determined by the reach of waves or the spray of the high tide (Bird, 2011; Kennedy et al., 2014; Summerfield, 1991).

Salt weathering is also a significant form of weathering which occurs along the coastline, primarily those with porous geologies which absorb sea water and spray (Summerfield, 1991). Mottershead (1989) identified that salt spray weathering contributed to the vertical lowering of greenschist bedrock along the Start-Prawle peninsular (South Devon). Vertical downwearing averaged 0.625

mm yr^{-1} over a seven-year period, a rate considered high for a rocky coastline (Mottershead., 1989). Salt spray weathering is often more influential in environments where temperatures are higher, which increases the evaporation of water from the salt spray (Mottershead., 1989; Stephenson., 2000; Summerfield., 1991). The removal of the water by high rates of evaporation result in the crystallization of elements, such as sodium and magnesium within the rock pores. This results in the degradation of the natural rock making it vulnerable to significant vertical downwearing (Ruiz-Agudo et al., 2007).

Lastly, solution weathering is also a significant process of weathering along rocky coastlines, especially those composed of limestone (Summerfield, 1991). Solution weathering is associated with sea water, sea spray or rainwater, which incorporates CO_2 from the atmosphere, creating carbonic acid which dissolve the shore platforms or rocky coasts upper surfaces (Bird, 2011; Rau et al., 2007).

The influence of weathering processes alters with latitude. The higher temperatures and greater possibility for evaporation nearer to the equator means that weathering processes (e.g. salt weathering) are more prevalent on coastlines at these latitudes (Summerfield, 1991). However, solution weathering is more likely to be more effective in lower latitudes, as the ability for water to hold CO_2 in solution decreases with increases in temperature (Dredge, 1992; Ruiz-Agudo et al., 2007). Overall, it is important to consider the possible influence of weathering process in the vertical downwearing, and overall evolution, of rocky coastline geomorphology. Weathering also varies at the local and individual shore platform scale. Work by Porter et al (2010) identifies that tidally generated weathering (e.g. water layer weathering and solution weathering), generally results in higher downwearing and vertical erosion rates within the upper intertidal zone of the shore platform, decreasing substantially towards the lower intertidal zone

(Kennedy et al., 2011). This is evident from the in-field results from Porter et al (2010), where upper intertidal zone downwearing rates were 1.5 mm a year, decreasing to around 0.24 mm a year in the lower intertidal zone.

Weathering rates also vary as a result of the shore platforms morphology, as well as the impact weathering rates have on altering and contributing to the overall morphology and formation of the shore platform (Porter et al., 2010). MEM measurements suggest that weathering dominated the downwearing processes which operate on subhorizontal (Type-B) shore platforms, especially those located in environments with microtidal ranges (e.g. Australia) (Stephenson and Kirk, 1998). Stephenson and Kirk (2000) identified that the formation of Type-B shore platforms along the Kaikoura Peninsula (New Zealand) can primarily be attributed to weathering, similar to conclusions drawn by Trenhaile and Porter (2007) on Type-B platforms at Mount Louis (New Zealand). Weathering significantly reduces the comprehensive strength of the rock, specifically along many resistant rocky coastlines which are dominated by microtidal ranges and weak wave environments (Stephenson, 2000; Stephenson and Kirk, 1998; Alan S. Trenhaile, 2001).

However, this is greatly debated, with some studies reporting there is ultimately no evidence which supports the theory of weathering being responsible for the overall shore platform morphology (Trenhaile, 2000; Trenhaile and Porter, 2007). Due to the difficulties in measuring long term absolute weathering rates on many shore platform morphologies, mathematical models are commonly used to evaluate the contribution of weathering, such as Trenhaile, (2001), Trenhaile (2008) and Trenhaile and Porter (2007). These studies all acknowledge and identify that weathering plays an important role in the development of shore platform morphologies, yet they also acknowledge it should be considered a

secondary process to wave erosional processes (Trenhaile., 2001). Weathering alone cannot account for the initiation of shore platforms or specific characteristics, such as the relationship between tidal range and platform gradient, the overall width of the platform and the platforms elevation (Trenhaile., 2001; Trenhaile and Porter.,2007). Furthermore, Trenahile (2008) also states that even severe weathering, such as that seen on Type-B platform, has minor importance in the long term evolution of shore platform morphology.

Therefore, it is often reported that wave dominated erosion and weathering, work in combination to develop both Type-A and Type-B shore platforms, with the relative and absolute degree of influence of each process varying through time and space (Trenhaile., 2004; Trenahile., 2008). Model runs and field evidence suggests that the most important role of weathering on shore platforms is to significantly reduce the overall comprehensive strength of rocks within the intertidal zone, which in turn increases the efficiency of waver erosion and shore platform development (e.g. quarrying) (Stephenson., 2000; Trenahile.,2008).

1.2.2.3. Other processes at work

In addition to mechanical erosion and weathering, biological and biochemical processes are also acting upon the coastline. However, their contribution to the horizontal or vertical movement of the coastline is often unknown, but appears to vary significantly between environments (Donn and Boardman, 1988; Summerfield, 1991). In some environments, bioerosion can remove rocky material as quickly as the physical erosion and weathering operating along the coast (Donn and Boardman, 1988; Healy, 1968). There are two main types of bioeroders. ‘Grazers’ (e.g. snails and urchins), which scrape and remove sediment from the rock surface, as part of their feeding, whereas ‘borers’ (e.g.

muscles and barnacles) dig into the rock for homes and protection (Donn and Boardman, 1988; Healy, 1968; Schönberg et al., 2017; Summerfield, 1991). These two types of bioeroders have different influences on coastlines, causing direct erosion but also facilitating and influencing other weathering and erosional processes (Naylor et al., 2012, 2010a). Sediment produced by grazing bioeroders are silt-grain size and can contribute to mechanical erosive processes, such as abrasion (Donn and Boardman, 1988). In contrast, borers create holes in the cliff face which can be filled with air on the impact of waves against the substrate, weakening the rocks lithology for hydraulic erosive processes (Bird, 2011).

Due to bioeroders, some rocky coastlines can experience significant erosion due to biochemical processes. Rocky carbonate coastlines on Andros Island (Bahamas), experienced erosion rates between 1.8 m and 2.6 m every 100 years within the intertidal zone, the majority of which can be sufficiently accounted for by bioerosion (Donn and Boardman, 1988). The significant influence of bioerosion is also noted by Viles (1987), where layers of microorganisms over the limestone coastline play a significant role in erosion and textural changes along the near surface zone of the coastline.

Similarly, bioeroders have influence over the vertical lowering of shore platforms in the higher latitudes, addressed in research located in Cornwall and Wales by Naylor et al (2012). This study identifies that erosion by bioeroders is not spatially uniform, and that it can be direct cause for landform responses, such as the formation of rock pools (Naylor et al., 2012). However, similar high latitude research in Tuscany (Italy), show that barnacles along rocky coastlines can in

fact act to protect the rocks from erosion and weathering (Pappalardo et al., 2018).

Changes to the coastline can also be driven by human influence. Humans have influenced a significant proportion of the wider environment, changing the natural behaviour of hundreds of miles of coastline, as well as the more local environment, such as changes to waterways, beach sediments and sea defences (Cencini, 1998; Hapke et al., 2013; Leveau et al., 2016). The extent of human influence over the erosion of the coastline is seen along the Qinhuangdao coastline (China). Between 1996 and 2003 the coastline was eroding on average 1.5 m/yr^{-1}, with higher rates of erosion around river mouths (Xue et al., 2009). The significant amount of erosion is associated with sediment starvation to the coastline, as a direct result of dams constructed along rivers that debouche along the coastline and provide sediment. This is seen especially from the main sediment supplier to the coastline, the Luan River, where there has been a decrease of 9% in the amount of sediment reaching the coastline since 1979 (Xue et al., 2009). Furthermore, humans have significantly influenced the removal of more than 80% of Taiwan's sand coasts over the last three decades due to increased development, removing the natural protection for the backing cliffs (Hsu et al., 2007).

Through the alteration of sediment regimes, humans have significantly increased the vulnerability of the coastline to erosion, yet there are also areas across the globe that have used different practices to protect the coastline. This is seen across a vast amount of coastline along the UK, through the adoption of coastal management plans and defences (Turner et al., 1998). These defences are often in place to protect buildings and infrastructure, through reducing the impact of coastal erosion and cliff retreat. Research has identified a relationship between

overall coastal erosion and accretion along coastlines, and the amount of human development (Hapke et al., 2013). These changes extend over long periods of time and over large spatial scales, suggesting that the influence of people is overriding the geomorphological processes and signal that drives the evolution of the coastline (Hapke et al., 2013).

1.3. Coastline evolution

The processes outline above play a significant role in the evolution of the coastline we see today. Typically, the evolution of the coastline follows the steps outlined in the diagram by Violante (2009) (Figure 1.3). However, this is a very simplified version, with deviations from the cycle occurring frequently. Furthermore, the timescales at which coastal evolution occurs varies significantly, as a result of lithology, climate and processes dominating the area (Bird, 2011). These variations are seen in Figure 1.4, which has been adapted from (Sunamura, 1995) by Naylor et al (2012), where all the possible contributing factors of coastal erosion have been identified.

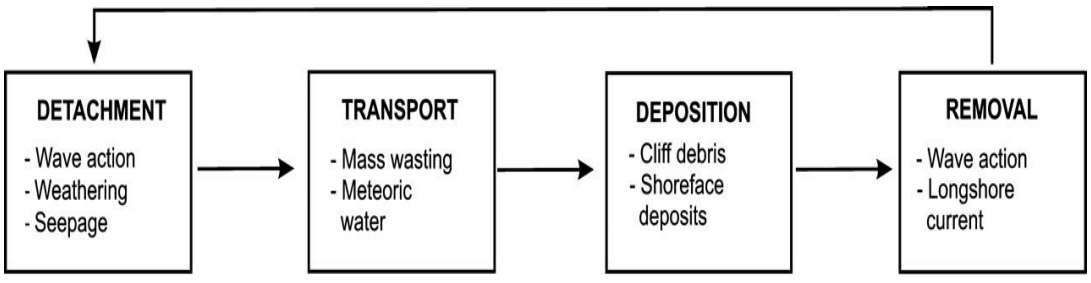

Figure 1.3: A simplified *schematic depicting the cyclitic nature coastline evolution, created by (Violante, 2009).*

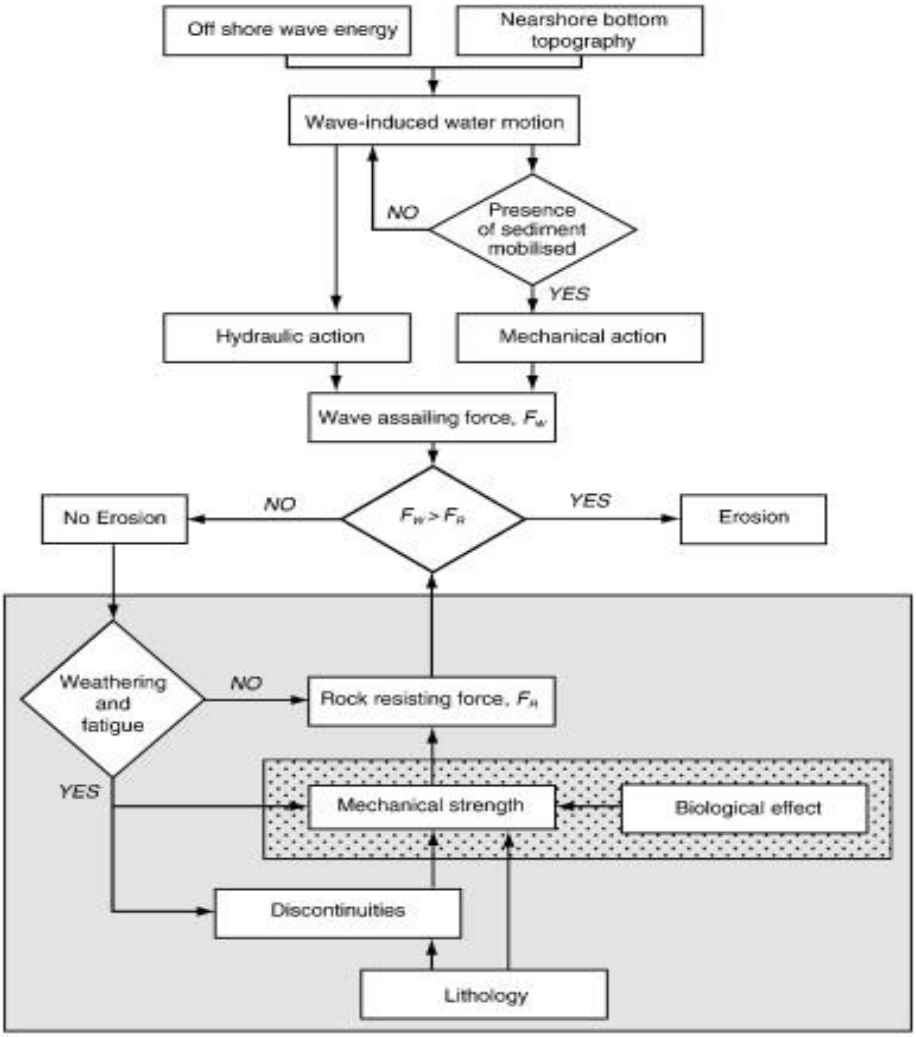

Figure 1.4: *This schematic shows the more complex factors that affect rocky coast erosion. The dominating processes are wave assailing force (FW) and rock resistance force (FR). Erosion occurs when FW > FR (Sunamura, 1995). The large grey box outlines biotic rock interactions and the stippled box shows the biotic interaction identified by the original model (Naylor et al., 2012).*

The rate of rocky coastline evolution is typically undetermined, with processes being significantly influenced by many parameters, such as climate, lithology and sediment availability (Bird, 2011; Kennedy et al., 2014). While there have been attempts to improve the quantification of rocky coastline evolution, the slow development of the coastline often extends beyond the life times of individual researchers meaning there is a lack of observations and data (Matsumoto et al., 2016b).

1.3.1. Existing Coastal Evolution Research

For as long as coastal areas have been inhabited, changes and the evolution of the coastline have been of great interest. Catastrophic and extreme events are recounted in ancient texts such as the Bible (Bentor, 1989; Carter and Woodroffe, 1997), and attempts to mitigate against such events, and the erosion of the coastline, have been witnessed since the middle ages, in China, Japan and the Mediterranean (Pranzini, 2018). Research has often focused on understanding coastal processes and mechanisms, outlined previously, and the influence they have on the rate of coastline evolution (Griggs and Trenhaile (1994). In: Carter and Woodroffe, 1997) Coastal evolution is highly non-linear, exhibiting complex behaviour and trends (Burningham and French, 2017). As a direct result of this, there has been significant debate over which methodologies are most suitable to understand coastal evolution. Through time the development of several suitable methodologies, which aim to understand and quantify coastal evolution around the world. Within the following section I will outline the methodologies which are often used to understand coastal evolution, criticising them in relation to their application in rocky coastline evolution.

1.3.1.1. In-field measurements and observations

In-field measurements and observations primarily underpin our overall understanding of coastal processes and geomorphology, as well as crudely quantifying a rate of evolution over time. Many of these studies focus on specific areas of coastline, observing and identifying specific morphological features such as elevation, topography, high and low water lines (HWL/LWL) and shoreline position (Hart and Gosling, 2018; Kim et al., 2017; Mottershead et al., 1987; Pajak and Leatherman, 2002; Stive et al., 2002). Studies, such as Stive et al (2002) plot these specific coastal features against time, to understand coastal advance and retreat along the Netherlands coastline. In-field mapping of features, such as GPS tracking of the HWL/LWL, is deemed to have a higher accuracy than more modern techniques, such as photo-interpretation (Pajak and Leatherman, 2002). However, the digitisation of shoreline position from aerial photographs or older maps, can support in-field studies to determine the age and antiquity of the coastline (Esteves et al., 2009; Kim et al., 2017). This is usually done to extend the timeframe of the study, aiming to identifying the oldest position of the coast, and subsequent coastline positions, up to the present day (Esteves et al., 2009). For example, in Esteves et al (2009), where in-field measurements and digitised HWL from ordinance survey maps created a time-lapse of coastal evolution from 1848 to 2005.

In addition to this, in-field measurements and observations can be used to determine the main controls and processes (natural and anthropogenic), which influence coastal evolution. In-field measurements taken between 2014 and 2015 from the Malamocco Marghera Channel (lagoon of Venice Italy), outlined that the speed of significant erosion in the lagoon is dependent on the distance from the main navigation channel (Zaggia et al., 2017). Areas of the lagoon proximal to

the channel experienced greater rates of erosion than more distal regions, this was attributed to greater water energies which resulted in higher rates of erosion (Zaggia et al., 2017).

However, the use of in-field measurements to quantify the rate of rocky coastline evolution is often difficult. This is due to the episodic nature of mass movement events, as well as very minimal incremental loses, which are the primary drivers of rocky coastline evolution (section 1.2.2). Consequently, significant changes in a coastline's position and geomorphological features occur over centuries to millennia. As a result, rocky coastlines cannot always be accurately observed and quantified in a study restricted to a short timeframe, due to the selected methodologies, data, or without plans for future research (Marques et al., 2011). Hence, many in-field methodologies are not always suitable for determining the long-term evolution of rocky coastlines.

In contrast to this, in-field measurements and observations of inherited and relict coastal geomorphology (e.g. raised shore platforms), has increased our understanding of past climates and their influence on rocky coastline evolution. In-field measurements and observations of such features are often localised in nature, as seen in work by Hart and Gosling (2018) and Mottershead et al (1987), which is discussed later in section 1.5.

Recent years have seen research focused on collating localised studies, creating national to international scale databases, which can be used to understand the way in which previous sea-levels influenced the evolution of coastlines. An example of this is seen in research by Ferranti et al (2006), which focuses on identifying the impact of palaeo sea-levels on coastline evolution through accurate in-field elevation measurements, at a high spatial resolution. Ferranti et

al (2006) lists accurate elevations of 246 interglacial depositional, erosional and biological high stand indicators, which outline the interglacial sea-level and the impact of long-term vertical land movement in the central Mediterranean (Ferranti et al., 2006). This is similar to recent research carried out by Rovere et al (2016a), who collated 987 studies globally, reporting sea-level indicator elevations related to the last interglacial. Similarly, Hibbert et al (2018), collected and combined 194 biological and geomorphological sea-level indicator studies in the UK, for both the careful assessment and reconstruction of sea-levels between 0-25 Ka BP, including the Holocene transgression.

These studies are dependent on observations and measurements of geomorphological features, which are currently situated at today's modern sea-level. As a result, the determination of which processes create palaeocoastal features often remains speculative. Therefore, many studies focus on observing and reporting just the morphological characteristics of geomorphological features.

1.3.1.2. Modelling coastline evolution

Numerical modelling is another key method used to understand coastal evolution and cliff retreat, across a broad range of environments, at various spatial and temporal scales (Carpenter et al., 2015; Kennedy et al., 2017a; Limber and Murray, 2015). Models of coastal evolution have been published as early as 1866, such as Fisher (1866), initially developing the parameters used to represent coastal evolution. These earlier models of coastal evolution stereotyped many rocky coastal environments with simple observations, which assumed rocky coastlines were straight forward in nature. Consequently, some earlier studies fail

to determine links and processes which operate as part of rocky coastline evolution (Carter and Woodroffe, 1997).

Tsuguo Sunamura has published some of the most cited work related to quantifying erosional processes, retreat rates and coastal evolution through numerical modelling (Sunamura, 1976, 1978a, 1978b). Wave tank and basin experiments by Sunamura (1976) modelled the erosional impact of different cliff profiles on open and closed coastal systems. The models demonstrated that the maximum eroding force can be increased by a magnitude of 4.5 due to the presence of sediments (Sunamura, 1976). Later models by Sunamura (1978a, 1978b) are more mathematical in nature, focusing on the temporal development of submarine platforms and continental shelves, and are often supported by laboratory and in-field observations. For example, Sunamura's (1978b) model correlates with observations from the Byobugaura area of Japan (Sunamura, 1978b). However, recent work by Sunamura (2015) has focused on softer coastlines, further highlighting the greater research efforts made to understand these faster evolving coastlines over their rocky counterparts.

Similar modelling techniques are seen in research led by Alan Trenhaile. Mathematical wave erosional models are used to determine the formation of palaeocoastal features, and rocky coastline evolution. Trenhaile and Layzell (1981) outline a wave erosional model, used to simulate shore platform evolution in east Canada, Australia, New Zealand and Britain. Trenhaile and Layzell's (1981) model is described as mathematically simple, maintaining the historical generalization of rocky coastline processes and evolution. Despite this, the model develops a technique which facilitates the understanding of the relationships between platform morphologies and morphogenic geological factors (e.g. erosion and tidal range) (Trenhaile and Layzell, 1981). Additional work, by Trenhaile and

Bryne (1986), further developed the mathematical wave erosional model. Model runs incorporate various environmental factors, to determine which environmental parameters are required to create specific geomorphological features and patterns of coastal evolution (Trenhaile and Bryne, 1986). The model results also fit consistently with the limited field evidence at the time of publication (Trenhaile and Bryne, 1986; Trenhaile and Laysells, 1981).

Trenhaile (2001a) further modified the models to include parameters which simulate the effect of physical and chemical weathering on the development of shore platforms (Trenhaile, 2001a; Trenhaile, 2000). In the same year, Trenhaile (2001b), developed a subsequent mathematical model to identify the impact of sea-level variation due to glaciations on rocky coastline evolution, specifically shore platform development and erosional continental shelves over the Quaternary. This model was further developed by Trenhaile (2002), to explore the impact of glacially induced eustatic sea-level changes, as well as the interactions between wave dynamics, tides, coastal morphology and rock erosion at the shoreline. Model descriptions and assumptions can be identified and explored in Trenhaile (2000).

The numerical models can be run hundreds and thousands of times, with different variable combinations, identifying changes over multiple temporal and spatial scales. Long model runs can ensure the inclusion of the 26 glacial cycles of the Quaternary period (2.5 million years – present), to understand the differing influence of environmental changes to coastal evolution (A. S Trenhaile, 2002). More recent work by Trenhaile (2016b) includes less generalised variables, focusing on more localised parameters, such as geology and slope gradient (Trenhaile, 2016b).

Whilst studies by Sunamura and Trenhaile can be considered pioneering work in the modelling of rocky coastline evolution, many other researchers have successfully developed new, robust and consistent exploratory models which further increase our understanding (Hanson et al., 2003; Larson et al., 2003; Matsumoto et al., 2016b; Nicholls, 2016; Skrivanek et al., 2018; Thébaudeau et al., 2013). For example, work produced by Limber and Murray (2011) is use to investigate rocky coast evolution over a million year time scale, focused on the large-scale and long-term emergent geomorphic interactions (Limber and Murray, 2011; Murray, 2007). Later theoretical models by Limber and Murray (2014) are similar, and have outlined the influence of differing lithologies and rock strength on rocky coastline evolution. These models have identified which variables cause more rapid erosion in the coastal environment, such as the influence of wave forcing, rock strength, beach width and the sediment richness of the coastline (Limber and Murray, 2014). While these models allow for the production of vast amounts of data, it is not always considered valuable, as it is not always grounded in reality or underpinned by in-field data (Carter and Woodroffe, 1997).

To address this disadvantage, studies such as Thébaudeau et al (2013), focus on specific areas of coastline to model and simulate coastline evolution over past and future timescales at a specific location. Thébaudeau et al (2013) specifically simulates rocky shoreline evolution in Northern Ireland, driven by local sea-level changes over 16,000 years. Multiple model runs identified the significant role of inheritance along the coastline of Northern Ireland, as well as its influence in shore platform formation over time (Thébaudeau et al., 2013). Model results report that many shore platforms and terrace features along rocky coastlines are partially inherited from earlier stadials and sea-levels (Blanco Chao et al., 2003;

Cloetingh and Haq, 2015; Thébaudeau et al., 2013). Similarly, numerical and analytical modelling of sea-stack formation was carried out by Limber and Murray (2015), using specific data from the California Coastal Records Project (Santa Cruz and Santa Barbra). This is a similar approach to the modelling of localized landsliding in Auckland (New Zealand), which utilizes existing available data to reduce the assumptions in the model itself (Dickson and Perry, 2016). Modelling specific coastlines allows for the comparison of model outputs with in-field observations of coastal evolution, increasing the relevance and validity of the models (Matsumoto et al., 2016a; Matsumoto et al., 2016b; Thébaudeau et al., 2013).

However, there is no universal model to analyse and predict rocky coastline evolution, resulting in a significant lack of consistency between different research methods and results (Carter and Woodroffe, 1997; Hanson et al., 2003). There are additional challenges associated with the upscaling of localised studies to boarder spatial scales, such as the national and global, due to inconsistent long-term data along rocky coastlines (Kennedy et al., 2017a). To address this issue there has been a development of programmes, which aim to collate localised models and available data together, such as iCOAST (Nicholls, 2016), Coastline Evolution Model 2D (Morris et al., 2018) and GlobR2C2 (Prémaillon et al., 2018). These programmes aim to model the longer-term morphodynamics of rocky coastlines, as well as extrapolating coastal evolution over longer timescales to quantifying possible responses to future projected sea-levels (Morris et al., 2018; Nicholls, 2016; Prémaillon et al., 2018). Thus, localised studies, which aim to understand the coastal evolution of specific rocky coastlines, are vital in increasing the data available to test, calibrate and validate numerical models

which are focused on creating a global understanding of rocky coastline evolution.

1.3.1.3. Dating coastal evolution

Various dating techniques have been used in coastal research in order to extend the record of past rocky coastline evolution. Building accurate chronologies allows us to further the understanding of rocky coastline evolution, as well as improve the forecasting of future coastal changes (Oliver et al., 2015). In the coastal environment, there are a variety of sediments and materials, which can be dated to create a chronology of coastal retreat and evolution (Lang et al., 1999). Dating coastal sediments is well established in literature and is an area of significant development in its application and analysis, such as in research which aims to determine the antiquity of palaeocoastal features and mass movement events (Pánek, 2015).

The most suitable dating technique is determined by the environment, materials and timeframes which are being investigated. The material that is dated further determines if the obtained age is relative or absolute. Many earlier studies use dating techniques to produce a relative age of a feature or event, not by directly dating the rocks surface, but rather obtaining the age from dateable material underlying, overlying or combined within the area of interest (e.g. a shell suspended in a raised beach, or organic material mixed with the remnants of a mass movement) (Walker, 2005). These ages are interpreted as either the minimum or bracketing ages of the mass movement or palaeocoastal feature (Flageollet, 1996; Pánek, 2015).

The erosional nature and lithology of some study areas, such as palaeocoastal shore platforms, means dating is often difficult. In these circumstances, relative

dating is often the best alternative to understand their age and if they are inherited (Hatrushi, 2017). This method requires readily available biogenic material and deposits within the erosion setting, which allows radiocarbon dating to be used (Bezerra et al., 2017; Yoshida and Moriwaki, 1979). This is a widely used methodology along many of the worlds coasts, which measures the amount of Carbon-14 (^{14}C) within the sample to determine the age (Bezerra et al., 2017). An example of such work is a study by Yoshida and Moriwaki (1979) who used radiocarbon dating to cluster a number of elevated beaches near Syowa Station (Antarctica), into specific time intervals (either between 2000 – 8000 kyr BP or 20,000 – 35,000 kyr BP). Similarly, Amino Acid Racemization (AAR) has also been used to date organic marine remains, measuring ratios of D-alloisoleucine/L-isoleucine (A/I) amino acids to obtain a relative age of the deposits they are suspended in, such as Mottershead et al (1987) (section 1.6.3) (Walker, 2005). Absolute ages, from either radiocarbon dating or AAR, can indicate which geologic period palaeocoastal geomorphological features are inherited from, highlighting the degree of inheritance along the coastline of interest.

These techniques can also be used to create chronologies of mass movement events, such as within research by Flageollet, (1996), where radiocarbon dating of fossil wood embedded within the mass movement ruminants provided a minimum age for when the event occurred. A synthesis by Lang et al (1999) and Pánek (2015) further discuss similar techniques which have been implemented and developed to understand the timings of similar mass movement events on a global scale.

However, the use of radiocarbon dating and AAR to obtain relative ages of mass movements and palaeocoastal features can be problematic (Lang et al., 1999;

Pánek, 2015; Walker, 2005). Both techniques often encounter issues of contamination. Ages obtained from radiocarbon dating can be contaminated by younger soluble carbon (e.g. organic matter, such as bones), where a sampled material may come into contact during its burial (Bezerra et al., 2017; Walker, 2005). Consequently, calculated ages may report as relatively older or younger than the true age (Bezerra et al., 2017). The degree of contamination is dependent on the material that is being dated, and can result in procedural and interpretation difficulties. Contamination can be reduced through careful sample collection and decontamination methods, as outlined in Walker (2005). Similar contamination can occur in AAR dating, due to the “open” nature of the sampled biogenic material (Kaufman and Miller, 1992). As well as this, significant variations in the climate, such as temperature, which alters the rate of A/I degradation and thus the obtained ages (Walker, 2005). As a way to counteract this, calibration curves for specific regional areas have been developed, to calculate the influence of climatic shifts on A/I ratios (Mottershead et al., 1987; Walker, 2005; Wehmiller et al., 2012). However, calibration curves are not available at a global scale, and can change significantly across regions and frequently become outdated (Walker, 2005). This can lead to the wrongful interpretation of the dated samples (Mottershead et al.,1987; Walker., 2005). As a result, AAR dating has reduced in its applicability in more modern studies (Walker, 2005).

Recent research has seen a shift towards other dating techniques to obtain relative ages which are less prone to contamination and its associated errors. For example, Torgersen et al (2015) utilises K/Ar and $^{40}Ar/^{39}Ar$ analysis of synkinematic clays, to constrain the timings of mass movement events, and thus major controls of coastal evolution. The dating highlights plausible ages of fault

initiation, without directly dating the faults or faces themselves and with a reduced risk of sample contamination (Torgersen et al., 2015). Similarly, tephrochronology is another technique that can be used to obtain relative and bracketing ages, enhanced through the use of dating techniques such as $^{40}Ar/^{39}Ar$ or fission track dating (Flageollet, 1996; Pánek, 2015). However, these forms of relative dating require specific materials, conditions and variables to be present (e.g. tephra layer), reducing their applicability in certain environments or locations (McCarroll, 1993).

Due to the disadvantages and inaccuracies associated with relative dating, significant developments in dating techniques have focused on the absolute dating of mass movement events and palaeocoastal features (Bezerra et al., 2017; Oliver et al., 2015; Pánek, 2015; Thomas, 2009). Absolute dating (direct or chronometric dating), refers to dating the features surface directly, obtaining a date with unwarranted certainty or accuracy (Walker, 2005). Absolute dating has been utilized in recent years, such as by Rémillard et al (2015) and Lamothe (2016) who utilise Optically-Stimulated Luminescence dating to directly date sandy beach ridge sediments and raises features, which can occur along rocky coastlines, to provide the first chronological framework of palaeocoastal features. Absolute dating increases our understanding of coastal evolution through establishing direct and precise chronologies from the palaeocoastal features themselves (Lamothe, 2016; Rémillard et al., 2015).

During the last century there have been few studies which have absolutely dated rocky coastline evolution. Those which have, utilise established techniques which are often used in other environmental settings (Pánek, 2015). An example of this is the application of cosmogenic nuclide exposure dating, which is now being

used to absolutely date the remnants of mass movements, cliff faces and palaeocoastal features (Martinod et al., 2016; Pánek, 2015; Soldati et al., 2018).

1.3.1.3.1. Cosmogenic nuclide exposure dating

Cosmogenic nuclide dating is often used to reconstruct glacial recession and thinning, providing direct surface exposure ages (see section 2.1 for a full explanation of the methodology), as well as erosion rates of bedrock surfaces and vertical lowering (Davies, 2014; Owen et al., 2005). Recently, there has been an increase in studies which utilise cosmogenic dating to determine site specific chronologies of coastline retreat, via rock exposure of distinctive rocky coastline features, such as shore platforms and the remnants of mass movement (Choi et al., 2012; Hurst et al., 2016; Stone et al., 1996). Cosmogenic nuclide dating has begun to address the uncertainties of slow rocky coastal evolution throughout history, something that has remained an apparently elusive goal until now (Regard et al., 2012).

Research from Stone et al (1996) is one of the earliest studies which utilises cosmogenic nuclide dating to understand rocky coastline evolution, specifically the formation of shore platforms. Absolute ages, based on the accumulation of ^{36}Cl in exposed surfaces, were used to calculate a late glacial age for the main rock platform in western Scotland (Stone et al., 1996). Isometric modelling of ^{36}Cl concentrations successfully quantified the platforms formation to the Younger Dryas period, with samples dating between 8.9 ka BP and 10.4 ka BP (Stone et al., 1996). Consequently, the authors suggest that the platforms width was created over a 1500 year time frame of stable relative sea-levels and severe climate conditions, with excessive cliff retreat rates of 10-20 mm per year (Stone et al., 1996). This rate is much higher than typically estimated for rocky coastlines,

perhaps highlighting a heightened response of these coastlines to environmental change, where material is removed in vast amounts in a short timeframe (Stone et al., 1996).

Other cosmogenic nuclides, such as ^{10}Be, have also been used to measure rocky coastline evolution. Choi et al (2012) used ^{10}Be to unravel the antiquity of a rocky shore platform in the west coast of Korea. Samples collected from the platform had varied ages between 4 ka BP (Holocene), nearer the cliff face, and 148 ka BP (Pleistocene) from sample collected at the furthest point from the sea cliff (Choi et al., 2012). This can be used to measure the sea-cliff retreat, which lead to shore platform widening. Older ages further from the cliff show a longer period of exposure than those nearer the cliff face exposed by more recent cliff retreat. Regard et al (2012) also proposed a similar method which utilises the pattern of cosmogenic nuclide concentrations along a shore platform, to evaluate the long-term retreat of cliffs located along the English Channel at Mesnil-Val. Overall, the method highlighted that retreat rates appear to be less than ~30 cm/yr at the site under the most “ideal conditions” (Regard et al., 2012). The obtained concentrations of 10Be have a characteristic “bump” or “hump” is stated to represent steady cliff retreat since Holocene RSL rise stabilization which occurred around 7000 – 6000 years ago (Regard et al., 2012). Similar results to both studies are obtained by Hurst et al (2016), who used ^{10}Be to quantify and identify recent accelerations in coastal cliff retreat along the south coast of Great Britain. Obtained concentrations replicate a similar pattern of age distribution (humped), with older ages also measured further from the cliff face, before decreasing in age nearer the cliff face (Choi et al., 2012; Hurst et al., 2016; Regard et al., 2012). The concentrations of ^{10}Be remained consistent with relatively slow retreat rates of the chalk cliffs (2-6 cm yr^{-1}), up until a few hundred

years ago, at which point cliff retreat rates appear to accelerate, based on historical observations (Hurst et al., 2016). The use of cosmogenic nuclides and isotopes in these studies provide a quantification of shore platform formation and the possible rates of cliff retreat, resulting in the platforms widening.

Cosmogenic nuclide dating has also be used to associate palaeocoastal features to specific climate stadials and past sea-levels. Giuliano et al (2014) measured 50 samples from the French Mediterranean shore platforms for ^{36}Cl concentrations. The dating of shore platforms highlighted fluctuations in sea-level, related to climatic changes, within the study site. The concentration of ^{36}Cl was used to identify that shore platforms situated at elevations at present sea-level are contemporary in age, whereas those that are around 8-14 m above sea-level are likely to be associated to the last interglacial and higher sea-levels (Giuliano et al., 2014).

Another way in which cosmogenic nuclides have been used to understand the episodic cliff retreat and evolution of rocky coastlines is through dating cliff faces and talus, which have been identified as relic mass movement events (Recorbet et al., 2010). Recorbet et al (2010) used cosmogenic nuclide dating and morphometric analysis to better understand areas of possible cliff collapse along Cap Canaille cliff (southeast France). The measurement of ^{10}Be and ^{36}Cl, on the cliffs face and collapse blocks, identified age clusters around 3.5 ka BP and 6.7 ka BP and older ages around 9 ka BP and 12 ka BP, suggesting four major episodic collapse events (Recorbet et al., 2010). Older ages coincide with the approach of the present day sea-level, and younger with significant storm events and further alterations in sea-level (Recorbet et al., 2010). The study concludes that sea-level changes have a significant influence over rocky coastline retreat,

through large episodic mass movements, which in turn controls rocky coastline evolution (Recorbet et al., 2010; Regard et al., 2012).

The studies outlined above identify the use and development of cosmogenic nuclide exposure dating in understanding rocky coastline evolution, through dating geomorphic features, relic cliff faces and the remnants of past mass movement events. While there are few studies which currently employ the technique in this manner, those which have highlight that the implementation of cosmogenic nuclides allows for increased understanding, making it a viable technique to capture rocky coastline evolution over a longer timescale.

1.3.1.4. Aerial imagery, LiDAR and Photogrammetry

It is relatively recently that unmanned aerial vehicles (UAVs), such as drones, and Structure-from-Motion (SfM) photogrammetry algorithms have been applied in coastal evolution research (Smith et al., 2016). The increased application of UAV and SfM is often related to the method's ease, low cost, rapid application and reproducibility over different temporal and spatial scales (Clark, 2017; Micheletti et al., 2015; Westoby et al., 2012). These advantages have seen UAV and SfM replace more traditional and expensive survey methods, such as light detection and ranging methods (LiDAR) (Rohling et al., 2008). However, due to the adolescence of combined UAV-SfM techniques in geography, the Earth sciences and rocky coastal research, many published applications are often proof-of-concept studies (Barlow et al, 2017; Smith et al., 2016). However, studies have begun to measure specific coastal evolution. For example Barlow et al (2017), use UAV-SfM to perform close-range digital photogrammetry on the chalk cliffs of Telscombe (UK). The use of UAV-SfM highlighted that the structural

geology of Telscombe's coastline is the primary control of slope failure and evolution (Barlow et al., 2017).

UAVs initially started to have significant applications in research focused on dynamic coastal environments, such as beaches and dunes. An example of this is seen in research conducted by Long et al (2016) in a lagoon inlet in the Bay of Biscay (France). UAVs used within this study were able to capture high resolution images and orthomosaics (between 4.6 cm and 2 cm), via a non-intrusive aerial survey, which captures inter-tidal and supra-tidal topography over a large geographical area (Long et al., 2016). The study also demonstrates the reproducibility of UAV data collection, conducting three campaigns over a three month time period, allowing the authors to create a high resolution time series of digital surface models (DSM) and orthomosaics (Long et al., 2016). Long et al (2016) concluded that the use of UAV allowed new perspectives and understandings of dynamic coastal environments, on large and small scales. High resolution measurements offer new perspectives and opportunities to understand fluxes of sand in lagoon systems, allowing for better parametrisation of features and processes in process-based models (Clark, 2017; Long et al., 2016).

Rapid increases in the applicability of UAV techniques within dynamic coastal environments, has seen routine surveys reduce in novelty, with many publications outlining the way these environments evolve over certain timescales (Barlow et al., 2017; Dewez et al., 2016; Turner et al., 2016) For example, QuestUAV (2017) are used in the UK to monitor stretches of coastline, which are potentially dangerous, inaccessible and rapidly eroding. As well as this, it demonstrates the ability for rapid data collection to occur after storms or major coastline alterations (Klemas, 2015; QuestUAV, 2017; Whitehead and

Hugenholtz, 2014). Frequent monitoring of the Northumberland coastline (UK), an Area of Outstanding Natural Beauty, is an example of QuestUAVs work. QuestUAV obtained annually collected 2.9 cm resolution images and orthomosaics of this coastline since 2008, as well as after significant storm and flooding events of 2013 and 2017 (QuestUAV, 2017). Time-series images and orthomosaics collected from the UAV show the impact of the 2017 floods, which alter the frontline of the dunes by 1-2 m, and eroded around 850 tonnes of dune foot along an 80 m stretch of the Northumberland coastline (QuestUAV, 2017). Additionally, predictions can also be made from QuestUAV interpretation of UAV images and orthophotos, such as the visible retreat of the high water mark by 2.2 m which is expected to trigger slumps and the erosion of the cliff toe by around 300 tonnes a year (QuestUAV, 2017).

Recent research has highlighted SfM algorithms and techniques as a powerful tool to process images acquired by UAVs (Mancini et al., 2013). The combination of UAV-SfM has been applied in coastal environments, such as the monitoring of topographical changes in beaches, dunes or coastal zoning (Smith et al., 2016). Furthermore, UAV-SfM reduces the time needed for data collection by around 80%, when compared to similar LiDAR surveys, allowing for rapid monitoring to measure such distinctive behaviour of the coastline (James and Robson, 2012). Casella et al (2016) used UAV-SfM to monitor beach topography and changes in the Ligurian Sea (northwest Mediterranean), utilising the ease and reproducibility of the technique. Regular monitoring of the area provides new insights and understanding into human and natural processes that alter the beaches topography on different temporal and spatial scales (Casella et al., 2016). Similar to monitoring by QuestUAV (2017), the regular monitoring of the beaches coincided with two significant storm events, throughout the winter months of 2013

and 2014 (Casella et al., 2016). The use of UAV-SfM by Casella et al (2016) identified that easterly and north easterly waves resulted in a coastline retreat of around 7 m in some areas, whereas waves propagating from the southeast resulted in deposition and advancement of the coastline by 5 m in some areas.

Furthermore, UAV-SfM has been shown to create higher resolution 3D topographical models and DSMs of beach dune systems, than when compared to other techniques (e.g. LiDAR), through the collection and creation of images, orthomosaics and point cloud data sets (Mancini et al., 2013). This allows for large portions of the coast to be monitored (up to km in length), at a cm resolution (Mancini et al., 2013).

The high-resolution of UAV-SfM can be used to identify coastline and new beach characteristics and geomorphologies. Papakonstantinou et al (2016) used UAV-SfM (with a small commercial camera), to identify coastal zones of a sandy and a rubble beach, creating DSMs, orthophotos and orthomosaics with a resolution of a few centimetres. Due to the accurate and confident visualisations of both beaches, several traces that represent previous sea-levels were identified on the sandy beach, as well as erosion crests, berm zones and sand dunes on both beaches (Papakonstantinou et al., 2016). Similar to research by Long et al (2016), this allows us to further understand coastal environments on a variety of spatial and temporal scales, as well as on a number of different platforms and morphologies (Gienko and Terry, 2014).

SfM has also been used in combination with other image collecting techniques, such as multi-view measurements (MVM) with a digital camera (Gienko and Terry, 2014; Klemas, 2015; Smith et al., 2016). Gienko and Terry (2014), applied SfM in combination with MVM, to individual coarse and clastic coastal boulders

as an alternative to traditional in-field techniques to measure boulder volume. MVMs were taken around the boulder, being processed and assessed on site (if required) by the researcher to give rapid results and clarification of the images suitability for further analysis (Gienko and Terry, 2014). MVMs were formulated into a point-cloud data set, then transitioned into a 3D model with the use of SfM and feature-detection algorithms, creating precise, measurable and textured models. Gienko and Terry (2014) concluded that the use of SfM to create 3D models of coastal boulders has certain advantages over traditional techniques, which do not utilise image based measurement methods and are more complex to use within the coastal environment.

What is evident from the literature is the advantages that UAV-SfM data collection techniques have in the study of physical geography and earth sciences. However, the majority of research that utilises these advantages within coastal environments is focused on more dynamic landforms and topographies, which change drastically over small timescales (e.g. beaches and dune systems). There is little research that currently applies UAV-SfM techniques on rocky coastlines. UAV-SfM can be used to identify key geomorphic features along rocky coastlines and can be used to conduct a high resolution morphometric analysis of these features. The use of UAV-SfM has advantages over more traditional and existing methodologies, such as manual in-field measurements, to understand coastal evolution over time.

1.4. Sea-level change

1.4.1. Eustatic and steric sea-level changes

Sea-level changes occur on multiple spatial and temporal scales, and are caused by a variety of Earth system processes (Cloetingh and Haq, 2015). Sea-level change is directly related to variations in continental ice volume (e.g. ice sheets, ice caps and glaciers). During colder periods, continental ice expands and sea-level lowers (Rovere et al., 2016b). These changes are counterbalanced by equivalent variations in global ocean mass and land-based ice mass during warmer climatic conditions, where both factors are a consequence of the principle of mass conservation (Meier et al., 2007).

These changes in the ocean's mass are due to changes in the mass of continental ice are described by the term "eustasy", coined by Edward Suess in 1888 (Rovere et al., 2016b; Suess, 1904). Eustasy implies that the solid earth is rigid and non-deformable, with local gravitational effects being neglected (Spada and Stocchi, 2007). At shorter timescales, a lot of eustatic sea-level changes are a direct result of coupled ocean-atmospheric processes (Rovere et al., 2016b). Small perturbations to variables, such as CO_2 concentration in the atmospheric and sea surface temperature or isolation, result in ice volume changes (Davidson-Arnott, 2010). However, eustatic sea-level rise is not uniform across the globe, varying significantly as a result of a series of other variables, which are discussed below (Fairbanks, 1989).

Sea-level changes can also occur as a result of steric effects, including thermosteric (changes in ocean temperature) and halosteric (changes in ocean salinity) (Hu and Bates, 2018). Melting continental ice not only results in eustatic changes, but also causes ocean freshening (Antonov et al., 2002). Fresh water

influx decreases ocean salinity, which in turn decreases ocean density and increases its volume (Antonov et al., 2002). Work by Munk (2003) highlight that halosteric sea-level change can contribute 0.05 ± 0.02 mm a year to eustatic sea-level changes, agreeing with other research which categorises halosteric contributions as minimal (Antonov et al., 2002). Thermal expansion, or thermosteric affect, of the ocean also contributes to rising sea-levels. Thermosteric affects also alters the oceans volume, as a result of density decrease followed by the addition of heat into the ocean (Antonov et al., 2005; Hu and Bates, 2018). Warming of the oceans can be attributed to global climate change, which can have natural or anthropogenic drivers (Steele and Ermold, 2007). Antonov et al (2005) notes that thermal expansion of the oceans contributes a larger proportion to sea-level rise, contributing around 0.33 mm per year.

However, many studies highlight that these steric affects are highly localised in nature, with temperature and salinity changes not being geographically uniform (Antonov et al., 2005; Ishii et al., 2006). This is seen within Japan, where thermostatic sea-level changes have significantly impacted sea-level rise between 1969 and 2003, to an extent where it eliminated the impact of crustal movements (Ishii et al., 2006). As a result, steric affects are seen to have a more profound impact on localised relative sea-levels, rather than the global ocean scale.

1.4.2. Relative sea-level changes

Relative Sea-Level (RSL) refers to changes in the land reference base, rather than the ocean volume itself through eustatic changes (Rovere et al., 2016b). Changes in RSL can be induced by land based ice-melt, as well as changes

which stem from the mean land surface (geoid), as a result of uplift (e.g. tectonics) or natural and anthropogenic subsidence (e.g. groundwater drainage) (Church et al., 2010). RSL changes occur at regional and local scales, unlike eustatic sea-level, which refer to global scale change (Rovere et al., 2016b).

1.4.2.1. Glacial-isostatic adjustment

Most RSL changes, resulting from changes in land-ice mass, are governed by a process called glacial- and hydrostatic adjustments, also referred to as glacial-isostatic adjustment (GIA) (Massey et al., 2008; Murray-Wallace and Woodroffe, 2014; Toscano et al., 2011). GIA is a continual viscoelastic response of the Earth to former changes in ice mass, in accordance with ice sheet and glacier fluctuations throughout glacial and interglacial cycles (Kopp et al., 2015). During glacial cycles, ice loading results in the deformation of the land below, migrating the mantle material to intermediate areas in adjacent regions, in turn uplifting them (Kopp et al., 2015; Rovere et al., 2016b). The uplift of land contributes to the fall in RSL during glacial periods, alongside additional climatic variables (Church et al., 2010). During interglacial periods and the unloading of ice, the mantle flows back to the glaciated area as a result of the collapsing forebulge, leading to RSL fall at glacial margins and RSL rise at far-field locations (Figure 1.5) (Rovere et al., 2016b).

The proximity of a location to formerly glaciated areas determines the rate of GIA and RSL change seen at particular locations (Church et al., 2010). Areas located within intermediate areas and former glaciated high latitudes experience greater rates of RSL rise, than those considered far field (Khan et al., 2015). There are few high latitude coastal areas which experience RSL fall, as a result of GIA, such as vast areas of Scotland (UK) (Rovere et al., 2016b). An example of such

isostatic change due to GIA can be seen at the UK scale, where Shennan et al (2009) identifies clusters of subsiding and uplifting areas (Figure 1.6). However, examples are seen across the world, such as RSL fall (1 cm/year) and isostatic uplift in Hudson Bay (Canada), which are occurring due to its proximity to the former Laurentide ice sheet. In contrast, RSL rise and isostatic subsidence is occurring along the east and west coast of the USA (1-3 mm/year), due to its intermediate distance from the ice sheets maximum thickness (Kopp et al., 2015).

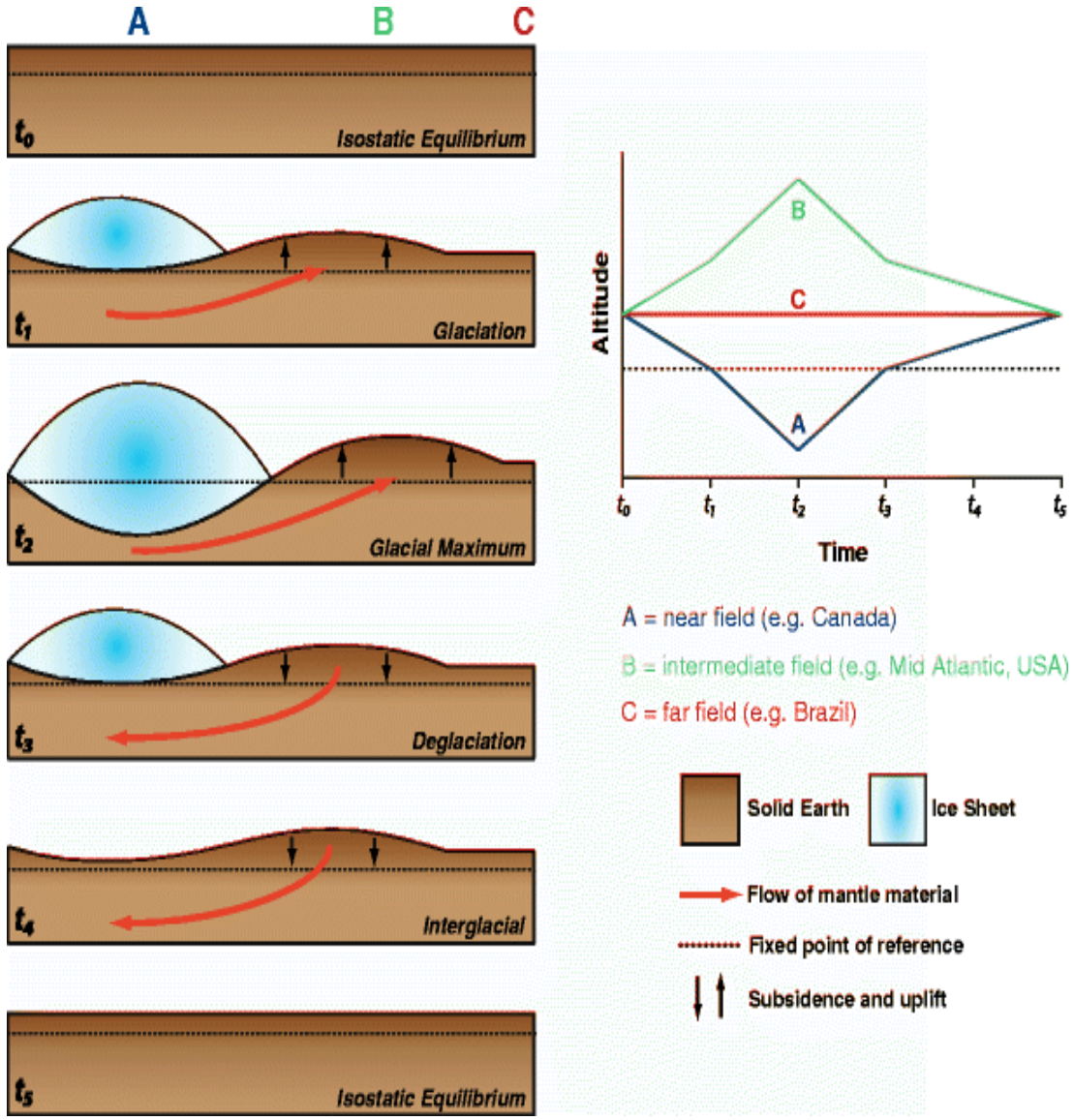

Figure 1.5: *Schematic representation of GIA, taken from Khan et al (2015). The creation and collapse of the forebulge is depicted. The influence of the geological proximity to the ice sheet is also shown, presenting a visual on isostatic influence in RSL heights.*

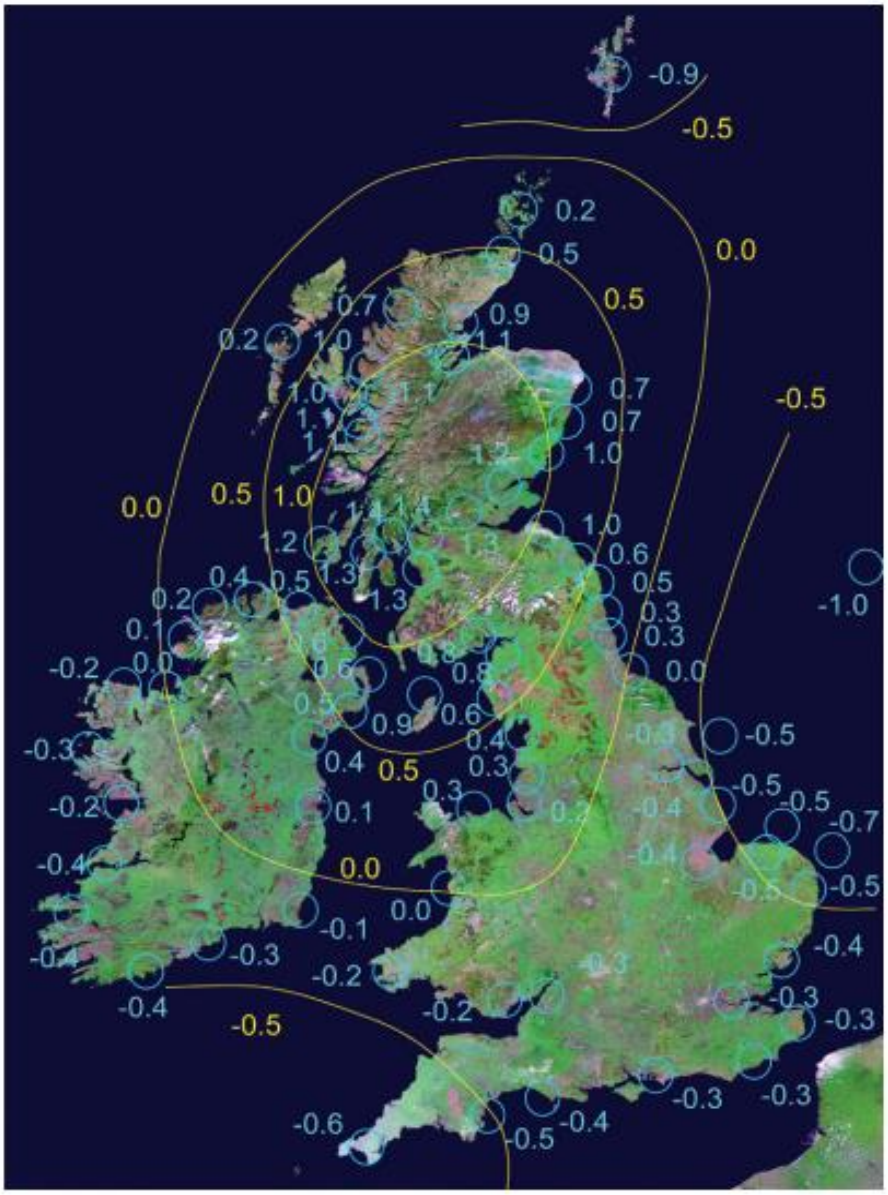

Figure 1.6: *Figure from Shennan et al (2009), identifying areas of isostatic uplift and subsidence around the UK, measured in mm/yr$^{-1.}$ The centre of relative uplift is located over central Scotland (Shennan et al., 2009).*

1.4.3. Palaeo sea-levels

Significant changes in both eustatic and RSL occurred around the world, during the transition between glacial and interglacial cycles which have preceded the present day. These changes are presented in palaeo sea-level indicators, located along the world's coastline. These indicators identify that sea-level changes are characterised by strong regional variability (Andrews et al., 1970; Daly, 1915;

Stocchi et al., 2018). Examples of this can be seen from fossilized corals in the Caribbean which show a RSL rise, from the Last Glacial Maximum (LGM) to present day, which is in line with the hypothetical eustatic trends (Fairbanks, 1989). However, ice proximal or even formerly glaciated areas show a large RSL drop, larger than the so-called eustatic (Andrews et al., 1970; Pedoja et al., 2014; Tushingham and Peltier, 1991).

Palaeo sea-level indicators show that the solid Earth is not rigid, but deformable, behaving like a highly viscous body under ice and ocean load variations (Andrews et al., 1970; Toscano et al., 2011). Accordingly, these palaeo sea-level indicators (e.g. geological, geomorphological or archaeological) do measure the RSL changes (Ávila et al., 2015; Hatrushi, 2017; Rovere et al., 2016a).

1.4.3.1. Marine isotope stages (MIS)

Over the Earth's geological timescale, sea-level has fluctuated significantly, as a result of cyclic and orbital changes triggering significant climatic changes, often referred to as Milankovitch cycles (Crowley et al., 2015; Short et al., 1991). Such climatic changes alternate between the growth and expansion of ice masses during colder glacial periods, followed rapidly by deglaciations and post-glacial rebounding in warmer interglacials. These climatic changes are subdivided into a series of MIS, pioneered and developed by Cesare Emiliani during the 1950's, who refined oxygen isotope data to determine palaeotemperatures and delineate the MIS stages (Berger, 2002; Emiliani, 1955). There are 104 MIS stages, which have been identified and collated across several research projects, beginning 2.6 million years ago, yet the most researched MIS stages extend back to MIS 21 (Figure 1.7) (Lisiecki and Raymo, 2005).

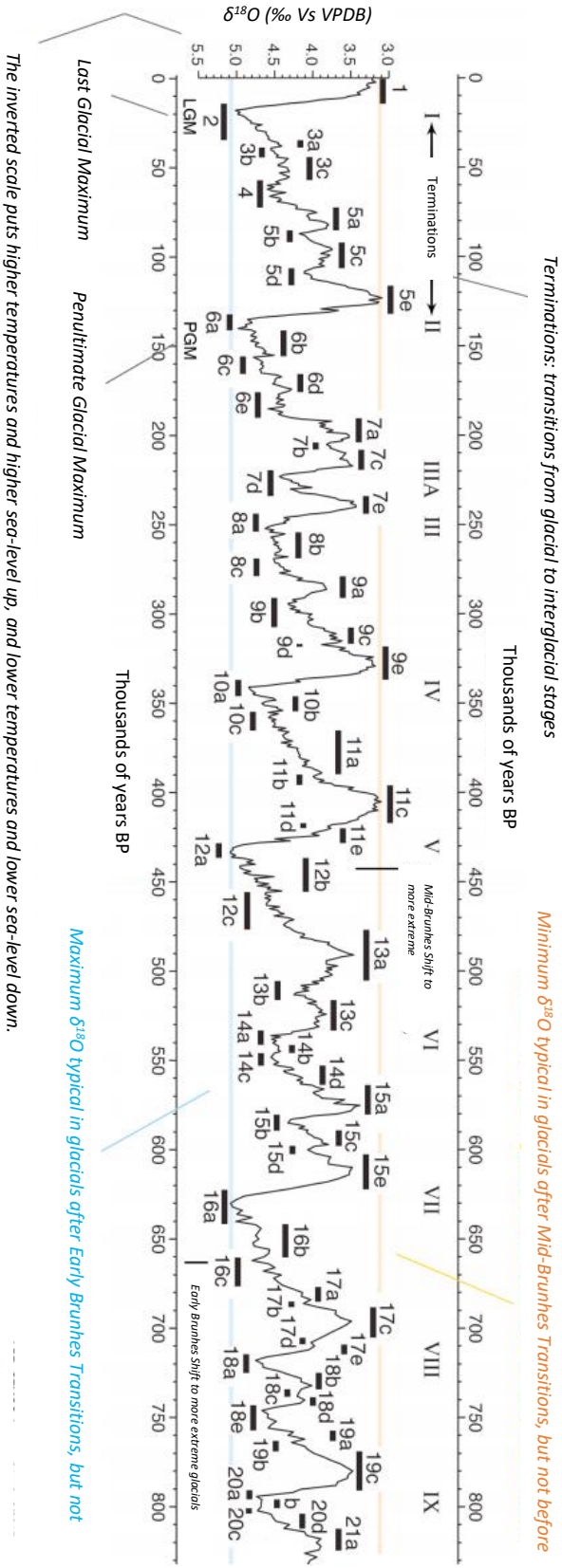

Figure1.7: *This figure is adapted from Railsback et al (2015). It shows climate perturbations, which are categorised from MIS 1 to MIS 21. $\delta^{18}O$ is a proxy for temperature.*

MIS 5e is one of the most studied periods of this period of the Earth's history, and is commonly referred to as the Eemian or Ipswichian, dating between 125 ka BP and 118 ka BP (Medley et al., 2006; Rovere et al., 2016b; Stocchi et al., 2018) MIS 5e is one of five sub-divisions, usually applied to the MIS 5 (Table 1.3) (Shackleton et al., 2003). MIS 5e was characterized by surface temperatures at least 2 ºC warmer than present on a global scale (Abad et al., 2013; Rohling et al., 2008). As a result of elevated temperatures, deglaciation of the Laurentide and Fennoscandian ice sheets and significant shrinking of the Antarctic and Greenland ice sheets resulted in eustatic sea-level rise several meters above the present sea-level (Abad et al., 2013; Antonioli et al., 2018; Galili et al., 2007; Hearty et al., 2007; Hearty and Tormey, 2017; Polyak et al., 2018; Rohling et al., 2008; Rovere et al., 2016b). MIS 5e is often seen as an analogue for understanding the present interglacial (Holocene), assisting in our understanding and projections of future scenarios (Hearty and Tormey, 2017). There is an abundance of palaeocoastal features situated along many stable coastlines, which can be measured to improve our understanding and reconstruction of MIS 5e sea-levels (Gill, 1972; Stocchi et al., 2018).

Sub-Division	**Ka BP**	**Climate**
MIS 5a	82	Peak of last interglacial sub-stage
MIS 5b	87	Peak of glacial sub-stage
MIS 5c	96	Peak of last interglacial sub-stage
MIS 5d	118	Peak of glacial stage
MIS 5e	125	Peak of Eemian last interglacial sub-stage (or Ipswichian in Britain)

Table 1.3: *Sub-division of MIS 5, adapted from work done by (Shackleton et al., 2003)*

1.4.4. Palaeo sea-level Indicators

1.4.4.1. Rocky coastline inheritance

Due to sea-level changes and the slow evolution of rocky coastlines, their geomorphology often has a significant amount of palaeocoastal features, and thus inheritance (Swirad et al., 2016). Inheritance refers to the rocky coastal morphology, which has persisted over time from earlier environments and higher sea-level to the present day, and these are often referred to as palaeo sea-level indicators (Bird, 2011; Masselink et al., 2014; Sunamura, 1992; Trenhaile et al., 1999). Palaeo sea-level records and consideration of inheritance suggest that present day marine processes are likely to be modifying shore platforms and cliffs that were formed during Pleistocene interglacials, where sea-level was higher than present day (Blanco Chao et al., 2003; Trenhaile et al., 1999). However, inheritance is difficult to quantify within many rocky coastal areas, due to the lack or removability of datable sediments, as discussed by Trenhaile et al (1999). Mathematical models have been used to determine the degree of inheritance of shoreline platforms in western Galicia (north-western Spain), concluding that most platforms along this coastline contain significant inheritance from one or more interglacial stages (Blanco Chao et al., 2003; Trenhaile et al., 1999). However, without specific dates attributed to features alongside the shore platform, or the platform itself, it is difficult to run realistic models (section 1.4.2).

To fully understand the timescales and process which contribute to the evolution of rocky coastlines, palaeo sea-level indicators must be analysed to establish a chronology and to quantify rocky coastline evolution throughout time. This can be done through a variety of methods, the choice of which is dependent on the study area.

1.4.4.2. Measurement of palaeo sea-level indicators

Palaeo sea-level indicators can be categorized into three distinctive categories: depositional, biological and geomorphological, identifying the height of palaeo sea-levels (Table 1.4). The best preserved MIS 5e sea-level indicators are situated along stable coastlines, where uplift and GIA are minimal, with palaeo sea-level indicators depicting the near 'true height' of the past sea-level with which they are associated (Galili et al., 2007; Hearty et al., 2007). It is vital to understand the height of the MIS 5e sea-level. While it isn't a direct analogue of future sea-level scenarios, the high concentration of palaeo sea-level indicators, and its accessibility in the most recent geological history, allows us to understand the possible future changes to the coastal environment under a warmer world (Hearty and Tormey, 2017; Kopp et al., 2009; Rohling et al., 2008).

Study Location	Palaeocoastal sea-level Indicator	Methodology	Measured SL Height of MIS 5e	Reference
Mediterranean	Depositional indicators: Cemented beach and shallow marine deposits Biological indicators: benthic organism fossils on hard substrates. Geomorphological indicators: fossil shore platforms and tidal notches.	Measured and assessed the elevations from 11 "stable" sites throughout the Mediterranean. Followed Rovere et al (2016a) to calculate palaeo sea-level. Solved the Sea Level Equation (Section 2.3) through the SELEN model. The sea-level model	MIS 5e RSL highstand range of 2 m to 10 m above present sea-level	(Stocchi et al., 2018)

		ANICE-SELEN coupled ice-sheet – sea-level model to account for the GIA induced sea-level.		
Island of Mallorca, Western Mediterranean Sea	Depositional: Phreatic overgrowths on speleothems (POS) – pieces/powder of calcium carbonate encrustations at the brackish water level (equivalent to sea-level).	Careful collection and sampling of 4 samples for U-series analysis. Stratigraphic progression of sampling to determine a growth rate of the speleothem, to represent SL stability over the POS growth. Based off present-day POS forming at present sea-level GIA compensated by sea-level and corrected using Dendy et al (2017).	RSL highstand showed stability between 1.4 m 2.1 m above mean present sea-level RSL peak between >126.6 c 0.4 ka BP and <123.6 ± 0.5 ka BP. RSL highstand ended ~116.0 ± 0.8 ka BP	(Polyak et al., 2018)
Central Mediterranean Sea	Geomorphological: Fossil tidal notches (FTN) and present tidal notches (PTN).	Dating of the FTN obtained through correlating them with biologic material dated via radiometric analyzed/fossiliferous content. Measurements of 80 study sites –	MIS 5e notches range between 2.09 m and 12.48 m (mean 5.7 m) – these are reflective of the RSL during MIS	(Antonioli et al., 2018)

		measured with different tools (GPS/RTK, levelling surveys, total station, telescopic rod, tape and digital altimeter) - estimated vertical errors range from ± 1 cm to 5 cm. SLE solved using SELEN (includes GIA feedbacks). ANICE-SELEN coupled ice-sheet – sea-level model to account for the GIA induced sea-level.	5e, and its max height GIA for the area ~1 m to 2.5 m.	
Bahamas and Bermuda	Depositional: Carbonate-sediment dominated platforms. Geomorphology/biological: Tectonically elevated reef terraces and megaboulders.	U/Th dating of fossil coral reefs. AAR dating of coral reefs. Stratigraphic analysis of features/data.	RSL stood 2 m to 3 m above present for several thousand years during MIS 5e. Later MIS 5e sea-level rose abruptly to 6 – 9 m RSL. Megaboulders provide evidence of large wave events in last MIS 5e	(Hearty et al., 2007)

Egyptian coast, northern Red Sea	Depositional: Sediment cores Biological: Fossil coral reefs.	$\delta^{18}O$ records taken from the two collected cores – 0.5-2 cm resolution throughout the MIS 5 stage. $\delta^{18}O$ from planktonic foraminifera from the central Red Sea. $\delta^{18}O$ converted into sea-level estimates Compared to coral data to cross-refence results.	RSL of MIS 5e is a long-term mean of up to 6 m higher than present mean sea-level (in agreement with coral data). RSL peaked twice, once = 5 m and another = 9 m above present sea-level.	(Rohling et al., 2008)
Carmel coastal plain, northern Israel	Depositional/Geomorphology: beachrock (dated to 125 ka BP).	Lithology and chronostratigraphic analysis. Presence of the index fossil Lentigo latus. Th/U, AAR and RTL dating Flint artifacts.	Peak RSL of MIS 5e highstand was ~ 5 m to 10m above present sea-level.	(Galili et al., 2007)
Strait of Gibraltar, North of Africa	Depositional: Beach deposits/speleothems/ marine samples. Geomorphology: Cliff/cliff notch/shore platform. Biological: Bioerosive structures in Mesozoic limestones/boulders/ cobbles.	Logging of feature details for palaeoenvironmental interpretation. Measured topographic elevations of geomorphic markers and deposits with a	RSL height of + 10 m above present sea-level can be inferred for MIS 5e.	(Abad et al., 2013)

		high-resolution altimeter. U-series dating of speleothems and marine samples.		
Coastline of Italy, Mediterranean	Depositional: Beach/lagoon deposits and backshore/foreshore deposits. Geomorphological: inner margin of marine terrace, marine terrace and tidal notch. Biological: top of lithophaga hole band and Dendropoma reef.	Review and update of the MIS 5e markers. Number of field observations of the highstand markers Elevations and presence of several indicators are taken, representing palaeo sea-level. Burrows of specific species (eg. The pelecypod Lithophaga lithophaga) is a reliable marker of sea-level.	This study was used to look at the uplift of the area (tectonic implications), rather than the height of the RSL.	(Ferranti et al., 2006)
Abrolhos islands, west Australia	Biological: Fossil coral core from the Turtle Bay.	U-series measured by thermal ionization mass spectronomy of fossil corals throughout the core Stated to be a "moderately reliable" method to obtain ages.	RSL reached a height of ~ 3.3 m above present sea-level, at the start of MIS 5e. Sea-level dropped below its current	(Eisenhauer et al., 1996)

			position ~ 116 ka BP.	
Pacific Coast, North America	Geomorphology: Marine terraces Biology: corals.	Dated 10 terrace sequences from south Oregon to south Baja California Sur, using U-series techniques and alpha spectronomy.	Evidence that RSL was around = 6 m above the present sea-level.	(Muhs et al., 1994)

Table1.4: Collection of research, focused on identifying and dating palaeocoastal features around the world to MIS 5.

The listed studies above (Table 1.4) are just a few of the individual case studies of sea-level during MIS 5e. There are over 980 palaeoshoreline sequences around the world that can be associated with the last interglacial (Pedoja et al., 2014, 2011; Rovere et al., 2016b). MIS 5e indicators tend to be clustered around certain areas of the world's coastline, such as the Mediterranean and southwest England (Rovere et al., 2016a). Individual studies can be collated together to determine a global sea-level for the MIS 5e (Kopp et al., 2009). Frequently cited work by Kopp et al (2009) provides an extensive compilation of local sea-level indicators, as well as extensive statistical analysis to determine likely sea-level during the MIS 5e. From the study, the following was determined for a global sea-level rise: 95% probability that MIS 5e sea-level reached a peak of at least 6.6m higher than present mean sea-level; 67% probability that sea-level exceeded 8.0m; 33% probability that the sea-level exceeded 9.4m (Kopp et al., 2009).

Collating a series of localized studies has several issues, such as the variation in palaeo sea-level indicator descriptions and the use of different datum references

(not always mentioned in the studies) (Rovere et al., 2016a, 2016b). The lack of high-resolution studies prior to 2010 also results in uncertainty when determining a global sea-level for the MIS 5e. This can result in systematic errors (Pedoja et al., 2014, 2011), or the selection of specific studies where detailed measurement errors are included (Kopp et al., 2009). These factors must be considered in the application of certain methodologies, as well as the comparison of this research alongside previously published literature.

1.5. Study Site: North Torbay

The UK has an array of lithology types which can be dated to almost every geological time period. The coastline of the UK mimics this variety, showing significant geological changes over small spatial scales (BGS, 2017). The changes within coastline lithologies can be classified as weak and sedimentary or rocky and resistant bedrock (BGS, 2017). This underlying geology of the UK coastline is what governs the coastal topography, producing a series of inlets and bays in the more susceptible materials, and headlands in the erosion-resistant lithologies (May and Hansom, 2003). The southwest of England is home to many palaeo sea-level indicators, as a result of resistant lithologies which are interspersed around its coastline, such as Torbay.

1.5.1. Torbay, Devon

Torbay is an almost perfect example of rocky coastlines within the UK, consisting of resistant Devonian shale and limestone lithologies, as well as a series of plunging cliffs and shoreline platforms. Torbay is located on the southwest peninsula of England, and is a good example of the numerous crescent bays that are located along the UK's coastline (Figure 1.10). Torbay is a significant socioeconomic and cultural asset to Devon and the southwest. Torbay consists

of three towns: Torquay, Paignton and Brixham, and is commonly referred to as “The English Riviera”. It is a highly valued UNESCO Global Geopark due to its complex Devonian geology, overlain by some of the oldest Permian “Red-Beds” (Figure 1.8 and Figure 1.9). These red beds are variegated sequences of detrital sedimentary rocks, which have distinctive reddish-brown ferric oxide pigments dispersed throughout the matrix. The differences in resistance between the Devonian and Permian sediments can be seen in Figure 1.8, a photograph of the defensive sea wall at Star Bay (Torbay), which was constructed with both of these sediments. The geological contrast between these two lithologies is thought to be the reason for the distinctive bay of Torbay and the protruding headlands, due to the coastal retreat of softer sediments located between the resistant headlands of Hopes Nose and Berry Head (Page, 2004) (Figure 1.9 and 1.10)

Figure 1.8: *Photograph of the sea-wall at Star Bay (Torbay), highlighting the difference in characteristics and lithology between the Devonian limestone and Permian red-beds. (Authors photograph).*

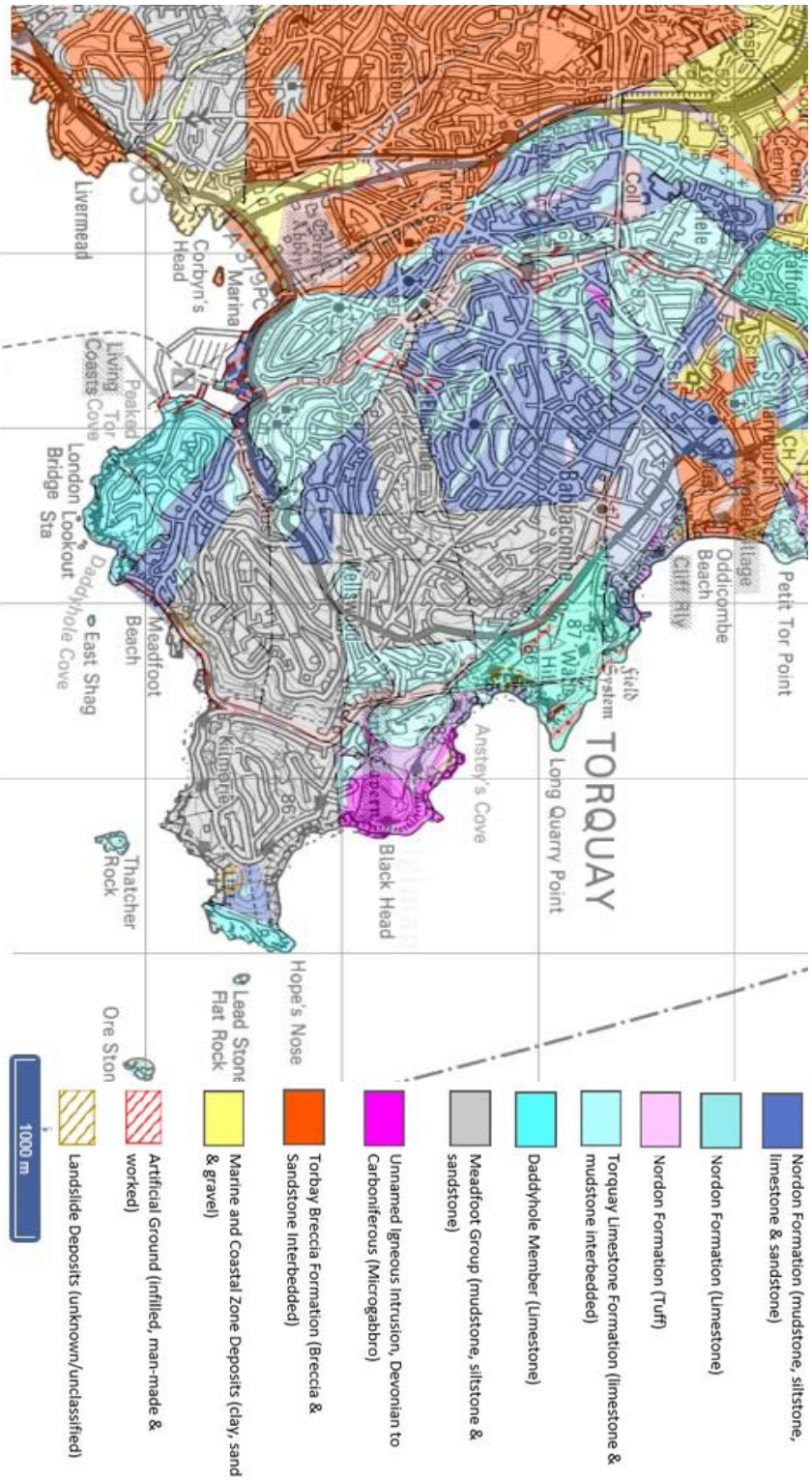

Figure 1.9: Geology map of the north Torbay area, with particular interest in the Devonian geology of the northern peninsular, as well as the Permian “red beds” situated directly below it (Digimap, 2019).

Torbay is a macrotidal coastline and has a maximum tidal range of 4-5 m during spring tides and around 1.7 m during neap tides (SCOPAC, 2012). Between 2008 and 2012 the prevailing wind and wave direction at Torbay was recorded to derive from east-south-east (SCOPAC, 2012). It has been reported that the mean significant wave height at Torbay is between 2.5 and 3 m (Harwood, 1983). However, data obtained from the Plymouth Coastal Observatory highlights that the average wave height is below this, yet the range of wave height varies significantly on both an annually and monthly basis (Table 1.5) (PCO, 2018).

	1st January 2018 – 31st December 2018	1st June 2019 – 30th June 2019
Average wave height (m)	0.76	0.64
Minimum wave height (m)	0.08	0.09
Maximum wave height (m)	9	4.73

Table 1.5*: Wave height data obtained from wave buoys situated in the bay of Torbay.*

Previous measurements of RSL change within the southwest have considerable variation, for example Holocene sea-level rates vary from 0.8 – 1.6 mm/year (Gehrels et al., 2011). Research conducted specifically along the south Devon coastline by Massey et al (2008) suggests that RSL has risen by 21±4 m over the last 9000 years, where around 8±1 m of this has occurred during the last 7000 years. However, there is minimal research which successfully quantifies the rate of RSL changes over the last interglacial cycle in Devon, despite the vast array of elevated palaeocoastal features within the region. Some studies draw conclusions on MIS 5e sea-levels based upon existing palaeocoastal features, such as Hart and Gosling (2018) and Mottershead (1987). Both of

these studies concluded that previous RSL heights reached between 6 and 8 m above present. However, this data is purely observational and fails to model the entirety of RSL change over the last interglacial, MIS 5e. Consequently, many studies which focus on raised morphological features rely on larger UK scale or global average modelled RSL measurements, such as Hearty et al (2007). This is problematic due to the significant variability in RSL related to tides, GIA and other local variables (Devoy, 1982).

1.5.2. North Torbay coastline

This research focuses on the northern peninsula of Torbay. Figure 1.10 outlines the selected study sites, which are located along the coast and tip of the peninsula. Site specific details are outlined in the section below. Furthermore, photographs taken from the study sites can be seen in Appendix 1.

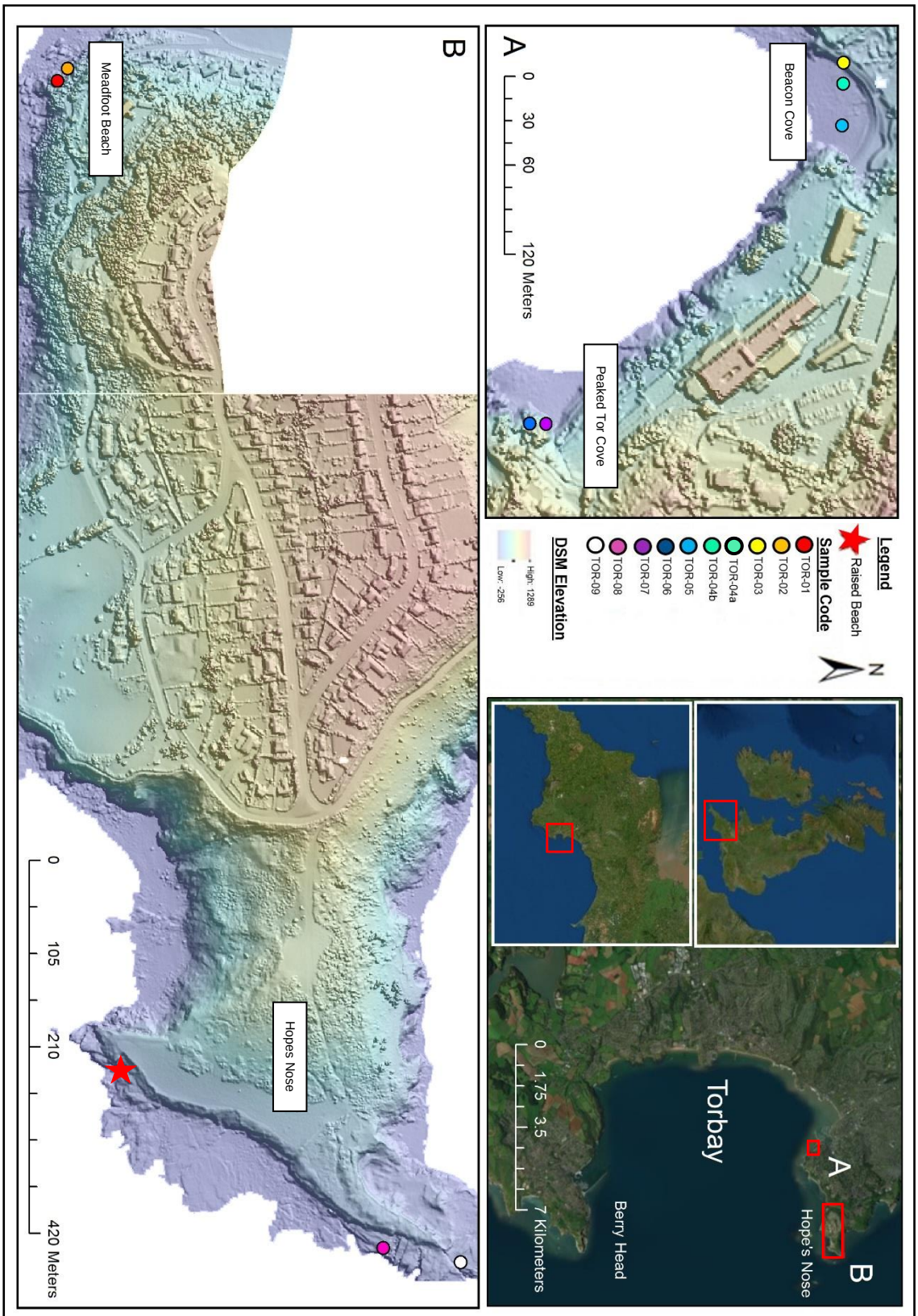

Figure 1.10: *Site map of the North Torbay area. The raised beach is depicted, as well as the sampling locations for ^{36}Cl exposure dating. Data sourced from the Plymouth Coastal Observatory 2016/17 LiDAR (PCO, 2018).*

1.5.2.1. Meadfoot Beach (Figure 1.10B)

Meadfoot beach is a shingle beach situated along an open coastline, with sediments that are considered part of the Lower Devonian Meadfoot Group (Leveridge and Shail, 2011). These Lower Devonian sediments are particularly visible during low tide, in the form of Devonian slates and sandstones that are likely to come from a fluvial origin (West and Csorvasi, n.d.).

1.5.2.2. Beacon Cove (Figure 1.10A)

Beacon Cove is a small shingle pocket beach, which is situated on a sheltered part of the coastline, being classified as part of the Torquay limestone and Meadfoot Group slate (Goodger et al., 1984). The cove has plunging cliffs, as well as exposed limestone bedrock, which is exposed at low tide.

1.5.2.3. Peaked Tor Cove (Figure 1.10A)

Peaked Tor Cove is a small pebble pocket beach on an open section of the coastline, with high plunging cliffs. The cove is characterised by steep woods of Holm Oak, growing above a Devonian limestone cliff, which has evidence of large folds along an east-west axes (Shannon, 1928). There is evident talus at the foot of the plunging cliffs, which is in direct contact with the sea at high tide. A sign on the plunging cliff is a good example as to the reach and destructive nature of the pebble beach at Peaked Tor Cove (Appendix 1, Figure 6.3C and D).

1.5.3. Hopes Nose (Figure 1.10B)

Hopes Nose is the northern headland of Torbay, which protrudes into the British Channel. The geology of Hopes Nose is internationally unique, as it is made up of geologically renowned Devonian carbonates and clastics, in the form of limestone and shale. Limestone deposits at Hopes Nose are thought to have been formed during the Middle Devonian (Eiefelian) 394-388 million years ago,

in a shallow and tropical sea, at a similar latitude to that of Australia at present day (Page, 2004). The Devonian limestone is characterised as “Daddyhole Member Limestone” (Digimap, 2019).

Hopes Nose also has an array of palaeogeomorphological and Quaternary landforms. The most distinctive is the raised shore platform that is evident around the extent of Hopes Nose. It is estimated that the elevation of the platform is around 8m above sea-level and reaches 12 m above sea-level at its highest point, separating two sharp cliff faces with a gentle slope (Mottershead et al., 1987). The minimal amount of research conducted at Hopes Nose suggests that the shore platform is evidence of palaeo sea-levels during the Quaternary. However, there is no direct quantitative age for the shore platform, yet estimations have associated the shore platform with the last interglacial MIS 5e (Mottershead et al., 1987).

In addition to the shore platform, Hopes Nose has an exposed palaeocoastal raised beach, visible along the southern edge of the headland (Figure 1.10). The raised beach is around 9 m above the current sea level, and up to 12 m thick. The raised beach has been dated using AAR by Davies (1984) (Mottershead et al., 1987), and using unpublished data by Bowen et al (1985). Mottershead et al (1987) argued, that on the basis of a comparison with AAR data from raised beaches nearby on Thatcher’s Rock, the raised beach at Hopes Nose formed during MIS 7, whilst Thatcher’s Rock’s beaches formed in MIS 5e. However, the range of values does not support this conclusion. A/I values for *Patella vulgaris* range from 0.115 ± 0.014 to 0.181 ± 0.004 at Hopes Nose and are 0.118 ± 0.004 at Thatcher’s Rock, indicating overlapping populations. No full calibration of A/I exists for southern England, but a calibration from the east coast of the USA (Wehmiller et al., 2012) shows that the A/I curve is initially steep, thud values for

Hopes Nose are not likely to reflect an interglacial difference in age. Therefore, based on the presence of A/I values of 0.123 in a raised beach under a stalagmite dated to 121 +14/-12 ka BP on nearby Jersey (Keen et al., 1981), it is most likely that both raised beaches formed during the last interglacial period, MIS 5e. However, this still is not a direct measurement of the shore platform itself, with the raised beach simply being used as an indicator of a relative age.

1.5.4. Existing coastal management and protection

Despite the presence of geological and geomorphological Quaternary evidence and documentation, there is no active intervention or protection to the coastline by the governing bodies of Torbay, such as the Environment Agency (EA), Torbay Coast and Countryside Trust and the National Trust. The nearest shoreline management plans are controlled by the EA, and are located around 2.5 miles north of Hopes Nose in Oddicombe and around 1.3 miles to the South, between Daddy Hole Cave and Meadfoot beach (Figure 1.11) (Environment Agency, 2019). Both these areas are under similar management plans, holding the line and maintaining hard-engineering coastal defences.

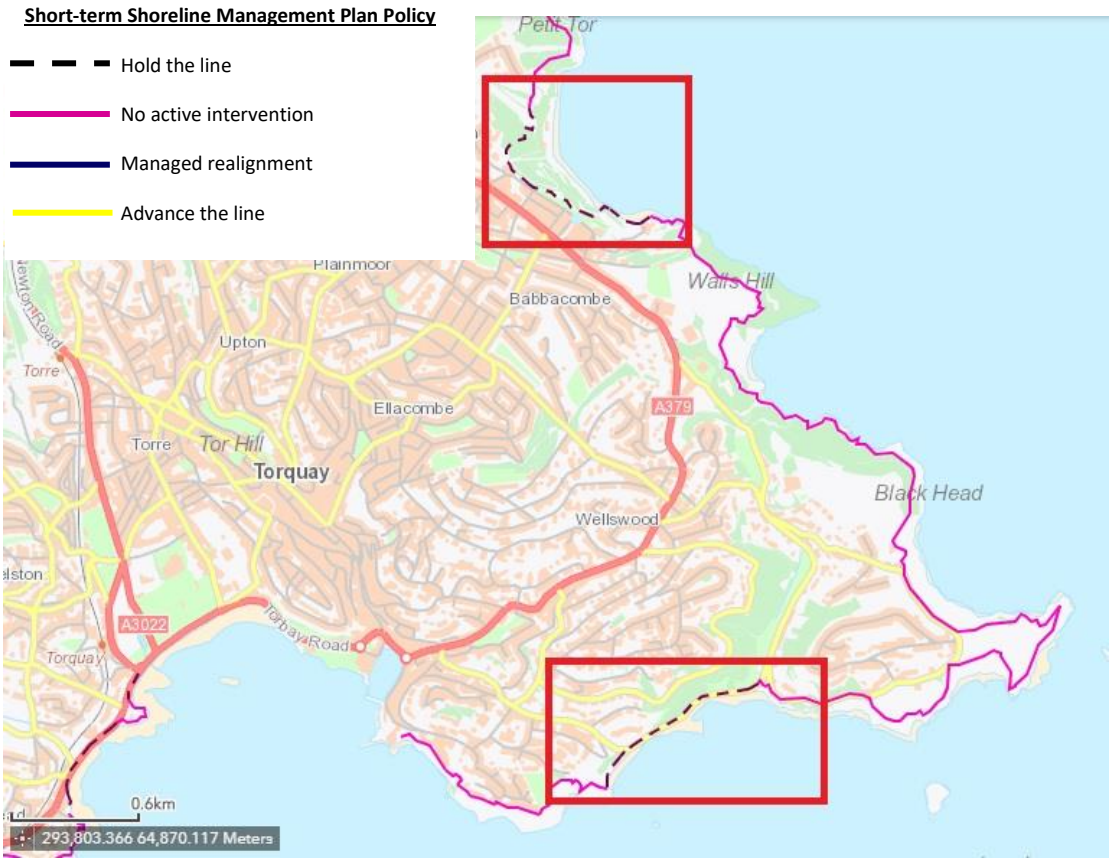

Figure 1.11: *Map outlining the short-term shoreline management plan for north Torbay. The red boxes highlight the "hold the line" policies at Oddicombe and between Daddhole Cave and Meadfoot beach. Modified from the (Environment Agency, 2019).*

These areas are under protection as they are eroding and receding significantly, a consequence of the soft nature of their red bed geology. Significant and dangerous landslides have occurred in the recent years, such as the Oddicombe landslide of 2013. The lack of coastal management around my chosen study sites can be explained by the assumptions of high resistance and therefore slow horizontal cliff retreat and erosion of the coastlines, this assumption is reinforced by the presence of the raised platform which is likely inherited from the Quaternary.

1.6. Study aims and objectives

Within this research I aim to address some research gaps within our current understanding of rocky coastline evolution to date. These research gaps have been outlined and discussed throughout my literature review above. Firstly, I aim to investigate the use of ^{36}Cl to understand the long term evolution of rocky coastlines. As outlined in section 1.3.1.3. exposure dating is a suitable methodology to analyse rocky coastline evolution, which occurs slowly over larger timescales than many modern methodologies available today (e.g. drone surveys). Furthermore, I will also investigate the use of ^{36}Cl exposure dating in the absolute dating of possibly inherited features along these slowly eroding rocky coastlines, in combination with other methodologies to fully understand the complex nature of inherited coastal features (e.g. sea-level modelling). SfM photogrammetry and morphometric analysis of the obtained data will be used to further increase our overall understanding of distinctive morphological characteristics along rocky coastlines, such as shore platforms. This data can be used in combination with those already stated, enabling comparison between varying rocky coastline evolutions, especially over longer time scales. To address the research gaps, I will focus on creating research questions which are specific to north Torbay. By doing this it will not only provide a test in methodological application but provide a pilot dataset for numerical models to direct and anchor models to replicate rocky coastline evolution.

Therefore, the aim of my research is to understand and quantify the evolution of rocky coastlines in north Torbay. This will be done by addressing the following research questions:

- How can ^{36}Cl cosmogenic nuclide exposure dating be used to quantify the rates of change on rocky coastlines and provide a chronology of rocky coastline evolution through mass movements?
- Can ^{36}Cl cosmogenic nuclide exposure dating be used to absolutely date and determine the antiquity of the raised shore platform at Hopes Nose?
- Can the raised shore platform at Hopes Nose be associated with a specific palaeo sea-level, providing evidence of inheritance along North Torbay's coastline?
- How can UAV-SfM photogrammetry contribute to understanding the mechanisms of shore platform evolution in the north Torbay study area, over short and long temporal scales?
- What are the dominant factors which control the erosion, and thus the evolution, of the rocky coast in north Torbay?

The aims of my research will be met through a series of objectives:

- Calculate the ^{36}Cl cosmogenic nuclide exposure ages for samples collected from around north Torbay, from the sites mentioned above.
- Conduct an UAV flight survey to obtain aerial images of Hopes Nose.
- Process aerial images with photogrammetry, specifically SfM algorithms, to create a 3D model of the study area.
- Conduct a morphometric analysis of Hopes Nose from the UAV-SfM photogrammetry data.
- Interpret and combine ^{36}Cl cosmogenic nuclide data and photogrammetry analysis to improve understanding of rocky coastline evolution in north Torbay.

- Produce a RSL curve for north Torbay to compare with cosmogenic exposure ages and UAV-SfM photogrammetry data, to understand sea-level influence on coastal erosion in north Torbay and to test assumptions that the raise platform dates to MIS 5e.

To address the questions outlined above and the build upon research and understanding of the surrounding rocky coastline evolution in north Torbay, I will combine two existing methodologies in a new and unique way. Firstly, ^{36}Cl cosmogenic nuclide exposure dating will be used to quantify a rate of rocky coastline evolution in north Torbay, from exposure ages obtained from the remnants of mass movement events. This will enable me to identify the frequency and magnitude of coastal retreat, as well as identify plausible triggers for significant mass movement events. Similarly, ^{36}Cl cosmogenic nuclide exposure dating will also be used to date the raised shore platform at Hopes Nose, to determine when it was initially carved from the resistant Devonian limestone within the area.

Secondly, UAV-SfM photogrammetry will be used to provide a high resolution data sets for Hopes Nose. A morphometric analysis will be done to extract additional data, to further understand rocky coastline evolution in Torbay, through cliff retreat and shore platform formation. Morphometric data and distinctive geomorphological characteristics will be compared to a site specific RSL curve, created by Dr Palao Stocchi. Throughout my research I will collate relevant research and place my findings into a global context, outlining the importance of localised studies in furthering our understanding of rocky coastline evolution under palaeo and present sea-levels.

A work plan figure can be seen in Appendix 9, which depicts the connections between the methodologies and the way in which each methodology will be used to address my research questions.

CHAPTER 2: METHODOLOGY

2.1. ^{36}Cl Cosmogenic Nuclide Exposure Dating

2.1.1. Background to cosmogenic nuclide exposure dating

Cosmogenic nuclide exposure dating has been used in the direct dating of a variety of geomorphic features and processes (e.g. glacial) (Barrows et al., 2002). Cosmogenic nuclide exposure dating utilises the build-up of rare isotopes within target minerals in rocks at or near the surface. These isotopes accumulate in the rock at a predictable time rate, which allows us to determine the date of first exposure, or rate of exhumation to the surface (e.g. erosion rate) (Darvill, 2013). Cosmogenic nuclide dating is applicable across a wide array of environments, materials and mineralogy, to investigate the exposure, burial, denudation of specific features (Alvarez-Marrón et al., 2008; Darvill, 2013; Dunai, 2010; Ivy-Ochs and Kober, 2008). The most common cosmogenic nuclei used in geomorphological studies are ^{10}Be, ^{26}Al, ^{36}Cl, ^{14}C, ^{3}He and ^{21}Ne. These nuclei have been used to date landforms, broadening our understanding of geomorphological features and processes on timescales expanding hundreds to millions of years (depending on the isotope used) (Darvill, 2013; Dunai, 2010).

Cosmogenic nuclides originate from the constant bombardment of the Earth's surface by cosmic rays. Cosmic rays are generated from supernovas outside of our solar system (Dunai and Lifton, 2014). The rays consist of high energy particles, such as protons (87%), alpha particles (12%) and heavy nuclei (1%), and are termed primary cosmic rays (Darvill, 2013). Rays are deflected by the Earth's magnetic field, with production rates of rays varying with altitude and latitude, between 15-35% (Dunai, 2010).

After passing through the atmosphere cosmic rays become secondary rays, experiencing an exponential energy decrease as they move deeper through the atmosphere (Dunai, 2010). This process is known as attenuation, which varies due to the mass of the atmosphere (130 g cm^{-2} at higher latitudes and 150 g cm^{-2} at the lower latitudes) (Darvill, 2013). When secondary cosmic rays reach the Earth's surface, they attenuate through the rock to a depth determined by the rock density and structure (Dunai and Lifton, 2014). Reactions between the target materials in the rocks (e.g. calcium) and the secondary cosmic rays are responsible for 98% of cosmogenic nuclide production (Dunai, 2010).

One way in which cosmogenic nuclides are formed is spallation. This process occurs in the top 3 m of the rock, where high energy nuclide collide with atomic nuclei and removes protons and neutrons, leaving behind a lighter residual nucleus (Dunai and Lifton, 2014). A second process which can create cosmogenic nuclide, is thermal neutron capture. This occurs when the speed of neutrons from the secondary cosmic rays slow to a point where their energy corresponds with the surrounding temperature (Dunai and Lifton, 2014). This allows the capture of other protons and nuclei, creating a heavier nucleus, which is vital for the production of cosmogenic nuclides in the top 20 cm of the rock surface (Darvill, 2013).

Finally, muonic reactions are another way in which cosmogenic nuclides are produced. Muons area heavy subatomic particles and relative to the electron, contributing to a significant proportion of cosmic radiation that reaches the earth's surface. At depths between 4 and 40 m negative muon capture is the dominant mode of cosmogenic nuclide production (Stone et al., 1998). Below 40 m fast muon induced reactions are the prominent production mechanisms of cosmogenic nuclide production (Gosse and Phillips, 2001). Muons are able to

penetrate to the great depths with attenuation length of 1500g cm^{-2} to 6500g cm^{-2}, significantly greater than neutrons and protons which contribute to spallation and thermal neutron capture (Braucher et al., 2013; Gosse and Phillips, 2001). Furthermore, they have significantly weaker reactions with the target material, allowing for further penetration into the material (Dunai, 2010; B. Heisinger et al., 2002).The weak interactions of muons and target materials are estimated to be around 2.3% of cosmogenic reactions at the surface, yet 100% of reactions beyond 3 m into the Earth's surface, due to the lack of spallation below this depth (Darvill, 2013; Dunai, 2010).

Within this research, ^{36}Cl was the main cosmogenic nuclide measured to calculate exposure ages for the samples collected in north Torbay. ^{36}Cl was used due to the high calcium content of the Devonian limestone and shale bedrock in the area, which is a key target element for the production of ^{36}Cl. Spallation of ^{39}K and ^{40}Ca is the dominant process of cosmogenic nuclide production in calcium rich material, accounting for 80-90% of ^{36}Cl production (Stone et al.,1996). However, later research by Stone et al (1998) highlights that up to 50% of ^{36}Cl production in significantly eroding limestone can be attributed to negative muon capture, due to the re-exposure of muons produced deeper in the rock, and this is often termed inheritance (section 1.5.4.1) (Barrows et al., 2002; Dunai, 2010). Inheritance can influence calculated exposure ages, making them appear older than they actually are, leading to wrongful interpretations or highlighting more complex exposure histories than originally estimated.

Within the coastal environment, topographic shielding of the exposed area, by cliff faces or over hanging rocks, reduces the cosmic ray flux and can influence the cosmic ray exposure and overall age. Topographic shielding is the most common form of shielding, accounted for with a function of height and lateral

extent to ensure accurate exposure ages (Dunai, 2010). Additionally, self-shielding can occur, relating to dips and bumps within a surface and the thickness of the material, yet this is harder to quantify and account for (Dunai, 2010; Dunai and Lifton, 2014). Finally, post-depositional overburden shielding also impacts exposure ages (Darvill, 2013; Dunai, 2010). Seasonal snow, vegetation and sediment cover can reduce cosmic ray flux by around 2-7% (Dunai, 2010). Corrections for shielding can be small at around 5%, but at the base of a vertical cliff the corrections can be around 50% (Hurst et al., 2017). These corrections are vital for reducing some of the uncertainties that surround the determination of exposure ages.

Scaling factors must be established to calculate a representable production rate, with different scaling factors accounting for variations in the production of in-situ nuclide. Production rates vary due to differences in the Earth's geomagnetic field, the cosmogenic nuclide decay, altitude, latitude, shielding, density and sample thickness (Darvill, 2013; Dunai, 2010; Dunne et al., 1999; Ivy-Ochs and Kober, 2008). Scaling factors associate values to these variations, describing the environment in which the sample was collected to establish a more accurate age (Masarik and Wieler, 2003). However, current scaling factors are more suited to a uniform environment, with flat surfaces and specific altitudes and pressures across the Earth's surface (Dunne et al., 1999; Reedy, 2013; Stone, 2000). Recent advances have recognised the bias of production rates towards more horizontal surfaces, and have begun to determine the rate of cosmogenic nuclide production in more complex sample environments (Dunne et al., 1999; Masarik and Wieler, 2003). Once a production rate has been determined, it is assumed that they remain constant, with little variation over time and space. However, it

must be noted that some changes within the earth geomagnetic field can influence and alter production rates by up to 10% (Dunai, 2010; Lifton et al., 2014)

2.1.2. ^{36}Cl Cosmogenic nuclide dating of Torbay's coastline

The application of cosmogenic nuclide exposure dating along North Torbay's coastline was used to model the progressive recession of a cliff face, similar to research on the Cretaceous chalk cliffs in east Sussex (UK), by Hurst et al., (2016). As outlined in section 1.2.2, landslides play a major role in the evolution of cliffed rocky coastlines. Exposure dating is an ideal method for dating deep-seated landslides, as it exposes fresh previously unexposed bedrock below a depth of around 3 m (Ivy-Ochs and Kober, 2008; Mcintosh and Barrows, 2011; Sewell et al., 2006). The episodic and infrequent nature of these collapse events means that newly exposed surface "reset" the exposure dating clock, before enabling cosmogenic nuclides to re-accumulate to detectable levels. However, this only occurs where the cliff retreat is slow, estimated to measure around <3 m per 1000 yrs. Exposure dating therefore provides a suitable method for determining the long-term evolution of slowly eroding rocky coastlines. North Torbay's coastline is predicted to be eroding slowly, due to the presence of palaeocoastal features, such as the raised beach and elevated shore platform.

2.1.2.1. Sample collection and analysis

Four sampling sites were chosen along north Torbay's coastline, as shown in Figure 1.9, and sample details are outlined in Table 2.1 with further context provided in images found in Appendix 1 (Figure 6.1 to 6.5). Samples were taken from both Devonian limestone and shale. Samples that were collected can be categorised into three distinctive settings. First, areas where the cliff face was

evidently exposed by mass movement events, such as rock falls or landslides, were targeted for sampling (Soldati et al., 2018). Three samples were collected from surfaces that were set back at least 3 m from the rest of the cliff face, with distinctive mass movement features such as detachment faces (TOR-01, TOR-02 and TOR-06). Vertical jointing and mass movements has promoted the production of near vertical plunging cliffs at Beacon Cove and Peaked Tor Cove, from these vertical faces TOR-3, TOR-05 and TOR-07 were collected. Samples collected from cliff faces were also taken relatively high up from the base of the cliff, in order to prevent the influence of marine processes and shingle impact. However, there is some severe shielding of cliff face samples, up to 56% of the horizon (Table 2.1), which was calculated using a clinometer and compass and must be considered to calculate an accurate exposure age following Dunne et al (1999). As seen from Figure 2.1, lower horizon correction values identify highly shielded areas to near vertical surfaces, with taller cliffs having a greater degree of shielding across the shore (Dunai, 2010; Hurst et al., 2017). A horizon correction value close to 1 indicates an area which is not shielded, and thus more exposed to the sky and incoming cosmic rays (Dunai, 2010; Hurst et al., 2017).

Sample Code	Sample Site	Lithology	Longitude (W)	Latitude (N)	Elevation (m)	Horizon Correction	Thickness (cm)
TOR-01	Meadfoot Beach	Shale	3˚29'-3.499"	50˚27'50.459"	1	0.8929	4
TOR-02	Meadfoot Beach	Shale/ Quartz Vein	3˚29'-3.499"	50˚27'50.459"	3	0.7704	1.5
TOR-03	Beacon Cove	Limestone	3˚31'-3.524"	50˚27'50.457"	3	0.755	5
TOR-04a	Beacon Cove	Limestone	3˚31'-3.523"	50˚27'50.457"	0.5	0.9649	2
TOR-04b	Beacon Cove	Limestone	3˚31'-3.523"	50˚27'50.457"	0.5	0.9649	4
TOR-05	Beacon Cove	Limestone	3˚31'-3.523"	50˚27'50.457"	1	0.6106	6
TOR-06	Peaked Tor Cove	Limestone	3˚31'-3.520"	50˚27'50.455"	5	0.8759	5
TOR-07	Peaked Tor Cove	Limestone	3˚31'-3.520"	50˚27'50.455"	2	0.5623	2
TOR-08	Hopes Nose	Limestone	3˚28'-3.520"	50˚28'50.463"	8	0.9903	2
TOR-09	Hopes Nose	Limestone	3˚28'-3.481"	50˚28'50.463"	8	0.9990	2

Table 2.1: *Site and sample data*

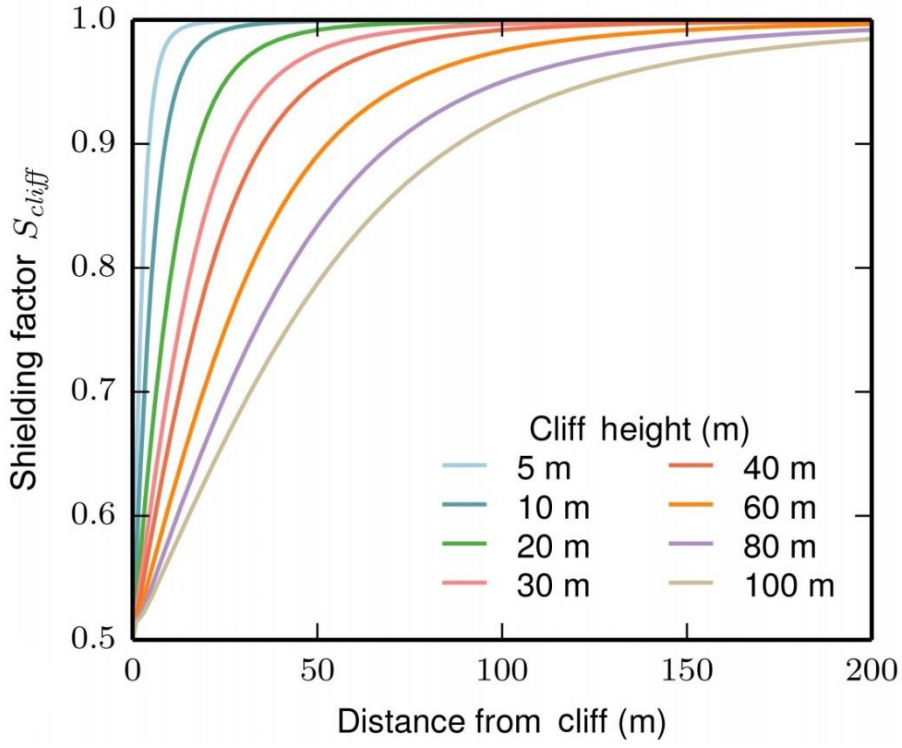

Figure 2.1: *Graph outlining the topographic shielding influence of sea cliffs.*

A shielding factor of 0.5 is deemed to be on the vertical cliff face Hurst et al (2017).

Second, I collected two samples from exposed limestone bedrock at exact sea-level in the swash zone at Beacon Cove (TOR-04a and TOR-04b). These surfaces were very smooth, similar to that of the backing sea wall, providing evidence of active and rapid abrasion by shingle impact during high wave conditions. Furthermore, the high water mark can be easily identified on the backing sea wall, with the upper section of the wall maintaining a rougher texture than that below the maximum water height (Appendix 1 Figure 6.2F). Due to the nature of this environment and the active erosion at the site, the cosmogenic nuclide concentrations here are best interpreted as erosion rates, rather than apparent exposure ages due to the lack of evidence suggesting the site is in dynamic equilibrium. Duplication of these samples provides an assessment of local variability.

Third, I collected two samples from the raised shore platform (TOR-08 and TOR-09) at Hopes Nose. The samples were collected from areas where there was minimal shielding from the backing cliff and the samples were collected away from solution pans located across the platform.

Sample elevations were estimated in the field, using a tape measure and visual estimation, in addition to some being taken from UAV data of Hopes Nose (collected in this research), which are deemed more accurate. Elevations are relative to the Ordnance Datum (OD) Newlyn for mainland Britain (Christie, 1994), as well as considering relative present-day high tide regimes specific to Torbay.

As highlighted, samples were composed mainly of Devonian limestone and shale, with minimal traces of quartz. Consequently, ^{36}Cl was chosen for analysis, which is suitable for these rocks which are rich in calcium, the target mineral for ^{36}Cl production (Stone et al., 1996). Samples were prepared following standard

samples preparation techniques as described in Barrows et al (2002). Targets for ^{36}Cl were measured by accelerator mass spectronomy at the Australian National University. However, TOR-02 had a lack of calcium-rich material, as a result of the quartz vein running through the cliff, this prevented the acquisition of ^{36}Cl concentrations to calculate an accurate exposure age. Similarly, insufficient calcium yield from TOR-03, due to the presence of other rock types veining through the cliff face, also prevented the calculation of efficient ^{36}Cl concentrations.

2.1.2.2. CRONUScalc and production rates

Exposure ages were calculated using the ^{36}Cl exposure age calculator version 2 (http://cronus.cosmogenicnuclides.rocks/2.0/html/cl/), as described in Marrero et al (2016a). CRONUScalc is an unified and multi-purpose code, created in association with the CRONUS-earth project, specifically for the use of calibrating specific production rates (Marrero et al., 2016b). This method has a user-friendly interface, simply requiring the input of relevant data, such as sample location information, sample chemical composition and associated uncertainties (Marrero et al., 2016a). The calculator includes seven possible production scaling factors, enabling the user to choose the most relevant scaling factor suitable to the study areas regional setting (Lifton et al., 2015; Marrero et al., 2016a, 2016b). Scaling factors are based on specific study site measurements, or numerical simulations based on certain physical principles, but is primarily a function of latitude and altitude changes (Dunai, 2010).

Production equations used within CRONUScalc are outlined in detail in Marrero et al (2016a). Firstly, spallation is the most dominant method of nuclide production at the surface (reference). The formula for the instantaneous production rate of

nuclides via spallation is obtained from Gosse and Phillips (2001) Schimmelpfennig et al (2008):

$$P_{\mathrm{s,m}}(Z) = S_T \sum_k S_{el,s} P_{\mathrm{m,k}}(0) C_{\mathrm{k}} \exp\left(-\frac{Z}{\Lambda_{\mathrm{f,e}}}\right), \quad \textbf{(1)}$$

$P_{m,k}(0)$ refers to sea-level, the high-latitude production rate of species m by spallation of element k (atoms g^{-1} a^{-1}; S_T represents the topographic shielding factor (unitless); $S_{el,s}$ refers to the geographical scaling factor for spallation reactions for the specific region/area of interest, which includes the temporal variation throughout production rates, as a result of fluctuations in the geomagnetic of solar magnetic fields (unitless); C_k is the concentration of the element k (atoms g^{-1} a^{-1}); Z is the depth (g cm^{-2}); and $\Lambda_{f,e}$ is the effective attenuation length for faster neutrons (g cm^{-2}) (Marrero et al., 2016a)

Attenuation length is also calculated by CRONUScalc. Attenuation length must be calculated as it is the best quantifier of the depth distribution of neutron production via spallation (Marrero et al., 2016a). as the angle of attenuation varies from vertical to horizontal the overall intensity of the cosmic ray decreases overall, as a result of the longer transport paths through the atmosphere (Dunai, 2010). The equation which accounts for this is seen in equation 2:

$$I(\theta) = I_0 \sin^m \theta, \quad \textbf{(2)}$$

Within thus equation I is the particle beam intensity, with θ representing the inclination angle from the vertical. The exponent m is significantly dependant on the energy and particle type, and is heavily discussed in Dunai (2010) (Marrero et al., 2016a). The attenuation-length model which his employed by CRONUScalc is based on atmospheric attenuation lengths, obtained from PARMA model of Sato et al (2008), and is altered to account for systematic

differences which occur between the atmospheric and lithospheric attenuation (Marrero et al., 2016a).

Thermal neutron capture also produces cosmogenics, mainly through cosmogenic epithermal neutron distribution with depth (Marrero et al., 2016a). Gosse and Phillips (2001) equation is used to obtain a production rate ($P_{th,m)}$ of cosmogenics through thermal neutron capture:

$$P_{th,ss,m} = \frac{f_{th,ss,m}}{\Lambda_{th,ss}} \Phi_{th,ss,total}(Z), \qquad \textbf{(3)}$$

$f_{th,ss,m}$ represents the fraction of absorbed thermal neutrons taken up by element k to produce nuclide m; $\Phi_{th,ss,total}$ is the thermal neutron flux; and $\Lambda_{th,ss}$ is the effective thermal neutron attenuation length (Marrero et al., 2016a). The calculation of thermal neutron capture is complicated and further details of how CRONUScalc calculated this variable are discussed in Marrero et al., 2016a).

As noted within in section 2.1.1, production of ^{36}Cl is high within calcium based materials (e.g. limestone), and contribute to the overall production of nuclides which are modelled by CRONUScalc (Marrero et al., 2016a). Muon production can occur in multiple ways, all of which are accounted for and discussed (with equations) in Marrero et al (2016a). the contribution of muonic production is minimal at the surface, increasing significantly with increased with depth, and accurate muon production formulas and modelling is vital for depth profiles which exceed 3 m (Dunia, 2010; Marrero et al., 2016a). CRONUScalc employs Heisinger et al (2002a) and Heisinger et al (2002b) as an improvement on Stone et al (1998), in addition to the Sato et al (2008) muon-flux model to create a specialised hybrid calculation of muon production (Marrero et al., 2016a). The

equations from each of these models are combined and discussed thoroughly within Marrero et al (2016).

Production rates in my study were scaled using the scheme of Saito (Sa (LSDn)), which accounts for secular geomagnetic variations, as described in Lifton et al (2014). This contrasts with the widely-used, more empirical scaling frameworks such as the schemes of Lifton et al (2005) (Lm) and Stone (2000) (St), which are included for comparison (Table 3.1). The Sa production scaling factor considers the analytical approximations of atmospheric cosmic-ray fluxes (e.g. Physical aspects of cosmogenic nuclide production), and is most suitable for this study due to the latitude and altitude upon which it is based (Lifton et al., 2014).

Spallation and low energy neutron capture (P_f) production rates under the Sa scaling factor can be seen in Table 2.2, including their associated uncertainties. Muon production rates for the Sa scaling framework are also outlined in Table 2.3. These production rates are calibrated from global high latitude, low altitude reference values, all of which has been taken from Marrero et al (2016b).

Scaling Framework	**Ca at ^{36}Cl (g Ca)$^{-1}$yr^{-1}**	**K at ^{36}Cl (g K)$^{-1}$yr^{-1}**	**P_f (0) neutrons (g air)$^{-1}$ yr^{-1}**
Sa (LSDn)	56.0 ± 4.1	155 ± 11	759 ± 180

Table 2.2: Sa production rates for spallation and low energy neutron capture (Marrero et al., 2016b).

Scaling Framework	Ca σ_0 ($10^{-30}cm^2$)	Ca F* (10^{-2})	K σ_0 ($10^{-30}cm^2$)	K F* (10^{-2})
Sa (LSDn)	8.3 ± 1.8	1.35 ± 0.27	9.4 ± 12.3	5.8 ± 1.7

Table 2.3: Sa muon production rates *(Marrero et al., 2016b)*. σ_0 *represents fast muon production. F* represents slow muon absorption.*

However, it must be noted that there are some issues with the online exposure programme itself. While the Sa scaling production rate errors are included, specific ^{36}Cl production rate errors for the samples themselves are not reported. As a result of this the exposure ages cannot be reported as accurately as desired within the results of my study.

2.2. UAV-SfM Photogrammetry

2.2.1. Background to photogrammetry

In recent decades, the use of remote sensing approaches to investigate Earth surface processes has expanded dramatically. Alongside this, multiple Geographical Information System (GIS) tools and methods have been developed to allow rapid and user-friendly visualisation, processing and analysis of remote sensing data (Sunamura, 2015; Woolard and Colby, 2002). This technological leap is most significant within geomorphological approaches, where the volume of 3D data and number of Digital Surface Models (DSM) have increased with the use of these methods (Micheletti et al., 2015). This has facilitated significant advances in modelling, mapping and understanding the environment. These methodologies are especially useful within coastal research, such as that

focused on coastline retreat and geomorphology, as outlines in section 1.4.4 (Boateng, 2012; Lefsky et al., 2002; Woolard and Colby, 2002).

Satellite, aerial and LiDAR images are the most common methods used within the field of coastal research. LiDAR has been embraced by coastal research in a number of ways, which primarily include work focused on floodplains, shoreline mapping, post-storm damage and coastal engineering projects (Woolard and Colby, 2002). The ability of LiDAR surveys to generate DSMs has resulted in expansion of datasets with dense spatial resolution and highly accurate vertical values, allowing the method to expand into quantifying erosion and retreat rates of coastlines (Clark, 2017).

The Plymouth Coastal Observatory have collated an extensive series of LiDAR datasets around the UK's coastline, including LiDAR of Hopes Nose between 2007 and 2017. Similarly, they have collected orthorectified 1 m resolution datasets repeatedly between 2007 and 2017, which are often used to analyse coastal changes and provide data for shoreline management schemes (PCO, 2018). GIS can be used to extract additional information from these data sets, and to visualise and quantify the movement of the coastline edge over the larger temporal and spatial scale, such as in Boateng (2012) and Swirad et al (2016). Despite the increasing usefulness of LiDAR datasets, they are hindered by expense, and the requirement of specialised user supervision (Klemas, 2015; Micheletti et al., 2015). Furthermore, LiDAR datasets are also hindered due to their coarse resolution, which miss significant details of coastal evolution (e.g. cliff-platform junction and solution pans), and can lead to a wrongful interpretation of results obtained from a morphometric analysis (Boateng., 2012; Woolard and Colby., 2002).

Due to these restrictions, I decided to use UAV-SfM photogrammetry in this study, to ensure an appropriate high resolution dataset is obtained to conduct a detailed morphometric analysis. UAV photogrammetry is a relatively new methodology, and the added application of SfM is even more recent (Eisenbeiss., 2009; Smith et al., 2016). While both techniques have existed and developed separately in coastal research, it is only recently they have been combined to understand coastal evolution (section 1.4.4).

Photogrammetry itself can be traced back to 1839 with the invention of photography (Schenk., 2005). From this point, photogrammetry has gone through four main generations of development, from the end of the last century to present day, developing alongside technology, especially computational power, increased storage capacity and digital imaging techniques (Schenk., 2005; Westoby et al., 2012)). A full break down of the history of photogrammetry is discussed in Schenk (2005). Traditional photogrammetry, without the application of SfM, relies on near parallel stereopairs of images from the same surface or environment, which have a minimum overlap of 60% (Carrivick et al., 2016; Fonstad et al., 2013; Micheletti et al., 2015). To allow for accurate processing of these images, traditional photogrammetry requires several ground control points (GCP) and the exact camera positions to be measured (Micheletti et al., 2015). Such strict requirements pose limitations to the technique and the environments which can be investigated, as well as the final topographic model which is produced (e.g. DEM and orthophotograph) (Westoby et al., 2012).

To overcome this, SfM algorithms were developed during the 1980s and 1990s, originating from the computer and machine vision community (Micheletti et al., 2015; Westoby et al., 2012). SfM can be used with a wide variety of imaging techniques, including videos stills, UAV images and commercial grade cameras

(Westoby et al., 2012). Unlike traditional photogrammetry, SfM uses a feature mapping algorithm to match distinctive features (e.g. geomorphic features and colours), in multiple overlapping images taken from different angles and viewpoints (Appendix 2, Figure 7.2) (Carrivick et al., 2016). In addition to this, the exact camera position or GCPs are not required, as it is internally and automatically determined by the SfM algorithm from the digital images themselves (Micheletti et al., 2015). The SfM algorithm produces a detailed point cloud, which represents the most prominent features within the environment (James and Robson, 2012). From these point clouds it is possible to generate a topographic surface, in multiple projections (e.g. geographic and planar), such as a high resolution DEM/DSM (Agisoft, 2018; Westoby et al., 2012).

UAVs and SfM packages have increase in their commercial and consumer availability in recent years. There are numerous UAVs available on the market (e.g. Phantom by DJI and eBee by senseFly), which can be used to capture high quality images to produce centimetre resolution topographic models. Similarly, several SfM packages have been developed to handle a variety of imaging techniques, including UAV (e.g. Agisoft Photoscan and Pix4D) (Micheletti et al., 2015). The commercialisation of SfM means the user is not required to understand the complex mathematical algorithms of SfM, making it more accessible to researchers new to the technique (Micheletti et al., 2015; Westoby et al., 2012).

Within my study, I will be using UAV images and a SfM software package to produce a high resolution DEM and orthophotograph of Hopes Nose. The availability and ease of UAV-SfM makes it a suitable aerial survey technique for Hopes Nose at a high resolution, to conduct a detailed morphometric analysis to understand its evolution over time.

2.2.2. UAV-SfM Photogrammetry of Hopes Nose

2.2.2.1. UAV image collection

UAV-SfM photogrammetry was employed within this study as a low cost, rapid, high-resolution and reproducible imaging technique, suitable for the desired centimetre spatial scale required for this study and allows for the possibility of future replication studies (Clark, 2017; Micheletti et al., 2015; Westoby et al., 2012). My study is the first to use of UAV-SfM, in combination with traditional dating methods, to understand and quantify rocky coastline evolution, specifically in north Torbay. The majority of existing UAV-SfM studies focus on more dynamic and rapidly eroding coastal environments, as outlined in section 1.4.4.

Aerial images were taken of Hopes Nose at low tide on 30th of January 2018, using a senseFly eBee RTK drone. RTK gives the exact camera position for each photograph taken, locating them in space and time. The flight plan was processed using e-motion (Roze et al., 2014), with 165 images of the study area being collected, covering a 0.14 km^2 area. The pre-defined flight path and initial image positions can be seen in Figure 2.2.

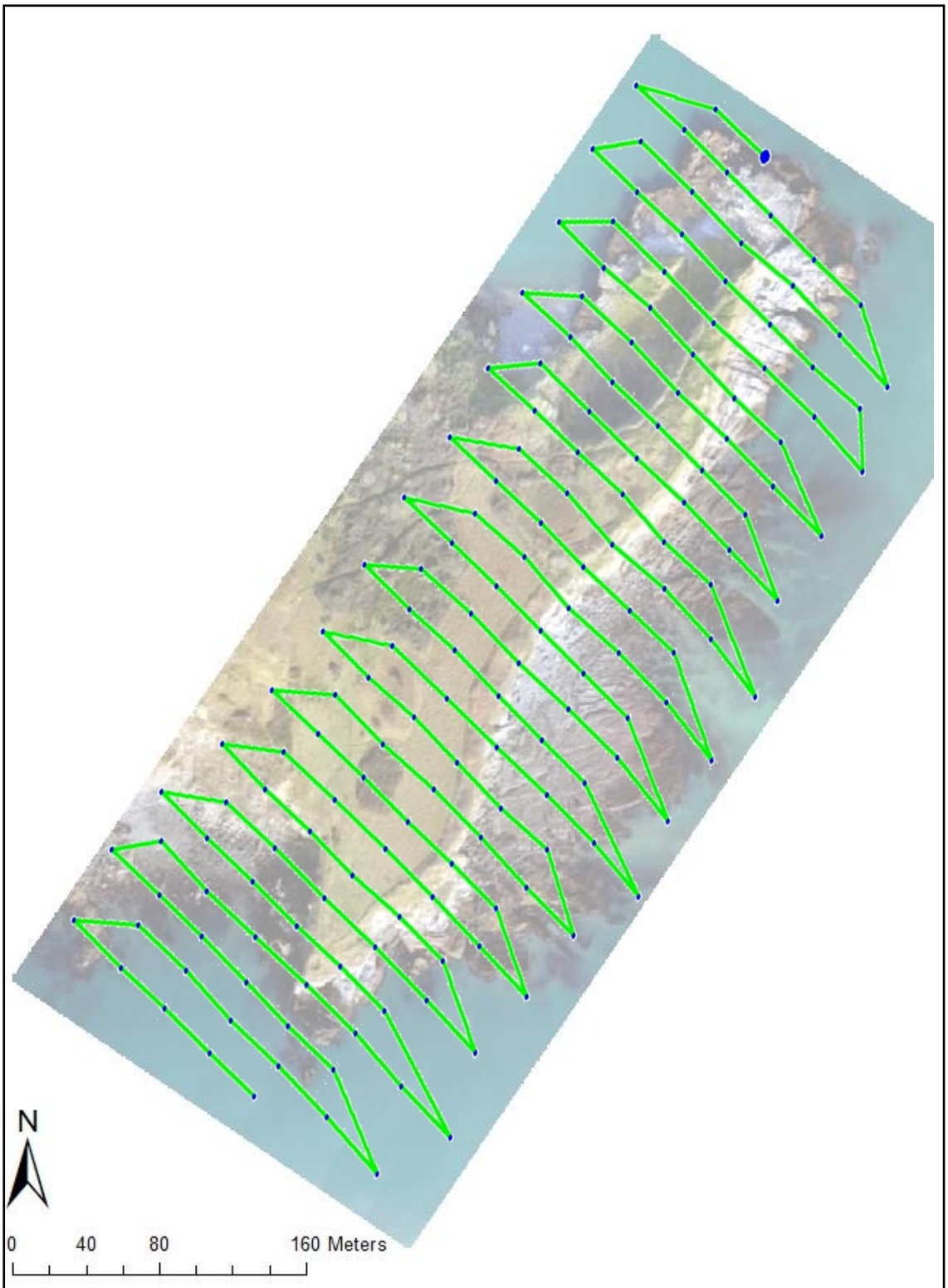

Figure 2.2: *Green line depicts the drone path flight line, with blue dots identifying where the images were taken.*

2.2.2.2. Post processing of images

Post-processing of the images was carried out using Agisoft Photoscan, which also produced an initial quality report for the drone flight survey and images (Agisoft LLC, 2018). A breakdown of the Agisoft process can be seen in Appendix 2, Figure 7.1.

Agisoft Photoscan enabled and calibrated 156/165 images (94%), with a 0.07% relative difference between initial and optimized inter camera parameters (Figure 2.3). In addition to this, Figure 2.4 indicates the overlap of the obtained images, which is essential for obtaining a seamless and high resolution UAV-SfM dataset (Long et al., 2016; Westoby et al., 2012).

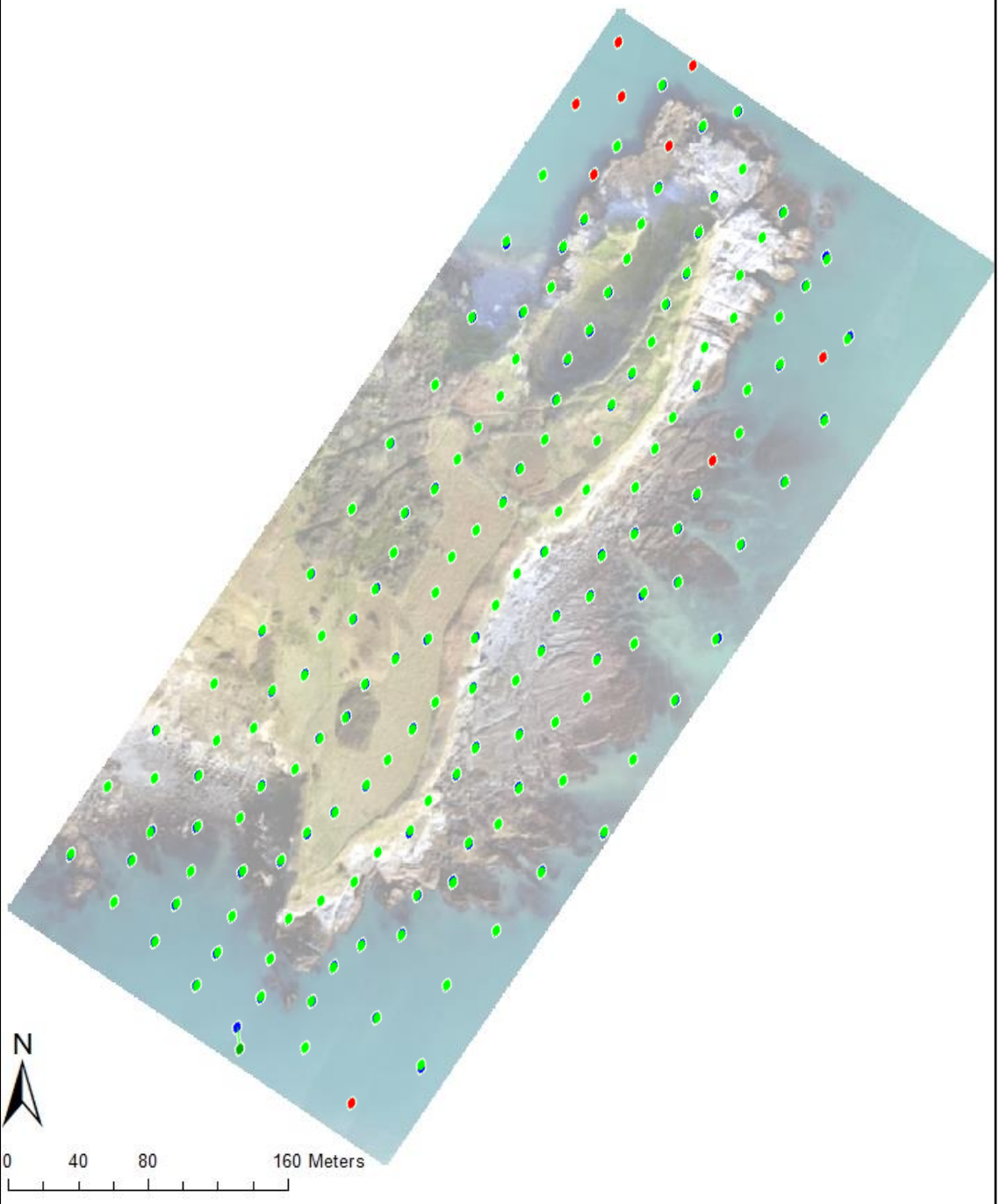

Figure 2.3 : *Offset between the initial images (blue dots) and the computed images (green dots). Red dots within the figure indicate disabled or uncalibrated.*

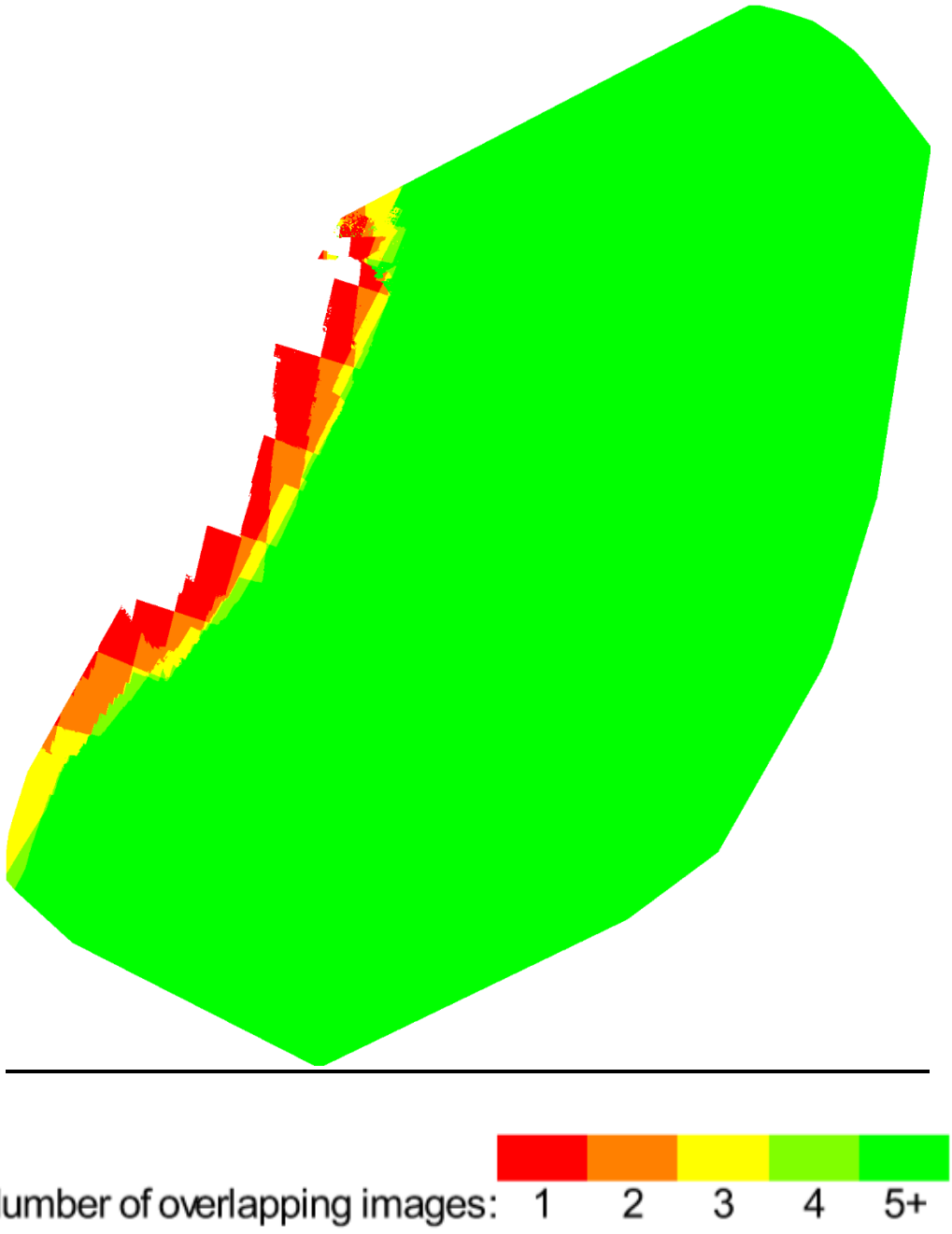

Figure 2.4 *: Number of overlapping images, computed for each pixel of the orthomosaic image. Red depicts areas of poor overlap, with green showing 5+ photos overlapping.*

It must be noted that issues arose with the elevations of the model, later related to projection and transformation issues. Drone images were collected in the coordinate system WGS_1984. Post-processing of the drone images in Agisoft Photoscan produced a model which had elevations around 50 m above what I anticipated (e.g. the elevated platform recorded 53 m to 58 m above present SL). Geoid height correction was calculated using an online calculator (UNAVCO, 2019), measured at -45 m. However, even with geoid corrections applied, elevations still exceeded the expected and observed elevations for the shore platforms at Hopes Nose. Consequently, elevations recorded from the drone images were run through the Ordnance Survey coordinate transformation tool (Ordnance Survey, 2019). This calculator transforms WGS_1984 coordinates and elevations to the relevant orthometric mean sea-level heights, in this case OD Newlyn (OSGB36), using the National Geoid Model 0SGM15 (Ordnance Survey, 2019). This brought the elevations in-line with those observed at the site, and within 1 – 2 m of those previously reported in Mottershead et al (1987). While Mottershead et al (1987) states elevations should not be regarded as exact, as they are observed and estimated, they provide good reference to ensure the elevation transformations were successful. In this study, elevations are thus reported relative to the OD Newlyn for mainland Britain (Christie, 1994). This issue acknowledges that the use of GCP, with known locations and elevations, would have been useful in preventing this situation from occurring in future research.

The use of UAV-SfM photogrammetry produced a high-resolution orthomosaic and DSM of Hopes Nose, with an average ground sampling distance of 3.59 cm (Figure 2.5).

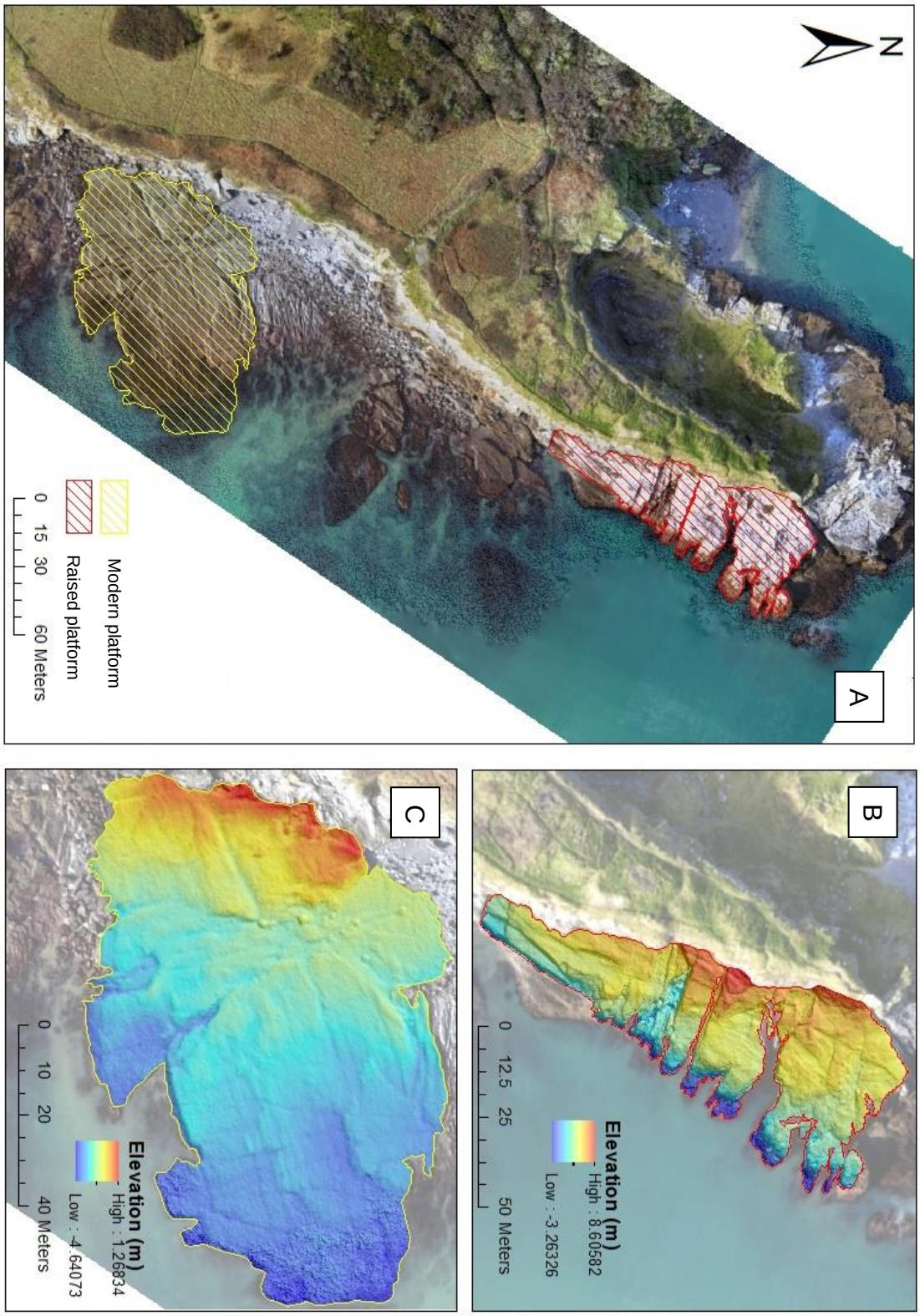

Figure 2.5: *A)* Orthomosaic image of Hopes Nose. The raised shore platform area of interest (AOI) is identified by red hatching and the modern platform by the blue hatching. B) Elevation distribution of the raised shore platform. C) Elevation distribution of the Modern shore platform.

2.2.2.3. Morphometric analysis

The UAV aerial images were focussed on the raised platform and the modern shore platform. Geoprocessing tools from ArcGIS were used to extract elevations of both platforms from the DSM. MATLAB R2018a was then used to present these results for interpretation, as well as analysing them for descriptive statistics. Platform areas of interest (AOI) were chosen to incorporate the main extent of the platforms (Figure 2.5A, B and C), whilst avoiding areas of uncertainty associated with water cover on the modern platform and significant post-depositional collapse from undercutting on the raised platform. Furthermore, I omitted the north side of the raised platform at Hopes Nose from my analysis, due to historical limestone quarrying. Elevations were extracted from the drone-derived DSM: over 63,000 points were taken from the elevated raised platform; and over 12,000 points from the modern platform.

From the morphometric data obtained from the UAV images several width measurements were also taken, with the maximum and average width of the shore platforms recorded. Widths were measured from the cliff-platform junction to the interpreted seaward edge of the shore platform. These measurements will be used to determine a possible cliff retreat rate for both the modern and raised shore platforms. The maximum shore platform width can be divided by what is deemed as the timescale of platform development, to estimate the magnitude of horizontal cliff retreat which widens and develops the shore platform (de Lange and Moon, 2005).

2.2.3. Multi-view Photogrammetry

In addition to the drone flight, ground-based photogrammetry was carried out on the sedimentary section which backed the raised shore platform, similar to that

done by Gienko and Terry (2014). A sub-millimetre scale (0.4 mm) model was created from 175 photos which were captured using an 18 Mega pixel digital camera and processed with Agisoft Photoscan (Figure 2.6). The imaging technique used to obtain these photographs is depicted in the schematic from Micheletti et al (2015) in the Appendix 2 (Figure 7.2).

2.3. Relative Sea-Level Modelling

The numerical modelling of RSL at Hopes Nose was conducted by Dr Paolo Stocchi at the Royal Netherlands Institute for Sea Research. While he also assisted with data interpretation, the overall analysis and conclusions were made by myself.

2.3.1. Modelling eustatic sea-levels

Variations in continental ice mass (ice sheets, ice caps, glaciers etc.), are counterbalanced by equivalent changes in the global ocean mass and volume, because of the principle of mass conservation. During glaciations water is taken from the oceans and stored in form of ice sheets, whilst during interglacials water flows back to the oceans. If it is assumed that the area of the oceans A_o is fixed in time (e.g. there is a vertical wall of infinite height along the coastlines), any ice-mass variation m_i (either positive or negative) corresponds to a sea level variation that is defined by:

$$S^E = -\frac{m_i}{\rho_w A_o}, \qquad (4)$$

where S^E is the so-called eustatic sea-level change and ρ_w is the density of sea water. As outline within section 1.5, eustasy implies that the solid Earth is rigid (non-deformable) and that gravity is neglected (Spada and Stocchi, 2007).

Accordingly, the oceans behave like a bathtub; for example, the eustatic sea-level change does not depend on the geographical location (Hay et al., 2014). However, recent evidence has outlined that this is not the case, as a result of steric sea-level changes and GIA contributions. Consequently, Eq. (1) and eustasy is not the most accurate representation for the RSL at Hopes Nose.

2.3.2. Background to modelling relative sea-levels

As noted within section 1.4.1, RSL refers to changes in the land reference base, in combination with changes in ocean volume through eustatic changes. The process of modelling RSL requires prior-knowledge of former geographical proximities and extents of Pleistocene ice sheets and a chronology of how these changed over time (Murray-Wallace and Woodroffe, 2014). Models must incorporate the coupled effects of solid earth deformations, gravitational perturbations, eustasy, the Earth's rotation and coastline migration, all of which occur as a direct consequence of time-variant ice and water loading at the Earth's surface (Spada and Stocchi, 2007). The contribution of GIA to regional RSL changes can only be evaluated by means of forward process-based numerical modelling (de Boer et al., 2017). Numerical models used to determine the relevant GIA feedback usually combine a pre-defined ice sheet model, which is the forcing function consisting in ice sheet thickness variation and a solid earth model. This operates as a response function, by returning solid earth deformations and mean sea surface variations (e.g. geoid). The outcome yields the space and time dependent RSL changes, which accompanies and follows the ice sheet fluctuations.

Consequently, the gravitationally self-consistent sea-level equation (SLE) must be solved (Farrell and Clark, 1976; Milne and Mitrovica, 1996). SLE models the

distribution of water between ice sheets and oceans on a deforming earth (Martinec et al., 2018). The SLE incorporates all the GIA feedbacks, yielding RSL changes which accompany and follow continental ice sheet thickness variations accurately (Spada and Stocchi, 2007).

Farrell and Clark (1976) state that sea-level changes are a function of space and time. The spatial and temporal response of sea-level change can be related to perturbations, specifically the geopotential and deformation of the Earth, as a response to climate induced ice and ocean mass re-distribution (Milne et al., 2006).

$S(\omega, t)$ is defined by:

$$S(\omega, t) = \frac{\phi}{\gamma} - U + c, \qquad \textbf{(5)}$$

where ϕ is incremental perturbation of the gravitational potential, γ is the gravity acceleration at the Earth's surface, U is the vertical displacement of the solid Earth's surface and c is a time-dependent function. In Eq. (2), S is the sea-level change which would be measured by a vertical meter stick that is attached to the solid boundary of the deformable Earth (e.g. a tide gauge). Therefore, S represents the RSL change.

Because the vertical variation:

$$N(\omega, t) = \frac{\phi}{\gamma} + c, \qquad \textbf{(6)}$$

corresponds to the change in radius of the geoid, Eq. (2) can be written as:

$$S(\omega, t) = N - U, \quad \textbf{(7)}$$

showing explicitly that S is determined by variations of the distance between the geoid and the solid Earth surface. This holds both on land and over the oceans, where N defines the change in radius of the equipotential sea surface in the absence of winds, tides, and ocean currents.

Therefore, N is usually measured by means of satellite altimetry, U is observed by means of GPS measurements and S is measured by tide gauges and by any geological and archaeological sea-level indicator.

Imposing the constraint of mass conservation gives:

$$c(t) = -\frac{m_i}{\rho_w A_o} - (\frac{\phi}{\gamma} - U), \quad \textbf{(8)}$$

where m_i is the ice mass variation, ρ_w is the density of water, A_o is the area of the surface of the oceans (assumed constant), and the overbar indicates the average over the surface of the oceans. Substituting Eq. (4) into Eq. (1) yields:

$$S(\omega, t) = (\frac{\phi}{\gamma} - U) + S^E - (\frac{\phi}{\gamma} - U), \quad \textbf{(9)}$$

where the first term on the right-hand side corresponds to the eustatic sea-level change of Eq. (1).

The SLE in the form (6) is an integral equation and cannot be solved explicitly, since both ϕ and U are determined by the surface load exerted by the ice sheets and by that due to the melt water, with the latter depending on S itself. The load function L stems, in fact, from an "ice" and a "water" component, with:

$$L(\omega, t) = \rho_i I + \rho_w SO, \qquad \textbf{(10)}$$

where ρ_i is the density of the ice and $O(\omega)$ is the so-called ocean function that locates the ocean loading term. Again, the loading function (eq. 7), which is needed to compute the sea-level change S, contains an ice-loading term and an ocean-loading term.

The latter is defined by the sea-level change S itself. Hence, the SLE is defined as an integral equation because it contains the unknowns on both the left and right side. Accordingly, solving the SLE requires an iterative procedure that usually terminates when the convergence is reached.

2.3.3. Relative sea-level modelling at Hopes Nose

The methodology used to produce the RSL for Hopes Nose is similar to methods used in recent research by Antonioli et al (2018), Stocchi et al (2018) and Toscano et al (2011). Similar to these studies SELEN, a Fortran 90 program (Spada and Stocchi, 2007), which solves the SLE by means of the pseudo-spectral approach, was employed specifically for this area of the southwest UK (Milne and Mitrovica, 1996). SELEN requires two main inputs: (i) an ice-sheet model, which describes the ice thickness variation in space and time, and (ii) a

rheological model, which describes the solid Earth and gravitational response to ice and equivalent water-load redistribution. ICE-5G and ICE-6G ice-sheet models are used to describe the last 123 ka BP of ice thickness variation (Argus et al., 2014; Peltier et al., 2015). The ICE-6G chronology starts at 123 ka BP and assumes that the Greenland and Antarctic Ice Sheets (GrIS and AIS, respectively) are smaller than todays. The ICE-6G chronology is combined twice in time, to account for the ice-sheets expansion during the MIS 6 and the following retreat, as well as the expansion and retreat during the LGM. However, it must be noted that this assumes that the MIS 6 glaciation was identical to the LGM, which is highly debated.

In addition to this, capturing the GIA contribution throughout the MIS 5e interval for the southwest is vital. Therefore, it is important to include the previous interglacial-glacial cycle to highlight the way in which the land deformed at this time. The ICE-6G model will be combined with the VM2 mantle profile to determine a local RSL for Hopes Nose, which considers both eustatic sea-level changes and the influence of GIA in the far-field site.

CHAPTER 3: RESULTS

3.1 ^{36}Cl Cosmogenic nuclide exposure dating

Exposure ages are presented within Table 3.1. The exposure ages obtained from Meadfoot Beach, Beacon Cove and Peaked Tor Cove fall within a range from 1.8 ± 0.2 ka BP to 5.89 ± 0.45 ka BP, which all fall within the late Holocene. Exposure ages for samples taken at Hopes Nose provided early Holocene ages of 8.35 ± 0.69 ka BP and 10.14 ± 0.81 ka BP. Exposure ages for TOR-04a and TOR-04b are apparent ages only. However, the measured ^{36}Cl concentrations and ages of TOR-4a and TOR-4b should be interpreted as incremental or vertical lowering rates of erosion, rather than exposure ages, due to their geological setting and the samples rocks lithology (Appendix 1, Figure 6.2C and 6.2D). I used the erosion rate equation from Lal (1991) to calculate an erosion rate for samples TOR-04a and TOR-04b (Table 3.2) using the scheme of (Stone, 2000). Concentrations of ^{36}Cl and other chlorine concentrations from the collected samples are presented within Table 3.3. Erosion rates were calculated at 0.58 ± 0.07 m/10^3Ka (TOR-04a) and 0.49 ± 0.05 m/10^3Ka (TOR-04b), yet these should be considered minimum rates as a result of possible reduced production rates related to water shielding of the samples (section 4.1 and 4.5.1). Exposure ages are placed in site context in Figure 3.1.

	Sa Scaling Factor	Lm Scaling Factor	St Scaling Factor
Sample	**Age (Ka BP)**	**Age (Ka BP)**	**Age (Ka BP)**
TOR-01	3.8 ± 0.72	3.9 ± 0.75	3.89 ± 0.76
TOR-04a	1.8 ± 0.2	1.98 ± 0.22	1.95 ± 0.23
TOR-04b	2.41 ± 0.23	2.58 ± 0.28	2.54 ± 0.28
TOR-05	5.89 ± 0.45	6.31 ± 0.61	6.23 ± 0.63
TOR-06	2.42 ± 0.21	2.6 ± 0.27	2.56 ± 0.28
TOR-07	4.5 ± 0.4	4.8 ± 0.5	4.72 ± 0.52
TOR-08	8.35 ± 0.69	9.1 ± 0.9	8.94 ± 0.93
TOR-09	10.14 ± 0.81	11 ± 1.1	10.8 ± 1.1

Table 3.1: ^{36}Cl exposure ages calculated using the Sa scaling scheme. Results from the St and Lm schemes calculated exposure ages are included for comparison.

Sample	Erosion Rate (m/10^3 Ka)
TOR-4a	0.58 ± 0.07
TOR-4b	0.49 ± 0.05

Table 3.2: Calculated erosion rates from limestone bedrock situated in Beacons Cove swash zone.

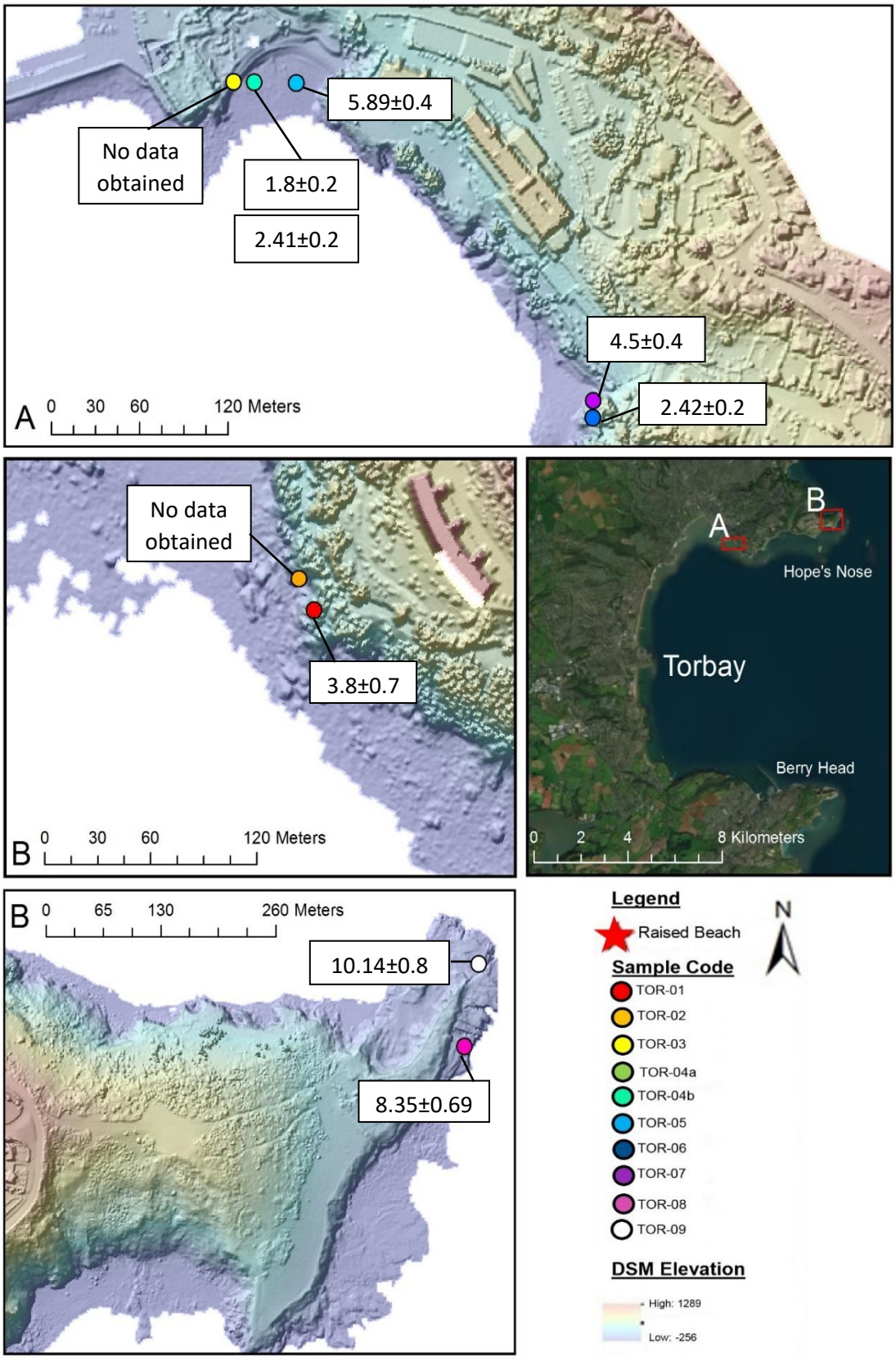

Figure 3.1: *Map showing the locations of exposure dating samples. Exposure ages are presented for each location, where data wasn't obtained has also been highlighted.*

Sample Name	^{36}Cl Concentration	Cl Concentration (ppm)	Cosmogenic Cl (atoms/g)	Radioactive Cl (atoms/g)
TOR-01	20580	20.71	11811.15	8768.854
TOR-04a	42650	28.94	41548.35	1101.649
TOR-04b	53330	27.7	52826.02	503.981
TOR-05	77610	20.69	77153.12	456.8782
TOR-06	43910	14.26	42964.76	945.2443
TOR-07	59700	20.89	58594.14	1105.859
TOR-08	190100	14.42	189765	334.9963
TOR-09	248400	43.3	246864.4	1535.607

Table 3.3*: Concentrations of 36Cl, Cl, Cosmogenic Cl and Radioactive Cl obtained from each sample taken from north Torbay.*

3.2. UAV-SfM Photogrammetry

3.2.1. Hopes Nose shore platforms

Distinctive differences are visible between the modern and raised platform elevations, depicted in Figure 3.2. The mean width of each of the platforms was measured from the orthophoto of Hopes Nose. Measurements of both shore platform widths were taken at 10 m intervals, over a 70 m area which encapsulated the main AOI. This enabled the measurements to extend across the entire width of the modern shore platform, yet only covers the widest area of the raised platform. This avoids the narrow sections which were possibly remodelled under present sea-levels. The modern platform has a maximum width of ~90 m (average 77 m wide), and the raised platform has a maximum width of ~50 m (average 39 m wide). The modern platform width obtained a standard deviation (SD) of 10.08 m, and the raised platforms width a SD of 6.47 m.

A possible erosion rate has been calculated using the shore platform maximum width data with the assumed formation time for each shore platform (data in section 3.3 and discussed in Chapter 4). Assuming the modern platform formed around 7000 years ago, when sea-level was ~5m below present (Appendix table 8.1), dividing the width by this time interval produced an annual erosion rate of 13 m is calculated (90 m / 7000 years = ~0.013 m a year or 13 m/1000 years). Similarly, if the maximum width of the raised shore platform divided by the duration of the sea-level highstand of the MIS 5e (Figure 3.4B and Appendix table 8.1), an annual erosion rate of 20 m is calculated (50 m / 2500 years = 0.02 m a year or 20 m/1000 years).

The skew on the elevation distribution for the modern platform is positive (Table 3.4.), which is evidence of a bias towards lower elevations (Figure 3.2). This is reiterated from the modal elevation taken from the modern platform, which is 3.08 m below OD Newlyn sea level (Table 3.4). In contrast, the skew on the elevation distribution for the raised shore platform is negative (Figure 3.2 and Table 3.4). This results from the platform having proportionately higher elevation areas, with the modal elevation being 3.75 m above current sea level, relative to OD Newlyn (Table 3.4). Kurtosis is greater than 3, for both the modern and the raised shore platform elevation distributions, meaning that the data sets are leptokurtic and have flatter tails with higher chances of extreme outliers existing (Table 3.4). From the statistics, it is evident that the raised shore platform has higher kurtosis, due to the wider spread of measured elevation values seen in Figure 3.2.

Elevation profiles of each of the platforms are shown in Figure 3.3, taken perpendicular to the coastline. The modern platform slopes gently seaward, with no steps or sudden elevation changes. However, profiles extracted from the raised platform show higher variability, both across and along the platform.

Despite this greater variability, all profiles exhibit a distinctive drop-off towards the seaward end of the profile.

	Modal Elevation (m)	Mean Elevation (m)	Max Elevation (m)	Min Elevation (m)	Skewness	Kurtosis
Modern Shore Platform	-3.08	-2.51	1.27	-4.64	0.8749	3.3542
Raised Shore Platform	3.75	3.37	8.61	-3.26	0.6803	3.5332

Table 3.4: *Summary statistics of elevation data extracted from the raised and modern shore platforms main extents Figure 2.5.*

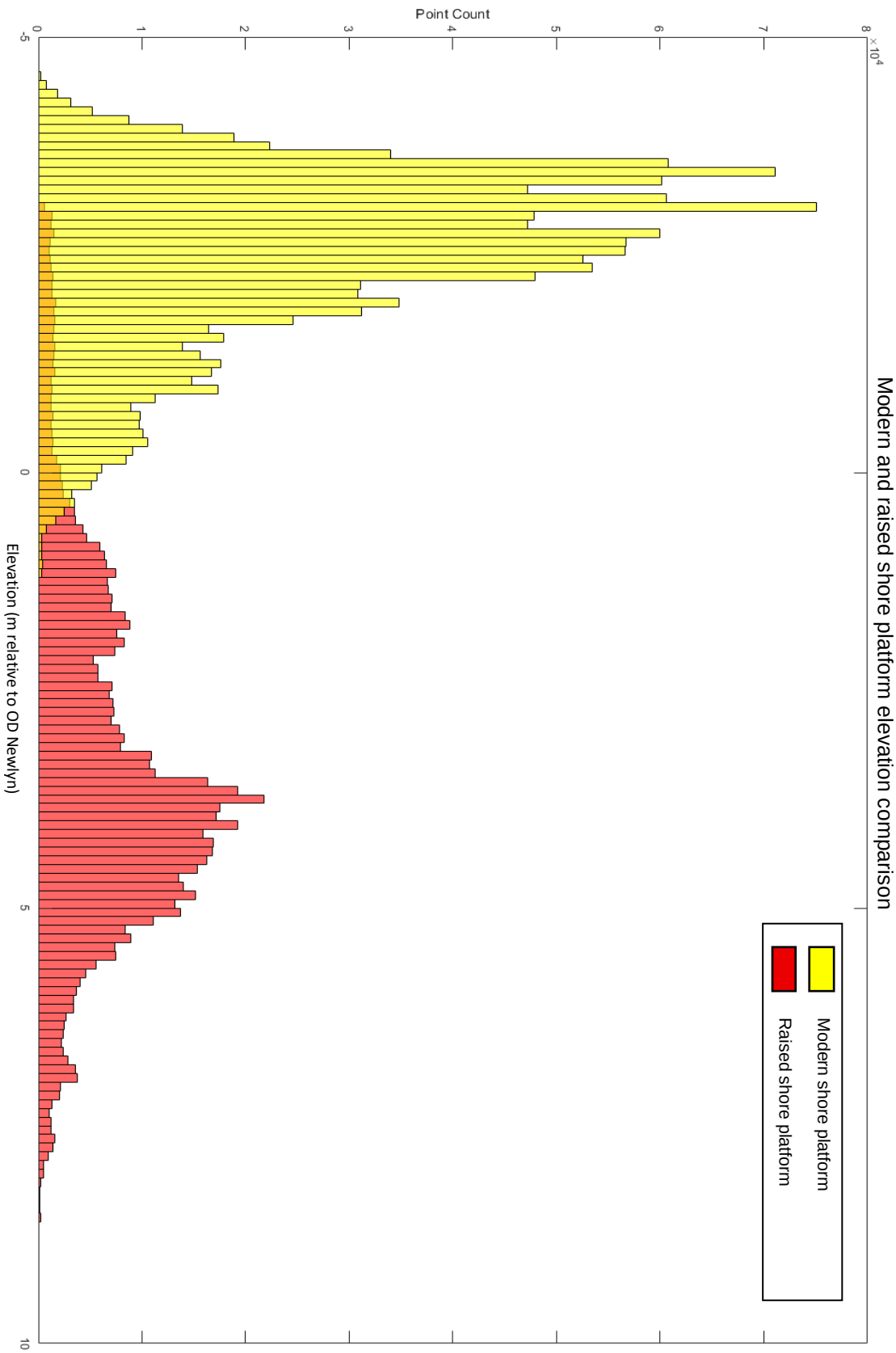

Figure 3.2: *Histogram showing the distribution of all elevations extracted from the platform AOI's. Summary statistics are outlined in Table 3.4.*

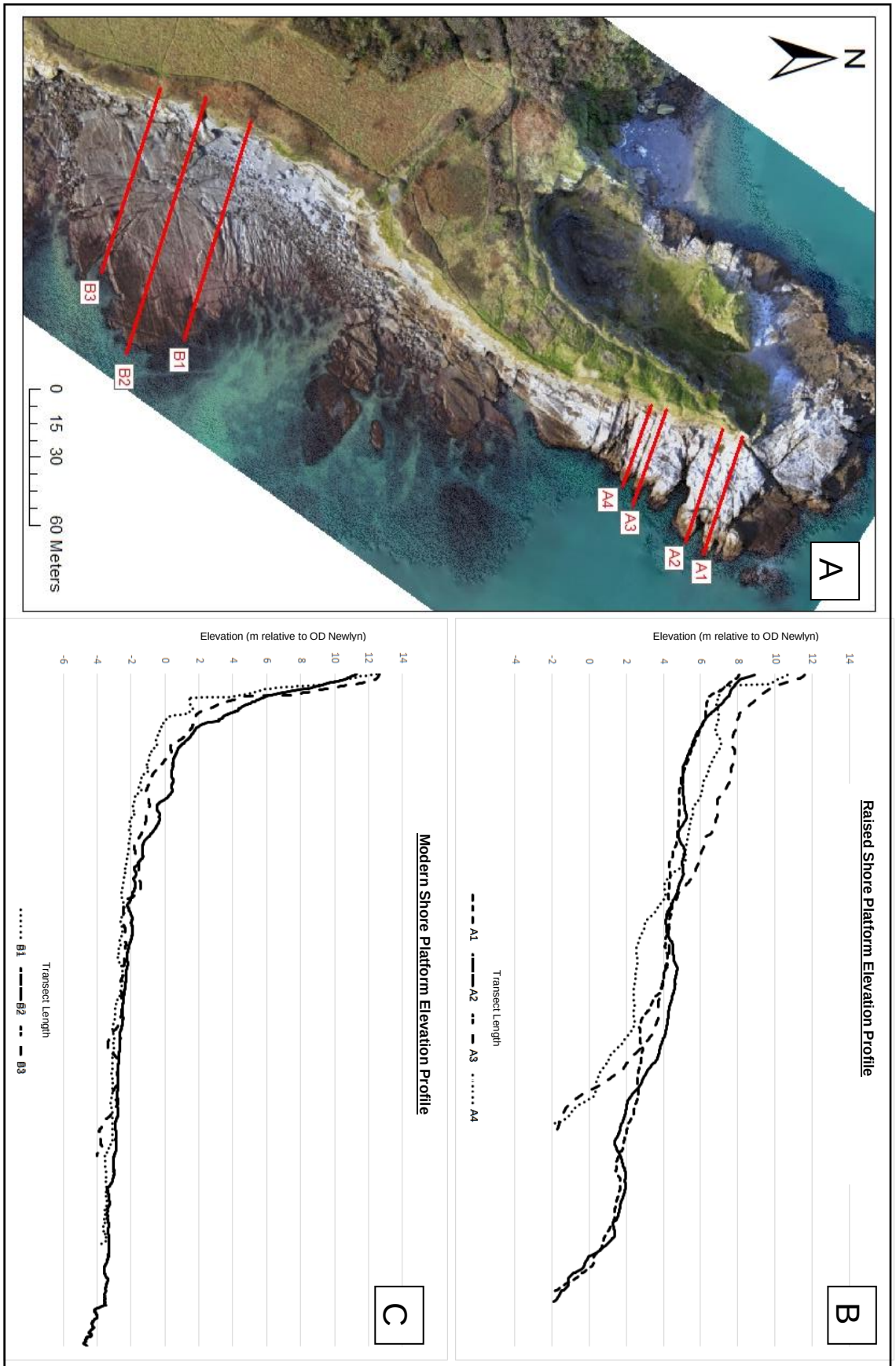

Figure 3.3: *A) Representative transects measured across the modern and raised platforms. B) Elevation profiles across the raised shore platform AOI. C) Elevation profiles across the modern shore platform AOI.*

3.2.2. Solifluction sediments

From the orthophoto, there is a distinctive underlying relict cliff, formed in flat lying Devonian limestone beds, which has a maximum vertical height of around 2 m. Overlying this there is a solifluction sheet with evident periglacial characteristics, such as cryoturbation. The width of the overlying solifluction sediments varies between 1.7 m and 2.5 m. The combined height of the relict cliff and the overlying solifluction sediments is between 3.7 m and 4.5 m at this site.

Figure 3.4: High resolution orthophoto and sedimentary log of the rocks and sediment backing the interglacial shore platform. The images are taken from the backing cliff along the northern section of the raised shore platform AOI (Figure 2.5B).

3.3. Relative sea-level modelling

The modelled RSL curve focused on, in this study is shown in Figure 3.5B, suggests that global mean sea-level at 123 ka BP was ~3 m above present day sea-level. This is also in accordance with the extended ICE-6G chronology, which covers the last 250 ka BP, confirming that the maximum MIS 5e eustatic highstand of ~3 m above present day sea-level (Figure 3.5 and Appendix table 8.2). It must be noted that results from the ICE-5G and ICE-6G models produced significantly different MIS 5e RSL curves for north Torbay (Figure 3.5A and 3.5B). Results from the SELEN ICE-5G model show a eustatic and GIA RSL peak between 122 and 123 ka BP, ~1 m above present sea-level, before rapidly falling below present sea-level (Figure 3.5A).

However, the output from SELEN ICE-6G is, overall, in line with the eustatic and predicts a RSL highstand of ~4 m above present day at Hopes Nose ~122 Ka (Torquay, Figure 3.5B) The latter is ~1 m higher than the predicted eustatic curve (Figure 3.5B). This peak occurs after a gradual increase from an initial peak at ~3 m at 125 Ka BP. Within SELEN ICE-6G the local RSL started to fall below present sea-level at ~120 ka BP, reaching 119 m below present at ~26.5 ka BP before rising again towards present-day (Figure 3.6).

RSL modelling, SELEN ICE-6G, for the Holocene (10 Ka Bp to present day) shows that RSL rises significantly over the Holocene, specifically before 7 Ka BP (Figure 3.7). Model predictions for the last 10 Ka BP can be seen in Figure 3.7 and Appendix 3, Table 8.1. At 10 Ka BP years sea-level is at 20.99 m below present, rising 15.9 m to 5.09 m at 7 Ka BP, at a calculated rate of 5.3 mm a year. After 7 Ka BP the rate of sea-level rise slows, rising 5.09 m to present day, at a rate of 0.72 mm a year. The recorded sea-level at 7 Ka BP is around 2 m lower

than the previously reported sea-level heights, which will be discussed further in Chapter 4.

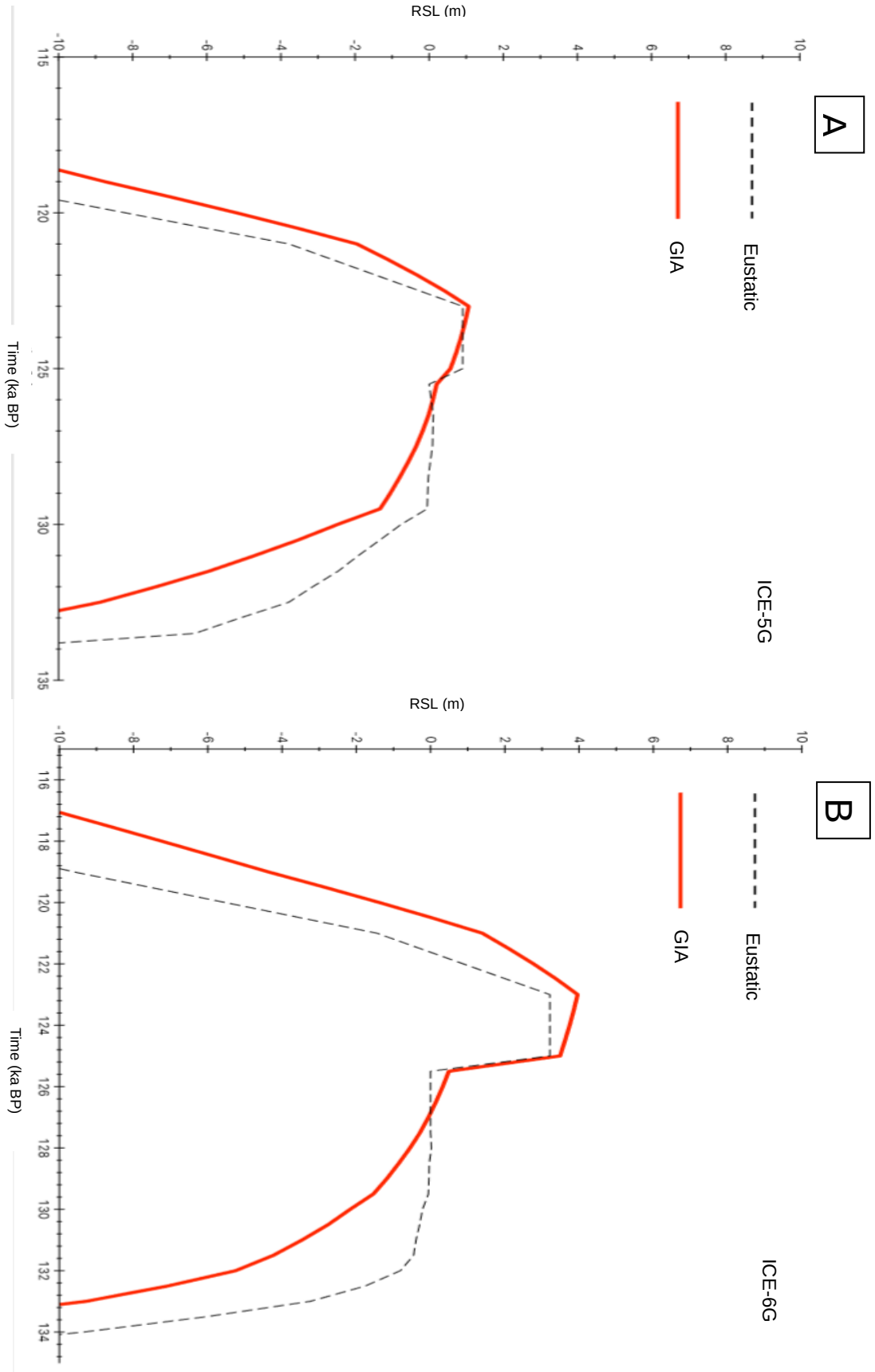

Figure 3.5: A) Eustatic curve vs the local RSL change at Hopes Nose, when ICE-5G ice sheet model is considered. B) Eustatic curve vs the local RSL change at Hopes Nose, when ICE-6G ice sheet model is considered.

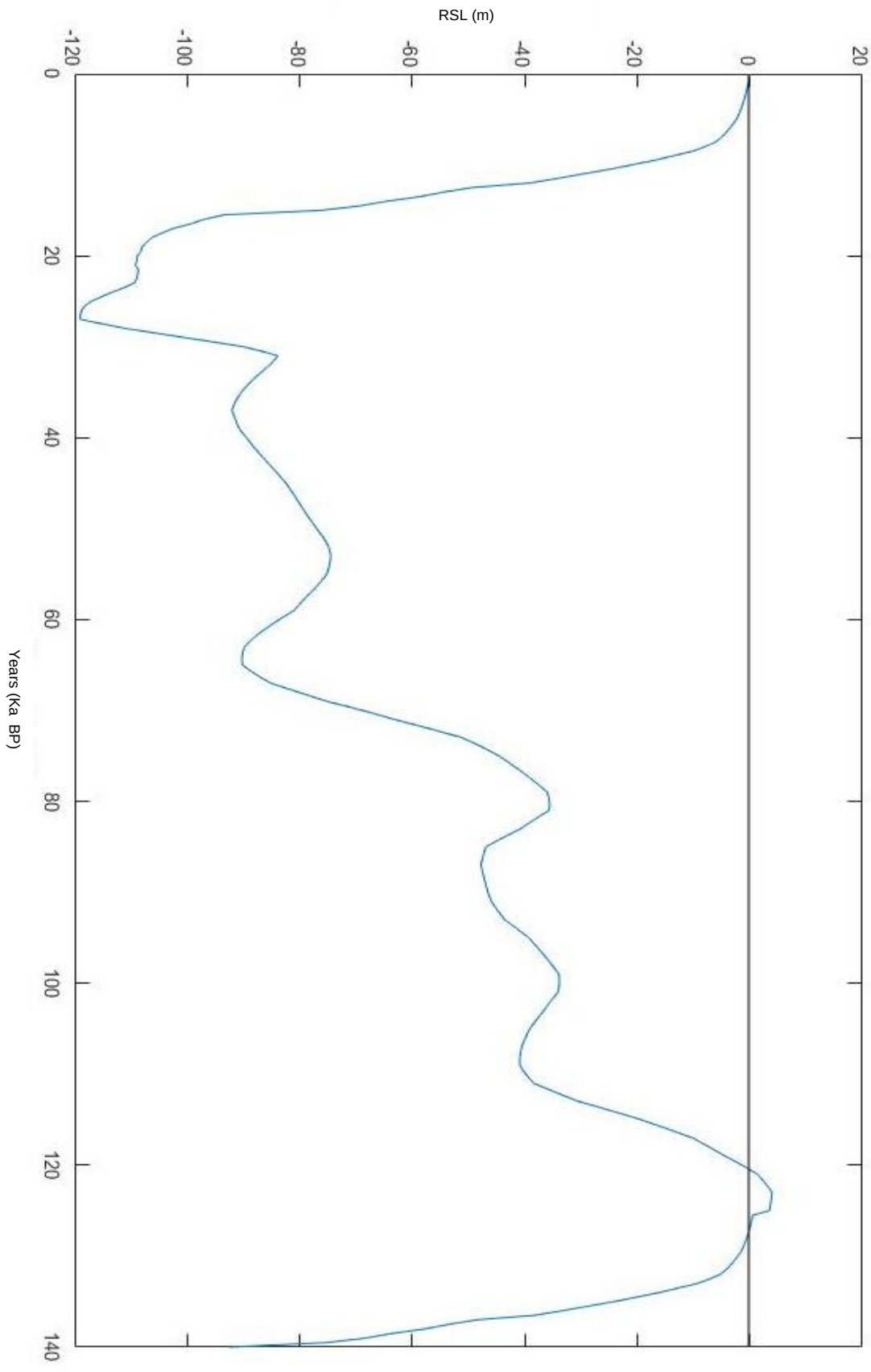

Figure 3.6: RSL curve, produced using the ICE-6G ice model. Present day sea-level is depicted by a horizontal line.

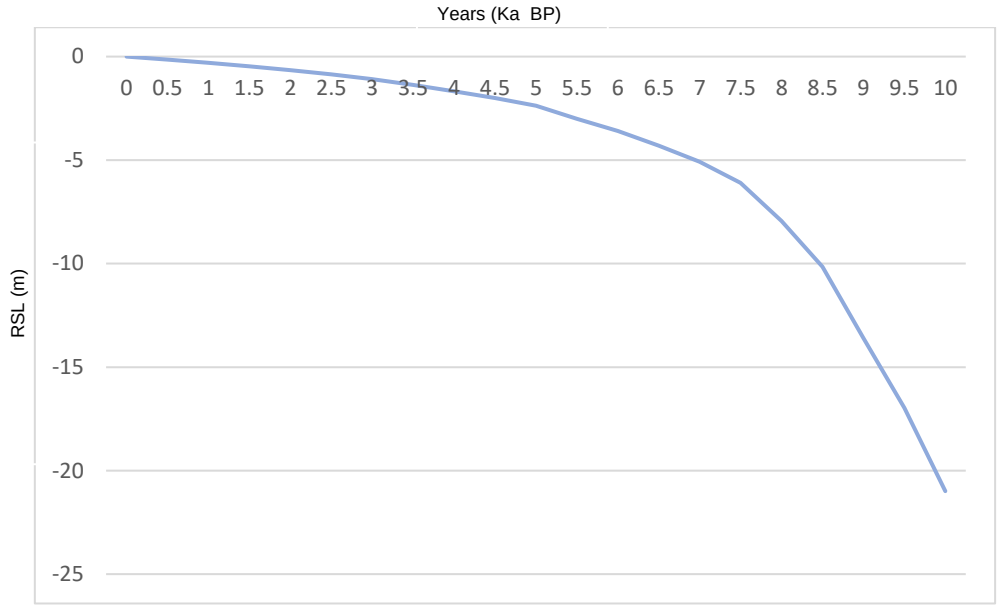

Figure 3.7: *A focused RSL curve from the data above, which highlights the RSL for the last 10,000 years of the Holocene. Present day sea-level is 0 m.*

CHAPTER 4: DISCUSSION

The results of my study indicate that the current coastline of north Torbay is actively eroding under modern RSL. Furthermore, north Torbay's coastline also has geomorphic features, which were formed ~125,000 years ago, and are currently subject to ongoing erosion processes today. In the following chapter, I re-evaluate the antiquity and age of the raised shore platform at Hopes Nose. In addition to this, I will also consider the Holocene evolution of the coastline, specifically cliff retreat and modern shore platform formation. Morphometric characteristics of modern and raised shore platforms are also analysed, providing an insight into the erosive processes currently acting upon north Torbay's coastline. Additionally, I will evaluate the unique combined application of cosmogenic nuclide exposure dating and UAV-SfM photogrammetry, as well as highlighting further areas of potential research.

4.1. Holocene Cliff Retreat

As summarised in section 1.2.2., previous studies have established that mass movements are the primary drivers of rocky coastline cliff retreat (Andriani and Walsh, 2007; Masselink et al., 2014; Recorbet et al., 2010; Rosser et al., 2013; Vann Jones (née Norman) et al., 2015). All cliff sections analysed along the north Torbay coastline are considered actively eroding during the Holocene. Specifically, all the mass movements occur after 6 ka BP (Table 3.1), once RSL was within 4 m of present day sea-level, as seen from the modelled RSL (Figure 3.3B). Modern tidal regimes in Torbay have a range of around 4-5 m in height (Mottershead et al., 1987). A similar RSL height is estimated to have occurred

along the north coast of Norfolk (UK) around 5300 Ka BP, by Boomer and Horton (2006), with RSL reaching ~ 4 m below present day RSL at this time.

Therefore, when RSL reached within 4 m of the present-day sea-level at Hopes Nose, it is likely that the water level at high tide reached the base of the cliff, especially during high swells and storms (Bird, 2011; Soldati et al., 2018; Trenhaile and Kanyaya, 2007). There is a strong relationship between these tidal movements and the associated seismic waves, which are transferred through the cliff, causing it to shake and trigger cliff failures in the form of mass movements (Lim et al., 2011; Vann Jones (née Norman) et al., 2015). As the tide reaches and submerges the cliff base at north Torbay there is an increase in the optimal delivery of wave energy (Lim et al., 2011). Consequently, any pre-existing and relict sea cliffs are subjected once again to mechanical and hydraulic erosive processes, as well as seismic shocks which trigger the stochastic mass movements driving rocky coastline evolution (McKenna et al., 1992; Savelli et al., 2017; Yanites et al., 2009). Modern day analogues of reactivated coastline retreat at previously abandoned coastlines can be found in Brittany, France, where a rise in sea-level and storm frequency resulted in the reactivation of coastal retreat and erosion in 2007 (Van Vliet-Lanoë et al., 2016). This previous study supports my hypothesis that reactivation of cliff retreat and erosion occurred at north Torbay's coastline around 6 ka BP.

The aspect of the cliff also appears to influence how the coastline of north Torbay erodes through mass movement events. Samples taken from cliffs at Meadfoot Beach (TOR-01), Beacon Cove (TOR-05) and Peaked Tor Cove (TOR-07) all show cliff failure during the early stages of RSL rise. It is possible to associate this occurrence with the open nature of the coves, as well as their south-westerly aspect. This combination situates them in the prime location for the prevailing

and dominant wave regimes in north Torbay. The relationship between dominant wave forces and the exposure of the coastline relative to wave direction is well documented in the literature, for example Kennedy et al (2018), Naylor and Stephenson (2010) and Trenhaile and Kanyaya (2007). These studies outline the influence of waves and the processes associated with them, as one of the primary controls of rocky coastline evolution over time (Abuodha and Woodroffe, 2010; Lim et al., 2011). The linear nature of exposed and open coastlines results in them being considered at “high risk” to changes in RSL, assailing wave forces, storms and swells (Abuodha and Woodroffe, 2010; Andrade et al., 2002; Council et al., 2007; Del Río and Gracia, 2009). As the RSL reached the base of the coastline in north Torbay around 6 ka BP, increased wave activity likely exceeded its resistant lithology, causing cliffs to yield to the wave energy and erosive forces. This is turn triggered the mass movements, which I have dated to the early Holocene.

Many studies acknowledge the importance of resistant lithologies, sometimes referred to as rock strength, which characteristic of rocky coastlines, Adams et al (2002), Dickson and Woodroffe (2005) and Andriani and Walsh (2007). However, these studies also identify the influence and importance of additional contributing factors, such as weathering, which lower the resistance and dominance of lithology as a significant control on coastal evolution (Gómez-Pujol et al., 2006). Research by Chelli et al (2010) identifies that where weathering rates are minimal, the lithology of the coastline is primarily dominant in influencing its strength and resistance to erosive processes. As weathering rates (and thus influence) increases within the environment, the role of lithology and overall rock strength decreases significantly (Chelli et al., 2010). In relation to my study, it is possible to assume that during the Last Glacial Maximum (LGM) the cliffs of

Torbay were subject to severe weathering conditions (e.g. wet/dry cycles and freeze/thaw cycles). Therefore, it is possible to assume that these conditions weakened the lithology of the cliffs, which increased their vulnerability. This in turn, decreased their resistance to increasing wave energies and erosive processes during the early Holocene (Dickson and Woodroffe, 2005).

In addition, it is not possible to rule out the influence of pre-existing fractures and inconsistencies within the cliffs lithology (Appendix 1 Figure 6.3), This could have possibly been exacerbated by weathering during the LGM and later by rising Holocene sea-levels (Bird, 2011; Masselink et al., 2014; Valvo et al., 2006). Joint inclination, tension fractures and discontinuities within cliff stratigraphy can all influence the way in which the cliff evolves over time (Bird, 2011; Rao et al., 1985). Tension fractures can be exacerbated by rain and groundwater seepage, which widen the fractures, and can trigger the loss of material through mass movements (e.g. rock falls) (Davies et al., 1998; Duperret et al., 2017). This type of coastal erosion can be seen along the Cornish coastline, as well as the near parallel coastal fractures along the Murgia Coastline (southeast Italy) (Andriani and Walsh, 2007; Bird, 2011). In addition to this, seeping water can also create new weaknesses within the cliff (e.g. cracks and holes), as well as expanding particular sediments (e.g. clay) or forming ice, which forces cracks to widen within the cliff (Davies et al., 1998; Masselink et al., 2014). Despite the influence and interest surrounding the influence of these variables in coastal erosion and evolution, it is often noted and argued that wave impact and the associated undercutting of the cliff face is the primary trigger of mass movement events, some of which is seen at Hopes Nose (Davidson-Arnott, 2010).

In contrast to previously mentioned samples and earlier mass movements, TOR-06 (also collected from Peaked Tor Cove), has a much younger exposure age

which indicates a more recent mass movement (Table 3.1) This can be attributed to the site being a relatively sheltered area, which faces a smaller body of water, rather than the open ocean as TOR-07 (Council et al., 2007). Typically, sheltered coastlines experience lower wave energies and tidal influence, possibly causing a time-lag between RSL changes and rocky coastline response (Abuodha and Woodroffe, 2010; Council et al., 2007; Davies et al., 2006). As a result, sheltered coastlines exhibit a more irregular wave pattern and slower evolution, which in turn creates distinct geomorphic components and environments, such as the undercut cliffs in Bermuda (Council et al., 2007; Neumann, 1966).

However, the assumption that these more recent mass movements are purely associated to their sheltered nature, disregards the possible occurrence of multiple mass movements in the last 7,000 years. Research suggests that mass movements reoccur on a cyclic basis, between steep and gentle profiles, that then return to a more stable profile, with the reoccurrence period driven by site-specific factors (Sunamura, 2015). An example of this can be seen in Black Ven (Dorset). Research by Brunsden and Chandler (1996) and Chandler and Brunsden (1995) identified a 50 – 60 year reoccurrence period or cycle of major activity and episodic landform change. Therefore, it is possible that the younger exposure ages are representative of reactivated coastal sites. If this is the case, the results still represent the episodic and stochastic nature of the mass movements along north Torbay's rocky coastline.

The corresponding timing of mass movements with RSL change implies that the attainment of modern sea-level is the controlling factor of cliff stability, and thus coastal evolution in north Torbay. These results are similar to the conclusions drawn from research on the coastline of Cassis, France (Recorbet et al., 2010). Although my dataset is limited in extent and sample size, there is no other obvious

pattern to the dated events. This is dissimilar to the specific clustering of events, which are associated with periods of elevated activity along the coastlines seen by Recorbet et al (2010), where ages cluster around 6.7 ka BP and 3.5 ka BP. Dated mass movement in my research are less consistent in time, indicating that cliff retreat rates along north Torbay's coastline are stochastic in nature, with thousand year intervals between some of the mass movement events. Interpretation and comparison of my results with previously published findings, also highlighst the coastal processes and environmental changes which trigger and control coastal mass movements in north Torbay.

It must be noted, that due to the low height of the cliffs (maximum height of 15 m), there is the possibility of inheritance in cliff face samples produced at depth by muons. Research by Hurst et al (2016) identified that ^{10}Be exposure ages of cliff inheritance from deep muonic production accounts for around 10-50% of the overall measured concentration of ^{10}Be. As discussed in section 2.1.1. muons play a significant role in the production of ^{36}Cl in calcium and thus the predominantly calcium carbonate cliffs at Torbay. However, it is difficult to estimate the magnitude of such inheritance. The tops of the cliffs are likely to be eroding in a quasi-steady state with regional denudation rates. The only available regional rates are for Dartmoor where cosmogenic nuclide measurements are consistent with denudation rates of 20-40 m/Ma on granite (Gunnell et al., 2013). These values are likely to be a minimum estimate on the much more easily eroded limestone and mudstone along the coast of Torbay. Consequently, a rate of coastal retreat at 40 m/Ma may result in an inheritance of ~1 ka on a limestone cliff 10 m high. For example, TOR-01 was obtained from a cliff around 10 m high, therefore the exposure age of 3.8 ± 0.72 Ka BP may be overestimated by ~1 Ka, resulting in an exposure age of ~ 2.8 - 3 Ka BP. While the role of inheritance plays

a possibly significant role in the exposure ages obtained along Torbay's coastline, the conclusions drawn on the sporadic nature of cliff retreat and the quick reactivation/rejuvenation of the coast in relation to RSL rise remain the same. To fully understand and calculate the degree to which inheritance influences the exposure ages of samples taken in my research I could collect further samples from sheltered areas (e.g. caves), or more recent landfall locations of a known age. From this a steady state concentration of muonic production could then be calculated using Lal (1991) and then subtracted from the overall exposure age obtained, for all the samples taken in north Torbay, to achieve a more accurate age for the coastline at Torbay.

Mass movement is not the only process that influences the retreat and erosion of rocky coastlines. Dislodged sediments from the cliff face cause mechanical erosion (e.g. abrasion), which result in the incremental loss of material from the cliff face and vertical lowering (de Lange and Moon, 2005). Incremental erosion rates of outcrops in the swash zone of Peaked Tor Cove range from 0.58 ± 0.07 m/Ka^{-1} and 0.49 ± 0.05 m/ Ka^{-1} (TOR-04a and TOR-04b). This vertical rate of erosion is associated with mechanical erosive processes, especially abrasion (section 1.2.2.2.), which is evident from the smooth surfaces of the rock and the backing seawall at Peaked Tor Cove (Appendix 1, Figures 6.2C, 6.2D and 6.2F). This is a significant rate of incremental erosion and vertical lowering for a rocky coastline, similar to vertical lowering rates along much warmer Portuguese limestone coastlines (Andrade et al., 2002). Lowering rates here are reported to be between 0.4 and 1.4 m/Ka (Andrade et al., 2002). However, the rate of incremental erosion in north Torbay is three orders of magnitude lower than the rocky incremental erosion rates recorded by Earlie et al (2015a) on the cliff faces of the Californian and Cornish coastlines, where incremental erosion rates fall

between 30 – 130 m/1000 years and 10 – 370 m/1000 years (Young et al., 2009). These incremental rates of erosion are similar to, or apparently exceed, rates measured from cliff faces consisting of softer lithologies, such as the Seven Sisters chalk cliffs (south coast of Great Britain), which retreat at 0.32 m/year equating to around 320 m every 1000 years (Hurst et al., 2016).

While it is possible that the use of alternating and nonuniform methodologies can results in some discrepancies, variations in the measured incremental erosion rates, either from the cliff face, bedrock situated in the swash zone or shore platforms, the rates are likely related to variations in lithology, geography, exposure and other environmental variables (Earlie et al., 2015a; Lee et al., 2001; Young et al., 2009). The apparent rate of incremental erosion in north Torbay, would be sufficient to remove any inheritance during the Holocene, from the bedrock outcrops, establishing steady-state erosion at the site. However, this remains an assumption due to the lack of information and understanding of Peaked Tor Cove's full exposure history. However, incremental erosion rates calculated from TOR-04a and TOR-04b are best interpreted as a minimum rate of erosion. This is due to the influence of water-shielding, related to daily tides in the short term and RSL changes over a longer time scale (Hurst et al., 2017; Regard et al., 2012). Water-shielding attenuates the cosmic ray flux to the bedrock, thus altering and lowering the overall production rate of ^{36}Cl over time in the bedrock (Hurst et al., 2017; Regard et al., 2012). This issue is further discussed within section 4.5.1. The influence of inheritance, discussed above, could also influence the incremental erosion rates, due to the high muon production of ^{36}Cl within limestone, sample location and frequent downwearing of the bedrock in the swash zone. As a result of this, the ^{36}Cl concentrations could

be overestimated, or at least skewed, by the existing/inherited ^{36}Cl already deep within the rock.

4.2. Dating Shore Platforms

4.2.1. Modern shore platform

The lower Holocene shore platform is being continuously created under the recently established modern sea-level and contemporary erosive processes, both vertical downwearing and horizontal cliff recession (section 1.2.2) (Trenhaile and Kanyaya, 2007). This is evident from the presence of the distinctive cliff-platform interface, located at current sea-level, as seen in the profiles taken across the platform (Figure 3.2). The interface marks the position of high tide and full inundation of the shore platform, covering the AOI outlined in Figure 2.5, as well as orientating itself with the dominant wave and tidal regimes at the site (Trenhaile, 2010; Trenhaile et al., 2015). The lowest recorded elevation from the modern shore platform AOI is 4.6 m below present sea-level. The modern shore platform could have been initiated shortly after 7 ka BP when sea-level (~ 5m below present), reached near this elevation. The modal elevation of the modern platform is 3.08 m below the present RSL. Similar Holocene shore platforms are seen along the Bristol Channel, some of which measure similar widths up to 100 m wide, such as at Nash Point (Glamorgon Heritage Coast) (Bryant and Haslett., 2007). These platforms are seaward sloping and are reported to have formed under sea-levels rising ~1 mm a year over the last 5000 years of the Holocene. This is a similar rate of RSL rise over the last 7000 years at Hopes Nose, where modelled RSL rose ~0.72 mm year (Trenhaile., 2010). Due to these similarities, it is possible to compare these examples and assume there is a possibility that the modern shore platform could have formed during this timeframe, especially

due to the increased wave exposure of Hopes Nose compared to the Bristol Channel.

Similar morphological features of shore platforms, along the Otranto coast, highlight a RSL stand-still around 3.8 m below the current RSL between 3400 and 2400 years BP (Sansò et al., 2016). The stand still at this time resulted in cliff recession through the development of deep notches along the Otranto coast(Sansò et al., 2016). It is possible such recession occurred during the evident slowing of RSL rise at Hopes Nose around this time (Figure 3.7), which could have carved the main body of the platform. However, the re-acceleration of RSL rise during the Holocene shifted high rates of horizontal cliff retreat and vertical lowering rates to higher elevations, with the cliff-platform junction eroding backwards with the rise in sea-level and tidal range.

In addition to this, there is abundant research which highlights that the seaward edge, defined as the point where active erosion of the bedrock/shore platform ceases, does not remain static over time and often shifts with changes in RSL (Kennedy., 2015). As a result, the width of the modern shore platform is likely an underestimate, meaning the shore platform could possibly be wider than reported within my research. At the seaward edge, the vertical lowering efficiency decreases with the increased water depth, and thus vertical lowering has appeared to have ceased within the lowest and oldest sections of the Holocene platform at Hopes Nose (Stephenson, 2000; Trenhaile, 2010). Therefore, caution must be taken when making such an interpretation of age, due to vertical downwearing of the shore platform resulting in post-inundation elevation changes (Moses et al., 2014). Vertical downwearing can range from <1 mm/year to a few cm/year, with more than one contributing process (Bird, 2011; Moses et al., 2014;

Trenhaile, 2010). Consequently, the estimation of platform initiation and formation is difficult to determine within 1 m.

However, due to the width of the modern shore platform there is also the possibility that it could be inherited from a previous interglacial cycle, where RSL was the same or similar to that of today. Studies, such as Trenhaile (2001), identify that platforms in resistant lithologies which exceed around 60 m in width are likely inherited from previous interglacial cycles. Platforms which exceed this width, in resistant and slowly eroding coastline, are often seen as the "main evidence" of inheritance along rocky coastlines (Trenhaile., 2001; 2002). As the width of the modern shore platform at Hopes Nose exceeds what is classified by Trenhaile (2001) as a "narrow platform" (40 – 60 m), the possible influence of inheritance cannot be ruled out without the direct dating of the platforms surface. Consequently, my interpreted Holocene age of the modern shore platform is based upon circumstantial interpretation of shore platform elevations, in relation to the modelled RSL of Hopes Nose, and is not certain without the use of direct dating methods.

4.2.2. Inherited shore platform

The exposure ages of samples taken from the raised shore platform at Hopes Nose were 8.35 ± 0.69 ka BP and 10.14 ± 0.81 ka BP respectively. These ages coincide with the approach of present day sea-level, However, it is not plausible for a platform as wide and as elevated as the one at Hopes Nose to have been created within this time period. This is evident from the RSL curve which places the sea-level at this time around –20m to –13m.

Dating of raised beaches at the site by Mottershead et al (1987), as outlined within section 1.5.3, provides relative dating of the shore platform in association

with a past interglacial period of higher sea level, which I have estimated to be MIS 5e. The elevations taken from the raised shore platform have a significant range, where the lowest elevation of the shore platform is measured as -3 m (Table 3.4) This elevation can be related to the post-formation erosion and erosion of the elevated platform at Hopes Nose, as it is slowly being destroyed under contemporary processes acting upon it, such as platform undercutting and destabilisation (A. S Trenhaile, 2002). Evidence of collapse can be seen in the aerial image in Figure 2.5 and Appendix 1 Figure 6.4, where undercutting of the shore platform has led to destabilisation and the formation of detachment grooves through the removal of material (Salzmann and Green, 2012). As a result, localised faulting of the platform has occurred, resulting in a downward displacement of a section of the platform.

The modal elevation of the raised platform measures 3.75 m above present mean sea-level. The junction of the palaeo-cliff and palaeo-platform is situated ~4-6 m above present sea-level (Figure 3.2 and Figure 3.4), which marks the mean high water mark of the elevated sea-level associated with MIS 5e (Stocchi et al., 2018; Wright, 1970). Comparison between the observed elevations of the raised shore platform and the modelled RSL curve indicates that the raised shore platform is most consistent with having been formed during the last interglacial (MIS 5e).

The maximum elevation of the raised shore platform is 8.6 m above present sea-level. This represents the maximum extent of inward growth of the shore platform, as well as recording the elevation of interglacial high tide (Shennan et al., 2014; Trenhaile, 1999). If the tidal height of north Torbay was the same as present (4-5 m), then the maximum elevation measured from the raised shore platform compares closely to predicted high tides during the last interglacial. These high tides possibly reached a maximum height between 8 m and 9 m above present

sea-level. At the southern end of the Hopes Nose, elevated beach sediments can be found 10-12m above present sea-level (Mottershead et al., 1987) (Figure 1.9). This is a familiar feature, as seen in west Galicia (northwest Spain), where shore platforms are closely associated with ancient beaches dated to the last interglacial (Blanco Chao et al., 2003). During the last interglacial, it is likely that these sediments were deposited towards the landward boundary of the shore platform by tidal and wave action (Twidale et al., 2005). As RSL dropped to present day levels, the beach sediments at Torbay are therefore situated beyond the reach of present tidal regimes, only being eroded during periods of high swells and storms (Blanco Chao et al., 2003). Thus, the elevations of these sediments are associated with the maximum elevation of the raised platform, which also confirms the MIS 5e age of both the raised shore platform and elevated raised beach sediments (Twidale et al., 2005).

It is unlikely that the elevated platform dates to older interglacials, such as MIS 7 and 9, as Hopes Nose is not an actively uplifting coastline where such ancient features are often observed (Lee et al., 2015; Pedoja et al., 2006; Rostami et al., 2000). Tectonically stable coastlines have insufficient rates of uplift to isolate features from reoccupation and reworking during other sea-level highstands such as the last interglacial, when sea-level heights exceeded those of MIS 7 and 9 (Mastronuzzi et al., 2007). This is also seen at Banks Peninsular (New Zealand), where tectonic stability and low rates of movement preserved shore platforms situated 6 – 8 m above the present sea-level (Lawrie, 1993). In addition to this, the modelled RSL curve highlights a period of RSL stability between 125 ka BP and 120 ka BP, with the low tide water level averaging ~3 m above current sea-level (Gill, 1972; Hearty et al., 2007; Stocchi et al., 2018). Similar stability is outlined in research by Hearty et al (2007), highlighting that such stability resulted

in the morphological imprint of the highstand along many rocky coastlines, such as the Mediterranean, Bermuda, Europe and western Australia. It is likely that the main body of the raised shore platform was carved from Torbay's coastline during the MIS 5e, where sea-level was ~3 m above the current sea-level.

4.2.3. Platform covering

Given the probability that the elevated shore platform was formed during MIS 5e, the exposure ages are much younger than expected, with TOR-08 producing an age of 8.35±0.69 Ka BP and TOR-09 an age of 10.14±0.81 Ka BP. During the MIS 5e interglacial, RSL and process which operated along the coast enabled considerable stripping of material and any inherited ^{36}Cl in the limestone from previous exposures, leading to surface renewal (Raimbault et al., 2018). As a result, it can be assumed that the exposure ages, obtained from the shore platform, are likely to be an accumulation of exposure over time. This indicates a complex exposure history with shielding of the platform from both exposure to cosmic rays and erosion (Dunai, 2010; Twidale et al., 2005). Consequently, this makes determining the shore platform age from the exposure dating extremely difficult (Blanco Chao et al., 2003; Choi et al., 2012; Trenhaile et al., 1999).

The most likely source of shielding is revealed in the back cliff. The detailed orthophotograph of this section shows low relict cliffs, covered by a solifluction layer, comprised of poorly sorted fine and clastic sediments, known as diamicton, (Gallagher et al., 2015). As well as this, periglacial features, such cryoturbation are also present, highlighting repeated freezing and thawing cycles within the environment (Figure 2.6) (Veit et al., 2017). The solifluction layer likely extended over the platform during the periods of lower sea-level, when this region likely formed a periglacial environment. This is dissimilar to other settings, where

sediments have more marine or colluvium origin, as seen in the backing sediments of shore platforms in Scotland (Firth et al., 2018; Shennan et al., 2014).

Due to the significantly younger ages obtained from the exposure dating, it is possible to assume that solifluction covered the platform in quick succession of the sea-level highstand termination around 119 ka BP by 40 m. This coincides with significant decreases in regional temperature, between 3 and 2 ºC, as recorded in the GRIP ice cores during MIS 5e/5d transition (Engels et al., 2010; Wohlfarth, 2013). Temperatures possibly reached 6 ºC lower than today, during the main part of MIS 5d (Capron et al., 2010; Engels et al., 2010; Hearty et al., 2007; Wohlfarth, 2013). From the combined heights of the relict cliff and overlying sediments, the solifluction sheet is likely to have measured between at least 3 and 4 m in depth above the shore platform. A sediment sheet of this thickness would effectively shield the underlying platform from most cosmic rays and prevent the accumulation of ^{36}Cl via spallation, post MIS 5d. However, muonic production of the cosmogenic nuclides can still occur, possibly contributing to the overall accumulative ages obtained from the raised shore platform (Dunia, 2010). The solifluction sheet persisted as a result of low sea-level until the late Holocene transgression. At this point sea-level began to reach levels where large swells, shore high-stands and storm surges were able to inundate the platform and erode the weakly consolidated solifluction sediments, re-exposing the shore platform once again (Blanco Chao et al., 2003; Twidale et al., 2005).

Further morphological evidence which suggests that the platform was likely covered for a substantial period of time is the presence and characteristics of the solution pans, which are common across the raised shore platform (Appendix 1 Figure 6.5). Solution pans which cover the shore platform measure an average depth of 9 cm, with some being as shallow as 4-5 cm, indicating a relatively short

period of exposure. Current rates of solution weathering on limestone have been measured by Wilson et al (2012), obtained on pavements in the Yorkshire Dales. Although not the same region, weathering rates in the Yorkshire Dales can provide a rough estimation of weathering on the raised shore platform in north Torbay. It is possible to assume that weathering of the raised shore platform would be around 2 m, if exposed for 122.5 ka BP after the drop in sea-level, effectively destroying the morphology of the platform. This must be considered a minimum rate of solution weathering, with the proximity of salt-bearing spray, wind and humid temperate conditions resulting in enhanced weathering rates, as well as significant local environmental variation (Mottershead, 1998). However, while this is not entirely representative of the significant limestone weathering which occurs along many coastlines, shielding of the elevated shore platform by the solifluction sediments explains the generally excellent preservation of such an old limestone landform.

4.3. Shore Platform Classification and Erosion

4.3.1. Shore platform classification

The presence of shore platforms on rocky coasts is not uncommon, and are found along approximately 20% of the coastline of England and Wales (Trenhaile, 1974). Many studies have attempted to understand the ways in which shore platforms develop, often categorising them through their morphological characteristics (Bird, 2011; Sunamura, 1992; Trenhaile, 1974). Shore platform characteristics vary in relation to geology, morphometric factors such as aspect, and marine factors such as tidal range and wave regimes (Bird, 2011; Ogawa et al., 2016). As outlined within section 1.2.1, Sunamura (1992) classifies Type-A and Type-B shore platforms, yet the relationship between these two

classifications are debated. While most literature agrees that Type-A and Type-B platforms are two distinct platform morphologies which are based upon site specific variables, there are some studies which present other theories (Trenhaile, 1987). For example, Gill and Lang (1983), argue that these platform types represent different stages of platform development, eventually evolving towards a profile in equilibrium. As a result, most single site studies on shore platforms apply the categories specifically to what appears to be occurring on the coastline of interest, making them localised in nature (Ogawa et al., 2016).

In addition to this, further debate surrounds the contribution of wave erosion and weathering on shore platform development (Bird, 2011; Matsumoto et al., 2018; Stephenson, 2000). It is often assumed that wave and tidal processes are responsible for the formation of seaward sloping Type-A platforms, whereas weathering is a dominating process in sub-horizontal Type-B platform formation (Cruslock et al., 2010; Matsumoto et al., 2018; Ogawa et al., 2016, 2011; Sunamura, 1992; Trenhaile and Kanyaya, 2007). The results of the morphometric analysis of the modern and raised shore platforms at Hopes Nose are considered alongside current literature to categorise them (relative to Sunamura (1992) Type-A and Type-B platforms), and determine the processes operating upon them.

The morphological characteristics of both shore platforms at Hopes Nose provide a key reflection of interactions between a series of dependent and independent variables, over varying timescales and under an array of different environmental conditions (Alvarez-Marrón et al., 2008). Transects taken along the modern shore platform show that it has a relatively smooth and gradual seaward sloping platform, from the distinctive cliff-platform interface (Figure 3.2). There are no sudden step changes or change in gradient, extending under the sub-tidal zone

(Duperret et al., 2017). These characteristics are similar to those shore platforms which are classified as “Type-A” shore platforms by Sunamura (1992). Type-A platforms are frequent around England and Wales, as well as many other exposed coastlines bordering highly energetic wave environments, such as the coastline of Ireland (Cullen and Bourke, 2018; Duperret et al., 2017; Trenhaile, 1974).

As previously highlighted in section 4.2.1, the modern platform has a distinctive cliff-platform interface, a common characteristic of contemporary Type-A shore platforms, situated at the current high tide mark (Matsumoto et al., 2017). However, it is likely that this was not the starting location of the interface following the modern shore platform possible initiation around 7000 – 6500 years ago, when RSL at Hopes Nose was located between 4-5 m below present day. Consequently, the modern shore platform was created under a rising sea-level. Trenhaile and Bryne (1986) highlight that Holocene RSL changes promoted the formation of wide and gently sloping Type-A shore platforms in the northern hemisphere, especially in areas located at the furthest point of the forebulge collapse areas, such as the southwest of England (Trenhaile., 2010; Trenhaile and Bryne., 1986). Similarly, Type-A shore platforms in the Bristol Channel were created under slow rising RSL, which averaged around 1 mm yr^{-1} over the last 5000 years (Trenhaile., 2010). Similar slow RSL rates are also seen over the last 5000 years of the Holocene at Hopes Nose, calculated at around 0.6 mm yr^{-1} from the modelled sea-level curve. Due to this, the wide and sloping Type-A characteristics of the modern shore platform can be partly attributed to RSL rises during the late Holocene period. However, current platform morphologies can only be partly explained by rising RSL. This can be influenced by other variables

including climatic changes, tidal range, wave intensity and rock resistance (Trenhaile and Bryne., 2010).

The gentle sloping platform surface and toe extending below the low tide level of the sea suggests that the modern platform is also dominated by the diurnal tidal cycle and processes associated with wave action (Duperret et al., 2017; Marshall and Stephenson, 2011; Stephenson et al., 2018). The gradient of Type-A platforms is strongly linked to spring tidal range and rock resistance of the platform, both of which are especially high within the macrotidal setting and Devonian sediments of Hopes Nose (Matsumoto et al., 2017; Trenhaile., 1999). This specific morphology exerts an important control on the amount of energy that reaches the inner platform, and consequently the backing cliff face (Marshall and Stephenson, 2011). The shore platform edge and sloping gradient promotes the formation of spilling breakers, making it the principal site of wave and energy dissipation, varying with the height of the tide (Earlie et al., 2018; Kennedy et al., 2017b; Kennedy et al., 2018; Marshall and Stephenson, 2011). This has been noted within many coastal settings around the world where Type-A platforms are identified, for example Mudstone Bay (Kaikoura, New Zealand) and Browns Creek (Apollo Bay, Australia) (Marshall and Stephenson, 2011).

In addition, Type-A morphology alters and exacerbates the erosive processes, such as abrasion (Matsumoto et al., 2017; Trenhaile, 1999). Abrasion is an important mechanism in shore platform development, as discussed in section 1.2.2.2. Abrasion takes place specifically in the shallow waters of the surf zone, particularly near the cliff and upper tidal limit, where shore platforms primarily develop (Beetham and Kench, 2011). As a result of the platforms sloping morphology, water depths are forced to transition from intermediate depths around 3–4 m at the platforms toe, to shallow depths of 0.5-1 m across the main

body of the platform, which is further influenced and changed by tidal regimes (Beetham and Kench, 2011; Trenhaile, 2000). In this zone sediments are suitably coarse and well mobilised, resulting in submarine abrasion an thus the removal of material weakened by weathering processes (Blanco-Chao et al., 2007; Bradley, 1958; Stephenson, 2000). Abrasion results in downwearing, which varies related to environmental factors and the lithology of the shoreline (Bird, 2011). Abrasion is seen as a consistent incremental loss of material within rocky coastline environments, which greatly increases during storms (Cullen and Bourke, 2018). Rising sea-levels, such as those seen during the early Holocene, also caused the abrasion zone to migrate gradually to the present high tide level (Blanco-Chao et al., 2007). This contributed to the difficulty of dating the initiation of modern shore platforms, which were likely initiated within the early Holocene, and discussed in section 4.5.2.

It is most likely that the raised shore platform is inherited from the last interglacial sea-level high-stand, as discussed in section 4.5.3. Under the elevated sea-level of MIS 5e, it is likely that the raised shore platform shared similar Type-A characteristics with the modern shore platform, as it was probably formed and shaped under a similar wave environment to what we see today at Hopes Nose (Alvarez-Marrón et al., 2008). This conclusion can be drawn from some of the more gently sloping profiles of the raise shore platform, as well as the similar range in the height of the cliff-platform junction to the contemporary modern platform (Trenhaile, 1974; Wright, 1970).

However, the raised shore platform is categorised as a sub-horizontal (or “Type-B”) shore platform profile at present, due to the abrupt change in the platforms profile towards the seaward edge (Raimbault et al., 2018; Sunamura., 1992). While it is possible the raised interglacial platform may have initially formed as a

Type-B platform, with a much smaller seaward drop than we see today, it is unlikely. If it is assumed the tidal regime at Hopes Nose was the same as present, a macrotidal environment with large tides ranging between 4 and 5 m, then the conditions are not conducive with the usual micro/mesotidal environments that Type-B platform morphologies are constructed under (Bourke et al.,2017). Type-B platforms are also seen to form at the present sea-level in weaker lithologies and low-energy inlets, such as Atia Point (Kaikoura, New Zealand) and Hayley Point (Marengo, Australia) (Marshall and Stephenson., 2011). This is not the case at Hopes Nose, which is situated on a rocky headland, dominated by high energy wave environments and comprised of resistant Devonian shales, as outlined in section 1.5.3.

However, the raised shore platforms distinctive morphology can be seen to reflect significant alterations within the environmental conditions which operated over the platforms evolution, from MIS 5e to the present day. Rapid changes in the RSL between MIS 5e and MIS 5d (Figure 1.6 and Figure 3.4), resulted in the abandonment of the shore platform and thus the formation of the abrupt seaward termination of the platform's profile (Bird., 2011; Sunamura., 1992). Consequently, it appears that the raised Type-B shore platform has evolved from a Type-A seaward sloping platform, which was initiated and created under the stable RSL of MIS 5e, as a result of RSL changes.

The abandonment of the raised shore platform has also altered the active processes which shape the platform from a wave dominated environment, to one dominated by subaerial weathering processes (Naylor and Stephenson., 2010). Solution weathering is the main weathering process on the raised shore platform. The effects of solution weathering is evident from lower and more horizontal gradient of the elevated shore platform profile, when compared to the modern

platform (Raimbault et al., 2018; Stephenson and Kirk., 1998). Weathering dominates the horizontal intertidal sections of many actively eroding Type-B platforms around the world, such as Mount Louis (Gaspé, Québec), as well as many shore platforms located in warmer environments (e.g. Australia and New Zealand) (Cruslock et al., 2010). As the shore platform is significantly elevated above the present RSL, the role of wave and tidal processes has diminished within the intertidal zone, disregarding high swells and storm surges (Ogawa et al., 2015; Trenhaile and Kanyaya., 2007). However, the terminating cliff of the platform results in highly reflective waves, which have a significant geomorphological importance in altering the platform profile evolution via undercutting (section 4.5.3.) (Laker, 2016; Ogawa et al., 2015).

Shore platform classification at Hopes Nose identifies the presence of the two types of platforms, as described by Sunamura (1992). The platforms at Hopes Nose highlight that while they can be considered within separate platform classifications at present, it is likely that the raised shore platform was once Type-A and then transition to Type-B, as a result of RSL changes. This supports arguments which suggest that the platform classifications are different stages of evolution, changing in combination with changes in its environment, moving towards an unknown state of platform equilibrium (Gill and Lang, 1983). In addition to this, it is possible to assume that wave erosion and weathering work synergistically with one another, in the development of both shore platform classifications (Matsumoto et al., 2018). Within this study I have not used methodologies which can be used to determine the degree of contribution of each process. However, it is clear that the processes which operate on the platforms are modulated by morphological and environmental characteristics, where wave

erosion dominants the modern Type-A shore platform and subaerial weathering dominants the raised interglacial Type-B platform present at Hopes Nose.

4.3.2. Shore platform erosion

In addition to classifying the shore platforms, I was also able to quantify a rate of retreat of the backing cliff, determined by the width of the shore platforms themselves. The width of shore platforms is determined by a number of factors, such as the lithology and time that has elapsed since platform initiation (Bird, 2011). How ever, it has been noted that there is a direct relationship between shore platform width and the exposure of the coastline to strong wave action (Ogawa et al., 2016; Trenhaile, 1999). This can be seen on the Japanese coastline, where sheltered platforms have an average width of around 40 m, while exposed platforms on the Pacific coast measure widths upwards of 60 m (Takahashi, 1977). On some exposed coastlines, it is possible for shore platforms to reach up to 170 m in width at low tide, such as in Glamorgan, if they are situated directly in prevailing and dominant winds and waves (Trenhaile, 1999).

The rate of shore platform formation for the modern shore platform, calculated in section 3.2.1 as 13 m a year, sits within our current understanding of shore platform development. This reiterates that shore platform development is a relatively short process, lasting only a few thousand years, with the seaward edge and width evolving through time (Raimbault et al., 2018; Sunamura, 1978a; Trenhaile, 1987). The calculated rate at Hopes Nose is at the high end of cliff retreat and erosion when compared to similar studies which use similar techniques, such as de Lange and Moon (2005), where cliff recession rates are 1.4±0.1 – 14.3±0.1 m every 1000 years. However, rate remain consistently lower than those seen along chalk or softer sediment coastlines.

However, as discussed within section 4.2.1 and throughout Stephenson (2008) (a commentary on de Lange and Moon, 2005), the seaward edge of shore platforms does not remain static through time, as suggested within de Lange and Moons methodology. The seaward edge moves in relation to changes in RSL and tidal range, sediment cover, erosional processes, as well as being obscured by the current wave and tides at Hopes Nose (Kennedy, 2015; Stephenson, 2008).

Furthermore, the possible role of inheritance on the modern shore platform must be considered, as there is the possibility that the entire modern platform width was not created over one interglacial cycle or the timeframe that I have specified. Stephenson (2008) stated that possible inheritance should mitigate against using this method, with results possibly being skewed by re-working of the coastline and other factors. Consequently, it is possible that the calculated erosion rates do not represent the true erosion rate of the shore platform, either resulting in an underestimate of cliff retreat due to the movement of the seaward edge, or overestimate of cliff retreat over the Holocene, as a result of inheritance from previous interglacial cycles.

Overall cliff retreat erosion rates of the modern platform can be attributed to the location of Hopes Nose, which is situated on a very exposed section of the coastline. As a result, there is frequent inundation of the platform from high swells and storm waves, with little protection, resulting in extensive mechanical and hydraulic erosion of the shore platform and its backing cliff (de Lange and Moon, 2005; Marshall and Stephenson, 2011; Matsumoto et al., 2017). It is unclear whether the differences between the results found at Hopes Nose and other studies can be attributed to the shore platforms geology, the processes operating on it or the environmental and geological setting of the coastline (Choi et al., 2012; Matsumoto et al., 2017).

The calculated rate of cliff erosion assumes a constant backwearing of the cliff over the selected time period. The exposure dating of north Torbay's coastline shows that rocky coastline retreat occurs through a series of larger stochastic and episodic falls. Consequently, it is possible to assume that cliff backing the shore platform experienced erosion which likely followed this episodic pattern and is not as systematic and consistent as the calculated retreat rates suggest (Duperret et al., 2017; Moses et al., 2014; Stephenson, 2000). In addition to this, it is recognised by many studies that as the platform increases in width, it starts to exert an important control on the amount of wave energy which reaches the backing cliff (Marshall and Stephenson, 2011). Consequently, it is possible that as the width of the shore platform at Hopes Nose increased, the amount of cliff erosion experienced diminished over time (Marshall and Stephenson, 2011; Ogawa et al., 2016). However, despite this and the difficulty of quantifying these variables, the calculated rates give us an understanding of the erosive magnitudes which are possible along the coastline of north Torbay.

The vertical downwearing of the shore platform is another important component to shore platform development (Blanco-Chao et al., 2007; Davidson-Arnott, 2010; Trenhaile, 2016a). Downwearing rates obtained from similar shore platforms and lithologies, such as Furlani and Cucchi (2013), measured and calculated a surface downwearing rate of 0.007 m to 0.205 m every 1000 years on the limestone shore platforms in the Gulf of Trieste (Italy). Due to similar wave environments, and the presence of sediments in the tidal and wave influenced area of the modern shore platform, downwearing rates and incremental erosion of the platform could have been accelerated, possibly placing the rate towards the upper end of this example or similar to Blanco-Chao et al (2007) (Dornbusch and Robinson, 2011; Robinson, 1977). These rates are measured along the

shore platforms in Galicia (northwest Spain), and are recorded between 0.13 and 1.8 m/1000 years (Blanco-Chao et al., 2007). However, without direct measurements from the modern shore platform at Torbay, expanding over several years and under different environmental conditions, the overall downwearing of the modern shore platform is not known and cannot be comment on with certainty.

4.4. Observed and Predicted Relative Sea-Level Changes

The extended ICE-6G chronology produced in this study was combined with the VM2 mantle profile, to create a RSL which considers the influence of GIA. This results in a local MIS 5e RSL curve that is not significantly different from the eustatic but is characterized by a ~1.0 m higher highstand. The latter is likely the combined result of the forebulge collapse which accompanied and followed the melting of the British Isles ice sheet (which were located further north), and of the far-field ice-sheets and meltwater redistribution, previously outlined in section 1.4.2.1.

Furthermore, the predicted RSL highstand for MIS 5e is in good agreement with the raised shore platform at Hopes Nose. The observed modal elevation of the platform measures a value of 3.76 m above present sea-level, and the modelled RSL is reported around 3 m above present sea-level. In addition to this, the highstand also correlates with findings by Hearty et al (2007), who suggests a period of stability within the MIS 5e highstand measuring a similar height, which likely persisted for a minimum of 2000 years to create the elevated shore platform.

Accordingly, it is possible to argue that:

1. The observed modal elevation of the raised shore platform corresponds with the RSL maximum of MIS 5e at Hopes Nose. This suggests that the MIS 5e highstand was characterised by a much lower eustatic sea-level than previously assumed.

2. Otherwise, it is possible that the observed modal elevation of the raised raised platform might not refer to the maximum MIS 5e peak in RSL, but could refer to a particular lower stand during the interglacial. This implies that the MIS 5e peak was characterized by two steps.

However, it is highly unlikely that the latter point is applicable to Hopes Nose. A two-step sea-level rise during MIS 5e would require the collapse and regrowth of ice sheets during the interglacial, yet there is no strong or significant evidence which suggests this occurred along Europe's northeast coastlines (Long et al.,2015). Similarly, there is minimal evidence of a two-step sea-level rise in either the ICE-5G or ICE-6G RSL models for Hopes Nose (Figure 3.3). However, there is evidence of the two-step within 3.6 Furthermore, the re-evaluation of evidence which supports the two-step theory also presents contradictory evidence (Dutton et al., 2015). For example, palaeocoastal features at Hergla (eastern Mediterranean) were previously dated to two MIS 5e RSL peaks, yet re-evaluation of the results has in-fact dated the features to two different substages of MIS 5 (global sea-level rise during MIS 5a and one later in MIS 5e) (Mauz et al., 2018).

Consequently, it is extremely likely that the modal elevations of the raised shore platforms represent the RSL maximum of MIS 5e, specifically for intermediate areas of coastline which are significantly influenced by GIA (Figure 1.5). When

GIA corrections are not applied to RSL models of similar intermediate and far-field sites (e.g. UK and Australia) a possible overestimation of 1–2 m can be seen in the eustatic sea-level for MIS 5e (Hay et al., 2014). As seen from Figure 3.3B, there is a departure from the predicted eustatic RSL curve for Hopes Nose, highlighting the influence and importance of GIA within the study areas RSL heights. Similar results are noted for other intermediate locations, such as Mallorca Island in the Mediterranean, where GIA corrected RSL for MIS 5e measured 2.15 ± 0.75 m above present (Polyak et al., 2018). Furthermore, in Figure 3.3B a gradual increase in RSL, around 0.5 m, is seen over the MIS 5e period. This could be related to the return of the mantle to previously loaded and glaciated areas, which gradually reduces the height of the forebulge and land over the interglacial period, thus increasing the RSL (Khan et al., 2015). This submergence and sea-level rise are currently seen throughout the Southwest during the Holocene, as discussed in section 1.5.2.1 (Shennan et al., 2009; Khan et al., 2015). However, while it is noted that the southwest is subsiding due to GIA, it is unlikely that this rate has distorted the true elevation of the raised shore platform to a great extent, as the platform elevations correspond significantly with the predicted RSL.

However, there are many studies across the globe which report much higher MIS 5e sea-levels from similar palaeocoastal features. For example, 9±1 in the Mediterranean (Mauz et al., 2012), 7.8–8.2 m from corals in the Seychelles (Dutton et al., 2015) and 6–8.5 m from marine sediments along African coastlines (Carr et al., 2010). The large variation of reported RSL at the global scale highlights significant spatial variability and can be attributed to local factors (e.g. uplift) and GIA feedbacks. Significant variations can possibly be attributed to the differences in the LGM and MIS 6 glacial extent, which are assumed to be the

same within my study. The glacial extent of the MIS 6 is greatly debated, and the possible occurrence of larger ice sheets during MIS 6 would increase the impact of GIA on RSL along coastlines similar to north Torbay. However, these conclusions are ambiguous, due to the uncertainties surrounding glacial extent during MIS 6, and are an ongoing challenge for glaciological and palaeoceanographic researchers (Hibbert et al., 2010; Long et al., 2015; Pawley et al., 2008)

4.5. Method Analysis

The novel combination and application of ^{36}Cl exposure dating and UAV-SfM photogrammetry was used to quantify the rate of coastal evolution in north Torbay, as well as determining the age of the raised shore platform at Hopes Nose. The following section outlines the effectiveness of the methods I have used in meeting my aims, as well as highlighting areas of uncertainty that have been considered. Furthermore, I will outline comparisons with existing literature, and include speculation of alternative methods which would produce similar results, but why they were not applicable to study of Hopes Nose. The aim of this analysis is to emphasise the suitability of cosmogenic nuclide dating and UAV-SfM within rocky coastline research, at both local and global scales.

4.5.1. ^{36}Cl Exposure dating

The application of cosmogenic nuclide exposure dating along north Torbay's coastline addressed the aims of my study. It revealed the stochastic nature of the Holocene cliff retreat, as well as contributing to our understanding in addressing the assumption that the elevated shore platform was inherited from a previous environmental period. As outlined within section 2.1.1, the application of this

technique is still in its infancy in application to rocky coastline environments. However, my study shows that it can be determined a suitable technique in similar research which focuses on rocky coastline evolution.

Cosmogenic nuclide exposure dating can be prone to random and systematic errors, which can influence the accuracy of calculated erosion rates and exposure ages (Dunai, 2010; Gosse and Phillips, 2001; Lang et al., 1999). These usually occur as a direct result of poorly known exposure histories, rates of incremental erosion and assumptions regarding the rate of production for the chosen isotope (Lang et al., 1999).

For example, water-shielding of samples obtained from bedrock at sea-level, TOR-04a and TOR-04b, can result in an underestimate and bias within the calculated incremental erosion rate, as briefly discussed in section 4.1. The degree of water-shielding varies with water depth and sample depth, as well as the time scale these changes occur (Hurst et al., 2017; Regard et al., 2012). Water attenuates the flux of cosmic rates and the overall production of cosmogenics (e.g. ^{36}Cl and ^{10}Be), within the sample, possible resulting in reduced production rates and thus underestimated exposure ages/erosion rates (Hurst et al., 2017). The location in which these samples were taken is extremely influenced by high and low tides, which results in water level and depth changes over the samples over short time scales (Regard et al., 2012). These simple diurnal or semi-diurnal tides can significantly influence and modify cosmogenic nuclide production within the surface of the rock sample (Hurst et al., 2017; Regard et al., 2012). Regard et al (2012) identifies that the periodic submergence of the upper intertidal zones of shore platforms during high tide, reduces overall cosmogenic production rates. However, the periodic exposure of the lower intertidal zone during low tides increases the production rate of cosmogenic

nuclides. Water level changes over larger timescales, such as RSL changes occurring across intertidal and glacial stadials, can also result in increased cosmogenic concentration (Hurst et al., 2017). As RSL rises, so does the water depth above the sample. This increased water depth results in decreased removal of material containing cosmogenic nuclides and thus an increased concentration (Hurst et al., 2017; Regard et al., 2012). Regard et al (2012) has developed mechanisms to account for, correct and calculate water-shielding adjusted production rates. While I have not applied these specific corrections to samples within this study, it is a possible area of future research, adjustment and methodological analysis.

Gosse and Phillips (2001) also calculated error magnitudes for other common error sources, to assist the understanding and accommodate the influence of errors on the calculated exposure ages. Similar errors are considered throughout this study, and are reduced through careful sample collection, calculation of an incremental erosion rates, as well as the selection of an appropriate scaling framework (Gosse and Phillips, 2001).

As outlined in section 4.1, cosmogenic nuclide dating successfully dated several mass movement events within the north Torbay region, in addition to providing an incremental rate of erosion. However, the application of cosmogenic nuclide exposure dating of the raised shore platform at Hopes Nose failed to provide a direct age (section 4.2). This can be attributed to the pre-conceived assumptions of the site's exposure history. The exposure ages obtained from the platform revealed it had a far more complex exposure history than previously assumed (section 4.2.3). This is in contrast to the study by Choi et al (2012), who obtained absolute ages ranging from 4 ka to 148 ka from the shore platform on the west coast of Korea, with no note of platform covering and shielding altering the

obtained age. The differences between these two studies highlight the importance of understanding the site's exposure history, to help ensure precise exposure ages are obtained, as well as the complex evolution of rocky coastline evolution.

Despite the success of cosmogenic nuclide exposure dating in assessing rocky coastline evolution at Hopes Nose, there are other techniques which could have been used to achieve similar results, which are synthesised in section 1.4 and Lang et al (1999). For example, radiocarbon dating is commonly used to provide an age of mass movement events, as outlined in section 1.4.3 and seen in research by Bertolini et al (2004) in the north Apennines (Italy). Additionally, lichenometry has been used to date mass movement events, which expose new rock surfaces for lichen to colonisation at a known rate (Lang et al., 1999). However, neither technique is as advanced or accurate as cosmogenic nuclide exposure dating, and requires either the presence of organic material for radiocarbon dating, or a specific lichen species for lichenometry measurements (Lang et al., 1999). Sampling sites at north Torbay had neither of these specific requirements, and if they were present there would be no guarantee they would provide accurate ages, which were directly associated with the mass movement or palaeocoastal feature itself.

Another plausible technique used to date exposed rock and palaeocoastal features is uranium-series dating (U-series) (Baker et al., 1996; Candy and Schreve, 2007; Knauss and Ku, 1980; Lang et al., 1999). U-series can be used to date carbonates, sinter-crusts and varnishes, which cover the rock face or reside above or within its cracks (Knauss and Ku, 1980; Lang et al., 1999). They commonly provide relative bracketing ages of mass movements or palaeocoastal features, rather than absolute or direct ages of the rock surface, which is possible

with cosmogenic nuclide dating (Candy and Schreve., 2007; Lang et al., 1999). However, it is unclear and unlikely that the appropriate sediments for U-series dating exist along north Torbay's coastline, as they usually only occur in arid or semi-arid environments (Knauss and Ku, 1980).

While it is clear there are other possible methods of dating, the application of cosmogenic nuclide exposure dating was the most suitable in assisting my understanding of coastal evolution in north Torbay.

4.5.2. UAV-SfM Photogrammetry

The use of UAV-SfM photogrammetry was extremely effective in my study, with results from the high resolution morphometric analysis of Hopes Nose addressing my studies aims. UAV-SfM furthered the understanding of erosive processes operating on the shore platform at Hopes Nose, both over long (millennia) and short (yearly or decadal) temporal scales. Furthermore, UAV-SfM provided an alternative to dating the elevated shore platform, where more traditional exposure dating techniques failed to do so.

However, similar to cosmogenic nuclide exposure dating, UAV-SfM photogrammetry also experiences errors and uncertainties, some of which are outlined in section 2.2.2. One major source of error relates to the amount of image overlap within the post-processing stage, and this can influence the overall quality of DEMs and orthophotos. Image sets with a low percentage of overlap restricts the orthomosaic production, reducing the accuracy of the final DEM (Gienko and Terry, 2014; Micheletti et al., 2015). This can be further exacerbated if images are excluded from the photogrammetric processing (e.g. due to low image quality) (Westoby et al., 2012). However, this was not a concern within my study, meaning the overall quality of the produced DEMs and orthomosaic were unhindered.

Another area of error, which can be specific to using either LiDAR or UAV-SfM photogrammetry to understand the morphology of shore platforms along rocky coasts, is the ability to delineate the seaward edge of the platform itself. This is noted within research by Carvalho and Woodroffe (2019), who acknowledge that even during low tides and calm weathering the remaining waves and white water may result in the inaccurate interpretation of the seaward edge. However, Carvalho and Woodroffe (2019) identify that tidal elevation appeared to be the most accurate and easiest variable to delineate the seaward edge of the shore platform. This variable was used within my study, ensuring that aerial images were acquired at a known time at low tide and in calmer weather, as suggested by Carvalho and Woodroffe (2019). This reduced the possible inaccuracies in shore platform morphological analysis.

Overall, the application of UAV-SfM photogrammetry at Hopes Nose has outlined its efficiency in producing a high resolution morphometric analysis. Similarly, recent research by Matsumoto et al (2017) identified the usefulness of using ground-based LiDAR as an alternative technique to acquire DEMs, used to understand past erosion events. However, UAV-SfM photogrammetry sill yields higher resolution data than those obtained via LiDAR measurements (<10 cm in UAV-SfM and >2 m in LiDAR) (Earlie et al., 2015a; Kennedy et al., 2014; Matsumoto et al., 2017). Consequently, UAV-SfM photogrammetry is more suitable in obtaining more precise elevations of palaeocoastal features. This is vital for the comparison of palaeocoastal features to RSL curves, where the coarse spatial resolution of LiDAR can result in palaeocoastal features being dated to the wrong environmental period (Kennedy et al., 2014; Polyak et al., 2018). Additionally, LiDAR's coarser spatial resolution increases the likelihood of missing or generalising vital geomorphological features (Earlie et al., 2015;

Kennedy et al., 2014). In doing so, key morphological features of shore platforms (e.g. cliff-platform junction and sea-ward edge), are not sufficiently captured and interpreted in high detail leading to wrongful interpretations (Kennedy et al., 2014; Swirad et al., 2016).

One similarity between LiDAR and UAV-SfM photogrammetry is the techniques in ability to collect data over deeper water, as seen through images in my study not being enabled in constructing the orthomosaic of Hopes Nose (Figure 2.3) (Duperret et al., 2017). Highly turbulent and turbid areas impact the light absorption which precludes the recognition of features which UAV-SfM photogrammetry is able to capture (Casella et al., 2017; Cook, 2017). LiDAR imagery is often limited to clear water depths up to 1 m, whereas UAV-SfM can penetrate deeper (<3.5 m) into more turbulent water (Charlton et al., 2003; Grenzdörffer and Naumann, 2016). Both LiDAR and UAV-SfM require specific adjustments to enable these photos within photogrammetry programming techniques. This characteristic of UAV-SfM is vital for looking at modern shore platforms at present sea-level, which is mainly covered by shallow and turbulent water (Kennedy et al., 2014; Smith et al., 2016).

Similarly, the MVM-SfM used to model the backing sediments at Hopes Nose also has an alternative technique, terrestrial laser scanning (TLS) which can also produce millimetre precision DEMs and orthomosaics (Caputo et al., 2016; Smith et al., 2016; Swirad et al., 2016; Teza et al., 2015; Veit et al., 2017). TLS provides the same opportunity as MVM-SfM, enabling contactless geometrical and morphological analysis, and is commonly used in coastal erosion studies (Bonneau and Hutchinson, 2019; Earlie et al., 2015a; Teza et al., 2015). TLS can also be used to further understand the overall lithology of a cliff face or backing sediments, where lithological changes can be identified and grain-sized

delineation is possible (Bonneau and Hutchinson, 2019; Teza et al., 2015). Consequently, this makes TLS a suitable alternative technique, which could have been utilised in the analysis of the backing sediments of Hopes nose. However, the use of MVM-SfM was more appropriate in my study, due to its more cost effective price, with TSL costing upwards of £30,000 (Smith et al., 2016). TLS is further limited by the lack of suitable acquisition locations within many coastal environments (Rosser et al., 2005; Smith et al., 2016; Westoby et al., 2012). Whereas, MVM-SfM allow for a wide variety of imaging techniques which can be used to construct the coastline of interest (section 2.2.1). This also reduces the amount of restricted areas available to the researcher, allowing complex coastlines and geomorphologies to be modelled and understood (Smith et al., 2016).

Overall, the use of UAV-SfM and MVM-SfM photogrammetry were the most suitable methods used to conduct my analysis of the shore platforms at Hopes Nose, when compared to the alternative techniques which are available. This is due to the higher resolution DEMs and orthomosaics that were obtained, which highlight key geomorphological features and allow for precise RSL comparison. Similarly, both UAV-SfM and MVM-SfM are more accessible to my research than more expensive techniques like TLS.

UAV-SfM is also significantly applicable to multi-temporal acquisition of data, allowing the potential measurement of erosion and costal evolution over time. This is seen in research by Swirad et al (2019), where SfM at a millimetre resolution was used at 15 sites to measure an average erosion rate of 0.528 mm/yr-1 along Hartle Loup (north Yorkshire, UK). This multi-temporal research identified important trends in erosion rates, highlighting considerable variability across the shore platform itself and the year of study, as well as increased erosion

during the summer months (Swirad et al., 2019). This is a potential avenue for future research using the USA-SfM and MVM-SfM technique within north Torbay, in addition to other areas of future research discussed further within the next section.

4.6. Wider Implications and Future Research

4.6.1. Future research at Torbay

Within my study I have revealed the complex processes, of both the past and the present, which influences the coastal evolution in north Torbay. However, further research in this region would be beneficial for increased understanding. This research should focus on increasing the overall understanding of the environmental and climatic variables, which control the erosional processes along the north Torbay coastline. Similarly, future work should aim to further quantify the rate at which overall erosion is taking place in north Torbay, as well as highlighting how these change in relation to climate driven changes within the area.

A possible way to further the work at north Torbay, would be to increase the cosmogenic nuclide exposure age database, through further sampling and dating of the rocky coastline between Hopes Nose and Torquay. As a direct result, factors which contributed to cliff instability and mass movements during the early Holocene, such as cliff aspect (section 4.4), could be analysed and reported with more detail. Furthermore, this would also establish a quantified frequency of mass movement events, extending over multiple climate scenarios, to help determine the long term rate of retreat and evolution in north Torbay. From this dataset it would be possible to identify areas of north Torbay's rocky coastline which are more vulnerable than previously assumed by current shoreline

management plans, where no intervention is currently in place, due to the apparent resistance of rocky coastline geology (Figure 1.10) (Cooper et al., 2002; Bernd-Cohen, 1999).

In addition to this, there is the possibility of extending this methodology and research around to the southern extent of Torbay, including the headland of Berry Head (Figure 1.9). Cosmogenic nuclide exposure dating of Berry Head would enable further understanding of how Torbay's crescent bay evolved. Similarly, this could also be compared with the findings from this study, to explore the influence of rising RSL and the cliffs aspect on mass movement events on both headlands at Torbay. Furthermore, research conducted by Hart and Gosling (2018) shows that Berry head hosts a number of elevated palaeocoastal features, such as raised beach sediments. UAV-SFM photogrammetry could be employed to obtained high resolution DEMs of these palaeocoastal features, which have previously been deemed inaccessible. These DEMs could be compared with RSL curves to obtain a confident age estimation of their formation. This would be useful to corroborate what has been found at Hopes Nose in my own study, but also to provide an additional reference point for RSL models of the southwest of the UK.

4.6.2. County level research

As well as the possibility of further research at north Torbay, the motivations, ideas and results from this study can influence and drive research at the county scale. Possible future research could focus on using the modelled RSL data for the MIS 5e within my study, to map and better understand the extent of submergence of the current coastline of southwest England under elevated RSLs (e.g. Exe Estuary), such as those predicted in future climate scenarios. This could

be achieved using ArcGIS digitisation of the modelled RSL extent, alongside mapping palaeocoastal features within and surrounding the submerged areas of coastline.

As well as this, there is the possibility of comparing other known palaeocoastal RSL indicators in the region. For example, the raised beach sediments at Saunton, Berry Head and Westward Ho!, where a 300 m wide shore platform is also present and likely to be a palaeocoastal feature (Keen and Campbell, 1998; Keene, 2011). The modelled RSL curve from my study could be used to possibly attain an age of formation for these palaeocoastal features, furthering the understanding inheritance and the influence of palaeo sea-levels on rocky coasts around the southwest.

Mapping the extent of interglacial sea-levels and correlating it with palaeocoastal features, can provide a proxy for future RSL rise within a region, such as the southwest of England. This is noted especially for MIS 5e, due to its similarity to our present Holocene interglacial, outlined by Hearty and Tormey (2017) and in section 1.5.3.1. Projecting future RSL in Devon, and other areas of the southwest, highlights areas which are at possible risk of flooding, increased erosion rates and overall loss of land and habitats. This information can be used to update or implement coastal management schemes along the county's coastline, which are in line with future RSL projections and possible risks.

4.6.3. Wider implications of research

In addition to the local understanding of coastal evolution in north Torbay, Devon and the southwest, my study has a series of wider implications, which both increase our understanding of the coastal environment, as well as opening rocky coastline research into a new frontier.

This study contributes to our overall understanding of the adjacent Jurassic Coast, which extends 95 miles between Orcombe Point (east Devon) and Studland Bay (Dorset). This high-resolution study of geomorphological change at Torbay builds upon research specific to the Jurassic coast, providing a nearby comparison of erosive magnitude, between a stochastically eroding coastline and one where erosive events occur more frequently (Bromhead and Ibsen, 2006; Brunsden and Jones, 1976).

In addition to this, the results of this study can be used as a comparison at the UK national scale, building on a series of works quantifying erosion and evolution around the coastline (Bromhead and Ibsen, 2006; Dornbusch and Robinson, 2011; Gallois, 2011; Hurst et al., 2016). For example, the erosion rates obtained from my research are comparable to those calculated by Jones and Williams (1991) along the west Wales coast (UK), where average erosion rates measure around 0.25 m yr^{-1}. Further comparison can be done from the individual cliffs measured within this study, such as erosion rates at Aberath (glacial embayment) and Aberaeron (clay), which both have high rates of incremental erosion, at 0.068 m yr^{-1} and 0.168 m yr^{-1}, than those calculated from TOR-04a and 4b at Torbay (Jones and Williams, 1991). Similarly, areas along the Suffolk coast are eroding at a much higher and frequent rate than the cliffs along north Torbay, with average erosion between 1883 – 1993 measuring 3.5 m yr^{-1}, rising to around 4.7 m yr^{-1} between 1993 – 2010 (Brooks et al., 2012). Through comparing erosion rates along the Uk's coastline, it is possible to distinguish the variables (e.g. lithology, tides, wave exposure, etc) which govern the way the cliffs evolve, either through low magnitude/high frequency events (Suffolk) or high magnitude/low frequency events (Torbay). Overall, this would allow us to determine the best and most effective methodology to manage the coastline.

This study can also provide a plausible comparative rate of erosion of other Devonian sediments, which are distributed around the UK coastline (Figure 4.1) (BGS, 2017). For example, Devonian sediments along the coast of South Cork (Ireland) erode at an estimated rate of 0.2 -1.6 m yr^{-1}, which is significantly higher than the rates measured for Devonian sediments in north Torbay (Clayton et al., 1979; DELG, 2001). Once again, comparing these studies allows for key morphological and lithological features to be determined and their influence on differing erosion rates in sediments deposited during the Devonian period.

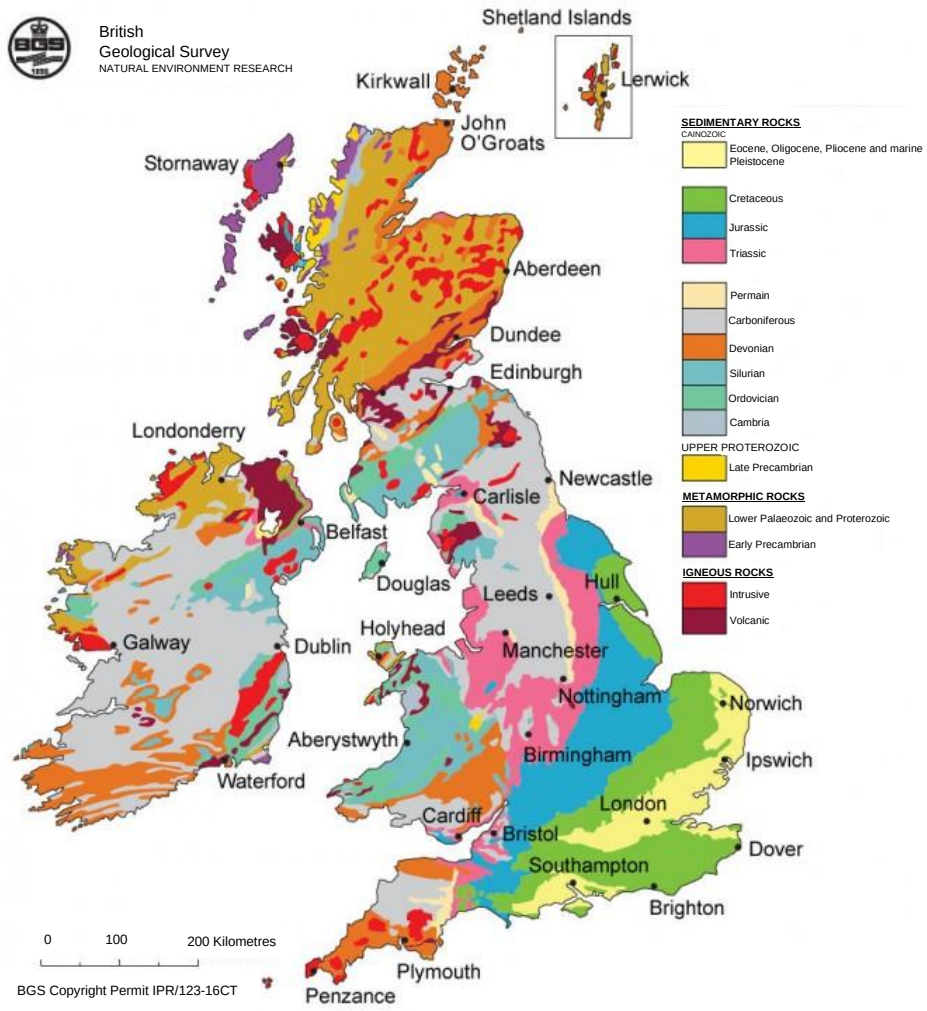

Figure 4.1: Geology of the UK, clearly highlighting areas of other Devonian sediments that could possibly be further understood as a result of this research (GB IPR_123-16CTGeologyMap) *(BGS, 2017)*.

Furthermore, this study contributes to the rocky coastline understanding around the world, addressing a need for such research in a synthesis by Naylor et al (2010). Additionally, my research highlights unique methodologies which can improve the dating and overall understanding of the long-term evolution of rocky coastlines (Naylor et al., 2010).

The background understanding of the main erosive processes which erode rocky coastlines is vital. Results from my research reiterate the stochastic nature of

mass movement events, which is in line with a wide array of current literature and theories (section 1.2.2). However, it also highlights the corresponding timing and relationship between these mass movement events and rising sea-level during the early Holocene. Rising sea-levels are predicted to change the controlling factors of mass movement events, including wave refraction patterns, tidal range, water depths, storm surges and high swells (Mauz et al., 2012; Naylor et al., 2010; Trenhaile, 2014). In addition to this, increasing temperatures and precipitation are also predicted to occur alongside rising sea-levels, possibly contributing to potential increases in mass movement frequency via saturation, or increased weathering and bioerosion rates (Trenhaile, 2014). These environmental changes are currently being documented and identified in this century, at a global scale, possibly increasing the frequency of mass movement events within coastal areas (Clark, 2017; Senfaute et al., 2009; Trenhaile, 2014). Consequently, the application of cosmogenic nuclide dating along some of the worlds coastline could construct an understanding of past mass movement events and incremental erosion rates. This can then be used as a proxy to project future changes under elevated sea-levels and environmental conditions.

Another successful component of my study focuses on the re-evaluation of the elevated shore platform at Hopes Nose, using UAV-SfM and modelled RSL to date and understand inheritance along north Torbay's rocky coastline. The results of my study are at a much higher resolution than previous studies, where low-accuracy and low resolution techniques are often employed, as noted in recent work by Rovere et al (2016a). Uncertainties are further exacerbated by the non-uniformity in measuring approaches commonly used to measure the geomorphological evidence of palaeo sea-levels at the global scale, thus hindering the collation of studies to create a global database (Rovere et al.,

2016a). However, my study demonstrates that UAV-SfM photogrammetry is a suitable alternative and effective methodology, which can be applied to many palaeogeomorphological features (e.g. elevated shore platforms or tidal notches), to produce centimetre resolution DEMs and orthomosaics which can be used to standardize the morphometric techniques within the research community.

Furthermore, the use of UAV-SfM photogrammetry to obtain morphometric data and model RSL, as discussed in section 4.6.2, can be used to date palaeocoastal features at the global scale. Applying UAV-SfM photogrammetry to palaeocoastal features at a global scale would produce useful insights into rocky coastal inheritance and evolution. Similarly, the technique can be used to estimate palaeo-RSL along many coastlines, possibly highlighting the significant variations in RSL between different locations on the global scale (Ferranti et al., 2006). Additionally, this can reveal significant temporal changes in RSL throughout the MIS stages, and how these differ between location. For example, the differences seen between north Torbay (section 4.4) and recent work by Polyak et al (2018) in the Mediterranean. Similarly, the high resolution elevations of palaeocoastal features can also be used as points of refence for existing modelled RSL curves at the global scale, which in turn will improve the overall accuracy of the models, as well as their future projections (Sloss et al., 2007).

Overall, it is evident that the methods used in my study have the potential to add significant and more accurate insights into rocky coastline evolution, at both the local scale and the global scale.

CHAPTER 5: CONCLUSION

The novel application of ^{36}Cl exposure dating and UAV-SfM photogrammetry in my study has provided insight into the complex history of evolution and antiquity of north Torbay's coastline. The application of exposure dating has highlighted that north Torbay's coastline is actively eroding, through a series of stochastic mass movements, which postdate the onset of sea-level stabilisation during the late Holocene. Within my results, there appears to be no pattern to the mass movements themselves. However, the influence of the open or closed aspect of the cliffs to prevailing waves and tides has some apparent influence over the possible timings of mass movement events, with open coastlines experiencing earlier falls than those in sheltered coastal environments. In contrast to this, differences in the exposure ages could possibly highlight the cyclic nature of cliff evolution, which cycles through periods of cliff destabilisation and stability.

I also calculated incremental erosion rate for bedrock situated in the swash zone at Peaked Tor Cove from ^{36}Cl concentrations, at between 0.4-0.6 m ka. This rate is a possible incremental erosion rate associated with mechanical erosion and weathering rates of the Devonian carbonates at north Torbay. These rates are high for rocky coastlines but remain three orders of magnitude lower than more sedimentary coastlines.

Exposure dating of the raised shore platform at Hopes Nose failed to provide a direct date, but identifies that the raised shore platform has had a complex exposure history. I identified this covering as solifluction sediments, through observations taken from a detailed orthomosaic of the cliff and sediments at the back of the platform. However, through the comparison of UAV-SfM photogrammetry elevations and modelled RSL at Hopes Nose, I have concluded

that it is possible that the raised shore platform is inherited from the last interglacial, MIS 5e.

I have attributed the preservation of the raised shore platform to the covering of the platform by solifluction sediments, which were likely removed during storms and swells throughout the Holocene. Morphometric analysis of the modern and raised shore platform profiles highlights how the platform geomorphology and erosive processes alters over time, as an indirect result of RSL changes. Furthermore, the measurement of shore platform widths, as well as the quantification of cliff retreat and erosion rates, supports similar research which concludes that shore platform formation requires a relatively short period of sea-level stabilisation for their formation.

Furthermore, the elevations measured from the morphometric analysis of Hopes Nose are consistent with the GIA prediction for north Torbay. My results imply that the maximum MIS 5e eustatic peak was lower than what has been assumed so far, rather than the MIS 5e highstand being characterized by two different highstands.

Lastly, extensive literature comparison and review highlights that the unique application of cosmogenic nuclide exposure dating and UAV-SfM photogrammetry was the most suitable methodology for this study area. The methods are well suited to the study area, as well as addressing the aims and scale of my research project. Additionally, this combination of methodologies has a wide application across several temporal and spatial scales (e.g. north Torbay to the global scale). Consequently, the techniques can develop our fundamental understandings of rocky coastline evolution throughout the Quaternary, through stochastic and incremental erosion. Similarly, high resolution morphometric

analysis of rocky coastlines can be collated to help understand the influence of palaeo-RSL on rocky coastline evolution, as well as utilizing results as an analogue of future coastal evolution under rising sea-levels.

5. REFERENCES

Abad, M., Rodríguez-Vidal, J., Aboumaria, K., Zaghloul, M.N., Cáceres, L.M., Ruiz, F., Martínez-Aguirre, A., Izquierdo, T., Chamorro, S., 2013. Evidence of MIS 5 sea-level highstands in Gebel Mousa coast (Strait of Gibraltar, North of Africa). Geomorphology 182, 133–146. https://doi.org/10.1016/j.geomorph.2012.11.004

Abuodha, P.A.O., Woodroffe, C.D., 2010. Assessing vulnerability to sea-level rise using a coastal sensitivity index: a case study from southeast Australia. J Coast Conserv 14, 189–205. https://doi.org/10.1007/s11852-010-0097-0

Adams, P.N., Anderson, R.S., Revenaugh, J., 2002. Microseismic measurement of wave-energy delivery to a rocky coast. GEOLOGY 30, 895–898. https://doi.org/10.1130/0091-7613(2002)030<0895:MMOWED>2.0.CO;2

Adams, P.N., Storlazzi, C.D., Anderson, R.S., 2005. Nearshore wave-induced cyclical flexing of sea cliffs. J. Geophys. Res. 110, F02002. https://doi.org/10.1029/2004JF000217

Agisoft LLC, 2018. Agisoft PhotoScan User Manual - Professional Edition, Version 1.4 127.

Alvarez-Marrón, J., Hetzel, R., Niedermann, S., Menéndez, R., Marquínez, J., 2008. Origin, structure and exposure history of a wave-cut platform more than 1 Ma in age at the coast of northern Spain: A multiple cosmogenic nuclide approach. Geomorphology 93, 316–334. https://doi.org/10.1016/j.geomorph.2007.03.005

Andrade, C., Marques, F., Freitas, M.C., Cardoso, R., Madureira, P., 2002. Shore platform downwearing and cliff retreat in the Portuguese west coast. The Changing Coast 1. Associacao Eurocoast Portrugal, 423-432. ISBN: 9728558090.

Andrews, J.T., Buckley, J.T., England, J.H., 1970. Late-Glacial Chronology and Glacio-Isostatic Recovery, Home Bay, East Baffin Island, Canada. GSA Bulletin 81, 1123–1148. https://doi.org/10.1130/0016-7606(1970)81[1123:LCAGRH]2.0.CO;2

Andriani, G.F., Walsh, N., 2007a. Rocky coast geomorphology and erosional processes: A case study along the Murgia coastline South of Bari, Apulia — SE Italy. Geomorphology, Studies in Weathering and Slope Movements 87, 224–238. https://doi.org/10.1016/j.geomorph.2006.03.033

Andriani, G.F., Walsh, N., 2007b. Rocky coast geomorphology and erosional processes: A case study along the Murgia coastline South of Bari, Apulia — SE Italy. Geomorphology, Studies in Weathering and Slope Movements 87, 224–238. https://doi.org/10.1016/j.geomorph.2006.03.033

Antonioli, F., Ferranti, L., Stocchi, P., Deiana, G., Lo Presti, V., Furlani, S., Marino, C., Orru, P., Scicchitano, G., Trainito, E., Anzidei, M., Bonamini, M., Sansò, P., Mastronuzzi, G., 2018. Morphometry and elevation of the last interglacial tidal notches in tectonically stable coasts of the Mediterranean Sea. Earth-Science Reviews 185, 600–623. https://doi.org/10.1016/j.earscirev.2018.06.017

Antonov, J.I., Levitus, S., Boyer, T.P., 2005. Thermosteric sea level rise, 1955–2003. Geophysical Research Letters 32. https://doi.org/10.1029/2005GL023112

Antonov, J.I., Levitus, S., Boyer, T.P., 2002. Steric sea level variations during 1957–1994: Importance of salinity. Journal of Geophysical Research: Oceans 107, SRF 14-1-SRF 14-8. https://doi.org/10.1029/2001JC000964

Argus, D.F., Peltier, W.R., Drummond, R., Moore, A.W., 2014. The Antarctica component of postglacial rebound model ICE-6G_C (VM5a) based on GPS positioning, exposure age dating of ice thicknesses, and relative sea level

histories. Geophysical Journal International 198, 537–563. https://doi.org/10.1093/gji/ggu140
Ávila, S.P., Melo, C., Silva, L., Ramalho, R.S., Quartau, R., Hipólito, A., Cordeiro, R., Rebelo, A.C., Madeira, P., Rovere, A., Hearty, P.J., Henriques, D., Silva, C.M. da, Martins, A.M. de F., Zazo, C., 2015. A review of the MIS 5e highstand deposits from Santa Maria Island (Azores, NE Atlantic): palaeobiodiversity, palaeoecology and palaeobiogeography. Quaternary Science Reviews 114, 126–148. https://doi.org/10.1016/j.quascirev.2015.02.012
Baker, A., Smart, P.L., Edwards, R.L., 1996. Mass spectrometric dating of flowstones from Stump Cross Caverns and Lancaster Hole, Yorkshire: palaeoclimate implications. Journal of Quaternary Science 11, 107–114. https://doi.org/10.1002/(SICI)1099-1417(199603/04)11:2<107::AID-JQS236>3.0.CO;2-E
Barlow, J., Gilham, J., Cofrã, I.I., 2017. Kinematic analysis of sea cliff stability using UAV photogrammetry. International Journal of Remote Sensing 38, 2464–2479. https://doi.org/10.1080/01431161.2016.1275061
Barrows, T.T., Stone, J.O., Fifield, L.K., Cresswell, R.G., 2002. The timing of the Last Glacial Maximum in Australia. Quaternary Science Reviews, EPILOG 21, 159–173. https://doi.org/10.1016/S0277-3791(01)00109-3
BBC, 2016. Coastal rail flood work "to cost £650m.". Viewed 06/04/2019, URL: https://www.bbc.co.uk/news/uk-england-devon-38025433
BBC, 2014. Storm-damaged rail line reopens. BBC News. Viewed 26/09/2017. URL: https://www.bbc.co.uk/news/uk-england-devon-26874503
Beetham, E.P., Kench, P.S., 2011. Field observations of infragravity waves and their behaviour on rock shore platforms. Earth Surface Processes and Landforms 36, 1872–1888. https://doi.org/10.1002/esp.2208
Bentor, Y. k., 1989. Geological events in the bible. Terra Nova 1, 326–338. https://doi.org/10.1111/j.1365-3121.1989.tb00382.x
Berger, W.H., 2002. Cesare Emiliani (1922–1995), pioneer of Ice Age studies and oxygen isotope stratigraphy. Comptes Rendus Palevol 1, 479–487. https://doi.org/10.1016/S1631-0683(02)00073-8
Bezerra, F.H.R., Vita-Finzi, C., Filho, F.P.L., 2017. The Use of Marine Shells For Radiocarbon Dating of Coastal Deposits. Revista Brasileira de Geociências 30, 211–213.
Bezerra, M.M., Moura, D., Ferreira, Ó., Taborda, R., 2011. Influence of Wave Action and Lithology on Sea Cliff Mass Movements in Central Algarve Coast, Portugal. Journal of Coastal Research 162–171. https://doi.org/10.2112/JCOASTRES-D-11-00004.1
BGS, (British Geological Survey), 2017. Geology of Britain | Discovering Geology | British Geological Survey (BGS) [WWW Document]. URL http://www.bgs.ac.uk/discoveringGeology/geologyOfBritain/home.html (accessed 12.28.17).
Bird, E.C.F., 2011. Coastal Geomorphology: An Introduction. John Wiley & Sons.
Blanco Chao, R., Costa Casais, M., Martínez Cortizas, A., Pérez Alberti, A., Trenhaile, A.S., 2003. Evolution and inheritance of a rock coast: western Galicia, northwestern Spain: Rock Coast Evolution in Northwestern Spain. Earth Surface Processes and Landforms 28, 757–775. https://doi.org/10.1002/esp.496
Blanco Chao, R., Pérez Alberti, A., Costa-Casais, M., Valcárcel Díaz, M., 2006. Abrasion processes in coarse-clastic beaches linked to rocky shore platforms.
Blanco-Chao, R., Pérez-Alberti, A., Trenhaile, A.S., Costa-Casais, M., Valcárcel-Díaz, M., 2007. Shore platform abrasion in a para-periglacial environment, Galicia,

northwestern Spain. Geomorphology 83, 136–151. https://doi.org/10.1016/j.geomorph.2006.06.028
Boaden, P.J.S., Seed, R., 1985. An introduction to coastal ecology. Blackie.
Boateng, I., 2012. An application of GIS and coastal geomorphology for large scale assessment of coastal erosion and management: a case study of Ghana. J Coast Conserv 16, 383–397. https://doi.org/10.1007/s11852-012-0209-0
Bonneau, D.A., Hutchinson, D.J., 2019. The use of terrestrial laser scanning for the characterization of a cliff-talus system in the Thompson River Valley, British Columbia, Canada. Geomorphology 327, 598–609. https://doi.org/10.1016/j.geomorph.2018.11.022
Boomer, I., Horton, B.P., 2006. Holocene relative sea-level movements along the North Norfolk Coast, UK. Palaeogeography, Palaeoclimatology, Palaeoecology 230, 32–51. https://doi.org/10.1016/j.palaeo.2005.07.004
Bourke, M., Flood, R., Goffo, F., Migge, K., Cullen, N., Nash, C., Naylor, L., 2017. Irish coastal platform location and type. Presented at the EGU General Assembly Conference Abstracts, p. 15557.
Bowen, D.Q., Sykes, G.A., Reeves (nee Henry), A., Miller, G.H., Andrews, J.T., Brew, J.S., Hare, P.E., 1985. Amino acid geochronology of raised beaches in south west Britain. Quaternary Science Reviews 4, 279–318. https://doi.org/10.1016/0277-3791(85)90003-4
Bradley, W.C., 1958. Submarine Abrasion and Wave-Cut Platforms. GSA Bulletin 69, 967–974. https://doi.org/10.1130/0016-7606(1958)69[967:SAAWP]2.0.CO;2
Braucher, R., Bourlès, D., Merchel, S., Vidal Romani, J., Fernadez-Mosquera, D., Marti, K., Léanni, L., Chauvet, F., Arnold, M., Aumaître, G., Keddadouche, K., 2013. Determination of muon attenuation lengths in depth profiles from in situ produced cosmogenic nuclides. Nuclear Instruments and Methods in Physics Research Section B: Beam Interactions with Materials and Atoms, Proceedings of the Twelfth International Conference on Accelerator Mass Spectrometry, Wellington, New Zealand, 20-25 March 2011 294, 484–490. https://doi.org/10.1016/j.nimb.2012.05.023
Bromhead, E.N., Ibsen, M.-L., 2006. A review of landsliding and coastal erosion damage to historic fortifications in South East England. Landslides 3, 341. https://doi.org/10.1007/s10346-006-0063-y
Brooks, S.M., Spencer, T., Boreham, S., 2012. Deriving mechanisms and thresholds for cliff retreat in soft-rock cliffs under changing climates: Rapidly retreating cliffs of the Suffolk coast, UK. Geomorphology 153–154, 48–60. https://doi.org/10.1016/j.geomorph.2012.02.007
Brunsden, D., Chandler, J.H., 1996. Development of an episodic landform change model based upon the Black Ven Mudslide 1946-1995, in: Advances in Hillslope Processes. John Wiley, Chichester, pp. 869–896.
Brunsden, D., Jones, D.K.C., 1976. A Discussion on valley slopes and cliffs in southern England: morphology, mechanics and Quaternary history - The evolution of landslide slopes in Dorset. Phil. Trans. R. Soc. Lond. A 283, 605–631. https://doi.org/10.1098/rsta.1976.0097
Bryant, E.A., Haslett, S.K., 2007. Catastrophic Wave Erosion, Bristol Channel, United Kingdom: Impact of Tsunami? The Journal of Geology 115, 253–269. https://doi.org/10.1086/512750
Burke, L.A., Kura, Y., Kassem, K., Revenga, C., Spalding, M., McAillister, D., 2001. Pilot Analysis of Global Ecosystems: Coastal Ecosystems. World Resources Institute.

Burningham, H., French, J., 2017. Understanding coastal change using shoreline trend analysis supported by cluster-based segmentation. Geomorphology 282, 131–149. https://doi.org/10.1016/j.geomorph.2016.12.029
Candy, I., Schreve, D., 2007. Land–sea correlation of Middle Pleistocene temperate sub-stages using high-precision uranium-series dating of tufa deposits from southern England. Quaternary Science Reviews 26, 1223–1235. https://doi.org/10.1016/j.quascirev.2007.01.012
Capron, E., Landais, A., Chappellaz, J., Schilt, A., Buiron, D., Dahl-Jensen, D., Johnsen, S.J., Jouzel, J., Lemieux-Dudon, B., Loulergue, L., Leuenberger, M., Masson-Delmotte, V., Meyer, H., Oerter, H., Stenni, B., 2010. Millennial and sub-millennial scale climatic variations recorded in polar ice cores over the last glacial period. Clim. Past 6, 345–365. https://doi.org/10.5194/cp-6-345-2010
Caputo, T., Somma, R., Marino, E., Matano, F., Troise, C., De Natale, G., 2016. Multi-temporal Terrestrial Laser Scanner monitoring of coastal instability processes at Coroglio cliff. Presented at the EGU General Assembly Conference Abstracts, pp. EPSC2016-7778.
Carpenter, N.E., Dickson, M.E., Walkden, M., Nicholls, R.J., Powrie, W., 2015. Lithological controls on soft cliff planshape evolution under high and low sediment availability. Earth Surface Processes and Landforms 40, 840–852. https://doi.org/10.1002/esp.3675
Carr, A.S., Bateman, M.D., Roberts, D.L., Murray-Wallace, C.V., Jacobs, Z., Holmes, P.J., 2010. The last interglacial sea-level high stand on the southern Cape coastline of South Africa. Quaternary Research 73, 351–363. https://doi.org/10.1016/j.yqres.2009.08.006
Carrivick, J.L., Smith, M.W., Quincey, D.J., 2016. Structure from Motion in the Geosciences. John Wiley & Sons.
Carter, R.W.G., Woodroffe, C.D., 1997. Coastal Evolution: Late Quaternary Shoreline Morphodynamics. Cambridge University Press.
Carvalho, R.C., Woodroffe, C.D., 2019. Morphological Exposure of Rocky Platforms: Filling the Hazard Gap Using UAVs. Drones 3, 42. https://doi.org/10.3390/drones3020042
Casella, E., Collin, A., Harris, D., Ferse, S., Bejarano, S., Parravicini, V., Hench, J.L., Rovere, A., 2017. Mapping coral reefs using consumer-grade drones and structure from motion photogrammetry techniques. Coral Reefs 36, 269–275. https://doi.org/10.1007/s00338-016-1522-0
Casella, E., Rovere, A., Pedroncini, A., Stark, C.P., Casella, M., Ferrari, M., Firpo, M., 2016. Drones as tools for monitoring beach topography changes in the Ligurian Sea (NW Mediterranean). Geo-Mar Lett 36, 151–163. https://doi.org/10.1007/s00367-016-0435-9
Cencini, C., 1998. Physical Processes and Human Activities in the Evolution of the Po Delta, Italy. Journal of Coastal Research 14, 775–793.
Chandler, J.H., Brunsden, D., 1995. Steady state behaviour of the black ven mudslide: The application of archival analytical photogrammetry to studies of landform change. Earth Surface Processes and Landforms 20, 255–275. https://doi.org/10.1002/esp.3290200307
Charlton, M.E., Large, A.R.G., Fuller, I.C., 2003. Application of airborne LiDAR in river environments: the River Coquet, Northumberland, UK. Earth Surface Processes and Landforms 28, 299–306. https://doi.org/10.1002/esp.482
Chelli, A., Pappalardo, M., Llopis, I.A., Federici, P.R., 2010. The relative influence of lithology and weathering in shaping shore platforms along the coastline of the Gulf of La Spezia (NW Italy) as revealed by rock strength. Geomorphology 118, 93–104. https://doi.org/10.1016/j.geomorph.2009.12.011

Choi, K.H., Seong, Y.B., Jung, P.M., Lee, S.Y., 2012. Using Cosmogenic 10Be Dating to Unravel the Antiquity of a Rocky Shore Platform on the West Coast of Korea. Journal of Coastal Research 641–657. https://doi.org/10.2112/JCOASTRES-D-11-00087.1

Christie, R.R., 1994. A New Geodetic Heighting Strategy for Great Britain. Survey Review 32, 328–343. https://doi.org/10.1179/sre.1994.32.252.328

Church, J.A., Aarup, T., Woodworth, P.L., Wilson, W.S., Nicholls, R.J., Rayner, R., Lambeck, K., Mitchum, G.T., Steffen, K., Cazenave, A., Blewitt, G., Mitrovica, J.X., Lowe, J.A., 2010. Sea-Level Rise and Variability: Synthesis and Outlook for the Future, in: Understanding Sea-Level Rise and Variability. John Wiley & Sons, Ltd, pp. 402–419. https://doi.org/10.1002/9781444323276.ch13

Clark, A., 2017. Small unmanned aerial systems comparative analysis for the application to coastal erosion monitoring. GeoResJ 13, 175–185. https://doi.org/10.1016/j.grj.2017.05.001

Clayton, G., Graham, J.R., Higgs, K., Holland, C.H., Naylor, D., 1979. Devonian Rocks in Ireland: A Review. Journal of Earth Sciences 2, 161–183.

Cloetingh, S., Haq, B.U., 2015. Inherited landscapes and sea level change. Science 347, 1258375. https://doi.org/10.1126/science.1258375

Coastal EBA, (UN Environment), 2017. The value of coastal ecosystems | Coastal Ecosystem-Based Adaptation [WWW Document]. Coatal Ecosystem-Based Adaptation. URL http://web.unep.org/coastal-eba/value-coastal-ecosystems (accessed 12.15.17).

Coastal Tourism Report, 2016. Coastal Tourism 2016 - new report! | National Coastal Tourism Academy [WWW Document]. URL https://coastaltourismacademy.co.uk/news/article/seaside-breaks--turning-the-tide-for-coastal-tourism (accessed 11.16.17).

Cochrane, J., 2008. Tourism, Partnership and a Bunch of Old Fossils: Management for Tourism at the Jurassic Coast World Heritage Site. Journal of Heritage Tourism 2, 156–167. https://doi.org/10.2167/jht057.0

Cook, K.L., 2017. An evaluation of the effectiveness of low-cost UAVs and structure from motion for geomorphic change detection. Geomorphology 278, 195–208. https://doi.org/10.1016/j.geomorph.2016.11.009

Cooper, N.J., Barber, P.C., Bray, M.J., Carter, D.J., 2002. Shoreline management plans: a national review and engineering perspective. Proceedings of the Institution of Civil Engineers - Water and Maritime Engineering 154, 221–228. https://doi.org/10.1680/wame.2002.154.3.221

Cotton, C.A., 1949. Plunging Cliffs, Lyttelton Harbour*. New Zealand Geographer 5, 130–136. https://doi.org/10.1111/j.1745-7939.1949.tb01256.x

Council, N.R., Studies, D. on E. and L., Board, O.S., Coasts, C. on M.S.E.A.S., 2007. Mitigating Shore Erosion Along Sheltered Coasts. National Academies Press.

Crowley, J.W., Katz, R.F., Huybers, P., Langmuir, C.H., Park, S.-H., 2015. Glacial cycles drive variations in the production of oceanic crust. Science 347, 1237–1240. https://doi.org/10.1126/science.1261508

Cruslock, E.M., Naylor, L.A., Foote, Y.L., Swantesson, J.O.H., 2010. Geomorphologic equifinality: A comparison between shore platforms in Höga Kusten and Fårö, Sweden and the Vale of Glamorgan, South Wales, UK. Geomorphology, Rock Coast Geomorphology 114, 78–88. https://doi.org/10.1016/j.geomorph.2009.02.019

Cullen, N.D., Bourke, M.C., 2018. Clast abrasion of a rock shore platform on the Atlantic coast of Ireland. Earth Surface Processes and Landforms 43, 2627–2641. https://doi.org/10.1002/esp.4421

Daly, R.A., 1915. The Glacial-Control Theory of Coral Reefs. Proceedings of the American Academy of Arts and Sciences 51, 157–251. https://doi.org/10.2307/20025572
Darvill, C.M., 2013. Cosmogenic Nuclide Analysis. British Society of Geomorphology Geomorphological Techniques.
Davidson-Arnott, R., 2010. Introduction to Coastal Processes and Geomorphology. Cambridge University Press.
Davies, B., 2014. Cosmogenic nuclide dating. AntarcticGlaciers.org. URL http://www.antarcticglaciers.org/glacial-geology/dating-glacial-sediments-2/cosmogenic_nuclide_datin/ (accessed 12.29.17).
Davies, K.H., 1984. The aminostratigraphy of British Pleistocene beach deposits. Unpublished Ph.D Thesis, University of Wales.
Davies, P., Sunamura, T., Takeda, I., Tsujimoto, H., Williams, A.T., 2006. Controls of Shore Platform Width: the Role of Rock Resistance Factors at Selected Sites in Japan and Wales, UK. Journal of Coastal Research 160–164.
Davies, P., Williams, A.T., Bomboe, P., 1998. Numerical analysis of coastal cliff failure along the Pembrokeshire Coast National Park, Wales, UK. Earth Surface Processes and Landforms 23, 1123–1134. https://doi.org/10.1002/(SICI)1096-9837(199812)23:12<1123::AID-ESP945>3.0.CO;2-F
Dawson, D., 2012. The impact of future sea-level rise on the London-Penzance railway line. University of Plymouth, _01 Research Theses Main Collection. Viewed 01/02/2019. URI: _http://hdl.handle.net/10026.1/912
de Boer, B., Stocchi, P., Whitehouse, P.L., van de Wal, R.S.W., 2017. Current state and future perspectives on coupled ice-sheet – sea-level modelling. Quaternary Science Reviews 169, 13–28. https://doi.org/10.1016/j.quascirev.2017.05.013
de Lange, W.P., Moon, V.G., 2005. Estimating long-term cliff recession rates from shore platform widths. Engineering Geology 80, 292–301. https://doi.org/10.1016/j.enggeo.2005.06.004
Del Río, L., Gracia, F.J., 2009. Erosion risk assessment of active coastal cliffs in temperate environments. Geomorphology 112, 82–95. https://doi.org/10.1016/j.geomorph.2009.05.009
Dendy, S., Austermann, J., Creveling, J.R., Mitrovica, J.X., 2017. Sensitivity of Last Interglacial sea-level high stands to ice sheet configuration during Marine Isotope Stage 6. Quaternary Science Reviews 171, 234–244. https://doi.org/10.1016/j.quascirev.2017.06.013
Department of the Environment and Local Government (DELG), 2001, Coastal Zone Management, Spatial Planning Unit, Dublin. [site visited 19/08/2006]
Devoy, R.J., 1982. Analysis of the geological evidence for Holocene sea-level movements in southeast England. Proceedings of the Geologists' Association 93, 65–90. https://doi.org/10.1016/S0016-7878(82)80033-3
Dewez, T.J.B., Leroux, J., Morelli, S., 2016. CLIFF COLLAPSE HAZARD FROM REPEATED MULTICOPTER UAV ACQUISITIONS: RETURN ON EXPERIENCE. ISPRS - International Archives of the Photogrammetry, Remote Sensing and Spatial Information Sciences XLI-B5, 805–811. https://doi.org/10.5194/isprs-archives-XLI-B5-805-2016
Dickson, M.E., Perry, G.L.W., 2016. Identifying the controls on coastal cliff landslides using machine-learning approaches. Environmental Modelling & Software 76, 117–127. https://doi.org/10.1016/j.envsoft.2015.10.029
Dickson, M.E., Woodroffe, C.D., 2005. Rock coast morphology in relation to lithology and wave exposure, Lord Howe Island, southwest Pacific. Zeitschrift für Geomorphologie 239–251.

Digimap., 2019. Geology Roam, UK Research Innovation (UKRI) (vendor), annual updating, viewed 14/1/2019, URL: https://digimap.edina.ac.uk/roam/map/geology

Donn, T.F., Boardman, M.R., 1988. Bioerosion of Rocky Carbonate Coastlines on Andros Island, Bahamas. Journal of Coastal Research 4, 381–394.

Dornbusch, U., Robinson, D.A., 2011. Block removal and step backwearing as erosion processes on rock shore platforms: a preliminary case study of the chalk shore platforms of south-east England. Earth Surface Processes and Landforms 36, 661–671. https://doi.org/10.1002/esp.2086

Dredge, L.A., 1992. Breakup of Limestone Bedrock by Frost Shattering and Chemical Weathering, Eastern Canadian Arctic. Arctic and Alpine Research 24, 314–323. https://doi.org/10.2307/1551286

Dunai, T.J., 2010. Cosmogenic Nuclides: Principles, Concepts and Applications in the Earth Surface Sciences. Cambridge University Press.

Dunai, T.J., Lifton, N.A., 2014. The Nuts and Bolts of Cosmogenic Nuclide Production. Elements 10, 347–350. https://doi.org/10.2113/gselements.10.5.347

Dunne, J., Elmore, D., Muzikar, P., 1999. Scaling factors for the rates of production of cosmogenic nuclides for geometric shielding and attenuation at depth on sloped surfaces. Geomorphology 27, 3–11. https://doi.org/10.1016/S0169-555X(98)00086-5

Duperret, A., Raimbault, C., Duguet, T., Le Gall, B., Costa, S., Vandycke, S., 2017. Long-term rocky coast erosion: the influence of structural pattern and lithological context, as evidenced in the chalk (NW Normandy) and granitic (SW Brittany) rocks, NW France. Presented at the EGU General Assembly Conference Abstracts, p. 19559.

Dutton, A., Webster, J.M., Zwartz, D., Lambeck, K., Wohlfarth, B., 2015. Tropical tales of polar ice: evidence of Last Interglacial polar ice sheet retreat recorded by fossil reefs of the granitic Seychelles islands. Quaternary Science Reviews 107, 182–196. https://doi.org/10.1016/j.quascirev.2014.10.025

Earlie, C., Masselink, G., Russell, P., 2018. The role of beach morphology on coastal cliff erosion under extreme waves. Earth Surface Processes and Landforms 43, 1213–1228. https://doi.org/10.1002/esp.4308

Earlie, C., Masselink, G., Russell, P., Shail, R., 2013. Sensitivity analysis of the methodology for quantifying cliff erosion using airborne LiDAR – examples from Cornwall, UK. Journal of Coastal Research 470–475. https://doi.org/10.2112/SI65-080.1

Earlie, Claire S., Masselink, G., Russell, P.E., Shail, R.K., 2015a. Application of airborne LiDAR to investigate rates of recession in rocky coast environments. J Coast Conserv 19, 831–845. https://doi.org/10.1007/s11852-014-0340-1

Earlie, Claire S., Young, A.P., Masselink, G., Russell, P.E., 2015b. Coastal cliff ground motions and response to extreme storm waves. Geophysical Research Letters 42, 847–854. https://doi.org/10.1002/2014GL062534

Economidou, E., 1982. The ecological value of coastal ecosystems on JSTOR. Coastal Planning and Management 49, 98–101.

Edwards, 1987. The UK Heritage Coasts: An Assessment of the Ecological Impacts of Tourism. Jonathan R. Edwards. Annals of Tourism Research, vol. 14, no. 1, pp. 71-87. Pergamon Press, Maxwell House, Fairview Park, Elmsford, New York 10523. 1987. $75 annual subscription. Journal of Travel Research 26, 43–43. https://doi.org/10.1177/004728758702600154

Eisenbeiss, H., 2009. UAV photogrammetry (Doctoral Thesis). ETH Zurich. https://doi.org/10.3929/ethz-a-005939264

Eisenhauer, A., Zhu, Z.R., Collins, L.B., Wyrwoll, K.H., Eichstätter, R., 1996. The Last Interglacial sea level change: new evidence from the Abrolhos islands, West Australia. Geol Rundsch 85, 606–614. https://doi.org/10.1007/BF02369014

Emery, K.O., Kuhn, G.G., 1982. Sea cliffs: Their processes, profiles, and classification. GSA Bulletin 93, 644–654. https://doi.org/10.1130/0016-7606(1982)93<644:SCTPPA>2.0.CO;2

Emiliani, C., 1955. Pleistocene Temperatures. The Journal of Geology 63, 538–578. https://doi.org/10.1086/626295

Engels, S., Helmens, K.F., Väliranta, M., Brooks, S.J., Birks, H.J.B., 2010. Early Weichselian (MIS 5d and 5c) temperatures and environmental changes in northern Fennoscandia as recorded by chironomids and macroremains at Sokli, northeast Finland. Boreas 39, 689–704. https://doi.org/10.1111/j.1502-3885.2010.00163.x

Environment Agency, 2019. Short-term Shoreline Management Plan Policy [WWW Document]. National Coastal Erosion Risk Mapping. URL https://environment.maps.arcgis.com/apps/webappviewer/index.html?id=9cef4a084bbb4954b970cd35b099d94c (accessed 2.5.19).

Esteves, L.S., Williams, J.J., Nock, A., Lymbery, G., 2009. Quantifying Shoreline Changes along the Sefton Coast (UK) and the Implications for Research-Informed Coastal Management. Journal of Coastal Research 602–606.

Fairbanks, R.G., 1989. A 17,000-year glacio-eustatic sea level record: influence of glacial melting rates on the Younger Dryas event and deep-ocean circulation. Nature 342, 637. https://doi.org/10.1038/342637a0

Farrell, W.E., Clark, J.A., 1976. On Postglacial Sea Level. Geophysical Journal of the Royal Astronomical Society 46, 647–667. https://doi.org/10.1111/j.1365-246X.1976.tb01252.x

Ferranti, L., Antonioli, F., Mauz, B., Amorosi, A., Dai Pra, G., Mastronuzzi, G., Monaco, C., Orrù, P., Pappalardo, M., Radtke, U., Renda, P., Romano, P., Sansò, P., Verrubbi, V., 2006. Markers of the last interglacial sea-level high stand along the coast of Italy: Tectonic implications. Quaternary International, Quaternary sea-level changes: contributions from the 32nd IGC 145–146, 30–54. https://doi.org/10.1016/j.quaint.2005.07.009

Firth, C., Smith, D., Barlow, N., Bradley, S., Hall, A., Jordan, J., Long, D., 2018. Quaternary sea level changes in Scotland. Earth and Environmental Science Transactions of the Royal Society of Edinburgh 107.

Fisher, O., 1866. On the Disintegration of a Chalk Cliff. Geological Magazine 3, 354–356. https://doi.org/10.1017/S0016756800167573

Flageollet, J.C., 1996. The time dimension in the study of mass movements. Geomorphology, Landslides in the European Union 15, 185–190. https://doi.org/10.1016/0169-555X(95)00069-H

Fonstad, M.A., Dietrich, J.T., Courville, B.C., Jensen, J.L., Carbonneau, P.E., 2013. Topographic structure from motion: a new development in photogrammetric measurement. Earth Surface Processes and Landforms 38, 421–430. https://doi.org/10.1002/esp.3366

Furlani, S., Cucchi, F., 2013. Downwearing rates of vertical limestone surfaces in the intertidal zone (Gulf of Trieste, Italy). Marine Geology 343, 92–98. https://doi.org/10.1016/j.margeo.2013.06.005

Galili, E., Zviely, D., Ronen, A., Mienis, H.K., 2007. Beach deposits of MIS 5e high sea stand as indicators for tectonic stability of the Carmel coastal plain, Israel. Quaternary Science Reviews 26, 2544–2557. https://doi.org/10.1016/j.quascirev.2007.06.027

Gallagher, C., Telfer, M.W., Cofaigh, C.Ó., 2015. A Marine Isotope Stage 4 age for Pleistocene raised beach deposits near Fethard, southern Ireland. Journal of Quaternary Science 30, 754–763. https://doi.org/10.1002/jqs.2808
Gallois, R.W., 2011. Natural and artificial influences on coastal erosion at Sidmouth, Devon, UK. Geoscience in South-West England : Proceedings of the Ussher Society 12, 304–312.
Garnett, R.H.T., 1962. Underwater geological exploration in the St. Agnes area, Cornwall. Proceedings of the Geologists' Association 73, 65-IN3. https://doi.org/10.1016/S0016-7878(62)80018-2
GCC, (Gosford City Council), nd. What is the value of our coastline? (Coastal Mangement).
Gehrels, W.R., Dawson, D.A., Shaw, J., Marshall, W.A., 2011. Using Holocene relative sea-level data to inform future sea-level predictions: An example from southwest England. Global and Planetary Change 78, 116–126. https://doi.org/10.1016/j.gloplacha.2011.05.013
Gienko, G., Terry, J., 2014. Three-dimensional modeling of coastal boulders using multi-view image measurements. Earth Surface Processes and Landforms 39, 583–564. https://doi.org/10.1002/esp.3485
Gill, E.D., 1972. The relationship of present shore platforms to past sea levels. Boreas 1, 1–25. https://doi.org/10.1111/j.1502-3885.1972.tb00141.x
Gill, E.D., Lang, J.G., 1983. Micro-erosion meter measurements of rock wear on the Otway coast of southeast Australia. Marine Geology 52, 141–156. https://doi.org/10.1016/0025-3227(83)90025-7
Griggs, G.B. and Trenhaile, A.S. (1994) Coastal Cliffs and Platforms. In: Carter, R.W.G. and Woodroffe, C.D., Eds., Coastal Evolution: Late Quaternary Shoreline Morphodynamics, Cambridge University Press, Cambridge, 425-450.
Giuliano, J., Godard, V., Lebourg, T., Dewez, T., Tric, E., Marçot, N., 2013. Large scale structural control on regional coastline orientations: example from South-eastern France. Journal of Coastal Research 1687–1691. https://doi.org/10.2112/SI65-285.1
Giuliano, J., Lebourg, T., Godard, V., Dewez, T., Braucher, R., Bourlès, D., Marçot, N., 2014. Cosmogenic nuclides application on French Mediterranean shore platform development. Presented at the EGU General Assembly Conference Abstracts, p. 15650.
Gómez-Pujol, L., Cruslock, E., Fornós, J.J., Swantesson, J., 2006. Unravelling factors that control shore platforms and cliffs in microtidal coasts : the case of Mallorcan, Catalonian and Swedish coasts. Zeitschrift für Geomorphologie, Supplementbände, 144.
Goodger, K.B., Buglass, A., Scrutton, C.T., 1984. Sequence of coralline faunas and depositional environments in the Middle Devonian Daddyhole Limestone Formation stratotype section, Torquay, Devon. 6, 13–24.
Gosse, J.C., Phillips, F.M., 2001a. Terrestrial in situ cosmogenic nuclides: theory and application. Quaternary Science Reviews 20, 1475–1560. https://doi.org/10.1016/S0277-3791(00)00171-2
Gosse, J.C., Phillips, F.M., 2001b. Terrestrial in situ cosmogenic nuclides: theory and application. Quaternary Science Reviews 20, 1475–1560. https://doi.org/10.1016/S0277-3791(00)00171-2
Grenzdörffer, G.J., Naumann, M., 2016. Investigations on the Possibilities of Monitoring Coastal Changes Including Shallow Under Water Areas with UAS Photo Bathmetry. The International Archives of the Photogrammetr, Remote Sensing and Spatial Information Sciences XLI-B1. https://doi.org/10.5194/isprs-archives-XLI-B1-843-2016

Gunnell, Y., Jarman, D., Braucher, R., Calvet, M., Delmas, M., Leanni, L., Bourlès, D., Arnold, M., Aumaître, G., Keddaouche, K., 2013. The granite tors of Dartmoor, Southwest England: rapid and recent emergence revealed by Late Pleistocene cosmogenic apparent exposure ages. Quaternary Science Reviews 61, 62–76. https://doi.org/10.1016/j.quascirev.2012.11.005

Hall, A.M., Hansom, J.D., Williams, D.M., Jarvis, J., 2006. Distribution, geomorphology and lithofacies of cliff-top storm deposits: Examples from the high-energy coasts of Scotland and Ireland. Marine Geology 232, 131–155. https://doi.org/10.1016/j.margeo.2006.06.008

Hanson, H., Aarninkhof, S., Capobianco, M., Jiménez, J.A., Larson, M., Nicholls, R.J., Plant, N.G., Southgate, H.N., Steetzel, H.J., Stive, M.J.F., Vriend, H.J. de, 2003. Modelling of Coastal Evolution on Yearly to Decadal Time Scales. Journal of Coastal Research 19, 790–811.

Hapke, C.J., Kratzmann, M.G., Himmelstoss, E.A., 2013. Geomorphic and human influence on large-scale coastal change. Geomorphology, Coastal Geomorphology and Restoration 44th Binghamton Geomorphology Symposium 199, 160–170. https://doi.org/10.1016/j.geomorph.2012.11.025

Hart, M.B., Gosling, D., 2018. New Observations on the Sandstone 'DYkes', Head Deposits and Raised Beach of Berry Head. Proceedings of the Ussher Society 14, 121–128.

Harwood L N (1983) Observations Made Regarding Cliff Erosion at Hollicombe Head, Torbay, Reports and Transactions of Devonshire Association for the Advancement of Science, 115, 71-78.

Trenhaile, A. S. and Layzell, M. G. J., 1980: Shore platform morphology and tidal-duration distributions in storm wave environments. In McCann, S. B. (ed.), The coastline of Canada, Geol. Surv. Canada Paper 80-10: 207-214

Hatrushi, S.M.A., 2017. Morphology of the Raised Shore Platforms along the Coastline between Daghmar and Dhabab, Sultanate of Oman. Journal of Arts and Social Sciences [JASS] 8, 13–24. https://doi.org/10.24200/jass.vol8iss2pp13-24

Hay, C., Mitrovica, J.X., Gomez, N., Creveling, J.R., Austermann, J., E. Kopp, R., 2014. The sea-level fingerprints of ice-sheet collapse during interglacial periods. Quaternary Science Reviews 87, 60–69. https://doi.org/10.1016/j.quascirev.2013.12.022

Healy, T.R., 1968. Bioerosion on shore platforms developed in the Waitemata Formation, Auckland. Earth Science Journal, 2(1), 26-37.

Hearty, P.J., Hollin, J.T., Neumann, A.C., O'Leary, M.J., McCulloch, M., 2007. Global sea-level fluctuations during the Last Interglaciation (MIS 5e). Quaternary Science Reviews 26, 2090–2112. https://doi.org/10.1016/j.quascirev.2007.06.019

Hearty, P.J., Tormey, B.R., 2017. Sea-level change and superstorms; geologic evidence from the last interglacial (MIS 5e) in the Bahamas and Bermuda offers ominous prospects for a warming Earth. Marine Geology 390, 347–365. https://doi.org/10.1016/j.margeo.2017.05.009

Heisinger, B., Lal, D., Jull, A.J.T., Kubik, P., Ivy-Ochs, S., Knie, K., Nolte, E., 2002. Production of selected cosmogenic radionuclides by muons: 2. Capture of negative muons. Earth and Planetary Science Letters 200, 357–369. https://doi.org/10.1016/S0012-821X(02)00641-6

Heisinger, B, Lal, D., Jull, A.J.T., Kubik, P., Ivy-Ochs, S., Neumaier, S., Knie, K., Lazarev, V., Nolte, E., 2002. Production of selected cosmogenic radionuclides by muons: 1. Fast muons. Earth and Planetary Science Letters 200, 345–355. https://doi.org/10.1016/S0012-821X(02)00640-4

Hibbert, F.D., Austin, W.E.N., Leng, M.J., Gatliff, R.W., 2010. British Ice Sheet dynamics inferred from North Atlantic ice-rafted debris records spanning the last 175 000 years. Journal of Quaternary Science 25, 461–482. https://doi.org/10.1002/jqs.1331

Hibbert, F.D., Williams, F.H., Fallon, S.J., Rohling, E.J., 2018. A database of biological and geomorphological sea-level markers from the Last Glacial Maximum to present. Scientific Data 5, 180088. https://doi.org/10.1038/sdata.2018.88

High, C., Hanna, F.K., 1970. method for the direct measurement of erosion on rock surfaces. Published for the British Geomorphological Research Group by Geo Abstracts.

Hsu, T.-W., Lin, T.-Y., Tseng, I.-F., 2007. Human Impact on Coastal Erosion in Taiwan. Journal of Coastal Research 961–973. https://doi.org/10.2112/04-0353R.1

Hu, A., Bates, S.C., 2018. Internal climate variability and projected future regional steric and dynamic sea level rise. Nature Communications 9, 1068. https://doi.org/10.1038/s41467-018-03474-8

Huntingford, C., Marsh, T., Scaife, A.A., Kendon, E.J., Hannaford, J., Kay, A.L., Lockwood, M., Prudhomme, C., Reynard, N.S., Parry, S., Lowe, J.A., Screen, J.A., Ward, H.C., Roberts, M., Stott, P.A., Bell, V.A., Bailey, M., Jenkins, A., Legg, T., Otto, F.E.L., Massey, N., Schaller, N., Slingo, J., Allen, M.R., 2014. Potential influences on the United Kingdom's floods of winter 2013/14. Nature Climate Change 4, 769–777. https://doi.org/10.1038/nclimate2314

Hurst, M.D., Rood, D.H., Ellis, M.A., 2017. Controls on the distribution of cosmogenic 10Be across shore platforms. Earth Surface Dynamics Discussions 5, 67–84. https://doi.org/10.5194/esurf-5-67-2017

Hurst, M.D., Rood, D.H., Ellis, M.A., Anderson, R.S., Dornbusch, U., 2016. Recent acceleration in coastal cliff retreat rates on the south coast of Great Britain. Proceedings of the National Academy of Sciences of the United States of America 113, 13336–13341. https://doi.org/10.1073/pnas.1613044113

Ishii, M., Kimoto, M., Sakamoto, K., Iwasaki, S.-I., 2006. Steric sea level changes estimated from historical ocean subsurface temperature and salinity analyses. J Oceanogr 62, 155–170. https://doi.org/10.1007/s10872-006-0041-y

Isla, F.I., 2009. Coastal Zones and Estuaries. EOLSS Publications.

Ivy-Ochs, S., Kober, F., 2008. Surface exposure dating with cosmogenic nuclides. Quaternary Science Journal 57/1–2, 179–209.

James, M.R., Robson, S., 2012. Straightforward reconstruction of 3D surfaces and topography with a camera: Accuracy and geoscience application. J. Geophys. Res. 117, F03017. https://doi.org/10.1029/2011JF002289

Jones, D.G., Williams, A.T., 1991. Statistical analysis of factors influencing Cliff erosion along a section of the West Wales coast, U.K. Earth Surface Processes and Landforms 16, 95–111. https://doi.org/10.1002/esp.3290160202

Jurrasic Coast Website, 2018. A Walk Through Time - About - Jurassic Coast [WWW Document]. Jurassic Coast World Heritage Site. URL http://jurassiccoast.org/about/what-is-the-jurassic-coast/ (accessed 10.30.17).

Kaufman, D.S., Miller, G.H., 1992. Overview of amino acid geochronology. Comparative Biochemistry and Physiology Part B: Comparative Biochemistry 102, 199–204. https://doi.org/10.1016/0305-0491(92)90110-D

Keen, D.H., Campbell, S., 1998. The Quaternary history of the Dorset, south Devon and Cornish coasts, in: Campbell, S., Hunt, C.O., Scourse, J.D., Keen, D.H., Stephens, N. (Eds.), Quaternary of South-West England, The Geological Conservation Review Series. Springer Netherlands, Dordrecht, pp. 155–189. https://doi.org/10.1007/978-94-011-4920-4_6

Keen, D.H., Harmon, R.S., Andrews, J.T., 1981. U series and amino acid dates from Jersey. Nature 289, 162–164. https://doi.org/10.1038/289162a0
Keene, P., 2011. Classic Landforms of the North Devon Coast. Thematic Trails.
Kendon, M., McCarthy, M., 2015. The UK's wet and stormy winter of 2013/2014. Weather 70, 40–47. https://doi.org/10.1002/wea.2465
Kennedy, D.M., Coombes, M.A., Mottershead, D.N., 2017a. The temporal and spatial scales of rocky coast geomorphology: a commentary. Earth Surface Processes and Landforms 42, 1597–1600. https://doi.org/10.1002/esp.4150
Kennedy, D.M., Ierodiaconou, D., Schimel, A., 2014. Granitic coastal geomorphology: applying integrated terrestrial and bathymetric LiDAR with multibeam sonar to examine coastal landscape evolution. Earth Surface Processes and Landforms 39, 1663–1674. https://doi.org/10.1002/esp.3615
Kennedy, David M., Ierodiaconou, D., Weir, A., Brighton, B., 2017b. Wave hazards on microtidal shore platforms: testing the relationship between morphology and exposure. Nat Hazards 86, 741–755. https://doi.org/10.1007/s11069-016-2714-1
Kennedy, D.M., Paulik, R., Dickson, M.E., 2011. Subaerial weathering versus wave processes in shore platform development: reappraising the Old Hat Island evidence. Earth Surface Processes and Landforms 36, 686–694. https://doi.org/10.1002/esp.2092
Kennedy, D.M., Vann Jones, E.C., Dickson, M.E., Rosser, N.J., 2018. Wind Waves and Cliff Shaking on Macrotidal Shore Platforms: A Case-study from North Yorkshire, U.K. Journal of Coastal Research 436–440. https://doi.org/10.2112/SI85-088.1
Khan, N.S., Ashe, E., Shaw, T.A., Vacchi, M., Walker, J., Peltier, W.R., Kopp, R.E., Horton, B.P., 2015. Holocene Relative Sea-Level Changes from Near-, Intermediate-, and Far-Field Locations. Curr Clim Change Rep 1, 247–262. https://doi.org/10.1007/s40641-015-0029-z
Kim, H.J., Park, W.K., Cho, W.C., 2017. Analysis of Coastal Erosion in Sanpo-Ri, Uljin-Gun (South Korea) using Field Survey and Measurement Data. Journal of Coastal Research 344–348. https://doi.org/10.2112/SI79-070.1
Klemas, V.V., 2015. Coastal and Environmental Remote Sensing from Unmanned Aerial Vehicles: An Overview. Journal of Coastal Research 1260–1267. https://doi.org/10.2112/JCOASTRES-D-15-00005.1
Kline, S.W., Adams, P.N., Limber, P.W., 2014. The unsteady nature of sea cliff retreat due to mechanical abrasion, failure and comminution feedbacks. Geomorphology 219, 53–67. https://doi.org/10.1016/j.geomorph.2014.03.037
Knauss, K.G., Ku, T.L., 1980. Desert Varnish: Potential for Age Dating via Uranium-Series Isotopes. Journal of Geology 88, 95–100. https://doi.org/10.1086/628476
Kopp, R.E., Hay, C.C., Little, C.M., Mitrovica, J.X., 2015. Geographic Variability of Sea-Level Change. Curr Clim Change Rep 1, 192–204. https://doi.org/10.1007/s40641-015-0015-5
Kopp, R.E., Simons, F.J., Mitrovica, J.X., Maloof, A.C., Oppenheimer, M., 2009. Probabilistic assessment of sea level during the last interglacial stage. Nature 462, 863–867. https://doi.org/10.1038/nature08686
Laker, C., 2016. Shore platform classification of central-southern NSW in relation to morphological variability and risk of drowning. Faculty of Science, Medicine & Health - Honours Theses.
Lal, D., 1991. Cosmic ray labeling of erosion surfaces: in situ nuclide production rates and erosion models. Earth and Planetary Science Letters 104, 424–439. https://doi.org/10.1016/0012-821X(91)90220-C

Lamothe, M., 2016. Luminescence dating of interglacial coastal depositional systems: Recent developments and future avenues of research. Quaternary Science Reviews 146, 1–27. https://doi.org/10.1016/j.quascirev.2016.05.005
Lang, A., Moya, J., Corominas, J., Schrott, L., Dikau, R., 1999. Classic and new dating methods for assessing the temporal occurrence of mass movements. Geomorphology 30, 33–52. https://doi.org/10.1016/S0169-555X(99)00043-4
Larson, M., Capobianco, M., Capobianco, M., Jansen, H., Rozynski, G., Southgate, H.N., Stive, M., Wijnberg, K.M., Hulscher, S.J.M.H., 2003. Analysis and modeling of field data of coastal morphological evolution over yearly and decadal time scales. Part 1 Background and linear techniques. J COASTAL RES 19, 760–775.
Lawrie, A., 1993. Shore platforms at +6–8 m above mean sea level on Banks Peninsula and implications for tectonic stability. New Zealand Journal of Geology and Geophysics 36, 409–415. https://doi.org/10.1080/00288306.1993.9514587
Lee, E.M., Hall, J.W., Meadowcroft, I.C., 2001. Coastal cliff recession: the use of probabilistic prediction methods. Geomorphology 40, 253–269. https://doi.org/10.1016/S0169-555X(01)00053-8
Lee, Yong, S., Seong, Bae, Y., Kang, Cheol, H., Choi, Hee, K., Yu, B.Y., 2015. Cosmogenic 10Be and OSL Dating of Marine Terraces Along the Central- East Coast of Korea: Spatio-Temporal Variations in Uplift Rates. The Open Geography Journal 7.
Lefsky, M.A., Cohen, W.B., Parker, G.G., Harding, D.J., 2002. Lidar Remote Sensing for Ecosystem StudiesLidar, an emerging remote sensing technology that directly measures the three-dimensional distribution of plant canopies, can accurately estimate vegetation structural attributes and should be of particular interest to forest, landscape, and global ecologists. BioScience 52, 19–30. https://doi.org/10.1641/0006-3568(2002)052[0019:LRSFES]2.0.CO;2
Leveau, P., Walsh, K., Trement, F., 2016. Environmental Reconstruction in Mediterranean Landscape Archaeology. Oxbow Books.
Leveridge, B.E., Shail, R.K., 2011. The marine Devonian stratigraphy of Great Britain. Proceedings of the Geologists' Association, The Marine Devonian of Great Britain 122, 540–567. https://doi.org/10.1016/j.pgeola.2011.03.003
Lewsey, C., Cid, G., Kruse, E., 2004. Assessing climate change impacts on coastal infrastructure in the Eastern Caribbean. Marine Policy 28, 393–409. https://doi.org/10.1016/j.marpol.2003.10.016
Lifton, N., Caffee, M., Finkel, R., Marrero, S., Nishiizumi, K., Phillips, F.M., Goehring, B., Gosse, J., Stone, J., Schaefer, J., Theriault, B., Jull, A.J.T., Fifield, K., 2015. In situ cosmogenic nuclide production rate calibration for the CRONUS-Earth project from Lake Bonneville, Utah, shoreline features. Quaternary Geochronology, The CRONUS-EARTH Volume: Part I 26, 56–69. https://doi.org/10.1016/j.quageo.2014.11.002
Lifton, N., Sato, T., Dunai, T.J., 2014. Scaling in situ cosmogenic nuclide production rates using analytical approximations to atmospheric cosmic-ray fluxes. Earth and Planetary Science Letters 386, 149–160. https://doi.org/10.1016/j.epsl.2013.10.052
Lifton, N.A., Bieber, J.W., Clem, J.M., Duldig, M.L., Evenson, P., Humble, J.E., Pyle, R., 2005. Addressing solar modulation and long-term uncertainties in scaling secondary cosmic rays for in situ cosmogenic nuclide applications. Earth and Planetary Science Letters 239, 140–161. https://doi.org/10.1016/j.epsl.2005.07.001

Lim, M., Rosser, N.J., Petley, D.N., Keen, M., 2011. Quantifying the Controls and Influence of Tide and Wave Impacts on Coastal Rock Cliff Erosion. Journal of Coastal Research 46–56. https://doi.org/10.2112/JCOASTRES-D-09-00061.1
Limber, P.W., Murray, A.B., 2015. Sea stack formation and the role of abrasion on beach-mantled headlands. Earth Surface Processes and Landforms 40, 559–568. https://doi.org/10.1002/esp.3667
Limber, P.W., Murray, A.B., 2014. Unraveling the dynamics that scale cross-shore headland relief on rocky coastlines: 2. Model predictions and initial tests. Journal of Geophysical Research: Earth Surface 119, 874–891. https://doi.org/10.1002/2013JF002978
Limber, P.W., Murray, A.B., 2011. Beach and sea-cliff dynamics as a driver of long-term rocky coastline evolution and stability. Geology 39, 1147–1150. https://doi.org/10.1130/G32315.1
Lisiecki, L.E., Raymo, M.E., 2005. A Pliocene-Pleistocene stack of 57 globally distributed benthic δ18O records. Paleoceanography 20. https://doi.org/10.1029/2004PA001071
Long, A.J., Barlow, N.L.M., Busschers, F.S., Cohen, K.M., Gehrels, W.R., Wake, L.M., 2015. Near-field sea-level variability in northwest Europe and ice sheet stability during the last interglacial. Quaternary Science Reviews 126, 26–40. https://doi.org/10.1016/j.quascirev.2015.08.021
Long, N., Millescamps, B., Guillot, B., Pouget, F., Bertin, X., 2016. Monitoring the Topography of a Dynamic Tidal Inlet Using UAV Imagery. Remote Sensing 8, 387. https://doi.org/10.3390/rs8050387
Mancini, F., Dubbini, M., Gattelli, M., Stecchi, F., Fabbri, S., Gabbianelli, G., 2013. Using Unmanned Aerial Vehicles (UAV) for High-Resolution Reconstruction of Topography: The Structure from Motion Approach on Coastal Environments. Remote Sensing 5, 6880–6898. https://doi.org/10.3390/rs5126880
Marques, F., Matildes, R., Redweik, P., 2011. Statistically based sea cliff instability hazard assessment of Burgau-Lagos coastal section (Algarve, Portugal). Journal of Coastal Research 927–931.
Marrero, S.M., Phillips, F.M., Borchers, B., Lifton, N., Aumer, R., Balco, G., 2016a. Cosmogenic nuclide systematics and the CRONUScalc program. Quaternary Geochronology 31, 160–187. https://doi.org/10.1016/j.quageo.2015.09.005
Marrero, S.M., Phillips, F.M., Caffee, M.W., Gosse, J.C., 2016b. CRONUS-Earth cosmogenic 36Cl calibration. Quaternary Geochronology 31, 199–219. https://doi.org/10.1016/j.quageo.2015.10.002
Marshall, R.J.E., Stephenson, W.J., 2011. The morphodynamics of shore platforms in a micro-tidal setting: Interactions between waves and morphology. Marine Geology 288, 18–31. https://doi.org/10.1016/j.margeo.2011.06.007
Martinec, Z., Klemann, V., van der Wal, W., Riva, R.E.M., Spada, G., Sun, Y., Melini, D., Kachuck, S.B., Barletta, V., Simon, K., A, G., James, T.S., 2018. A benchmark study of numerical implementations of the sea level equation in GIA modelling. Geophys J Int 215, 389–414. https://doi.org/10.1093/gji/ggy280
Martínez, M.L., Intralawan, A., Vázquez, G., Pérez-Maqueo, O., Sutton, P., Landgrave, R., 2007. The coasts of our world: Ecological, economic and social importance. Ecological Economics 63, 254–272. https://doi.org/10.1016/j.ecolecon.2006.10.022
Martinod, J., Regard, V., Riquelme, R., Aguilar, G., Guillaume, B., Carretier, S., Cortés-Aranda, J., Leanni, L., Hérail, G., 2016. Pleistocene uplift, climate and morphological segmentation of the Northern Chile coasts (24°S–32°S): Insights from cosmogenic 10Be dating of paleoshorelines. Geomorphology 274, 78–91. https://doi.org/10.1016/j.geomorph.2016.09.010

Masarik, J., Wieler, R., 2003. Production rates of cosmogenic nuclides in boulders. Earth and Planetary Science Letters 216, 201–208. https://doi.org/10.1016/S0012-821X(03)00476-X
Masselink, G., Hughes, M., Knight, J., 2014. Introduction to Coastal Processes and Geomorphology, Second Edition. Routledge.
Masselink, G., Hughes, M.G., Knight, J., 2011. Introduction to Coastal Processes and Geomorphology. Hodder Education.
Masselink, G., Russell, P., 2008. Coastal erosion and coastal geomorphology (Marine Climate Change Impacts Partnership), MCCIP Annual Report Card 2007-2008 Sceintific Revew. Plymouth University.
Massey, A.C., Gehrels, W.R., Charman, D.J., Milne, G.A., Peltier, W.R., Lambeck, K., Selby, K.A., 2008. Relative sea-level change and postglacial isostatic adjustment along the coast of south Devon, United Kingdom. J. Quaternary Sci. 23, 415–433. https://doi.org/10.1002/jqs.1149
Mastronuzzi, G., Quinif, Y., Sansò, P., Selleri, G., 2007. Middle-Late Pleistocene polycyclic evolution of a stable coastal area (southern Apulia, Italy). Geomorphology 86, 393–408. https://doi.org/10.1016/j.geomorph.2006.09.014
Matsumoto, H., Dickson, M.E., Kench, P.S., 2018. Modelling the relative dominance of wave erosion and weathering processes in shore platform development in micro- to mega-tidal settings. Earth Surface Processes and Landforms 43, 2642–2653. https://doi.org/10.1002/esp.4422
Matsumoto, Hironori, Dickson, M.E., Kench, P.S., 2016. Modelling the Development of Varied Shore Profile Geometry on Rocky Coasts. Journal of Coastal Research 597–601. https://doi.org/10.2112/SI75-120.1
Matsumoto, H., Dickson, M.E., Kench, P.S., 2016. An exploratory numerical model of rocky shore profile evolution. Geomorphology 268, 98–109. https://doi.org/10.1016/j.geomorph.2016.05.017
Matsumoto, H., E. Dickson, M., Masselink, G., 2017. Systematic analysis of rocky shore platform morphology at large spatial scale using LiDAR-derived digital elevation models. Geomorphology 286. https://doi.org/10.1016/j.geomorph.2017.03.011
Mauz, B., Fanelli, F., Elmejdoub, N., Barbieri, R., 2012. Coastal response to climate change: Mediterranean shorelines during the Last Interglacial (MIS 5). Quaternary Science Reviews, Coastal Change during the Late Quaternary 54, 89–98. https://doi.org/10.1016/j.quascirev.2012.02.021
Mauz, B., Shen, Z., Elmejdoub, N., Spada, G., 2018. No evidence from the eastern Mediterranean for a MIS 5e double peak sea-level highstand. Quaternary Research 89, 505–510. https://doi.org/10.1017/qua.2017.111
May, V.J., Hansom, J.D., 2003. An Introduction to the Coasatal Geomorphology of Great Britain, in: Coastal Geomorphology of Great Britain, Geological Conservation Review Series. Joint Nature Conservation Committee, Peterborough, p. 754.
McCarroll, D., 1993. Modelling late-holocene snow-avalanche activity: Incorporating a new approach to lichenometry. Earth Surface Processes and Landforms 18, 527–539. https://doi.org/10.1002/esp.3290180606
Mcintosh, P.D., Barrows, T.T., 2011. Morphology and age of bouldery landslide deposits in forested dolerite terrain, Nicholas Range, Tasmania. Zeitschrift für Geomorphologie 55, 383–393. https://doi.org/10.1127/0372-8854/2011/0044
McKenna, J., Carter, R.W.G., Bartlett, D., 1992. Coast Erosion in Northeast Ireland:-Part II Cliffs and Shore Platforms. Irish Geography 25, 111–128. https://doi.org/10.1080/00750779209478724

McLean, R.F., Davidson, C.F., 1968. The role of mass-movement in shore platform development along the Gisborne coastline, New Zealand.
Medley, S.E., Lea, D., Peterson, L.C., 2006. A new climate record from the Cariaco Basin: Marine Isotope Stage 5. American Geophysical Union.
Meier, M.F., Dyurgerov, M.B., Rick, U.K., O'Neel, S., Pfeffer, W.T., Anderson, R.S., Anderson, S.P., Glazovsky, A.F., 2007. Glaciers Dominate Eustatic Sea-Level Rise in the 21st Century. Science 317, 1064–1067. https://doi.org/10.1126/science.1143906
Melo, C.S., Ramalho, R.S., Quartau, R., Hipólito, A., Gil, A., Borges, P.A., Cardigos, F., Ávila, S.P., Madeira, J., Gaspar, J.L., 2018. Genesis and morphological evolution of coastal talus-platforms (fajãs) with lagoons: The case study of the newly-formed Fajã dos Milagres (Corvo Island, Azores). Geomorphology 310, 138–152. https://doi.org/10.1016/j.geomorph.2018.03.006
Micheletti, N., Chandler, J.H., Lane, S.N., 2015. Structure from motion (SFM) photogrammetry. British Society for Geomorphology. Geomorphological Techniques, Chapter 2, Section 2.2. ISSN 2047-0371.
Milne, G.A., Mitrovica, J.X., 1996. Postglacial sea-level change on a rotating Earth: first results from a gravitationally self-consistent sea-level equation. Geophysical Journal International 126, F13–F20. https://doi.org/10.1111/j.1365-246X.1996.tb04691.x
Milne G.A, Shennan I, Youngs B.A.R, Waugh A.I, Teferle F.N, Bingley R.M, Bassett S.E, Cuthbert-Brown C, Bradley S.L, 2006. Modelling the glacial isostatic adjustment of the UK region. Philosophical Transactions of the Royal Society A: Mathematical, Physical and Engineering Sciences 364, 931–948. https://doi.org/10.1098/rsta.2006.1747
Morris, C., Coulthard, T., Parsons, D.R., Manson, S., Barkwith, A., 2018. Modelling coastal dynamics under sea level rise with the Coastline Evolution Model 2D (CEM2D). Presented at the EGU General Assembly Conference Abstracts, p. 14888.
Moses, C., Robinson, D., Barlow, J., 2014. Methods for measuring rock surface weathering and erosion: A critical review. Earth-Science Reviews 135, 141–161. https://doi.org/10.1016/j.earscirev.2014.04.006
Mottershead, D.N., 1998. A Morphological Study of Greenschist Weathering on Dated Coastal Structures, South Devon, UK - Mottershead - 1997 - Earth Surface Processes and Landforms - Wiley Online Library. Earth Surface Processes and Landforms 22, 491–506. https://doi.org/10.1002/(SICI)1096-9837(199705)22:5<491::AID-ESP745>3.0.CO;2-4
Mottershead, D.N., 1989. Rates and patterns of bedrock denudation by coastal salt spray weathering: A seven-year record. Earth Surface Processes and Landforms 14, 383–398. https://doi.org/10.1002/esp.3290140504
Mottershead, D.N., Gilbertson, D.D., Keen, D.H., 1987. The raised beaches and shore platforms of Tor Bay: A re-evaluation. Proceedings of the Geologists' Association 98, 241–257. https://doi.org/10.1016/S0016-7878(87)80042-1
Muhs, D.R., Kennedy, G.L., Rockwell, T.K., 1994. Uranium-Series Ages of Marine Terrace Corals from the Pacific Coast of North America and Implications for Last-Interglacial Sea Level History. Quaternary Research 42, 72–87. https://doi.org/10.1006/qres.1994.1055
Munk, W., 2003. Ocean Freshening, Sea Level Rising. Science 300, 2041–2043. https://doi.org/10.1126/science.1085534
Murray, A.B., 2007. Reducing model complexity for explanation and prediction. Geomorphology, Reduced-Complexity Geomorphological Modelling for River

and Catchment Management 90, 178–191. https://doi.org/10.1016/j.geomorph.2006.10.020
Murray-Wallace, C.V., Woodroffe, C.D., 2014. Quaternary Sea-Level Changes. Cambridge University Press.
Mwaipopo, R., Shalli, M., 2016. Aesthetic, cultural and spiritual services from coastal and marine environments, in: Regional State of the Coast Report. Organisation for Economic Co-operation and Development, pp. 242–250.
Naylor, L.A., Coombes, M.A., Viles, H.A., 2012. Reconceptualising the role of organisms in the erosion of rock coasts: A new model. Geomorphology 157–158, 17–30. https://doi.org/10.1016/j.geomorph.2011.07.015
Naylor, L. A., Stephenson, W.J., 2010. On the role of discontinuities in mediating shore platform erosion. Geomorphology, Rock Coast Geomorphology 114, 89–100. https://doi.org/10.1016/j.geomorph.2008.12.024
Naylor, L.A., Stephenson, W.J., Trenhaile, A.S., 2010a. Rock coast geomorphology: Recent advances and future research directions. Geomorphology, Rock Coast Geomorphology 114, 3–11. https://doi.org/10.1016/j.geomorph.2009.02.004
Naylor, L.A., Stephenson, W.J., Trenhaile, A.S., 2010b. Rock coast geomorphology: Recent advances and future research directions. Geomorphology, Rock Coast Geomorphology 114, 3–11. https://doi.org/10.1016/j.geomorph.2009.02.004
Neumann, A.C., 1966. Observations on coastal erosion in bermuda and measurements of the boring rate of the sponge, cliona lampa1,2. Limnology and Oceanography 11, 92–108. https://doi.org/10.4319/lo.1966.11.1.0092
NGS, (National Geographic Society), 2017. coast [WWW Document]. URL https://www.nationalgeographic.org/encyclopedia/coast/ (accessed 12.15.17).
Nicholls, R.J., 2016. Understanding and Predicting Decadal Coastal Evolution. Presented at the EGU General Assembly Conference Abstracts, pp. EPSC2016-5199.
Nicholls, R.J., 2010. Impacts of and Responses to Sea-Level Rise, in: Understanding Sea-Level Rise and Variability. John Wiley & Sons, Ltd, pp. 17–51. https://doi.org/10.1002/9781444323276.ch2
Norman, E.C., Rosser, N.J., Brain, M.J., Petley, D.N., Lim, M., 2013. Coastal cliff-top ground motions as proxies for environmental processes. Journal of Geophysical Research: Oceans 118, 6807–6823. https://doi.org/10.1002/2013JC008963
Ogawa, H., Dickson, M.E., Kench, P.S., 2016. Generalised observations of wave characteristics on near-horizontal shore platforms: Synthesis of six case studies from the North Island, New Zealand. New Zealand Geographer 72, 107–121. https://doi.org/10.1111/nzg.12121
Ogawa, H., Dickson, M.E., Kench, P.S., 2015. Hydrodynamic constraints and storm wave characteristics on a sub-horizontal shore platform. Earth Surface Processes and Landforms 40, 65–77. https://doi.org/10.1002/esp.3619
Ogawa, H., Dickson, M.E., Kench, P.S., 2011. Wave transformation on a sub-horizontal shore platform, Tatapouri, North Island, New Zealand. Continental Shelf Research 31, 1409–1419. https://doi.org/10.1016/j.csr.2011.05.006
Oliver, T.S., Dougherty, A.J., Gliganic, L.A., Woodroffe, C.D., 2015. Towards more robust chronologies of coastal progradation: Optically stimulated luminescence ages for the coastal plain at Moruya, south-eastern Australia. The Holocene 25, 536–546. https://doi.org/10.1177/0959683614561886
ONS, (Office of National Statistics), 2016. Population Estimates for UK, England and Wales, Scotland and Northern Ireland - Office for National Statistics [WWW Document]. www.ons.gov.uk. URL https://www.ons.gov.uk/peoplepopulationandcommunity/populationandmigratio

n/populationestimates/bulletins/annualmidyearpopulationestimates/latest (accessed 11.2.17).
Ordnance Survey, 2019. Coordinate Transformation Tool [WWW Document]. OS-Net | Ordnance Survey. URL https://www.ordnancesurvey.co.uk/gps/transformation/ (accessed 2.5.19).
Owen, L.A., Finkel, R.C., Barnard, P.L., Haizhou, M., Asahi, K., Caffee, M.W., Derbyshire, E., 2005. Climatic and topographic controls on the style and timing of Late Quaternary glaciation throughout Tibet and the Himalaya defined by 10Be cosmogenic radionuclide surface exposure dating. Quaternary Science Reviews 24, 1391–1411. https://doi.org/10.1016/j.quascirev.2004.10.014
Page, D.K.N., 2004. A review of the geological heritage of Torbay with guidance for its management and a strategy for sustainable use., Torbay Heritage Forum. Torbay Coast and Countryside Trust.
Pajak, M.J., Leatherman, S., 2002. The High Water Line as Shoreline Indicator. Journal of Coastal Research 18, 329–337.
Palmer, M., Howard, T., Tinker, J., Lowe, J.A., Bricheno, L., Calvert, D., Edwards, T., Gregory, J., Harris, G., Krijnen, J., Pickering, M., Roberts, C., Wolf, J., 2018. UK Climate Report 18 - Marine Report (UKCP18). MetOffice, Environment Agency, DEFRA and DBEIS.
Pánek, T., 2015. Recent progress in landslide dating: A global overview. Progress in Physical Geography: Earth and Environment 39, 168–198. https://doi.org/10.1177/0309133314550671
Papakonstantinou, A., Topouzelis, K., Pavlogeorgatos, G., 2016. Coastline Zones Identification and 3D Coastal Mapping Using UAV Spatial Data. ISPRS International Journal of Geo-Information 5, 75. https://doi.org/10.3390/ijgi5060075
Pappalardo, M., Maggi, E., Geppini, C., Pannacciulli, F., 2018. Bioerosive and bioprotective role of barnacles on rocky shores. Science of The Total Environment 619–620, 83–92. https://doi.org/10.1016/j.scitotenv.2017.10.281
Pawley, S.M., Bailey, R.M., Rose, J., Moorlock, B.S.P., Hamblin, R.J.O., Booth, S.J., Lee, J.R., 2008. Age limits on Middle Pleistocene glacial sediments from OSL dating, north Norfolk, UK. Quaternary Science Reviews 27, 1363–1377. https://doi.org/10.1016/j.quascirev.2008.02.013
PCO, 2018. Plymouth Coastal Observatory map viewer and data catalogue. Chanel Coastal Observatory (Vendor), annual updating. Date Viewed 2/3/2019, URL: https://www.channelcoast.org/southwest/
Pedoja, K., Husson, L., Johnson, M.E., Melnick, D., Witt, C., Pochat, S., Nexer, M., Delcaillau, B., Pinegina, T., Poprawski, Y., Authemayou, C., Elliot, M., Regard, V., Garestier, F., 2014. Coastal staircase sequences reflecting sea-level oscillations and tectonic uplift during the Quaternary and Neogene. Earth-Science Reviews 132, 13–38. https://doi.org/10.1016/j.earscirev.2014.01.007
Pedoja, K., Ortlieb, L., Dumont, J.F., Lamothe, M., Ghaleb, B., Auclair, M., Labrousse, B., 2006. Quaternary coastal uplift along the Talara Arc (Ecuador, Northern Peru) from new marine terrace data. Marine Geology 228, 73–91. https://doi.org/10.1016/j.margeo.2006.01.004
Pedoja, K., Regard, V., Husson, L., Martinod, J., Guillaume, B., Fucks, E., Iglesias, M., Weill, P., 2011. Uplift of quaternary shorelines in eastern Patagonia: Darwin revisited. Geomorphology 127, 121–142. https://doi.org/10.1016/j.geomorph.2010.08.003
Peltier, W.R., Argus, D.F., Drummond, R., 2015. Space geodesy constrains ice age terminal deglaciation: The global ICE-6G_C (VM5a) model. Journal of

Geophysical Research: Solid Earth 120, 450–487. https://doi.org/10.1002/2014JB011176
Polyak, V.J., Onac, B.P., Fornós, J.J., Hay, C., Asmerom, Y., Dorale, J.A., Ginés, J., Tuccimei, P., Ginés, A., 2018. A highly resolved record of relative sea level in the western Mediterranean Sea during the last interglacial period. Nature Geoscience 1. https://doi.org/10.1038/s41561-018-0222-5
POST Report 363, 2010. Sea Level Rise. Houses of Parlimen, Parlimentary Office of Science and Technology.
Pranzini, E., 2018. Coastal erosion and shore protection: A brief historical analysis. J Coast Conserv 22, 827–830. https://doi.org/10.1007/s11852-017-0521-9
Prémaillon, M., Regard, V., Dewez, T.J.B., Auda, Y., 2018. GlobR2C2 (Global Recession Rates of Coastal Cliffs): a global relational database to investigate coastal rocky cliff erosion rate variations. Earth Surface Dynamics 6, 651–668. https://doi.org/10.5194/esurf-6-651-2018
QuestUAV, 2017. QuestUAV Drones - Reliable and Accurate Tools for Coastal Monitoring. URL https://www.questuav.com/media/case-study/questuav-drones-reliable-accurate-tools-coastal-monitoring/ (accessed 1.16.18).
Railsback, L.B., Gibbard, P.L., Head, M.J., Voarintsoa, N.R.G., Toucanne, S., 2015. An optimized scheme of lettered marine isotope substages for the last 1.0 million years, and the climatostratigraphic nature of isotope stages and substages. Quaternary Science Reviews 111, 94–106. https://doi.org/10.1016/j.quascirev.2015.01.012
Raimbault, C., Duperret, A., Regard, V., Molliex, S., Wyns, R., Authemayou, C., Le Gall, B., 2018. Quaternary geomorphological evolution of a granitic shore platform constrained by in situ 10 Be concentrations, Penmarc'h, SW Brittany, France. Marine Geology 395, 33–47. https://doi.org/10.1016/j.margeo.2017.09.011
Rao, P.P., Nair, M.M., Raju, D.V., 1985. Assessment of the role of remote sensing techniques in monitoring shoreline changes: a case study of the Kerala coast. International Journal of Remote Sensing 6, 549–558. https://doi.org/10.1080/01431168508948477
Rau, G.H., Knauss, K.G., Langer, W.H., Caldeira, K., 2007. Reducing energy-related CO2 emissions using accelerated weathering of limestone. Energy 32, 1471–1477. https://doi.org/10.1016/j.energy.2006.10.011
Recorbet, F., Rochette, P., Braucher, D., Benedetti, L., Hantz, D., Finkel, R.C., 2010. Evidence for active retreat of a coastal cliff between 3.5 and 12ka in Cassis (South East France). Geomorphology 115, 1–10. https://doi.org/10.1016/j.geomorph.2009.04.023
Reedy, R.C., 2013. Cosmogenic-nuclide production rates: Reaction cross section update. Nuclear Instruments and Methods in Physics Research Section B: Beam Interactions with Materials and Atoms, Proceedings of the Twelfth International Conference on Accelerator Mass Spectrometry, Wellington, New Zealand, 20-25 March 2011 294, 470–474. https://doi.org/10.1016/j.nimb.2011.08.034
Regard, V., Dewez, T., Bourlès, D.L., Anderson, R.S., Duperret, A., Costa, S., Leanni, L., Lasseur, E., Pedoja, K., Maillet, G.M., 2012. Late Holocene seacliff retreat recorded by 10Be profiles across a coastal platform: Theory and example from the English Channel. Quaternary Geochronology 11, 87–97. https://doi.org/10.1016/j.quageo.2012.02.027
Rémillard, A.M., Buylaert, J.-P., Murray, A.S., St-Onge, G., Bernatchez, P., Hétu, B., 2015. Quartz OSL dating of late Holocene beach ridges from the Magdalen Islands (Quebec, Canada). Quaternary Geochronology, LED14 Proceedings 30, 264–269. https://doi.org/10.1016/j.quageo.2015.03.013

Robinson, L.A., 1977. Marine erosive processes at the cliff foot. Marine Geology 23, 257–271. https://doi.org/10.1016/0025-3227(77)90022-6
Rohling, E.J., Grant, K., Hemleben, C., Siddall, M., Hoogakker, B. a. A., Bolshaw, M., Kucera, M., 2008. High rates of sea-level rise during the last interglacial period. Nature Geoscience 1, 38–42. https://doi.org/10.1038/ngeo.2007.28
Rosser, N.J., Brain, M.J., Petley, D.N., Lim, M., Norman, E.C., 2013. Coastline retreat via progressive failure of rocky coastal cliffs. Geology 41, 939–942. https://doi.org/10.1130/G34371.1
Rosser, N.J., Petley, D.N., Lim, M., Dunning, S.A., Allison, R.J., 2005. Terrestrial laser scanning for monitoring the process of hard rock coastal cliff erosion. Quarterly Journal of Engineering Geology and Hydrogeology 38, 363–375. https://doi.org/10.1144/1470-9236/05-008
Rostami, K., Peltier, W.R., Mangini, A., 2000. Quaternary marine terraces, sea-level changes and uplift history of Patagonia, Argentina: comparisons with predictions of the ICE-4G (VM2) model of the global process of glacial isostatic adjustment. Quaternary Science Reviews 19, 1495–1525. https://doi.org/10.1016/S0277-3791(00)00075-5
Rovere, A., Raymo, M.E., Vacchi, M., Lorscheid, T., Stocchi, P., Gómez-Pujol, L., Harris, D.L., Casella, E., O'Leary, M.J., Hearty, P.J., 2016a. The analysis of Last Interglacial (MIS 5e) relative sea-level indicators: Reconstructing sea-level in a warmer world. Earth-Science Reviews 159, 404–427. https://doi.org/10.1016/j.earscirev.2016.06.006
Rovere, A., Stocchi, P., Vacchi, M., 2016b. Eustatic and Relative Sea Level Changes. Curr Clim Change Rep 2, 221–231. https://doi.org/10.1007/s40641-016-0045-7
Rovere, A., Stocchi, P., Vacchi, M., 2016c. Eustatic and Relative Sea Level Changes. Curr Clim Change Rep 2, 221–231. https://doi.org/10.1007/s40641-016-0045-7
Roze, A., Zufferey, J.-C., Beyeler, A., McClellan, A., 2014. eBee RTK Accuracy Assessment 7.
Ruiz-Agudo, E., Mees, F., Jacobs, P., Rodriguez-Navarro, C., 2007. The role of saline solution properties on porous limestone salt weathering by magnesium and sodium sulfates. Environ Geol 52, 269–281. https://doi.org/10.1007/s00254-006-0476-x
Salzmann, L., Green, A., 2012. Boulder emplacement on a tectonically stable, wave-dominated coastline, Mission Rocks, northern KwaZulu-Natal, South Africa. Marine Geology 323–325, 95–106. https://doi.org/10.1016/j.margeo.2012.07.001
Sansò, P., Gianfreda, F., Leucci, G., Mastronuzzi, G., 2016. Cliff evolution and late Holocene relative sea level change along the Otranto coast (Salento peninsula, southern Apulia, Italy). GeoResJ 9–12, 42–53. https://doi.org/10.1016/j.grj.2016.07.001
Sato, T., Yasuda, H., Niita, K., Endo, A., Sihver, L., 2008. Development of PARMA: PHITS-based Analytical Radiation Model in the Atmosphere. Radiation Research 170, 244–259. https://doi.org/10.1667/RR1094.1
Savelli, D., Troiani, F., Cavitolo, P., Nesci, O., 2017. Rocky Cliffs Joining Velvet Beaches: The Northern Marche Coast, in: Soldati, M., Marchetti, M. (Eds.), Landscapes and Landforms of Italy, World Geomorphological Landscapes. Springer International Publishing, Cham, pp. 271–280. https://doi.org/10.1007/978-3-319-26194-2_23
Schenk, T., 2005. Introduction to Photogrammetry. The Ohio State University Department of Civil and Environmental Engineering and Geodetic Science, 100.

Schimmelpfennig, I., Benedetti, L., Pik, R., Burnard, P., Blard, P.H., Dunai, T., Bourlès, D., 2008. In situ cosmogenic 36Cl production rate calibration from Ca and K in lava flows. Geochimica et Cosmochimica Acta Supplement 72, A831.

Schönberg, C.H.L., Fang, J.K.H., Carreiro-Silva, M., Tribollet, A., Wisshak, M., 2017. Bioerosion: the other ocean acidification problem. ICES J Mar Sci 74, 895–925. https://doi.org/10.1093/icesjms/fsw254

SCOPAC, S.C. on P. associated with the C., 2012. Literature Review - Berry Head to Hope's Nose Tor Bay Sediment Transport Study [WWW Document]. Sediment Transport Study 2012. URL http://www.scopac.org.uk/sts/bh-hn-literature-review.html (accessed 8.26.19).

Senfaute, G., Duperret, A., Lawrence, J.A., 2009. Micro-seismic precursory cracks prior to rock-fall on coastal chalk cliffs: a case study at Mesnil-Val, Normandie, NW France. Natural Hazards and Earth System Sciences 9, 1625–1641. https://doi.org/10.5194/nhess-9-1625-2009

Sewell, R.J., Barrows, T.T., Campbell, S.D.G., Fifield, L.K., 2006. Exposure dating (10Be, 26Al) of natural terrain landslides in Hong Kong, China, in: Special Paper 415: In Situ-Produced Cosmogenic Nuclides and Quantification of Geological Processes. Geological Society of America, pp. 131–146. https://doi.org/10.1130/2006.2415(08)

Shackleton, N.J., Sánchez-Goñi, M.F., Pailler, D., Lancelot, Y., 2003. Marine Isotope Substage 5e and the Eemian Interglacial. Global and Planetary Change, The Eemain Interglacial: A Global Perspective 36, 151–155. https://doi.org/10.1016/S0921-8181(02)00181-9

Shanmugam, G., Wang, Y., 2015. The landslide problem. Journal of Palaeogeography 4, 109–166. https://doi.org/10.3724/SP.J.1261.2015.00071

Shannon, W.G., 1928. The geology of the Torquay district. Proceedings of the Geologists' Association 39, 103-136. https://doi.org/10.1016/S0016-7878(28)80020-4

Shennan, I., Long, A.J., Horton, B.P., 2014. Handbook of Sea-Level Research. John Wiley & Sons.

Shennan, I., Milne, G., Bradley, S.L., 2009. Late Holocene relative land - and sea-level changes : providing information for stakeholders. GSA today. 19, 52–53. http://dx.doi.org/10.1130/GSATG50GW.1

Short, D.A., Mengel, J.G., Crowley, T.J., Hyde, W.T., North, G.R., 1991. Filtering of Milankovitch Cycles by Earth's Geography. Quaternary Research 35, 157–173. https://doi.org/10.1016/0033-5894(91)90064-C

Skrivanek, A., Li, J., Dutton, A., 2018. Relative sea-level change during the Last Interglacial as recorded in Bahamian fossil reefs. Quaternary Science Reviews 200, 160–177. https://doi.org/10.1016/j.quascirev.2018.09.033

Sloss, C.R., Murray-Wallace, C.V., Jones, B.G., 2007. Holocene sea-level change on the southeast coast of Australia: a review. The Holocene 17, 999–1014. https://doi.org/10.1177/0959683607082415

Smith, M.W., Carrivick, J.L., Quincey, D.J., 2016. Structure from motion photogrammetry in physical geography. Progress in Physical Geography 40, 247–275. https://doi.org/10.1177/0309133315615805

Soldati, M., Barrows, T.T., Prampolini, M., Fifield, K.L., 2018. Cosmogenic exposure dating constraints for coastal landslide evolution on the Island of Malta (Mediterranean Sea). J Coast Conserv 22, 831–844. https://doi.org/10.1007/s11852-017-0551-3

Spada, G., Stocchi, P., 2007. SELEN: a Fortran 90 program for solving the "Sea Level Equation. Comput. Geosci 538–562.

Steele, M., Ermold, W., 2007. Steric Sea Level Change in the Northern Seas. J. Climate 20, 403–417. https://doi.org/10.1175/JCLI4022.1
Stephenson, W., 2008. Discussion of de Lange, W. P. and Moon V. G. 2005. Estimating long-term cliff recession rates from shore platform widths. Engineering Geology 80, 292–301. Engineering Geology 101, 288–291. https://doi.org/10.1016/j.enggeo.2008.04.008
Stephenson, W.J., 2000. Shore platforms: a neglected coastal feature? Progress in Physical Geography: Earth and Environment 24, 311–327. https://doi.org/10.1177/030913330002400301
Stephenson, W.J., Kirk, R.M., 1998. Rates and patterns of erosion on inter-tidal shore platforms, Kaikoura Peninsula, South Island, New Zealand. Earth Surf. Process. Landforms 23, 1071–1085. https://doi.org/10.1002/(SICI)1096-9837(199812)23:12<1071::AID-ESP922>3.0.CO;2-U
Stephenson, W.J., Naylor, L.A., Smith, H., Chen, B., Brayne, R.P., 2018. Wave transformation across a macrotidal shore platform under low to moderate energy conditions. Earth Surface Processes and Landforms 43, 298–311. https://doi.org/10.1002/esp.4245
Stive, M.J.F., Aarninkhof, S.G.J., Hamm, L., Hanson, H., Larson, M., Wijnberg, K.M., Nicholls, R.J., Capobianco, M., 2002. Variability of shore and shoreline evolution. Coastal Engineering, Shore Nourishment in Europe 47, 211–235. https://doi.org/10.1016/S0378-3839(02)00126-6
Stocchi, P., Vacchi, M., Lorscheid, T., de Boer, B., Simms, A.R., van de Wal, R.S.W., Vermeersen, B.L.A., Pappalardo, M., Rovere, A., 2018. MIS 5e relative sea-level changes in the Mediterranean Sea: Contribution of isostatic disequilibrium. Quaternary Science Reviews 185, 122–134. https://doi.org/10.1016/j.quascirev.2018.01.004
Stone, J., Lambeck, K., Fifield, L.K., Evans, J.M., Cresswell, R.G., 1996. A Lateglacial age for the Main Rock Platform, western Scotland. Geology 24, 707–710. https://doi.org/10.1130/0091-7613(1996)024<0707:ALAFTM>2.3.CO;2
Stone, J.O., 2000. Air pressure and cosmogenic isotope production. J. Geophys. Res. 105, 23753–23759. https://doi.org/10.1029/2000JB900181
Stone, J.O.H., Evans, J.M., Fifield, L.K., Allan, G.L., Cresswell, R.G., 1998. Cosmogenic Chlorine-36 Production in Calcite by Muons. Geochimica et Cosmochimica Acta 62, 433–454. https://doi.org/10.1016/S0016-7037(97)00369-4
Suess, E., 1904. The face of the earth. Рипол Классик.
Summerfield, M.A., 1991. Global geomorphology: an introduction to the study of landforms. Longman Scientific & Technical.
Sunamura, T., 2015. Rocky coast processes: with special reference to the recession of soft rock cliffs. Proceedings of the Japan Academy, Series B 91, 481–500. https://doi.org/10.2183/pjab.91.481
Sunamura, T., 1995. Rock control in coastal geomorphic processes. International Journal of Rock Mechanics and Mining Sciences and Geomechanics Abstracts 3, 103A.
Sunamura, T., 1992. Geomorphology of rocky coasts. J. Wiley.
Sunamura, T., 1978a. A mathematical model of submarine platform development. Mathematical Geology 10, 53–58. https://doi.org/10.1007/BF01033299
Sunamura, T., 1978b. A model of the development of continental shelves having erosional origin. GSA Bulletin 89, 504–510. https://doi.org/10.1130/0016-7606(1978)89<504:AMOTDO>2.0.CO;2
Sunamura, T., 1976. Feedback Relationship in Wave Erosion of Laboratory Rocky Coast. The Journal of Geology 84, 427–437. https://doi.org/10.1086/628209

Swirad, Z.M., Rosser, N.J., Brain, M.J., 2019. Identifying mechanisms of shore platform erosion using Structure-from-Motion (SfM) photogrammetry. Earth Surface Processes and Landforms 44, 1542–1558. https://doi.org/10.1002/esp.4591

Swirad, Z.M., Rosser, N.J., Brain, M.J., Vann Jones, E.C., 2016. What controls the Geometry of Rocky Coasts at the Local Scale? Journal of Coastal Research 612–616. https://doi.org/10.2112/SI75-123.1

Takahashi, T., 1977. Shore Platfrom in Southwestern Japan - Geomorphological Study. Oska, Japan. Coastal Landform Study Society of Southwestern Japan 177.

Teixeira, S.B., 2006. Slope mass movements on rocky sea-cliffs: A power-law distributed natural hazard on the Barlavento Coast, Algarve, Portugal. Continental Shelf Research, Coastal Hazard Assessment in the Gulf of Cádiz 26, 1077–1091. https://doi.org/10.1016/j.csr.2005.12.013

Teza, G., Marcato, G., Pasuto, A., Galgaro, A., 2015. Integration of laser scanning and thermal imaging in monitoring optimization and assessment of rockfall hazard: a case history in the Carnic Alps (Northeastern Italy). Nat Hazards 76, 1535–1549. https://doi.org/10.1007/s11069-014-1545-1

Thébaudeau, B., Trenhaile, A.S., Edwards, R.J., 2013. Modelling the development of rocky shoreline profiles along the northern coast of Ireland. Geomorphology, Continental Shelf Drowned Landscapes (INQUA-CMP and IGCP-526) 203, 66–78. https://doi.org/10.1016/j.geomorph.2013.03.027

Thomas, P.J., 2009. Luminescence Dating of Beachrock in the Southeast Coast of India—Potential for Holocene Shoreline Reconstruction. Journal of Coastal Research 1–7. https://doi.org/10.2112/07-0916.1

Thompson, R.C., Crowe, T.P., Hawkins, S.J., 2002. Rocky intertidal communities: past environmental changes, present status and predictions for the next 25 years. Environmental Conservation 29, 168–191. https://doi.org/10.1017/S0376892902000115

Tina Bernd-Cohen, M.G., 1999. State Coastal Program Effectiveness in Protecting Natural Beaches, Dunes, Bluffs, and Rocky Shores. Coastal Management 27, 187–217. https://doi.org/10.1080/089207599263839

Torgersen, E., Viola, G., Zwingmann, H., Harris, C., 2015. Structural and temporal evolution of a reactivated brittle–ductile fault – Part II: Timing of fault initiation and reactivation by K–Ar dating of synkinematic illite/muscovite. Earth and Planetary Science Letters 410, 212–224. https://doi.org/10.1016/j.epsl.2014.09.051

Toscano, M.A., Peltier, W.R., Drummond, R., 2011. ICE-5G and ICE-6G models of postglacial relative sea-level history applied to the Holocene coral reef record of northeastern St Croix, U.S.V.I.: investigating the influence of rotational feedback on GIA processes at tropical latitudes. Quaternary Science Reviews 30, 3032–3042. https://doi.org/10.1016/j.quascirev.2011.07.018

Trenhaile, A., 2016a. Rocky coasts ― their role as depositional environments. Earth-Science Reviews 159, 1–13. https://doi.org/10.1016/j.earscirev.2016.05.001

Trenhaile, A., 2016b. Modelling coastal notch morphology and developmental history in the Mediterranean. GeoResJ 9–12, 77–90. https://doi.org/10.1016/j.grj.2016.09.003

Trenhaile, A.S., 2014. Chapter 2 Climate change and its impact on rock coasts. Geological Society, London, Memoirs 40, 7–17. https://doi.org/10.1144/M40.2

Trenhaile, A.S., 2011. Predicting the response of hard and soft rock coasts to changes in sea level and wave height. Climatic Change 109, 599–615. https://doi.org/10.1007/s10584-011-0035-7

Trenhaile, A.S., 2010. The effect of Holocene changes in relative sea level on the morphology of rocky coasts. Geomorphology, Rock Coast Geomorphology 114, 30–41. https://doi.org/10.1016/j.geomorph.2009.02.003
Trenhaile, A.S., 2008. Modeling the role of weathering in shore platform development. Geomorphology 94, 24–39. https://doi.org/10.1016/j.geomorph.2007.04.002
Trenhaile, A. S, 2002. Modeling the development of marine terraces on tectonically mobile rock coasts. Marine Geology 185, 341–361. https://doi.org/10.1016/S0025-3227(02)00187-1
Trenhaile, Alan S, 2002. Rock coasts, with particular emphasis on shore platforms. Geomorphology, 29th Binghamton Geomorphology Symposium: Coastal Geomorphology 48, 7–22. https://doi.org/10.1016/S0169-555X(02)00173-3
Trenhaile, Alan S., 2001. Modeling the Effect of Weathering on the Evolution and Morphology of Shore Platforms. Journal of Coastal Research 17, 398–406.
Trenhaile, A. S., 2001. Modelling the Quaternary evolution of shore platforms and erosional continental shelves. Earth Surf. Process. Landforms 26, 1103–1128. https://doi.org/10.1002/esp.255
Trenhaile, A.S., 2000. Modeling the development of wave-cut shore platforms. Marine Geology 166, 163–178. https://doi.org/10.1016/S0025-3227(00)00013-X
Trenhaile, A.S., 1999. The Width of Shore Platforms in Britain, Canada, and Japan. Journal of Coastal Research 15, 355–364.
Trenhaile, A.S., 1987. The geomorphology of rock coasts, Oxford research studies in geography. New York: Oxford University Press.
Trenhaile, A.S., 1974. The Morphology and Classification of Shore Platforms in England and Wales. Geografiska Annaler. Series A, Physical Geography 56, 103–110. https://doi.org/10.2307/520431
Trenhaile, A.S., Alberti, A.P., Cortizas, A.M., Casais, M.C., Chao, R.B., 1999. Rock coast inheritance: an example from Galicia, northwestern Spain. Earth Surface Processes and Landforms 24, 605–621. https://doi.org/10.1002/(SICI)1096-9837(199907)24:7<605::AID-ESP977>3.0.CO;2-1
Trenhaile, A.S., Bryne, M.-L., 1986. A Theoretical Investigation of the Holocene Development of Rock Coasts, with Particular Reference to Shore Platforms. Geografiska Annaler: Series A, Physical Geography 68, 1–14. https://doi.org/10.1080/04353676.1986.11880154
Trenhaile, A.S., Kanyaya, J.I., 2007. The Role of Wave Erosion on Sloping and Horizontal Shore Platforms in Macro- and Mesotidal Environments. Journal of Coastal Research 23, 298–309.
Trenhaile, A.S., Layzell, M.G.J., 1981. Shore Platform Morphology and the Tidal Duration Factor. Transactions of the Institute of British Geographers 6, 82–102. https://doi.org/10.2307/621974
Trenhaile, A.S., Porter, N.I., Prestanski, K., 2015. Shore platform and cliff notch transitions along the La Paz Peninsula, southern Baja, Mexico. Geologica acta 13, 0167–0180. https://doi.org/10.1344/GeologicaActa2015.13.2.7
Trenhaile, A.S., Porter, N.J., 2018. Shore platform downwearing in eastern Canada; A 9–14 year micro-erosion meter record. Geomorphology 311, 90–102. https://doi.org/10.1016/j.geomorph.2018.03.024
Trenhaile, A.S., Porter, N.J., 2007. Can shore platforms be produced solely by weathering processes? Marine Geology 241, 79–92. https://doi.org/10.1016/j.margeo.2007.03.005
Tsujimoto, H., 辻本英和, ツジモトヒデカズ, 1986. Dynamic conditions for shore platform initiation. Science Report, Institute of Geoscience. University of Tskuba, Section A.8, 45-93. Article ID (NAID) 10006395787. Identifier: http://hdl.handle.net/2241/5800

Turner, I.L., Harley, M.D., Drummond, C.D., 2016. UAVs for coastal surveying. Coastal Engineering 114, 19–24. https://doi.org/10.1016/j.coastaleng.2016.03.011
Turner, R.K., Lorenzoni, I., Beaumont, N., Bateman, I.J., Langford, I.H., McDonald, A.L., 1998. Coastal Management for Sustainable Development: Analysing Environmental and Socio-Economic Changes on the UK Coast. The Geographical Journal 164, 269–281. https://doi.org/10.2307/3060616
Turrill, K., 2017. Britain's cheapest seaside towns to buy a house REVEALED | Property | Life & Style | Express.co.uk [WWW Document]. Express. URL https://www.express.co.uk/life-style/property/788709/buying-a-house-cheapest-seaside-towns-uk (accessed 12.15.17).
Tushingham, A.M., Peltier, W.R., 1991. Ice-3G: A new global model of Late Pleistocene deglaciation based upon geophysical predictions of post-glacial relative sea level change. Journal of Geophysical Research: Solid Earth 96, 4497–4523. https://doi.org/10.1029/90JB01583
Twidale, C.R., Bourne, J.A., Vidal Romani, J.R., 2005. Beach etching and shore platforms. Geomorphology, Weathering and landscape evolution 67, 47–61. https://doi.org/10.1016/j.geomorph.2003.11.008
UNAVCO, 2019. Geoid Height Calculator (Software) [WWW Document]. URL https://www.unavco.org/software/geodetic-utilities/geoid-height-calculator/geoid-height-calculator.html?fbclid=IwAR0x6w0v__TiEIT0zjNhe1XsBdQOoqvxKvVvORySB9g5j_v4nGtYJgTSl2g (accessed 2.5.19).
United Nations (UN), 2007. Percentage of total population living in coastal areas. Accessed 01/11/2017. URL: http://www.un.org/esa/sustdev/natlinfo/indicators/methodology_sheets/oceans_seas_coasts/pop_coastal_areas.pdf
Valvo, L.M., Murray, A.B., Ashton, A., 2006. How does underlying geology affect coastline change? An initial modeling investigation. Journal of Geophysical Research: Earth Surface 111. https://doi.org/10.1029/2005JF000340
Van Vliet-Lanoë, B., Goslin, J., Hénaff, A., Hallégouët, B., Delacourt, C., Le Cornec, E., Meurisse-Fort, M., 2016. Holocene formation and evolution of coastal dunes ridges, Brittany (France). Comptes Rendus Geoscience, Coastal sediment dynamics 348, 462–470. https://doi.org/10.1016/j.crte.2015.01.001
Vann Jones (née Norman), E.C., Rosser, N.J., Brain, M.J., Petley, D.N., 2015. Quantifying the environmental controls on erosion of a hard rock cliff. Marine Geology 363, 230–242. https://doi.org/10.1016/j.margeo.2014.12.008
Varnes, D.J., 1978. Slope Movement Types and Processes. Transportation Research Board Special Report.
Veit, H., Trauerstein, M., Preusser, F., Messmer, T., Gnägi, C., Zech, R., Wüthrich, L., 2017. Late Glacial/Early Holocene slope deposits on the Swiss Plateau: Genesis and palaeo-environment. CATENA 158, 102–112. https://doi.org/10.1016/j.catena.2017.06.012
Viles, H.A., 1987. Blue-green algae and terrestrial limestone weathering on Aldabra Atoll: An S.E.M. and light microscope study. Earth Surf. Process. Landforms 12, 319–330. https://doi.org/10.1002/esp.3290120310
Violante, C., 2009. Rocky coast: geological constraints for hazard assessment. Geological Society, London, Special Publications 322, 1–31. https://doi.org/10.1144/SP322.1
Walker, M., 2005. Quaternary Dating Methods. John Wiley & Sons, Incorporated, New York, UNITED KINGDOM.

Wehmiller, J.F., Harris, W.B., Boutin, B.S., Farrell, K.M., 2012. Calibration of amino acid racemization (AAR) kinetics in United States mid-Atlantic Coastal Plain Quaternary mollusks using 87Sr/86Sr analyses: Evaluation of kinetic models and estimation of regional Late Pleistocene temperature history. Quaternary Geochronology 7, 21–36. https://doi.org/10.1016/j.quageo.2011.09.005

Wentworth, C.K., 1938. Marine bench-forming processes : water-level weathering. Journal of Geomorphology 1, 6–32.

West, I., Csorvasi, N., n.d. Torquay - Geological Field Guide by Ian West [WWW Document]. URL http://www.southampton.ac.uk/~imw/Torquay.htm (accessed 12.28.17).

Westoby, M.J., Brasington, J., Glasser, N.F., Hambrey, M.J., Reynolds, J.M., 2012. 'Structure-from-Motion' photogrammetry: A low-cost, effective tool for geoscience applications. Geomorphology 179, 300–314. https://doi.org/10.1016/j.geomorph.2012.08.021

Whitehead, K., H. Hugenholtz, C., 2014. Remote sensing of the environment with small unmanned aircraft systems (UASs), part 1: A review of progress and challenges. Journal of Unmanned Vehicle Systems 02, 69–85. https://doi.org/10.1139/juvs-2014-0006

Wilson, P., Barrows, T.T., Lord, T.C., Vincent, P.J., 2012. Surface lowering of limestone pavement as determined by cosmogenic (36Cl) analysis. Earth Surface Processes and Landforms 37, 1518–1526. https://doi.org/10.1002/esp.3260

Wohlfarth, B., 2013. A review of Early Weichselian climate (MIS 5d-a) in Europe 70. Department of Geological Sciences, Stockholm University. ISSN 1404-0344. SKB TR-13-03. ID 1358661. URL: http://www.skb.se/upload/publications/pdf/TR-13-03.pdf

Woodroffe, C.D., 2002. Coasts: Form, Process and Evolution. Cambridge University Press.

Woolard, J.W., Colby, J.D., 2002. Spatial characterization, resolution, and volumetric change of coastal dunes using airborne LIDAR: Cape Hatteras, North Carolina. Geomorphology, 29th Binghamton Geomorphology Symposium: Coastal Geomorphology 48, 269–287. https://doi.org/10.1016/S0169-555X(02)00185-X

Wright, L.W., 1970. Variation in the level of the cliff/shore platform junction along the south coast of Great Britain. Marine Geology 9, 347–353. https://doi.org/10.1016/0025-3227(70)90023-X

Xue, Z., Feng, A., Yin, P., Xia, D., 2009. Coastal Erosion Induced by Human Activities: A Northwest Bohai Sea Case Study. Journal of Coastal Research 723–733. https://doi.org/10.2112/07-0959.1

Yanites, B.J., Tucker, G.E., Anderson, R.S., 2009. Numerical and analytical models of cosmogenic radionuclide dynamics in landslide-dominated drainage basins. Journal of Geophysical Research: Earth Surface 114. https://doi.org/10.1029/2008JF001088

Yoshida Y., Moriwaki K., 1979. Some Consideration on Elevated Coastal Features and Their Dates around Syowa Station, Antarctica 13, 220–226.

Young, A.P., Flick, R.E., Gutierrez, R., Guza, R.T., 2009. Comparison of short-term seacliff retreat measurement methods in Del Mar, California. Geomorphology 112, 318–323. https://doi.org/10.1016/j.geomorph.2009.06.018

Zaggia, L., Lorenzetti, G., Manfé, G., Scarpa, G.M., Molinaroli, E., Parnell, K.E., Rapaglia, J.P., Gionta, M., Soomere, T., 2017. Fast shoreline erosion induced by ship wakes in a coastal lagoon: Field evidence and remote sensing analysis. PLOS ONE 12, e0187210. https://doi.org/10.1371/journal.pone.0187210

6. APPENDIX 1

A collection of images from the three north Torbay fieldtrips in January and February 2016, June 2017, January and March 2018. The follow photographs show sampling locations within the chosen study sites, as well as some of the distinctive geomorphology at the study sites located along north Torbay. Additionally, some of the drone images collected during the January 2018 eBee flight have also been included.

6.1. Meadfoot Beach

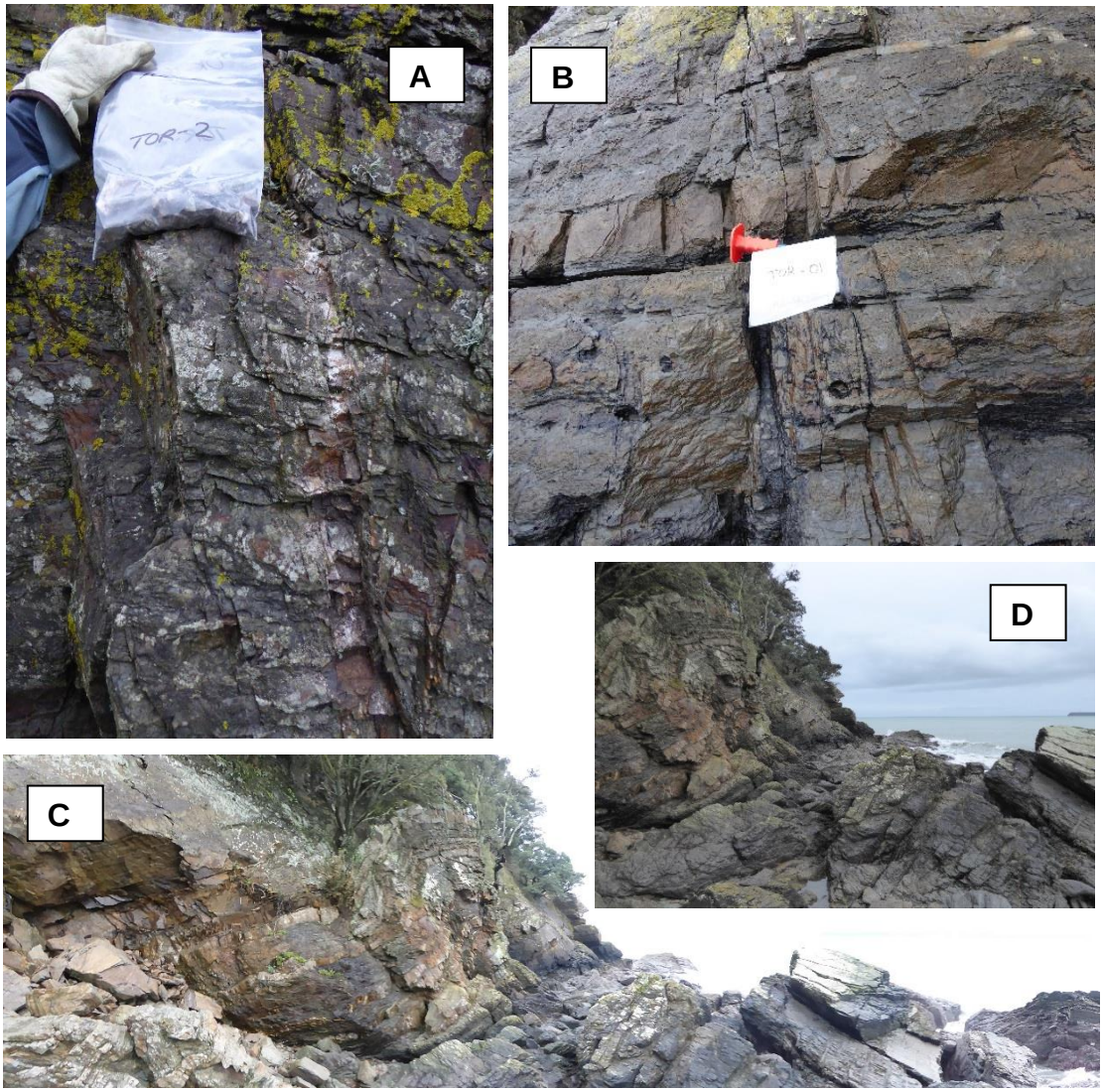

Figure 6.1: *A series of photographs taken at Meadfoot Beach.*
A) Photograph of the cliff sample TOR-02 (shale, with a quartz vein).
B) Photograph of the cliff sample TOR-01 (shale).
C) Photograph of a relic rotational landslide within the sampling site.
D) Same rotational landslide, from a closer perspective.

6.2. Beacon Cove

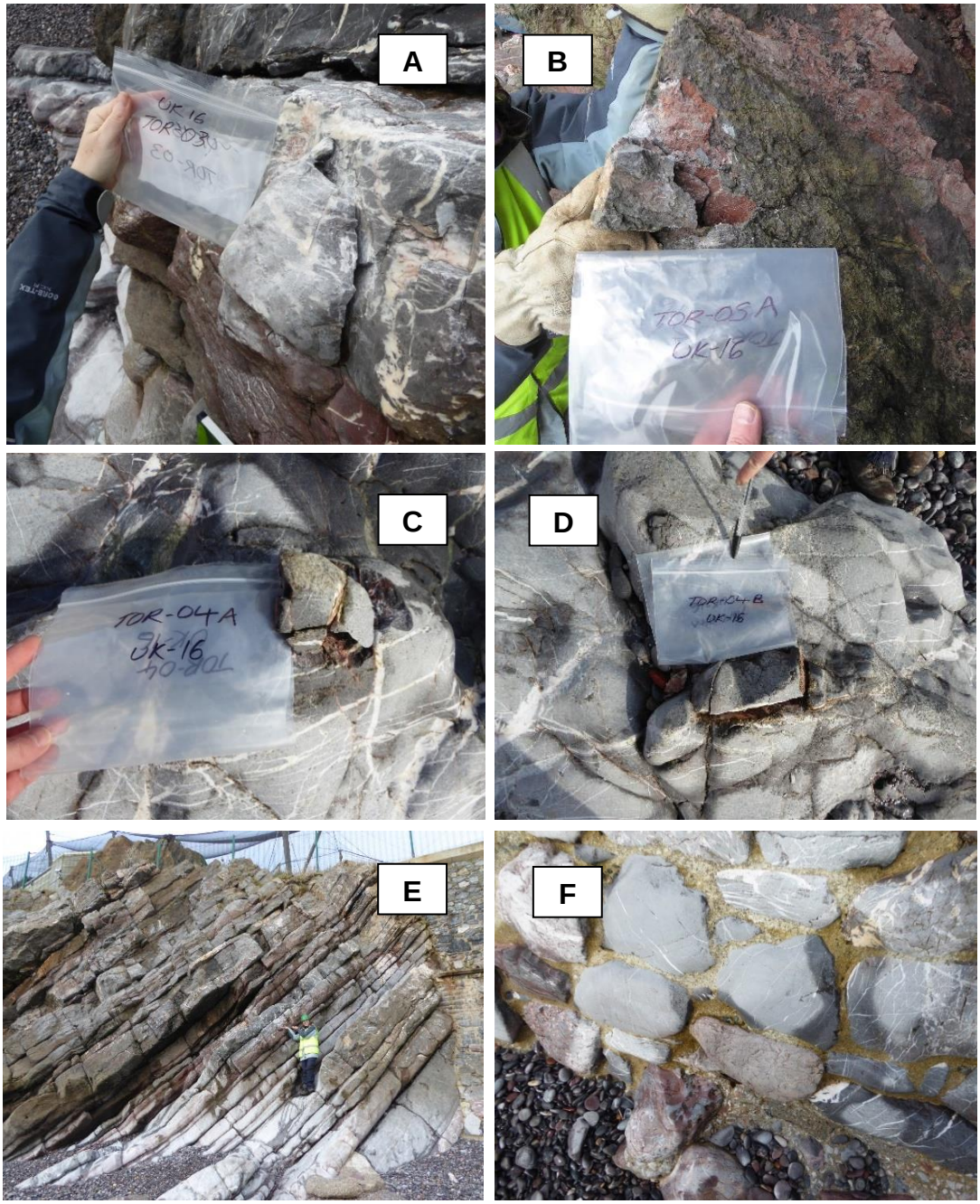

Figure 6.2: *A series of photographs taken at Beacon Cove.*
A) Photograph of the cliff face sample TOR-03 (limestone).
B) Photograph of the cliff face sample TOR-05 (limestone).
C) Photograph of the bedrock sampled in the swash zone for TOR-o4a (limestone).
D) Photograph of the bedrock sampled in the swash zone for TOR-04b (limestone).
E) Example of a relic landslide, or topple, within Beacon Cove (TOR-03 taken here).
F) Photograph of the backing sea-wall (Victorian period) at Beacon Cove, which have the same smooth texture as the sampled bedrock.

6.3. Peaked Tor Cove

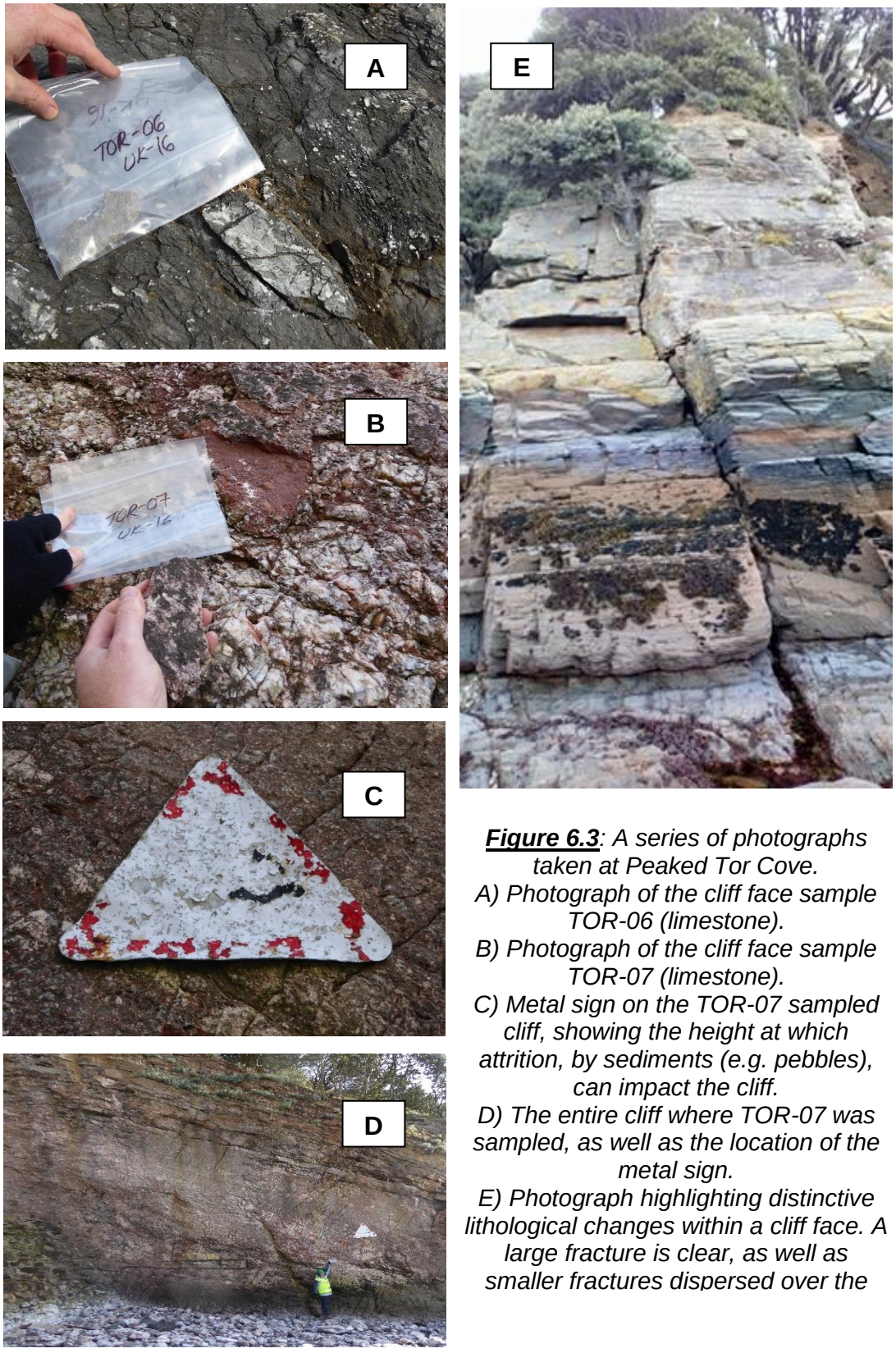

***Figure 6.3**: A series of photographs taken at Peaked Tor Cove.*
A) Photograph of the cliff face sample TOR-06 (limestone).
B) Photograph of the cliff face sample TOR-07 (limestone).
C) Metal sign on the TOR-07 sampled cliff, showing the height at which attrition, by sediments (e.g. pebbles), can impact the cliff.
D) The entire cliff where TOR-07 was sampled, as well as the location of the metal sign.
E) Photograph highlighting distinctive lithological changes within a cliff face. A large fracture is clear, as well as smaller fractures dispersed over the

6.4. Hopes Nose

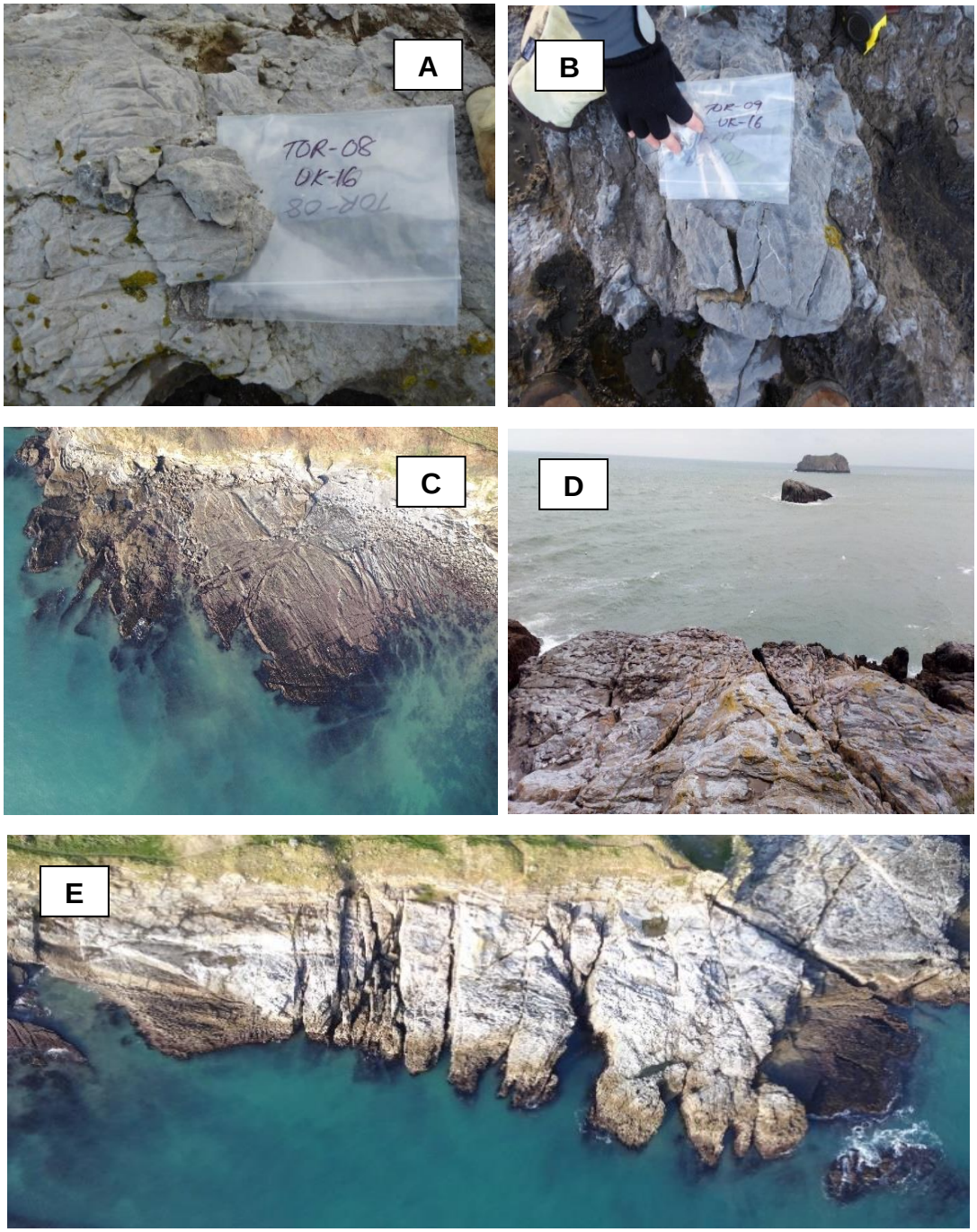

Figure 6.4: *A series of photographs taken from Hopes Nose, including two images from the EBee drone.*
A) Sample TOR-08 taken from the raised shore platform at Hopes Nose (Limestone).
B) Sample TOR-09 taken from the raised shore platform at Hopes Nose (Limestone).
C) eBee drone image of the modern shore platform AOI.
D) Photograph showing the slope of the raised platform towards the sea.
E) eBee drone image of the raised (interglacial) shore platform AOI).

Figure 6.5: *Additional images collected on the raised (interglacial) shore platform at Hopes Nose.*
A) The palaeo limestone cliff towards the back of the platform.
B) Image showing the elevated cliff-platform junction (red box) at Hopes Nose.
C) Photograph showing the extent of the palaeo-cliff and overlying solifluction sediments.
D) Shallow solution pans that are scattered across the surface of the raised shore platform.
E) Example of the sediments which are seen across both the raised (interglacial) and modern shore platforms.
F) Example of limestone that has undergone significant solution weathering at the toe of the raised (interglacial) shore platform.

7. APPENDIX 2

This section outlines the basic principles behind the Agisoft Photoscan SfM process, as well as the multi-view photogrammetry imaging technique to construct the sub-millimetre model of the backing sediments at Hopes Nose.

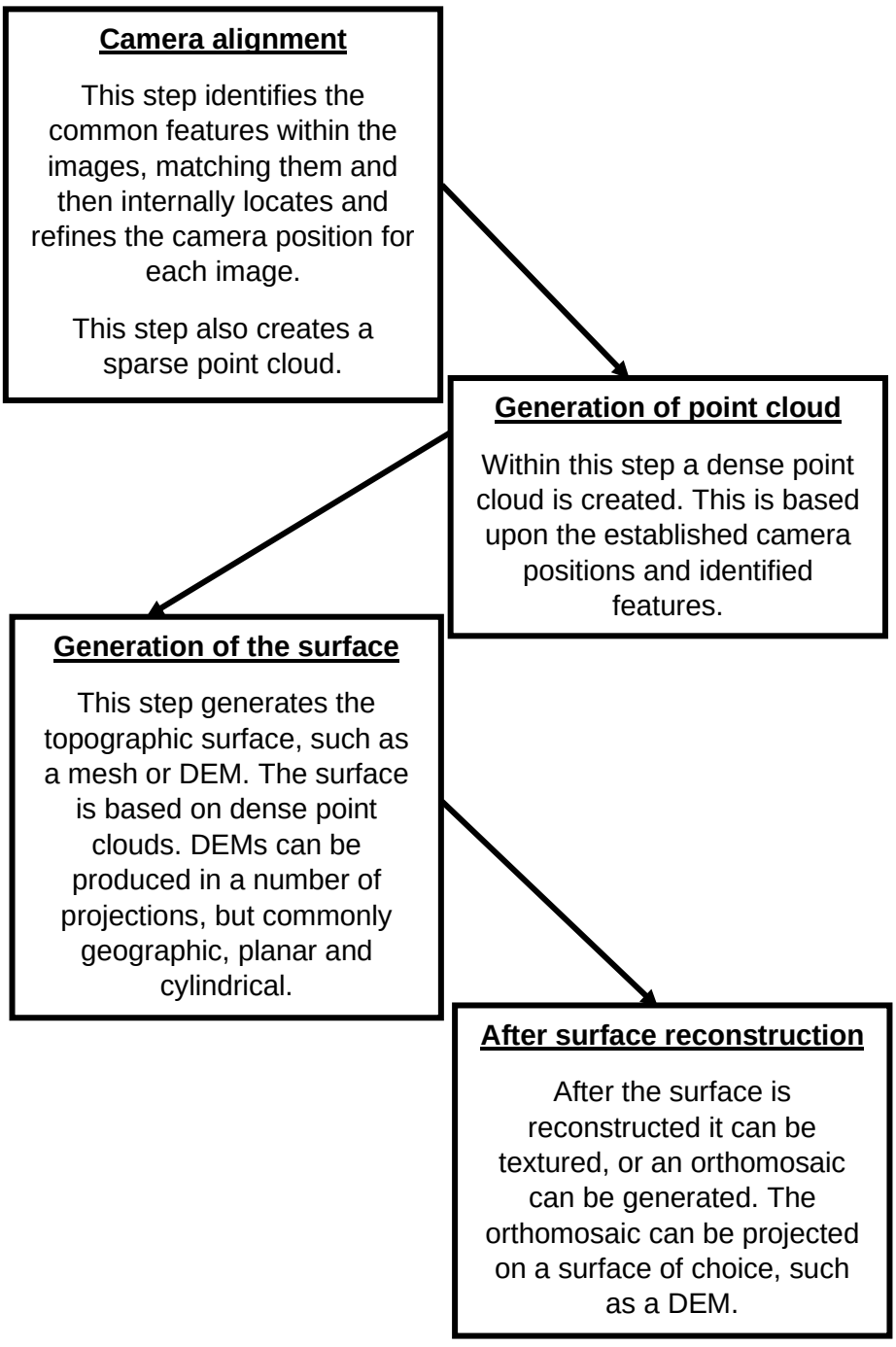

Figure 7.1: *Basic flowchart depicting the basic process of SfM within the Agisoft programme (Agisoft., 2018).*

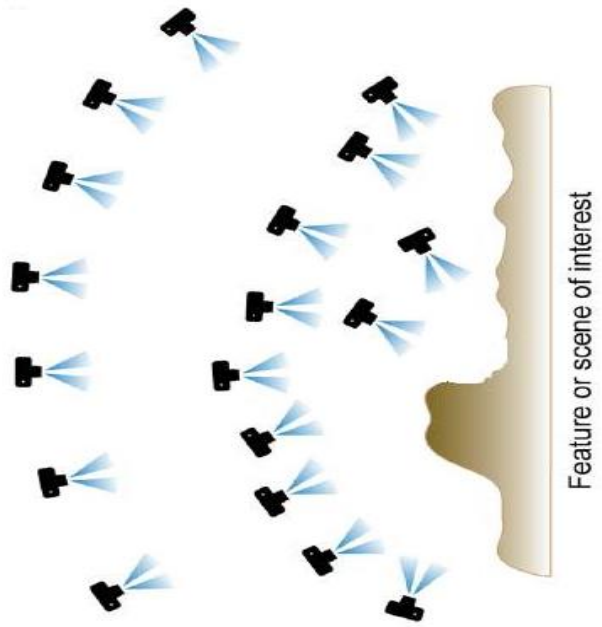

Figure 7.2*: Schematic from Micheletti et al (2015), showing how the images were collected to construct the backing sediment orthomosaic model.*

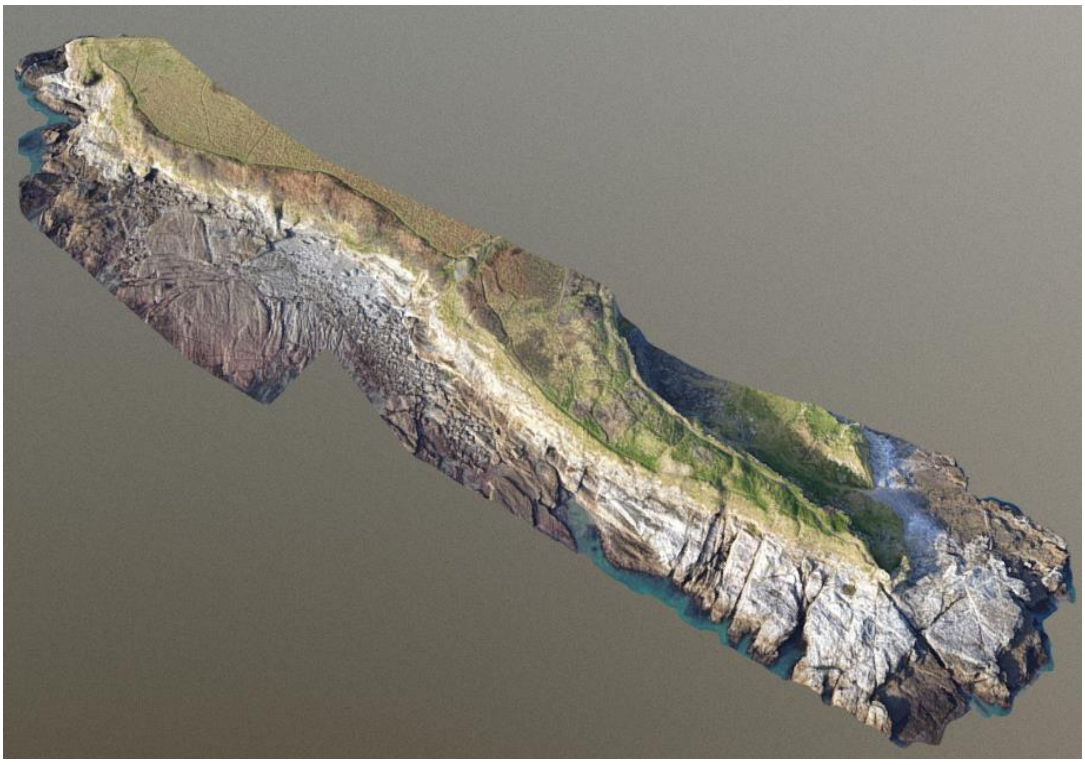

Figure 7.3*: Screenshot of 3D model obtained from the point cloud created during the Agisoft Photoscan post-processing. The model is available at: https://skfb.ly/6IWIS*

8. APPENDIX 3

Age (Ka BP)	Relative sea-level (m)
0	0
0.5	-0.14
1	-0.29
1.5	-0.46
2	-0.65
2.5	-0.86
3	-1.09
3.5	-1.37
4	-1.67
4.5	-2.00
5	-2.37
5.5	-3.00
6	-3.56
6.5	-4.31
7	-5.09
7.5	-6.11
8	-7.94
8.5	-10.15
9	-13.60
9.5	-16.97
10	-20.99

Table 8.1: *Sea-level predictions for the last 10,000 years of the Holocene. Sea-level was modelled specifically to Hopes Nose using the SELEN ICE-6G model.*

Age (Ka BP)	Relative sea-level (m)
119	-4.38
119.5	-2.86
120	-1.38
120.5	4.244
121	1.39
121.5	2.104
122	2.77
122.5	3.397
123	3.96
123.5	3.86
124	3.75
124.5	3.62
125	3.49
125.5	0.49
126	0.33
126.5	0.15
127	-5.69
127.5	-0.28
128	-0.55

Table 8.2: *Sea-level predictions for the last interglacial period, MIS5e (Eemian), which dates between 125 ka BP and 119 ka BP. Sea-level was modelled specifically to Hopes Nose using the SELEN ICE-6G model.*

9. APPENDIX 4

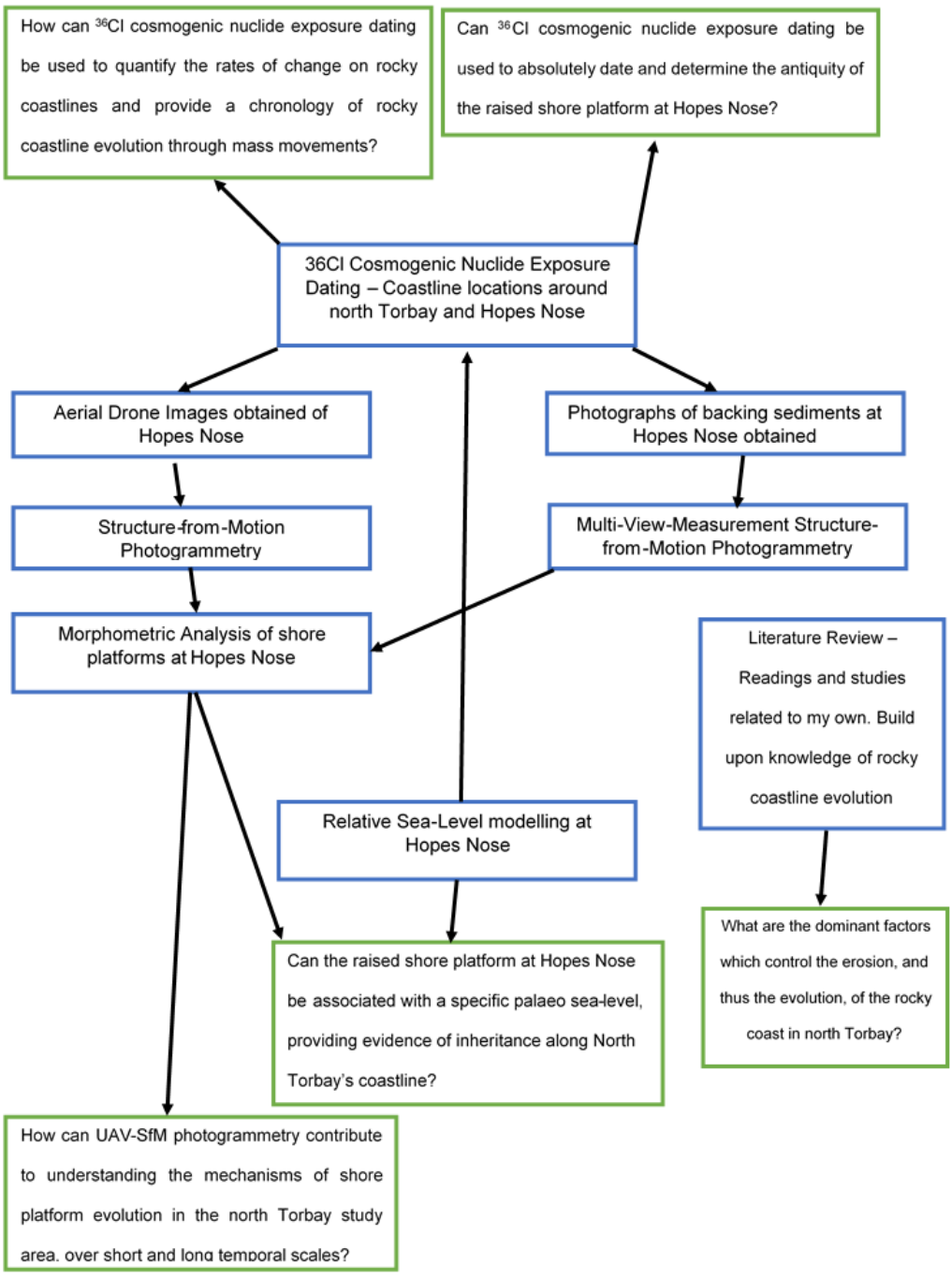

Figure 9.1: *Work plan figure outlining the ways in which the analytical approaches tie together, and which methodologies address which research questions.*